The Development of Microreactor Technology for the Study of Multistep Catalytic Systems and Rapid Kinetic Modelling

Conor John Waldron

Department of Chemical Engineering

University College London

August 2019

A thesis submitted for the degree of Doctor of Philosophy

I, Conor Waldron, confirm that the work presented in this thesis is my own. Where information has been derived from other sources, I confirm that this has been indicated in the thesis.

Signature: _____

Date: _____

Abstract

Microreactor technology was applied to the study of catalytic systems because their high rates of heat and mass transport, improved safety and ease of automation makes them particularly effective research tools in this area.

A multistep flow system for the synthesis of benzylacetone from benzyl alcohol via oxidation, aldol condensation and reduction reactions was developed by utilising three micropacked bed reactors and a gas liquid membrane separator. This reaction had previously been conducted in batch cascade, however, the multistep flow system enabled the achievement of higher yields with lower catalyst contact times because separating each reaction into its own reactor allowed greater freedom to tailor the operating conditions for each reaction. The multistep system also allowed the catalysts to be studied in a process wide environment, leading to the identification of significant catalyst inhibition due to by and co-products from upstream reactions.

An automated closed loop microreactor platform was developed which utilised Model-Based Design of Experiments (MBDoE) algorithms for rapid kinetic modelling of catalytic reactions. The automated platform was first applied to the homogenous esterification of benzoic acid with ethanol using a sulfuric acid catalyst, where a campaign of steady-state experiments designed by online MBDoE led to the estimation of kinetic parameters with much higher precision than a factorial campaign of experiments. This reaction was then conducted with MBDoE designed transient experiments, which dramatically reduced the experimental time required. The same reaction was studied using a heterogeneous Amberlyst-15 catalyst, and by combining factorial designs, practical identifiability tests and MBDoE for model discrimination and parameter precision, a practical kinetic model was identified in just 3 days. The automated platform was applied to the oxidation of 5-hydroxymethylfurfural in a micropacked bed reactor with gas-liquid flow using AuPd/TiO_2 catalysts, however due to poor experimental reproducibility, a kinetic model was not identified.

Acknowledgments

To begin, I would like to convey my gratitude to my supervisor, Prof Asterios Gavriilidis, for his mentorship and support throughout my PhD. Prof Gavriilidis provided me not only with a wealth of technical knowledge and expertise, but additionally, he greatly assisted my academic and professional development by encouraging me to attend numerous conferences and to participate in a wide variety of interdisciplinary projects. I am very grateful to have been one of his students.

I would also like to thank Dr Federico Galvanin for introducing me to Model-Based Design of Experiments, and to Dr Enhong Cao who helped me develop my lab skills and my understanding of microreactors. I was very lucky to benefit from both of their complementing skill sets. Additionally, I would like to thank all of the other group members of Prof Gavriilidis' group, from who I obtained excellent advice and support throughout my PhD.

I want to acknowledge all of the assistance I obtained from the department technicians, and in particular Dr Simon Barrass, who always had time to help a PhD student. I also offer my appreciation to my collaborators in Prof Hutching's research group in Cardiff who provided me with the catalyst samples I needed for my research.

I would like to thank all of my friends in London, who have helped make my PhD an amazing experience. I have enjoyed every day living in London with you all and I have some memories I will never forget. In particular, I want to thank my house mates Niamh and Marco for their friendship, which has been such an important part of my life here.

Finally, I would like to dedicate this thesis to my parents, John and Saundra, who have been a constant source of support, love and inspiration throughout my life. Thank you for everything you have ever done for me.

Table of Contents

Contents

List of Figures

List of Tables

Nomenclature

Latin Variables

a	Specific surface area (m^{-1})
a_{cat}	Catalyst activity (-)
A	Area (m^2)
Bo	Bond Number (-)
C	Concentration (mol/L)
Ca	Capillary Number (-)
Cp	Heat capacity (J kg^{-1} K^{-1})
D_{ax}	Axial dispersion coefficient (m/s^2)
D_m	Molecular diffusion coefficient (m/s^2)
d_t	Tube diameter (m)
E	Residence Time Distribution (-)
Ea	Activation Energy (J/mol)
f	Stoichiometric coefficient of feed (-)
g	Gravitational constant (m/s^2)
h	Heat transfer coefficient (W m^{-2} K^{-1})
J	Trans membrane flux (m^3/s)
k	Rate constant (varies with reaction)
k_0	Pre-exponential factor (varies with reaction)
k_{GL}	Gas liquid mass transfer coefficient (m^2/s)
K_i	Adsorption parameter (L/mol)
k_{LS}	Liquid solid mass transfer coefficient (m^2/s)
$KP1, KP2$	Reparameterised kinetic parameters (-), (J/mol)
L	Length (m)
MW	Molecular weight (g/mol)
N	Number (-)
N_L	Vessel dispersion number (-)
Nu	Nusselt Number
p	Stoichiometric coefficient of product (-)
P	Pressure (Pa)
Pe	Pecklet Number (-)
Pr	Prandtl Number (-)
Q	Rate of heat transfer (W)
r_{ij}	Correlation between the i^{th} and j^{th} parameters(-)
r	Rate of reaction (mol L^{-1} s^{-1} or mol g^{-1} s^{-1})
Re	Reynolds Number (-)
R	Universal gas constant (J mol^{-1} K^{-1})
S_i	Selectivity of species i (-)
$t\text{-}value$	t-value (-)
t	Time (s)
T	Temperature (K)
U	Overall heat transfer coefficient (W m^{-2} K^{-1})
u	Velocity (m/s)
V	Reactor volume (m^3)

W	Catalyst mass (g)
We	Weber Number (-)
X	Conversion (-)
Y	Yield (-)

Greek Variables

α	Ramp rate (-)
δ	Membrane thickness (m)
K	Membrane permeability (m^2 Pa^{-1} s^{-1})
λ	Thermal conductivity (W m^{-1} K^{-1})
μ	Dynamic viscosity (kg m^{-1} s^{-1})
v	Flowrate (L/s)
ρ	Density (kg/m^3)
σ_{ij}	Standard deviation of measurement error ij (-)
σ	Surface tension (N/m)
τ	Residence time (s)
Φ	Objective function for parameter estimation (-)
Φ_{rxr}	Reactor voidage or porosity (-)
Φ_p	Catalyst pellet porosity (-)
χ^2	Chi square (-)
ψ	Objective function for model discrimination (-)

Latin Vectors & Matrices

$\mathbf{H}$	Hessian Matrix (-)
$\mathbf{M}$	Measurement Noise (-)
$\mathbf{Q}$	Sensitivity matrix (-)
$\mathbf{S}$	Total variance due to uncertainty and measurement noise (-)
$\mathbf{u}$	Inputs (-)
$\mathbf{V}$	Covariance matrix (-)
$\mathbf{x}$	State variables (-)
$\mathbf{y}$	System responses (-)
$\hat{\boldsymbol{y}}$	Model predicted system responses (-)

Greek Vectors & Matrices

$\boldsymbol{\theta}$	Parameter (-)
$\hat{\boldsymbol{\theta}}$	Maximum Likelihood Estimates (-)
$\boldsymbol{\varphi}$	Design vector (-)

Impact Statement

Catalysts are of great value to a wide variety of chemical industries with some reports estimating that catalysts are involved in the production of over 75% of all chemical products [1]. In financial terms the UK chemical industry was reported in 2013 to have a gross value added contribution to the UK economy of £195 billion per year, and it is projected to increase that contribution to £300 billion by 2030 [2]. In addition to having large commercial importance, catalysts are also seen as a key future technology for reducing humanity's environmental impact. It is hoped that new developments in catalysis will lead to major improvements in the bio-fuels and bio-feedstocks industries, and that improved heterogeneous catalysis will help make existing processes in the chemical industries greener by reducing the use of solvents, allowing reactions to occur at milder temperatures and by reducing greenhouse gas emissions [3, 4].

The work presented in this thesis shows ways to improve current catalyst testing methods through the application of flow microreactors, and hence due to the previously outlined importance of catalysis, positive economic and environmental impact can be expected due to incremental improvements in catalyst testing methods.

One area of this work was the use of microreactors in multistep flow systems to allow researchers to study how a catalyst will operate in the wider context of the process or plant design. Such a study provides scientists and engineers with a unique opportunity to identify problems due to up and downstream interactions before investing in a pilot scale plant. The publications and presentations made throughout this work helped to demonstrate this opportunity to the community as well as highlighting many of the challenges that are encountered when designing multistep flow systems.

In this work an autonomous reactor platform was created which was capable of rapidly identifying kinetic models for catalytic reactions. This would be of huge benefit to any catalysis lab as it allows lab resources to be used more efficiently while freeing up researcher time for more intellectually demanding tasks. Through the papers published in this work, the catalysis community now have more detailed instructions on how to automate reactors and analysis equipment, allowing the community to build similar platforms. Additionally, this work also helped to expose the catalysis community to Model-Based Design of Experiments, which is a technique that should be widely adopted for both steady-state and transient experiments, in order to minimise the number of experiments required to achieve a task, and hence to maximise lab productivity. Therefore, this work is expected to have a positive impact on the catalysis community's research productivity.

1 Introduction

1.1 Motivation & Objectives

Catalysts are of vital importance in a wide range of chemical industries, from petrochemicals, agrochemicals, bulk chemical production, pharmaceuticals to emission control, as shown by the estimate that 75% of all chemical products require a catalyst at some point in their production [1]. It is also clear that in order for the chemical industries to meet the ever increasing demands to reduce the cost and environmental impact of their production, that new and improved catalysts will need to be developed, studied and optimised. However, the design and testing of new catalysts is a very challenging problem due to the large number of complicated phenomena that occur during catalysis. For heterogeneous catalysis, which is of greatest industrial interest (80% of industrial catalytic processes are heterogeneous [1]), the important phenomena include surface reaction on the active site, internal heat and mass transfer in the catalyst particle, external heat and mass transfer surrounding the catalyst particle and also possible non-ideal reactor design effects and catalyst deactivation. Therefore, it is clear that studying and designing new catalysts, particularly heterogeneous catalysts, is a non-trivial problem. The development of new, improved catalysts is a process that requires the combination of knowledge and expertise from three areas of the catalytic community; multiscale modelling, catalyst synthesis and catalyst testing, as shown in Figure 1-1. However, the focus of this thesis is entirely on the application of microreactors for improving the current methods available for catalyst testing.

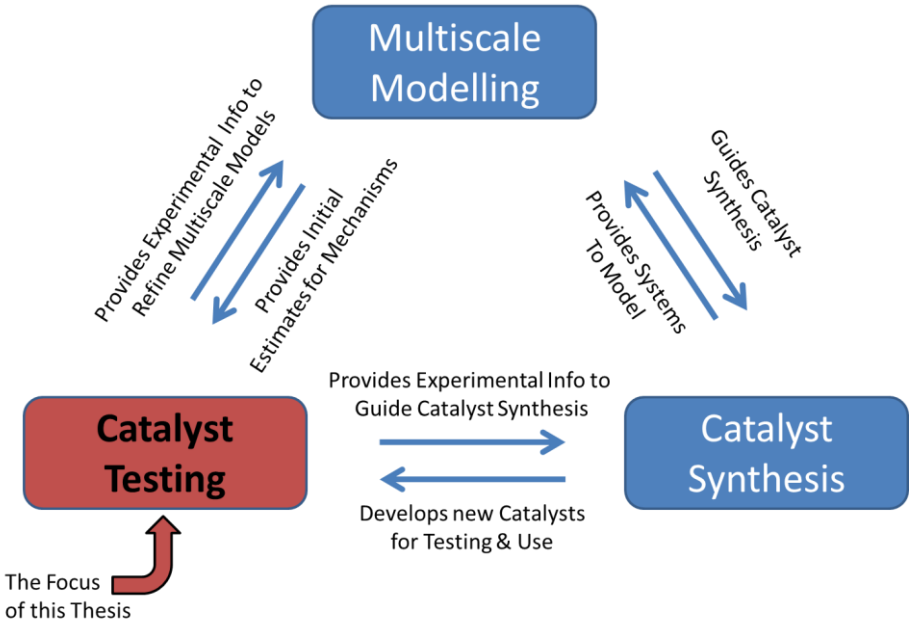

Figure 1-1 Holistic approach to catalyst design.

Catalyst testing is a very broad area and it can refer to many things including,

1. Activity studies to identify if a catalyst is active or selective for a particular reaction.
2. In-situ or Operando spectroscopic studies that may help determine the active site or reaction mechanism.
3. Kinetic studies which help determine the reaction mechanism as well as providing a model to assist in reactor design.
4. Deactivation studies to investigate if the catalyst is stable and hence industrially useful.
5. Reactor studies to investigate how the catalyst would behave in industrially relevant conditions, these are often conducted using catalyst pellets which may introduce heat and mass transfer resistances.
6. Studying how a catalyst would integrate in the wider chemical plant by considering up and downstream implications.

The fundamental motivation behind this thesis is the belief that the way in which lab based catalytic studies are currently being conducted can be significantly improved through the application of flow microreactors. This is because of a number of advantages offered by flow microreactors including,

1. Enhanced heat and mass transfer due to the increase in the surface area to volume ratio of the reactors [5-7].
2. Increased safety and access to higher temperatures and pressures [8-10].
3. Reduction in materials required [11].
4. Ease of automation and integration with online analysis [12-19].

While flow microreactors could be applied to many if not all of the previously outlined areas of catalyst testing, this work focuses just on two major areas in which lab based catalysis research can be enhanced. The first area is studying how a catalyst would integrate in the wider chemical plant by developing a multistep flow system to provide a lab scale representation of the chemical plant. The second area of this thesis is applying automated flow reactors with intelligent design of experiments to rapid kinetic studies.

1.1.1 Multistep Flow Systems for Studying Catalysts in a Wider Process Environment

Currently most catalyst studies are conducted by running a single reaction in isolation, commonly with the use of pure reagents and fresh powdered catalyst. Conducting experiments in such a controlled way is necessary due to the complexity of catalysis.

However, these studies often vary considerably from how the catalysts are actually used in industry in terms of the reactor configuration, the catalyst pellet size and the presence of impurities in the feed from upstream processes. Therefore, after identifying promising catalysts and developing some initial understanding of the catalysts from these controlled studies, further experiments should be conducted in more industrially relevant conditions. Multistep flow reactor systems, consisting of multiple reaction and separating steps, present a great opportunity to study the catalysts in a process environment rather than as a single unit operation environment [16, 19, 20]. This allows the study of the catalyst under more realistic conditions and enables the observation of any up and downstream interactions a catalyst has in a process, such as catalyst inhibition from an upstream reactor side product. Overall this enables the identification of the optimum system wide configuration for a process and it helps identify problems in current catalyst performance, and highlights areas for improvement in future catalyst design.

Only in recent years with improvements in microreactor technology including improved separation unit operations [21, 22] and reconfigurable plug and play reactors [16, 19] has it been possible to study catalysts in this multistep context in a safe and cost effective way in a single fume cupboard. Therefore, in this thesis a multistep flow system is presented for the synthesis of benzylacetone from benzyl alcohol with AuPd, Pt and Pd/TiO_2 catalysts in micropacked bed reactors. These catalysts were previously found to be suitable for this reaction in a batch cascade [23], and hence direct comparisons can be made to see how the reactor configuration (flow vs batch) affects catalyst performance. The combined aims were to try and optimise the system for benzylacetone production and also to study the catalyst to identify areas required for future improvement. In a more general way, this work also demonstrates some of the challenges and advantages of creating lab scale multi-step flow processes compared to using batch cascades.

1.1.2 Automated Microreactors for the Intensification of Catalytic Kinetic Studies

A kinetic model consists of a set of equations and parameter values that can be used to predict a reaction's behaviour. Reliable and robust kinetic models are of great value to chemical engineers and chemists as they can be used to assist in reactor design, optimisation, process control, improving plant safety and they can offer mechanistic insight into a reaction mechanism [24]. However, developing kinetic models is often a challenging, costly and time intensive process which involves identifying the most appropriate set of kinetic model equations from a large number of candidate models, and then precisely estimating the model parameters (pre-exponential factors, activation energies and adsorption terms). Both of these tasks require a significant amount of

resources to be spent to run kinetic experiments and collect experimental data [25], making kinetic studies one of the areas of catalyst testing which is the most tedious, requiring the repetition of a large number of similar experiments.

Currently most catalytic kinetic studies are conducted in batch reactors for three major reasons. First of all, because most chemists are trained with batch reactors, are familiar with them, find them easy to operate and because the same batch reactor can be used for a wide range of reactions, including single phase, multiphase or catalytic reactions, whereas often different flow reactors are required for different reactions. Secondly, powdered catalysts can be easily used in batch reactors which can help eliminate internal mass transfer resistances and allow access to intrinsic kinetics. Thirdly, because a single batch experiment is capable of generating a large amount of data through the use of automated sampling and online analysis techniques [24, 26, 27]. However, due to the advances in flow microreactors in the past 20 years, many kinetic studies could now be carried out more quickly and effectively in flow instead of in batch. This is because microreactors provide increased rates of heat and mass transfer which may be necessary for conducting isothermal intrinsic kinetic studies for very fast and exothermic reactions [28, 29]. They also allow safe access to a wide range of operating temperatures and pressures [11, 30, 31]. Most importantly, it is possible to automate a flow microreactor and combine it with a variety of online analysis techniques [12, 15, 17, 18, 32], hence kinetic experiments can be conducted without researcher supervision leading to significant time savings. Most often automated flow reactors conduct a series of steady-state experiments, however to speed up the rate of information collection, they can also be operated in transient mode, eliminating the need to wait for the reactor to reach steady-state for each new condition [12, 33-37]. In comparison, the automation of sequential experiments in a batch reactor remains challenging due to the requirement of emptying and cleaning the vessel between uses. Hence, kinetic studies in batch reactors remain labour intensive endeavours.

Even further time and resource savings can be made through the use of closed loop systems which combine an automated flow reactor with online analysis with a design of experiments algorithm. These closed loop systems allow the use of online Model-Based Design of Experiments (MBDoE), a technique which can be used to minimise the number of experiments required to identify an appropriate kinetic model from a list of other candidate models [38], and then to precisely estimate the parameter values of the chosen model [25]. Already automated systems utilising MBDoE techniques have been applied to kinetic studies [14, 39-41] however, so far these have only been applied to homogenous systems. In this thesis, an automated system is developed that

attempts to push the boundaries of the state-of-the-art in rapid kinetic studies by applying automation and MBDoE techniques for the first time to heterogeneous catalytic systems. This will involve a number of challenges that were not encountered in the homogenous systems including external and internal heat and mass transfer resistances and the possibility of catalyst deactivation. Additionally, as the systems get more complex to include gas liquid solid reactions, automated separation steps will be required before it is possible to conduct online analysis. The automated system developed in this thesis, is first validated with the homogenous esterification of benzoic acid and ethanol with sulfuric acid, before being applied to heterogeneous systems of increasing complexity including the heterogeneous esterification of benzoic acid and ethanol with Amberlyst-15 in a string reactor, and then the heterogeneous oxidation of 5-hydroxymethylfurfural (HMF) to 2,5-furandicarboxylic acid (FDCA) in a micropacked bed reactor with gas liquid flow and Au/TiO_2 and $AuPd/TiO_2$ catalysts. The automated system is designed to be as flexible as possible, so that it can be used with multiple different types of equipment and for different reactions, so that the time savings from automation are not outweighed by the time spent automating the system. The automated system is also designed to be able to operate in steady-state or transient mode, and as the literature has shown that the design of transient experiments is particularly difficult, often requiring the tuning of ramp rates [33], MBDoE techniques will be applied to transient experiments.

1.2 Outline of Thesis

A literature review is presented in Chapter 2 which gives a review of catalytic microreactors before focusing on the two major areas of this thesis, the use of catalytic microreactors in multistep flow systems and the use of automated microreactors with online MBDoE for rapid kinetic studies.

Chapters 3 and 4 are dedicated to the multistep flow synthesis of benzylacetone from benzyl alcohol. In Chapter 3 each of the three component reactions (oxidation, coupling and reduction) are studied in isolation, and in Chapter 4 the integration of the three reactions together into a single multistep system is presented. This work has been published in The Chemical Engineering Journal, “Three step synthesis of benzylacetone and 4-(4-methoxyphenyl)butan-2-one in flow using micropacked bed reactors”, 2018, **377**, 119976,.

Chapters 5 to 8 are all dedicated to the intensification of kinetic studies for increasingly complex catalytic reactions.

In Chapter 5 an autonomous closed loop reactor platform for sequential steady-state experiments is developed and validated using the case study reaction of benzoic acid and ethanol esterification with a homogenous sulfuric acid catalyst. In this chapter a comparison is made between a campaign of 8 experiments designed by the factorial method, and a campaign of 8 experiments designed by online MBDoE for improved parameter precision. This work has been published in Reaction Chemistry & Engineering, “An autonomous microreactor platform for the rapid identification of kinetic models”, 2019, **4**, 1623-1636. In Chapter 6 the same case study reaction is explored using single variable and multi variable ramped transient experiments which are also designed by MBDoE for improved parameter precision. This work has been accepted for publication in Reaction Chemistry & Engineering as an article titled “Model-Based Design of Transient Flow Experiments for the Identification of Kinetic Parameters”.

In Chapter 7 the solid-liquid esterification of benzoic acid and ethanol with the heterogeneous catalyst Amberlyst-15 is investigated using a string reactor. This work includes characterising the string reactor’s hydrodynamic and mass transfer behaviour before beginning kinetic experiments using the automated closed loop system for sequential steady-state experiments. In order to rapidly identify kinetic models with the minimum number of experiments, a five step methodology is developed which includes factorial experiments, offline practical model identifiability analysis and then online MBDoE for model discrimination and improved parameter precision. This was work has been accepted for publication in Industrial & Engineering Chemistry Research under the title “Closed Loop Model-Based Design of Experiments for Kinetic Model

Discrimination and Parameter Estimation: Benzoic Acid Esterification on Heterogeneous Catalyst"

In Chapter 8 the autonomous reactor platform is then applied to develop a kinetic model for the gas-liquid-solid oxidation of HMF using Au and AuPd/TiO_2 catalysts. This is also conducted using only steady-state experiments. First the automated reactor is used to screen five catalysts to identify the most active and stable catalyst. Then the chosen catalyst is used to conduct a campaign of factorial experiments where the catalyst activity is continuously monitored during the campaign by conducting a reference condition experiment at regular intervals. The entire factorial campaign was conducted using 6 different reactors (containing different masses of the same catalyst) but unfortunately large variations in catalyst activity from reactor to reactor were observed. This was attributed to a combination of non-reproducible catalyst and non-reproducible flow patterns in the micropacked bed. Due to the differences in activity between reactors, an adapted method of parameter estimation was needed in order to develop a model that fitted the collected data and online MBDoE was not applied to this system.

In the final chapter, Chapter 9, concluding remarks are presented as well as highlighting future areas for continuing this work. A graphical representation of the thesis structure is shown in Figure 1-2.

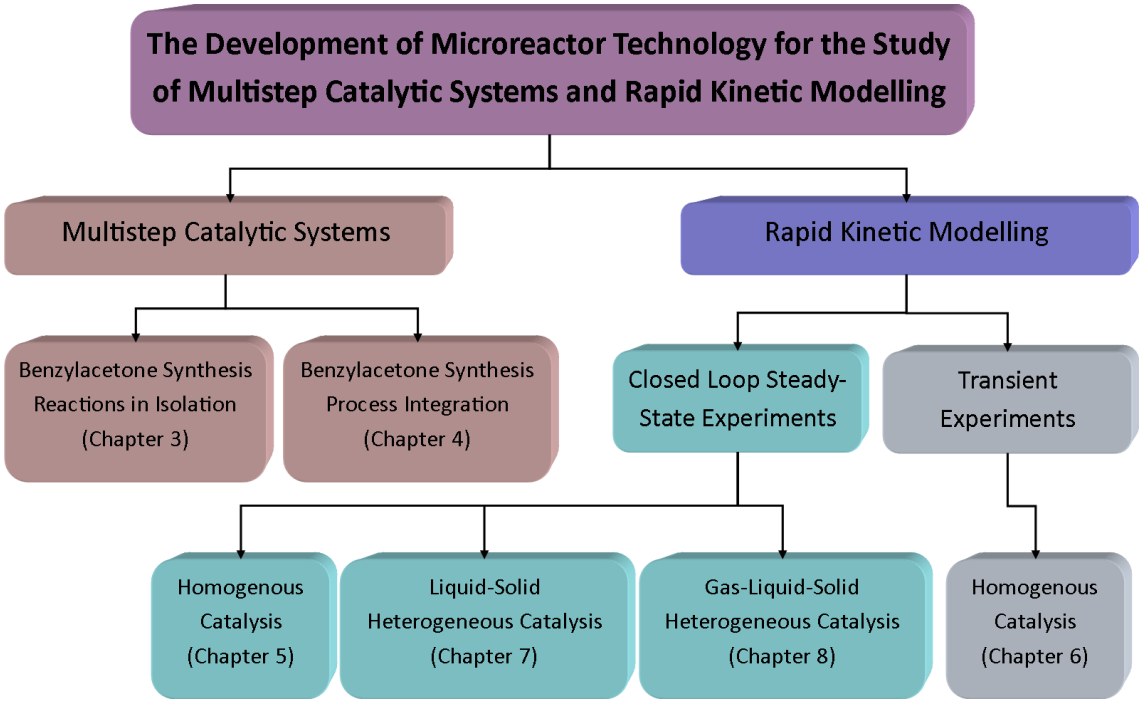

Figure 1-2 Thesis Outline

2 Literature Review

Catalytic studies are being increasingly conducted in microreactors due to their many benefits, including increased rates of heat and mass transfer, improved control over reaction conditions, access to a wider range of operating conditions and ease of automation and compatibility with many forms of online analysis. In this chapter, a brief description of catalytic microreactors is provided, before providing a detailed review of the two areas of this thesis, multistep catalytic flow systems and the application of closed loop microreactor platforms to catalytic kinetic studies.

2.1 Review of Microreactor Technology

2.1.1 Review of Catalytic Microreactors

Microreactors are reactors with a length scale in the sub millimetre range, with very large surface area to volume ratios which create a number of advantages that have led to them becoming an area of intense research interest over the past 20 years. Typical catalytic microreactors, some of which are shown in Figure 2-1, include micropacked bed reactors [5, 13, 29, 42-45], string reactors [46-49], wall coated reactors [28, 32, 50-55] or slurry reactors which can resemble continuous stirred tank reactors [56, 57], or plug flow reactors [58-61].

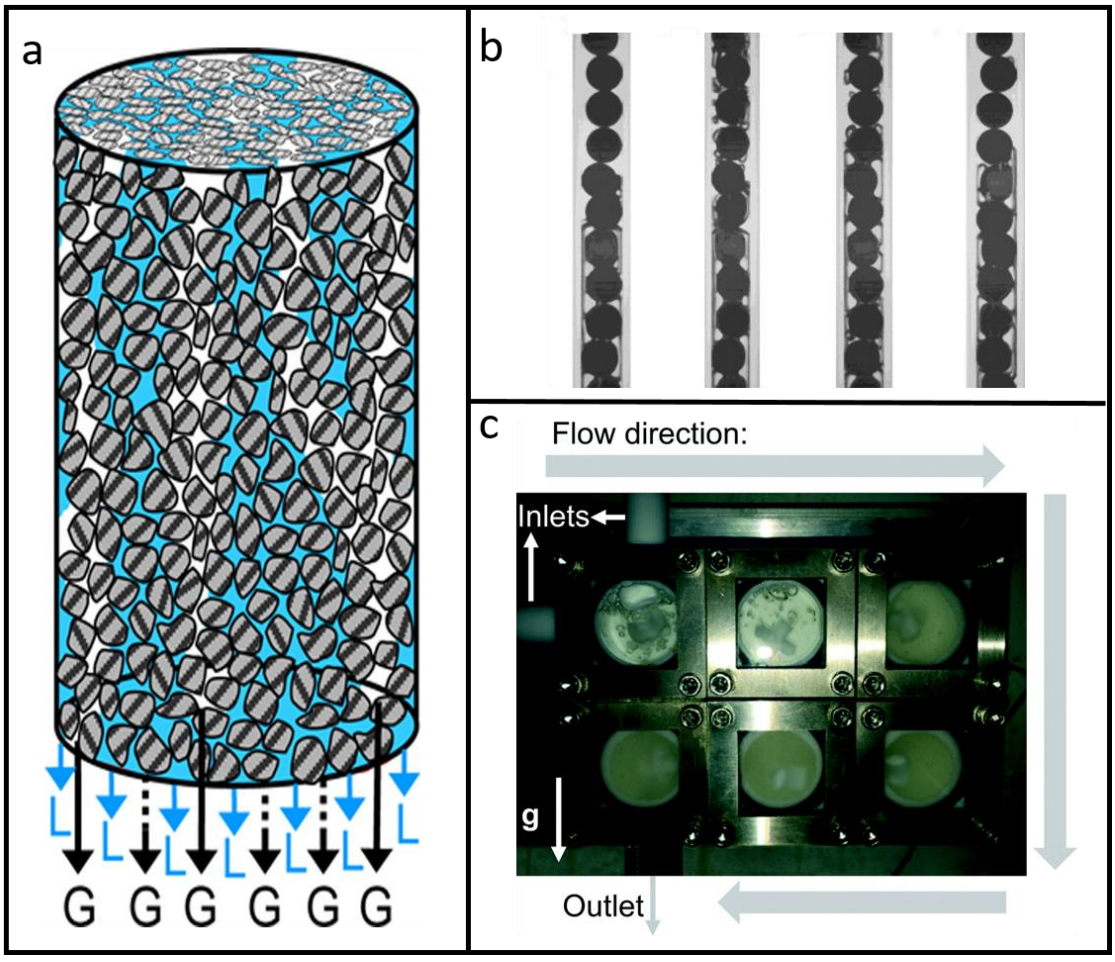

Figure 2-1 a) Representation of the flow in a micropacked bed reactor. Reprinted from Alsolami, B.H., et al., Catalyst Performance Testing in Multiphase Systems: Implications of Using Small Catalyst Particles in Hydrodesulfurization. Industrial & Engineering Chemistry Research, 2013. 52(26): p. 9069-9085. [42] [42] [42] [42] [42] [42] [42] with permission from American Chemical Society. b) Observed flow regimes in a string reactor. Reprinted from Bauer, T. and S. Haase, Comparison of structured trickle-bed and monolithic reactors in Pd-catalyzed hydrogenation of alpha-methylstyrene. Chemical engineering journal, 2011. 169(1-3): p. 263-269, with permission from Elsevier. c) Cascade of miniature solid containing CSTRs. Reprinted from Mo, Y. and K.F. Jensen, A Miniature CSTR Cascade for Continuous Flow of Reactions Containing Solids. Reaction Chemistry & Engineering, 2016. 1(5): p. 501-

507. [57] [57] [57] [57] [57] [57] [57], with permission from the Royal Society of Chemistry.

The flow behaviour and hence reaction performance of microreactors differs greatly from their conventionally sized equivalent reactors. This is due to their much larger surface area to volume ratio and because at the microscale surface tension and viscous forces dominant, while gravitational and inertial forces are comparatively unimportant [43, 62]. The relative significance of the various forces in micro and macro sized reactors can be most easily compared by examining several dimensionless numbers. For one of the most common catalytic microreactors, the micropacked bed reactor with gas liquid flow, this is demonstrated by examining the Bond number, *Bo*, Capillary number, *Ca*, and Weber number, *We*, which can be calculated using Equations (2-1), (2-2) and (2-3) where ρ_L and ρ_g are the densities (kg/m^3) of the liquid and gas, g is the gravitational constant (m/s^2), L is the diameter of the catalyst particles (m), σ is the surface tension (N/m), u the fluid superficial velocity (m/s) and μ the fluid viscosity (kg m^{-1}s^{-1}).

$$Bo = \frac{(\rho_L - \rho_g) g L^2}{\sigma} = \frac{gravitational\ force}{surface\ tension\ force} \quad (2\text{-}1)$$

$$Ca = \frac{u\mu}{\sigma} = \frac{viscous\ force}{surface\ tension\ force} \quad (2\text{-}2)$$

$$We = \frac{\rho u^2 L}{\sigma} = \frac{Inertial\ forces}{surface\ tension\ force} \quad (2\text{-}3)$$

The governing forces in a micropacked bed with gas liquid flow vary drastically from industrial trickle bed reactors as the Bond, Capillary and Weber numbers at the micro scale are typically in the range of 10^{-3}, 10^{-6} and 10^{-6}, whereas in industrial trickle bed reactors, these values are orders of magnitude larger, in the range of 1, 10^{-4} and 10^{-4} [43, 62]. These changes then result in a large difference in flow behaviour and reactor performance; including much larger liquid hold up [63], independence of bed orientation and flow history (pre wetting before start up) [62], different flow regimes [43, 64], different pressure drop correlations [65], and increased rates of mass transport [5, 6]. Due to these large differences between micropacked bed reactors and industrial trickle bed reactors, significant effort has been spent in the last decades studying the flow behaviour and mass transfer in micropacked bed reactors to try and develop new generalised correlations (for mass transfer coefficients, for pressure drop, for flow regime transition points etc.) that can be applied to micropacked beds. There have now been a large number of hydrodynamic studies [42, 43, 62-69] so that the flow in micropacked beds is reasonably well understood. It is known that the deviation from

plug flow is small, but that the gas and liquid flows may be quite segregated, as shown in Figure 2-1 a, with the liquid gathering in large regions leading to significant radial heat and mass transfer resistances. However, there have been far fewer mass transfer studies [62, 65], with most mass transfer studies simply reporting an overall mass transfer coefficient at a single or small set of operating conditions [5, 70]. Hence there is considerable need for further characterisation of mass transfer in micropacked bed reactors.

2.1.2 Advantages & Disadvantages of Microreactors

Due to their small size, some immediate benefits of microreactors include the requirement of smaller volumes of reagents and catalyst material, as well as minimising the health and safety risks of experiments due to the smaller reactor holdup and due to the small channels which help supress explosive propagation and extends the process window of safe operation for a reaction [71]. Many microreactor designs also allow the use of very high pressures and temperatures, with conditions of 450 ^{o}C and 950 bar [31] being reported in the literature for a steel capillary microreactor and up to 80 ^{o}C and 140 bar for a silicon-glass microreactor that still allowed optical access [8, 9]. Many microreactors are also compatible with a variety of different forms of online analysis techniques including IR [12, 18, 33, 72-76], UV-vis [39], Raman [13, 77] and X-Ray spectroscopy [18, 78] as well as online HPLC [14, 16, 34, 79-81], GC [32, 39, 82] and MS [15-17, 83, 84]. For catalytic studies this is particularly useful as it enables in situ or Operando studies where the catalyst surface and active sites are studied under realistic process conditions [85, 86]. These Operando studies can provide crucial mechanistic information to help understand how a catalyst works and how it can be improved. Flow microreactors are also quite easy to automate [87, 88], which provides many opportunities for high throughput continuous and discrete variable screening for reaction discovery and optimisation [15, 89, 90], for reaction monitoring [17, 82, 91] and for closed loop reactor control [14, 16, 32, 39, 73, 74, 84, 92-101]. Such techniques could lead to potentially huge time and cost savings, and they are paving the way for artificial intelligence and machine learning to play a greater role in lab based research [102-104]. However, the greatest advantage of microreactors derives from their large surface area to volume ratio which provides rates of heat and mass transport orders of magnitude greater than in conventional sized reactors [5] or in batch reactors [60]. This rapid heat transfer can be used to eliminate hot spots and can allow isothermal control of many highly exothermic reactions [28, 29]. The high rate of mass transport can be used to intensify mass transfer limited reactions [105], as well as eliminating mass transfer resistances for kinetic studies where it is important to access the kinetic regime [29]. Microreactors also allow the rapid change of and precise control of reaction

conditions [11], which combined with their fast mixing times and low residence times can be used to process highly unstable intermediates in what is called flash chemistry [106]. A more detailed discussion on the advantages of microreactors can be found in numerous review articles [11, 107-111].

Microreactors also have a number of drawbacks associated with them, most notably their difficulty in solids handling [112]. For reactions which produce solids, or where it would be desirable to use a catalyst in powder slurry form, clogging of the small channels is a common and serious problem. While many proposed solutions exist including periodic flushing of the reactor, the use of droplets in carrier fluids [113], ultra-sonication [59, 114] or a cascade of micro CSTRs [57] none of these strategies are ideal. Another disadvantage is the difficulty in scaling up a microreactor to meet the requirements of commercial production. This is challenging because as a microreactor is scaled up it begins to lose its rapid heat and mass transport rates. Additionally, even the strategy of numbering up is limited, as even with carefully designed flow manifolds it is difficult to ensure equal flow distribution between units [115]. Therefore, the use of microreactors for commercial production is generally limited to small volume high value products such as some APIs in the pharmaceutical industry [20, 116, 117], or else for materials with a very low shelf life where production at the point of use is required.

2.1.3 Applications of Microreactors

Since the reporting of their many early successes where microreactors far out perform conventional reactors, microreactors are now becoming a maturing technology with many industrial companies (Chemtirx, Corning, Dolomite, Ehrfeld, Little Things Factory) manufacturing their own microreactors for academic and industrial use. The applications of microreactors can be broadly divided into two separate areas, production and research.

Microreactors Applied to Production

Microreactors are currently being used for production in a number of industries which specialise in high value low volume products such as pharmaceuticals [15, 20, 112, 118] and nanomaterials synthesis [107]. In these industries the high rates of heat and mass transport, improved safety and tight control over reaction conditions provided by microreactors is used to achieve significant process intensification. In particular the pharmaceutical industry is expected to adopt microreactor technology as studies have highlighted that many typical pharmaceutical reactions would benefit from flow [112]. Furthermore, the U.S. Food and Drug Administration (FDA) is now encouraging pharmaceutical companies to produce products in flow instead of in batch [119-121], and several drugs including Orkambi, Prezista and Symdeko are already being

produced industrially in continuous flow reactors. Many micro or milli reactor systems have already been developed that can produce pharmaceutical products in flow, such as the system shown in Figure 2-2 [20]. In particular it is expected that microreactors may be used to produce the small quantities of Active Pharmaceutical Ingredients (API) required for clinical trials. The use of microreactors in the pharmaceutical industry is also expected to involve many catalytic reactors, such as the micropacked bed reactor, as estimates report that almost 20% of pharmaceutical reaction steps are catalytic hydrogenation reactions [122]. These catalytic hydrogenation reactions are ideal candidates for micropacked bed reactors because this reaction type is typically fast, highly exothermic and are often dangerous requiring flammable solvents. Therefore, these reactions have the most to gain from the advantages offered by microreactors [107, 123]. In other industries such as the fine chemicals industry there is expected to be some uptake in the use of catalytic microreactors for production, where they will most likely be used for fast, exothermic or dangerous reactions such as oxidation reactions [43, 124].

Figure 2-2 Millifluidic system for the synthesis of 4 different APIs, reprinted from Adamo, A., et al., On-Demand Continuous-Flow Production of Pharmaceuticals in a Compact, Reconfigurable System. Science, 2016. 352(6281): p. 61-67, with permission from AAAS.

Microreactors Applied to Research and Development

Rather than being used in production, microreactors can also be used as information gathering tools to intensify lab based research for the discovery of novel synthesis routes, for improved mechanistic understanding and for process development and optimisation.

Microreactors facilitate the discovery of novel synthesis routes in many ways. Primarily, they allow a chemist access to a wider range of chemistries than what can safely be accessed in batch and hence they enable the discovery of new reaction pathways. The increased window for safe chemistry is accomplished through the high temperatures and pressures achieved in microreactors [31], their fast mixing rates which allows the generation and then immediate use of highly unstable species [106] and also their ability to completely contain hazardous reagents such as ozone, hydrazoic acid, hydrogen cyanide and diazomethane by generating them in flow for immediate use [125, 126]. Together these opportunities have allowed organic chemists to develop many new reaction pathways, such as the Swern Moffat oxidation which previously needed to be conducted at -30 ^{o}C to avoid the degradation of an unstable intermediate, but now can be conducted at room temperature [106]. In another example, microreactors enabled the safe use of diazomethane, (which cannot normally be used due to safety considerations despite it being one of the most useful C1 building blocks in organic chemistry) for the synthesis of 8 different products [127]. A second way in which microreactors facilitate the discovery of new reaction pathways is the application of automated flow reactors for high throughput screening. Many automated microreactor platforms, such as the one shown in Figure 2-3, have been developed for continuous (temperature, pressure, concentration) and discrete (solvent, catalyst, ligand) variable screening [81, 89, 90], with one system reporting to screen Suzuki-Miyaura coupling reactions at a rate of >1500 per day, which is considered superior to high throughput batch systems [15]. Other automated microreactors have been used to identify reactions of highly functionalised molecules (bicyclo[3.2.1]octanoid scaffolds) which is considered a key step in drug discovery [89].

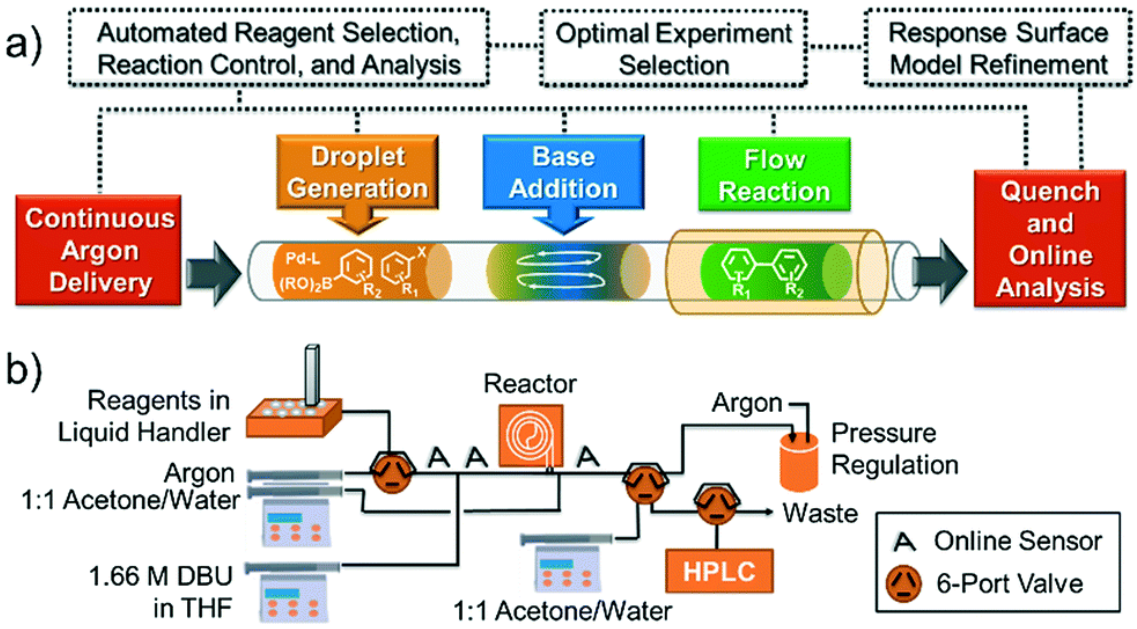

Figure 2-3 Example of an automated screening platform for discrete and continuous variables using a microreactor combined with online analysis. Reprinted from Reizman, B.J., et al., Suzuki-Miyaura cross-coupling optimization enabled by automated feedback. Reaction Chemistry & Engineering, 2016. 1(6): p. 658-666, with permission from the Royal Society of Chemistry.

Microreactors are also great research tools for enhancing our mechanistic understanding of a process. This is particularly evident in the field of catalysis where microreactors have enabled Operando catalytic studies to examine the catalyst active site during reaction [85]. A wide variety of microreactors have been developed that are compatible with X-ray diffraction and absorption spectroscopy [13, 128, 129], Raman [129], FT-IR [18] and scanning transmission electron microscopy [130].

Microreactors are used in many ways to generate information that is useful for process development and optimisation. Automated closed loop microreactors platforms can be used for self-optimisation of a reaction [32, 39, 100, 131-133], where a black box model of the reactor and optimisation algorithms are used to optimise reaction conditions to maximise criteria such as yield. While this may not provide significant understanding of the process, this information is very useful for complex processes where first principle models are not available. Microreactors can also be used to develop a lab scale multistep flow system which can be used to study an entire chemical process instead of just a single unit operation in isolation, hence allowing system wide optimisation. The development of multistep catalytic systems is the first major topic of this thesis, and a detailed literature review on batch cascades ad multistep flow reactions is provided in the following section. Finally, microreactors are excellent research tools for kinetic studies as their high rates of heat and mass transfer can be used to allow isothermal intrinsic kinetic studies [28, 29], and they can be combined with automated

microreactor platforms [134] and online MBDoE [14, 41] to significantly decrease the amount of time and labour to identify a kinetic model. The application of automated microreactors to the study of catalytic kinetics is the second major area of this thesis and therefore, a detailed literature review regarding kinetics in flow, automated reactors and MBDoE is provided in the following section.

2.2 Multistep Flow Systems

Multistep reaction systems are important as most chemical products require multiple reaction steps to be completed to convert raw materials into the final desired product. Multistep chemistry can be achieved in both batch and flow, and a review of the literature of both batch cascades and multistep flow systems are presented and compared to show the relevant advantages and disadvantages of both approaches for maximising the yield of a product and for allowing the collection of information that is useful for the design of industrial processes. In particular a review of the state of the art multistep flow systems is presented, highlighting their applications and the current challenges.

2.2.1 Review of Catalytic Multistep Systems

Using modern chemical synthesis techniques it is now possible to produce a wide variety of molecules with diverse functionalities. Most often in the lab new synthesis routes are developed using batch reactors which involve a series of reactions and intermediate work up steps, possibly with the use of protection groups. This approach can be very inefficient as it leads to low atom economy, the generation of large amounts of waste (high E factors) and requires significant labour [135]. In an effort to reduce both the environmental impact and cost of multistep synthesis in recent years there has been significant research into using selective catalysts more frequently to replace the use of stoichiometric inorganic reagents which produce significant amounts of waste [136]. Two approaches to the use of catalysts in multistep systems have been developed, the one-pot method [137] and multistep flow methods [138]. One-pot methods refer to conducting sequential reactions in a single flask without intermediate work up. Batch cascades are a sub category within one-pot methods where all of the reagents and catalysts are present in the flask from the start of the reaction, instead of sequentially adding reagents or catalysts as earlier reactions are finished. There are numerous examples of how these one-pot methods have increased atom economy for various reactions [23, 136, 137, 139-143]. However, this approach faces a major challenge in that all of the catalysts, reagents and products need to be compatible with one another and a single operating window of temperature, pressure and solvent needs to be found that suits all reactions [143]. While multifunctional catalysts (catalysts which have more than 1 type of active site) have been found for several

batch cascades, they are generally difficult to find or design, and in some cases interactions with other species in the flask can lead to catalyst deactivation [143].

In contrast using multistep flow systems or telescope systems, where multiple reactors and separators are connected in series, it is possible to physically separate the sequential reactions into different reactors, each using their own catalyst and operating temperature. While this doesn't completely remove the problems of compatibility of the catalysts in the systems, as the catalysts can still be inhibited by unreacted reagents or side products from upstream reactors, it does removes many of the constraints in the design of a multistep system. Multistep flow systems also allow the use of inline purification techniques such as liquid-liquid extraction [144, 145], distillation [146], gas liquid separation [147] and scavengers [148] and after the synthesis it is not necessary to filter out the catalyst as solid catalysts are normally used in fixed bed micropacked bed reactors [149]. Multistep flow systems offer many other advantages over batch one-pot methods, such as the increased rates of heat and mass transfer enabling rapid changes in temperatures between units, fast mixing for flash chemistry, and improved safety with the possibility of generation of dangerous intermediates immediately prior to their consumption [150]. Additionally, flow systems allow safe access to a wide range of temperatures and pressures, which may be of great interest for industrial applications.

Recently a large number of multistep flow systems have been reported in the literature in a wide range of research areas including pharmaceuticals [20, 116-118, 151-160], biofuels [149, 161, 162] and fine chemicals [16, 19, 145, 150, 163-166] industries. A common trend in nearly all of these systems is the use of milli and micropacked bed reactors and many of these systems report significant process intensification due to the benefits of flow. The current state of the art multistep flow systems are reconfigurable so that they can be used for many different products [20], and they also combine online analysis at different points across the flow system with closed loop control for system optimisation [16, 19]. The capabilities of these systems are impressive and they represent a disruptive technology which could dramatically change a number of industries. For example, a multistep flow system was developed that is only the size of a fridge that can produce hundreds to thousands of doses per day of 4 different APIs [20]. Compared to the current production method of drugs, which involves batch processing at multiple different locations leading to long production times and the potential for supply chain disruption, this multistep flow system could spark change in the industry towards manufacture at the point of use. Alternatively, multistep flow systems can be used for information generation instead of for production. One of most impressive examples of information generation using a multistep system is shown in

Figure 2-4, which involved the automated optimisation of an entire multistep synthesis for ketone generation and cycloaddition which involved three homogenous reactors [16]. This is particularly notable as the optimisation of a multistep system is a challenging problem due to the interactions between unit operations. This type of system rapidly generates process information and can be expected to considerably reduce process development time.

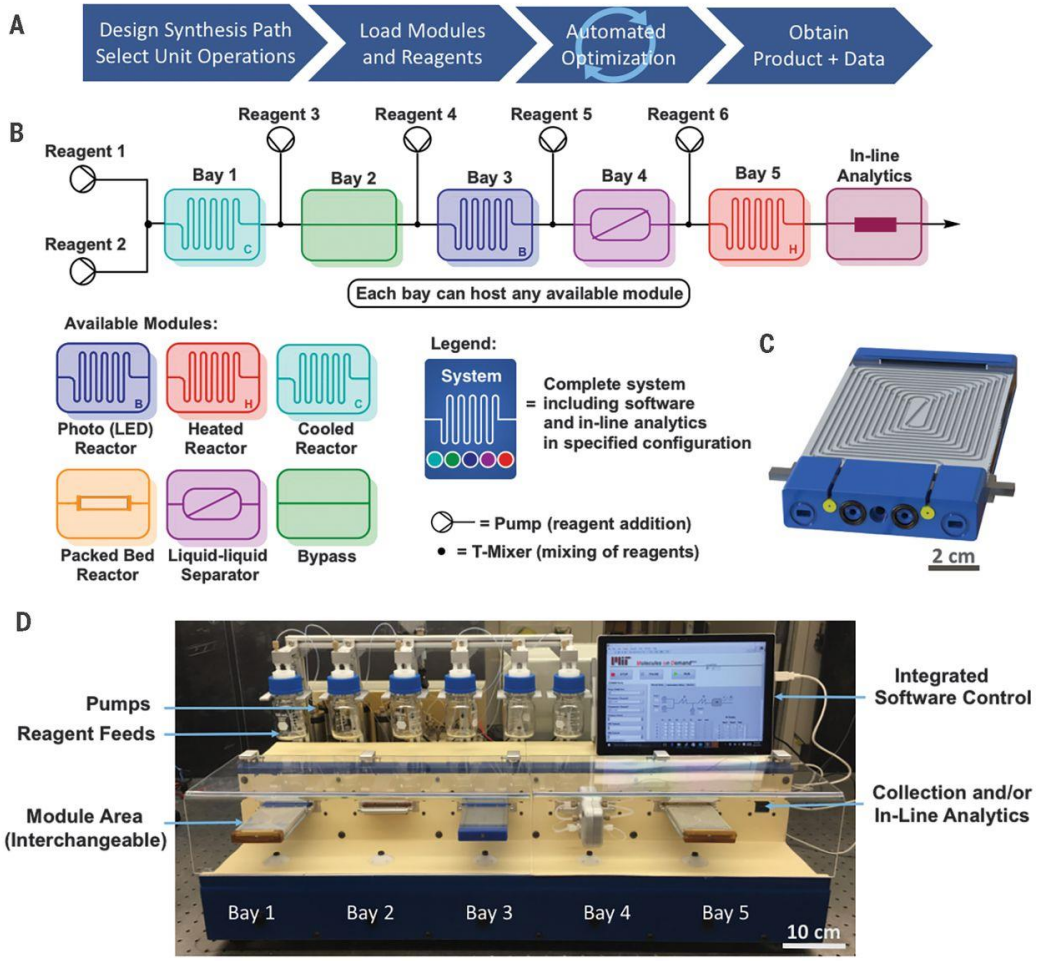

Figure 2-4 State of the art plug and play multistep flow system with online analysis used for self-optimising a multistep reaction. Reprinted from Bédard, A.-C., et al., Reconfigurable system for automated optimization of diverse chemical reactions. Science, 2018. 361(6408): p. 1220-1225, with permission from AAAS.

2.2.2 Current Challenges and Areas for Improvement in Multistep Flow Systems

A number of challenges still remain in the field of multistep flow systems that prevents their more widespread use in academia and industry. These include concerns around the suitability of multistep flow systems for reactions which use powder catalysts or which produce solids due to the high risk of clogging. While methods for solids handling have been demonstrated in isolation including the use of CSTRs [57] and sonication [59, 114], these have yet to been demonstrated in a multistep system. Another challenge for multistep flow systems revolve around pressure and flow management in

systems of increasing complexity such as those that use recycle streams or with unit operations that introduce a pressure drop that varies with flowrate (such as packed beds). It is necessary to show that these complicated flow systems can operate without instabilities or periodic oscillations in pressure and flow which may affect the performance of the other operations, many of which (liquid-liquid separation, gas-liquid separation and micro distillation) depend on precise control of pressure and flowrate.

Having reviewed the multistep catalytic flow literature, a gap in the literature was identified that this thesis could contribute to. Despite there being numerous examples of successful multistep flow systems and many papers claiming to have benefited from the process intensification offered by flow systems, the author was unable to find any direct comparisons of batch systems to flow systems to validate these claims for catalytic systems. Therefore, the first aim of this thesis is to convert a one-pot cascade system into a multistep flow system and to compare the advantages and disadvantages of flow compared to batch. This comparison will focus on which system achieves the greatest levels of process intensification, and also on which system presents the greatest opportunity for studying the catalyst. This research aim is explored using the case study of the three step synthesis of benzylacetone from benzyl alcohol, and of 4-(4-methoxyphenyl)butan-2-one from 4-methoxybenzyl alcohol via oxidation, coupling and reduction using Au, Pd and Pt supported catalysts.

2.3 Intensification of Catalytic Kinetic Studies Using Automated Flow Reactors and MBDoE

The second major research area of this thesis is the application of automated microreactor systems using online MBDoE for rapidly identifying kinetic models of heterogeneous catalytic reactions. Here a literature review is presented which describes the recent developments in kinetic studies in flow, automated reactor platforms and MBDoE.

2.3.1 Review of Catalytic Kinetic Studies Conducted in Microreactors

Microreactors have been successfully used for many catalytic kinetic studies because their high rates of heat and mass transfer allow isothermal intrinsic kinetic studies to be conducted for a large number of reactions. For gas phase catalytic reactions, many kinetic studies have been conducted where the catalyst is coated as a thin film on the walls of single channel or multichannel microreactors, including ethylene oxide formation [28] and methanol oxidation [53] over silver catalyst films, the oxidation of SO_2 on Pt/TiO_2 [55] and ethanol reforming using Rh/CeO_2 [54]. Another common reactor configuration is the packed bed reactor, which has been used to study the kinetics of the direct epoxidation of propene over a Au/TiO_2 catalyst [167]. There are

also numerous examples of micropacked bed reactors being used for kinetic studies for gas-liquid-solid reaction systems including the oxidation of benzyl alcohol over AuPd/TiO_2 [168], hydrogenation of aromatic nitro ketone on Pd/Al_2O_3 [29], hydrodeoxygenation of 4-propylguaiacol with NiMo/Al_2O_3 [45] and the direct H_2O_2 formation from O_2 and H_2 on Pd/SiO_2 [169]. Additionally, some gas-liquid-solid kinetic studies have also been conducted where gas liquid slugs flow through a catalyst coated capillary, such as the hydrogenation of citral on Au/TiO_2 films [170]. In many cases the use of microreactors was critical to the success of the previously mentioned studies, as for many highly exothermic and fast reactions it would not be possible to collect isothermal intrinsic kinetic data from a batch reactor [29].

2.3.2 Review of Automated Flow Reactor Systems Applied to Kinetic Studies

In recent years automated flow reactors have become increasingly common, and many flow reactors have already been combined with many forms of online analysis including GC [32, 39, 82, 91, 94], HPLC [14, 16, 17, 34, 79, 81, 92, 131, 171], MS [15-17, 83, 84], UV-vis [39], IR [12, 18, 33, 72-74], Raman [13, 77], X-ray absorption spectroscopy [18] and NMR [93]. Automated reactor platforms are a key technology for intensifying lab work as they allow experiments to be conducted without researcher supervision, potentially allowing experiments to be run 24 hours a day. Today automated flow reactors have already been successfully applied to unattended reaction monitoring [17, 82, 91] and high throughput continuous and discrete variable screening for reaction discovery and optimisation [15, 81, 89, 90], where they have dramatically reduced the amount of tedious manual labour that is typically required of highly trained scientists. The system complexity of automated reactor platforms is also steadily increasing, and now there are already several examples of gas-liquid-solid reactions [32, 172] and other multiphase reactors using separation at the reactor exit before analysis one of the phases. For example, the automated study of gas-liquid mass transfer in a micropacked bed reactor involved the separation of the gas and liquid by membrane separation before analysing the liquid via UV-vis spectrometry [6], and a study of a gas-liquid-solid hydrogenation reaction in a wall coated tube reactor used online GC analysis of the liquid product, as shown in Figure 2-5 [32]. However, to the best of the author's knowledge, these automated flow reactors have not yet been applied to studying the kinetics of heterogeneous catalytic systems. Instead automated flow reactors have only been applied to study the kinetics of relatively simple systems such as liquid phase homogenous reactions [14, 34, 80] and gas-liquid reactions [134].

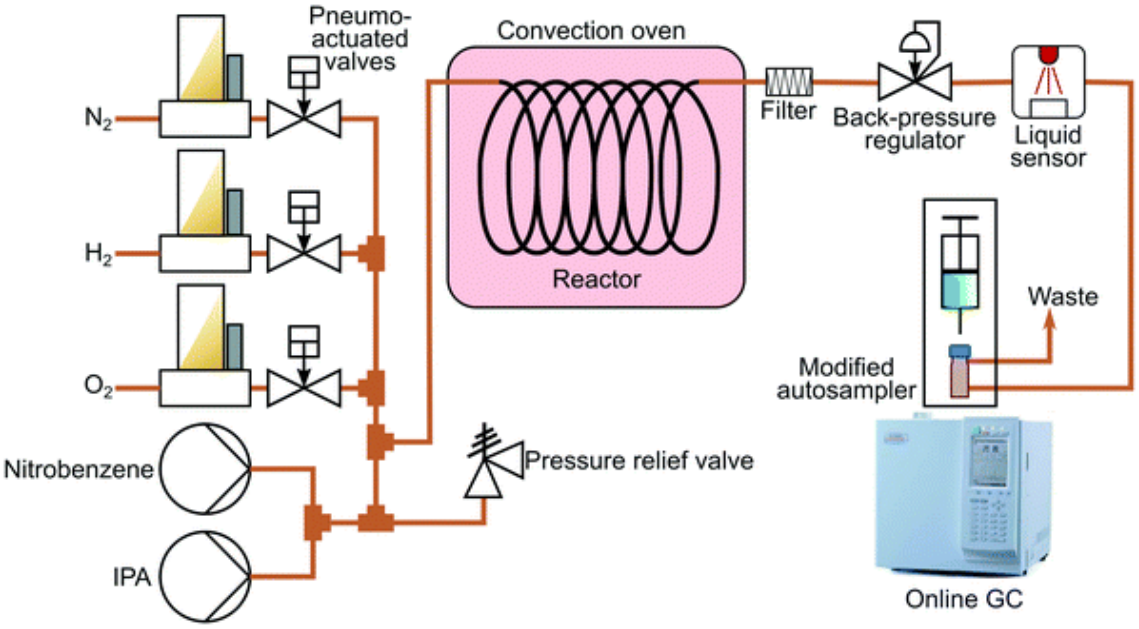

Figure 2-5 Self-optimising reactor platform used for gas-liquid-solids reactions in a wall coated tube reactor with online GC analysis. Reprinted from Cherkasov, N., et al., OpenFlowChem–a platform for quick, robust and flexible automation and self-optimisation of flow chemistry. Reaction Chemistry & Engineering, 2018. 3: p. 769-780., with permission from the Royal Society of Chemistry.

In addition to improving kinetic studies through the use of automation, it is also possible to make kinetic studies more efficient with improved Design of Experiments (DoE). Furthermore, the recent integration of automated reactors with online analysis techniques has enabled the use of automated online DoE in closed loop systems which use information gathered from previous experiments for the design of subsequent experiments. This offers considerable advantages as it allows for intelligent experimental design, such as MBDoE, instead of relying on factorial screening of the design space. While a large number of closed loop flow reactor systems have been reported in the literature in recent years for sequential steady-state experiments, most of these systems are for “self-optimising” reactors, where the reactor is described using black box models and optimisation techniques [173] are used to automatically identify the best operating conditions to maximise a given target, such as yield [32, 39, 73, 74, 84, 92-95, 97-101]. This approach is particularly useful for complicated processes where a first principles model is not available, however it is of relatively little value for identifying kinetic models. Some examples of the most advanced self-optimising reactors include the optimisation of a multistep sequence including reaction and separation steps [16] and the use of multiple objective functions where an optimal compromise between two competing variables (such as economics and environmental impact) are identified [39, 133]. In contrast, MBDoE is a much more appropriate DoE strategy for kinetic studies, however, there has only been limited application of online MBDoE to closed loop reactor platforms, such as the work of the Jensen group who

have applied MBDoE for designing sequential steady-state experiments for both model discrimination and improved parameter precision for a Diels-Alder reaction [14] and also the application of MBDoE for improved parameter precision to a reaction network [41]. These case studies were both very successful reducing the time, labour and number of experiments required to identify kinetic models, and hence these systems are considered as some of the most effective way of performing rapid kinetic studies. However, these two reactions were for homogenous reaction systems and to date no one has applied online MBDoE to heterogeneous catalytic systems.

There has also been significant interest in recent years in the application of automated flow reactors to perform dynamic kinetic studies, where one of the design variables is given a time varying profile such as a step change or ramp, and the reactor response is measured. These techniques are now considered state of the art in rapid kinetic investigation as they generate kinetic data without having to wait for the reactor to reach steady-state conditions. A common method for these experiments is to ramp the flowrate to a Plug Flow Reactor (PFR) and to monitor the outlet concentration, which is mathematically equivalent to running a batch reactor [12, 34, 36]. It is also possible to ramp other control variables such as temperature [174, 175], or to ramp multiple variables simultaneously to explore an even greater range of conditions in a single experiment [33, 37]. Alternative methods include introducing step changes to the PFR, however this is more difficult to achieve experimentally, as it is often not physically possible to achieve perfect step changes in many variables such as temperature or flowrate [176]. While transient PFR studies have proven to be very successful for generating kinetic data, recent work has shown that the design of the ramp transient experiment is crucial for producing highly informative data and that a good design is not intuitive, especially for experiments where multiple variables are ramped simultaneously. In these cases trial and error is often required to obtain satisfactory experiment designs [33]. Due to this challenging experimental design problem, the most advanced application of transient flow reactors to kinetic studies used offline MBDoE to successfully design a transient flow experiment for the purposes of discrimination between two candidate models for the reaction of phenylisocyanate with t-butanol [35].

2.3.3 Review of Model-Based Design of Experiments

Despite advances in automated flow systems allowing large numbers of experiments to be quickly conducted, the design of experiments still remains a critical part of kinetic studies, as poorly designed experiments may offer very little information for discriminating between multiple candidate kinetic models, or for precisely estimating kinetic parameters [25]. For example, Figure 2-6 demonstrates how experimental

design can dramatically influence the information content of an experiment where the goal is to precisely estimate a kinetic rate constant for a first order reaction in a batch reactor. In this example, due to experimental limitations it is only possible to take a single measurement of the process and hence the experimental design problem consists of picking the time at which to sample the reactor. The figure shows that sampling the reactor at a long time of 3.8 minutes would be a very poor experimental design as the predicted concentration profiles for multiple different rate constants overlap at this point, hence it is not possible to determine with high precision what the rate constant is. This figure also shows that the location of the optimum design depends on the true parameter value, for example if the value of the rate constant was 10 min^{-1} or 1.75 min^{-1}, then the optimum locations would be 0.4 min and 1.2 min respectively. This demonstrates that the location of MBDoE designs is influenced by the initial estimate of the parameter value, and hence that the design of numerous sequential experiments by MBDoE is particularly effective as with each new experiment the parameter estimate improves which in turn improves the design of future experiments.

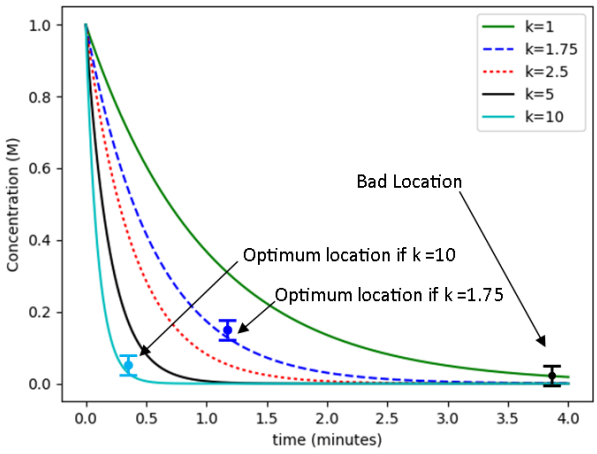

Figure 2-6 Concentration profiles in a first order batch reactor with different rate constants.

Traditionally, researchers have designed experiments using the one factor at a time approach, or by using factorial or fractional factorial designs. While these methods are useful for exploring the design space, especially when there is no model available for the system, there is no guarantee that they will lead to highly informative experiments. In contrast MBDoE is a method of designing experiments which uses the information already known about a system from its model structure and initial parameter estimates to design an experiment in an optimal way, most commonly with the objective of either distinguishing between two or more candidate models [177-179], or for precisely

estimating the parameter values in a single chosen model [25, 179-181]. MBDoE is a well-established field that was initially pioneered in the 1950s by Box and Lucas [182], Box and Hunter [183], Draper and Hunter [184], Box and Hill [185], Hill et al. [186], Hunter et al [187] and Bard [180] amongst others. MBDoE can be applied to both steady-state experiments, where a single value is optimised for each design variable, and for transient experiments, where an input profile is designed for each design variable. Due to the increased degrees of freedom in a dynamic experiment, the input profiles are often split into piecewise constant or piece wise linear profiles [25].

2.3.3.1 Background to Modelling and Parameter Estimation

A brief background to modelling and parameter estimation is presented here before reviewing the MBDoE literature.

A model consists of a set of **f** equations, state variables **x**, input variables **u** and a vector of N_θ non-measurable parameters $\boldsymbol{\theta}$, which can be used to predict the behaviour of a system and hence can predict experimentally measurable values $\hat{\mathbf{y}}$, as shown in Eq (2-4).

$$\hat{\mathbf{y}} = \mathbf{f}(\mathbf{x}, \mathbf{u}, \boldsymbol{\theta}) \tag{2-4}$$

Parameter estimation is the process of using experimental measurements to identify the value of the non-measurable parameters, $\boldsymbol{\theta}$, in a model. In a system where N_{exp} experiments are conducted, with each experiment consisting of N_m measurements, then the for the ith experiment and jth measurement the i,jth residual ρ_{ij}, is defined as the difference between the model predicted value $\hat{y}_{ij}$, and the experimentally measured value y_{ij}, as shown in Eq (2-5).

$$\rho_{ij} = y_{ij} - \hat{y}_{ij} \qquad for\ all\ i,j \tag{2-5}$$

One of the most common methods of parameter estimation is the maximum likelihood principle which assumes that i) the correct model structure is used ii) the experimental inputs **u** are perfectly controlled and iii) the residuals are caused by measurement errors which are normally distributed with a mean of 0 and a standard deviation σ_{ij} [25, 180]. Parameter estimation is then an optimisation problem to find the optimum parameter values to maximise the log likelihood function $\Phi(\boldsymbol{\theta})$ shown below in Eq (2-6) [180]

$$\max_{\boldsymbol{\theta}}\left(\Phi(\boldsymbol{\theta})\right) = \max_{\boldsymbol{\theta}}\left(\sum_{i=1}^{N_{exp}}\sum_{j=1}^{N_m}\left[-\frac{1}{2}ln(2\pi) - \frac{1}{2}ln\left({\sigma_{ij}}^2\right) - \frac{1}{2}\left(\frac{\rho_{ij}}{\sigma_{ij}}\right)^2\right]\right) \tag{2-6}$$

The resulting parameter estimates, $\widehat{\boldsymbol{\theta}}$, are then called the Maximum Likelihood Estimates (MLE). The quality of the obtained parameter estimates can be described by

their accuracy and precision, which are explained graphically in Figure 2-7. Accuracy is how close an estimate is to the true value, however, the true value is normally unknown so it is not possible to measure accuracy. Precision or variance is a measure of the spread in the distribution of parameter estimates that would be obtained if the same experiments were repeated.

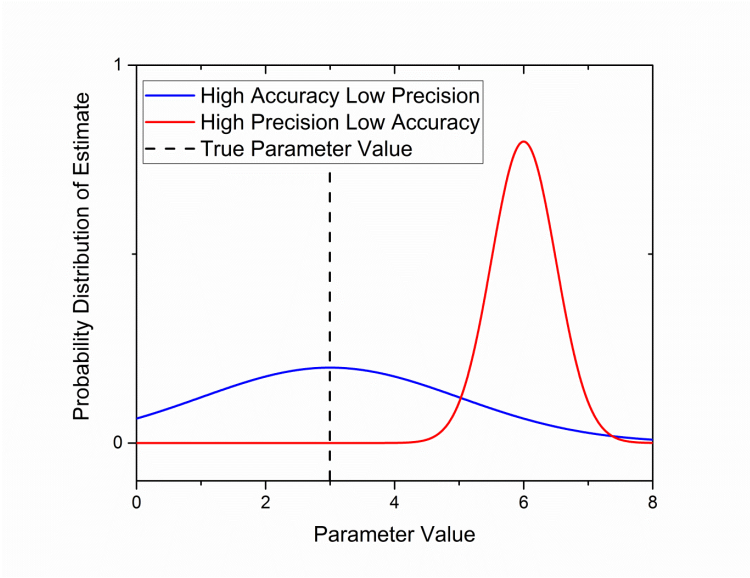

Figure 2-7 Graphical demonstration of accuracy and precision in parameter estimation.

The parameter precision is calculated from the covariance matrix, $\mathbf{V_\theta}$, which is a N_θ by N_θ matrix showing the variance and co-variance of each parameter and parameter pair. The covariance matrix $\mathbf{V_\theta}$ is approximated using the first term Taylor expansion, as the inverse of the Fisher information matrix $\mathbf{H_\theta}$

$$\mathbf{V_\theta} \approx \mathbf{H_\theta^{-1}} \tag{2-7}$$

The Fisher Information matrix is approximated using the sensitivity of the model responses to changes in the parameter estimates. This approximation is commonly used in the literature [25] and is shown for the k,lth element of the Fisher information matrix.

$$[H_\theta]_{kl} = \sum_{i=1}^{N_{exp}} \sum_{j=1}^{N_m} \frac{1}{\sigma_{ij}^2} \left[\left(\frac{\partial y_{ij}}{\partial \theta_k} \right) \left(\frac{\partial y_{ij}}{\partial \theta_l} \right) \right] \tag{2-8}$$

The precision of a parameter estimate is often quantified by calculating the 95% confidence intervals or the 95% t-test value. From the covariance matrix, the 95% confidence interval for the ith parameter is calculated as the square root of the variance element $v_{\theta,ii}$, obtained from the diagonal of the covariance matrix, multiplied by the student t-value at 95% confidence level for the given number of degrees of freedom.

$$95\%\ Confidence\ Interval_i = \sqrt{v_{\theta,ii}} * t(95\%, DoF) \quad \text{for i} = 1, \dots, N_\theta \tag{2-9}$$

The t-test statistic is calculated by dividing the parameter estimate by the confidence interval, as shown in Eq (2-10). The t-test is considered passed if the calculated t-value is greater than the reference t-value, which is found from statistical tables at a given level of significance and for the given degrees of freedom. If the t-value is high that means the parameter estimate is reliable [25].

$$t_i = \frac{\hat{\theta}_i}{95\%\ Confidence\ Interval_i} \tag{2-10}$$

After conducting parameter estimation the adequacy of the model is assessed using the χ^2 test, where the χ^2 value is calculated using Eq (2-11), and compared to the 95% reference value, χ^2_{ref} at the given number of degrees of freedom [180].

$$\chi^2 = \sum_{i=1}^{N_{exp}} \sum_{j=1}^{N_m} \left(\frac{\rho_{ij}(\hat{\boldsymbol{\theta}})}{\sigma_{ij}} \right)^2 \tag{2-11}$$

$$degrees\ of\ freedom = N_{exp} * N_m - N_\theta \tag{2-12}$$

If the χ^2 value is greater than the reference value, this is interpreted to mean that the model is not compatible with the experimental data and that the model should be rejected.

2.3.3.2 MBDoE for Model Discrimination

MBDoE comprises of a set of tools for designing experiments in an optimum way, using the information already known about the system from the model equations and the current parameter estimates [1]. MBDoE can be used for many different tasks but the two most common are for model discrimination [2] and improved parameter precision [1]. In all cases MBDoE involves choosing the optimum values for the entries in the design vector **φ**, which is a subset of the control vector **u**, and consists of the experimental variables which are to be optimised.

There are a variety of different objective functions that can be used to determine the optimum experimental conditions for a discriminating experiment. The simplest objective function, the Hunter Reiner criterion, is the difference in predicted values between each candidate model [178] and is shown in Eq (2-13) for the case of two candidate models, where $\hat{\mathbf{y}}_\mathbf{1}$ and $\hat{\mathbf{y}}_\mathbf{2}$ are both $1 \times N_m$ matrices containing all the predicted values for model 1 and model 2 respectively.

$$\max_{\boldsymbol{\varphi}}(\ \psi_{Hunter}(\boldsymbol{\varphi})\ ) = \max_{\boldsymbol{\varphi}} \left(\left(\hat{\mathbf{y}}_\mathbf{1}(\boldsymbol{\varphi}) - \hat{\mathbf{y}}_\mathbf{2}(\boldsymbol{\varphi}) \right)^T \left(\hat{\mathbf{y}}_\mathbf{1}(\boldsymbol{\varphi}) - \hat{\mathbf{y}}_\mathbf{2}(\boldsymbol{\varphi}) \right) \right) \tag{2-13}$$

This can be extended to any number of models by maximising the summation of the difference in model predictions for each combination of model pairings. This simple method relies entirely on the predicted values of each model without taking into account the uncertainty of the model prediction, which can potentially lead to a non-optimal design of experiments. Uncertainty in model prediction arises due to the fact that the parameter values are never exactly known and that each estimated parameter value has an associated uncertainty affecting the expected model responses. More sophisticated model discriminating criteria, such as the one proposed by Buzzi-Ferraris [38, 177, 185] take this into account by finding an optimal design vector **φ,** which maximises the divergence between candidate models, while also minimising the uncertainty of the model predictions. The Buzzi-Ferraris design criterion assuming the presence of two candidate model structures is shown in Eq (2-14).

$$\max_{\boldsymbol{\varphi}}\left(\ \psi_{Buzzi}(\boldsymbol{\varphi})\ \right) = \max_{\boldsymbol{\varphi}}\left(\left(\hat{\mathbf{y}}_{\mathbf{1}}(\boldsymbol{\varphi}) - \hat{\mathbf{y}}_{\mathbf{2}}(\boldsymbol{\varphi})\right)^{T}\mathbf{S}(\boldsymbol{\varphi})^{-1}\left(\hat{\mathbf{y}}_{\mathbf{1}}(\boldsymbol{\varphi}) - \hat{\mathbf{y}}_{\mathbf{2}}(\boldsymbol{\varphi})\right)\right) \quad (2\text{-}14)$$

Here, **S**(**φ**) is the total variance due to covariance of the measurement noise **M**, and the covariance of the model predictions of model 1, $\mathbf{P}_1$ and model 2, $\mathbf{P}_2$ as shown in Eq (2-15).

$$\mathbf{S}(\boldsymbol{\varphi}) = 2\mathbf{M} + \mathbf{P}_1(\boldsymbol{\varphi}) + \mathbf{P}_2(\boldsymbol{\varphi}) \quad (2\text{-}15)$$

The covariance of the measurement noise, **M**, is a $N_m \times N_m$ matrix where the diagonal entries are the standard deviation for each measurement and the off-diagonal entries are 0. The covariance of the model predictions for the kth model, $\mathbf{P_k}$, which is the uncertainty in the model prediction, is in turn calculated from the covariance matrix, $\mathbf{V}_{\theta,k}$, and the sensitivity matrix, $\mathbf{Q_k}(\boldsymbol{\varphi})$, for that model, as shown in Eq (2-16).

$$\mathbf{P}_k(\boldsymbol{\varphi}) = \mathbf{Q}_k(\boldsymbol{\varphi})\mathbf{V}_{\theta,k}\mathbf{Q}_k^T(\boldsymbol{\varphi}) \quad \text{for k } = 1 \text{ and } 2 \quad (2\text{-}16)$$

The i,jth element of the sensitivity matrix $\mathbf{Q_k}(\boldsymbol{\varphi})$ is the partial derivative of the kth model prediction for the ith model response variable with respect to parameter j at conditions **φ**.

$$[\mathbf{Q}_k(\boldsymbol{\varphi})]_{ij} = \left.\frac{\partial \hat{y}_{i,k}}{\partial \theta_j}\right|_{\boldsymbol{\varphi}} \quad (2\text{-}17)$$

Taking into account prediction uncertainty can lead to significantly improved discriminating experiments, as shown in Figure 2-8 where simply maximising the difference in model predictions leads to the poor design of a discriminating experiment with a control value of 4 as the two model predictions overlap. However, taking into account uncertainty leads to the improved design of a control value of 0 where the model predictions are more certain and do not overlap.

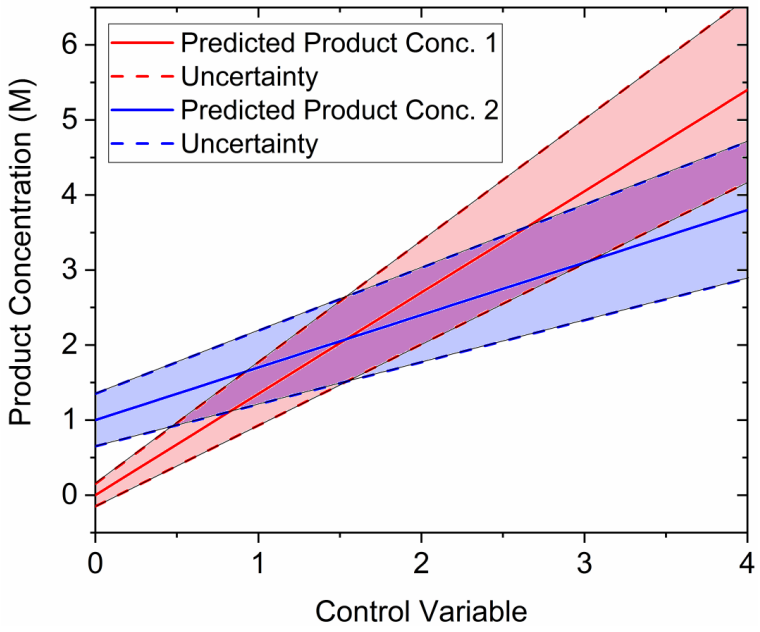

Figure 2-8 Graphical representation of the predicted responses from two rival models including the confidence intervals for the predicted responses due to uncertainty in the parameter estimation.

Box and Hill developed Bayesian approaches to the design of model discrimination which is particularly advantageous in the case of multiple candidate models, as the objective function is weighted towards the design of the optimum experimental conditions for the most likely models [185]. However, these approaches are more computationally expensive and hence less suited to online applications.

2.3.3.3 MBDoE for Improved Parameter Precision

Mathematically MBDoE for improved parameter precision is based on two principles, the first being that it is possible to predict the expected Fisher information of any planned experiment, $\mathbf{H_{expected}}$, using Eq (2-8) with some initial estimate for the parameter values $\boldsymbol{\theta}$, which can be obtained from the literature or from previously conducted experiments in the form of the MLE estimate $\hat{\boldsymbol{\theta}}$. The second principle is the additivity of Fisher information which allows the expected covariance matrix $\mathbf{V_{\theta,expected}}$, after N_{exp} already completed experiments and N_{new} new planned experiments, to be calculated according to Eq (2-18).

$$\mathbf{V_{\theta,expected}}(\boldsymbol{\varphi}) = \left[\mathbf{V_{\theta,0}^{-1}} + \sum_{i=1}^{N_{new}} \mathbf{H_{expected,i}}(\boldsymbol{\varphi})\right]^{-1} \tag{2-18}$$

where $\mathbf{V_{\theta,0}}$ is the prior covariance matrix obtained from the N_{exp} already conducted experiments and $\mathbf{H_{expected,i}}$ is the expected Fisher information obtained from the i^{th} planned experiment. Therefore, MBDoE for improved parameter precision is then an optimisation problem to design experiments to minimise some scalar measure of the

expected covariance matrix. The most common scalar measures of the covariance matrix used in MBDoE are described below [25] and shown graphically in Figure 2-9.

- A - minimising the trace of the covariance (sum of the elements in the main diagonal). This is proportional to the volume of the polyhedron circumscribing the confidence ellipsoid.

- D - minimising the determinant of the covariance. This is proportional to the volume of the confidence ellipsoid.

- E - minimising the largest eigenvalue of the covariance matrix. This is equivalent to minimising the length of the longest axis of the confidence ellipsoid, and can often be most useful in the event of high parameter correlation [25, 188]. The modified E-optimal objective function aims to minimise the ratio of the largest and smallest Eigen values in the covariance matrix, hence making the confidence region as spherical as possible [189].

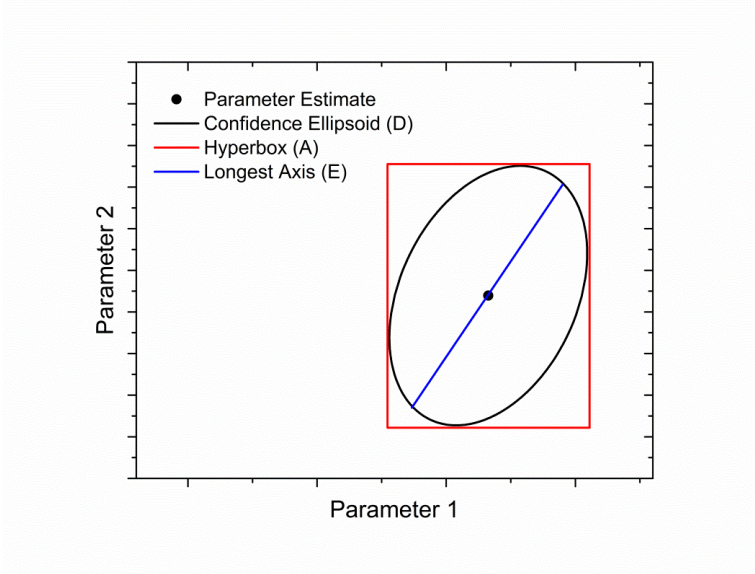

Figure 2-9 Example of a 95% confidence ellipsoid for a general two parameter model, with graphical representations of the A-, D- and E-optimal criteria for MBDoE for improved parameter precision.

Other MBDoE objective functions, such as the G or V-optimal designs, aim to increase the accuracy of model predictions under specific sets of operating conditions specified by the user [190]. In order to address one of the weaknesses of MBDoE, that the designed experiments depend on the initial parameter estimates, which may not be reliable leading to sub-optimal designs, robust MBDoE algorithms were developed that take into account the uncertainty of the initial parameter estimates [191-193].

Today many of the state-of-the-art objective functions are joint objective functions which find a trade-off between two, often competing aims, including:

- Joint optimisation of parameter precision and process performance [194]
- Joint optimisation of information gain and correlation reduction [195, 196]
- Joint optimisation of model discrimination and parameter precision [53]

2.3.3.4 Applications of MBDoE to Kinetic Studies

MBDoE has been successfully applied in many areas of science and engineering, but most often for chemical and biological modelling. In biological modelling, transient MBDoE has been particularly effective for identifying Monod type kinetics in fed batch reactors. It was shown that the Monod parameters were nearly unidentifiable for a batch reactor, however, by using MBDoE to design fed batch input profiles the parameters were successfully identified [40, 179, 197-202]. For chemical kinetics both steady-state and transient MBDoE have been applied for both model discrimination [35, 203-205] and improved parameter precision [39, 53, 196, 206, 207] to identify kinetic models, and many of these studies were for heterogeneous catalytic systems [53, 203-205]. Most of the applications of MBDoE to date have been offline applications through the iterative design of a new experiment every time new data is collected. While this has been very successful, it is also slow and labour intensive. Only recently with the development of closed loop reactor platforms has it become possible to perform online MBDoE [14, 41], and this presents great opportunities to extract the maximum combined benefits of flow reactors and MBDoE to intensify kinetic studies.

3 Multistep Flow Synthesis: Reactions in Isolation

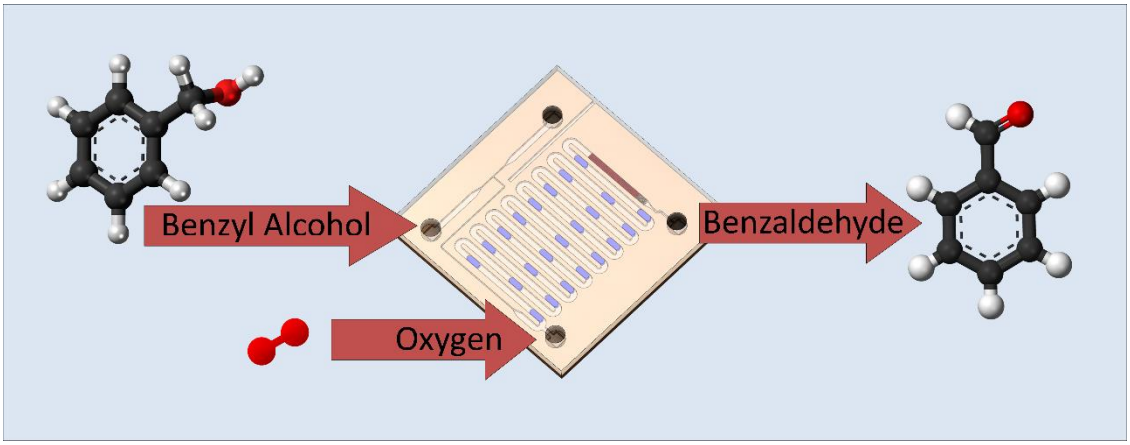

Abstract

Oxidation, aldol condensation and reduction, the three component reactions in the multistep synthesis of benzylacetone and 4-(4methoxyphenyl)butan-2-one, were each studied in separate flow reactors and suitable reaction conditions to ensure high conversion and selectivity were identified for each reaction. The aldol condensation reaction was identified to be the bottleneck in this system with a reaction rate one order of magnitude lower than the other two reactions. Furthermore, it was found that both the aldol condensation and reduction reactions suffered from catalyst deactivation and water inhibition, which presents a large problem as water is an unavoidable co-product of both the oxidation and aldol condensation reactions. This information was then used to assist in the design of the multistep flow system presented in Chapter 4.

The contents of this chapter have been published in
C. Waldron, E. Cao, S. Cattaneo, G.L. Brett, P.J. Miedziak, G. Wu, M. Sankar, G.J. Hutchings and A. Gavriilidis, “Three step synthesis of benzylacetone and 4-(4-methoxyphenyl)butan-2-one in flow using micropacked bed reactors”. *Chemical Engineering Journal,* 2019, **377**, 119976. https://doi.org/10.1016/j.cej.2018.09.137

3.1 Introduction

In this work it was desired to develop a multistep flow system and compare it against a batch cascade system to identify whether the flow system offered significant advantages in either process intensification or in studying catalyst behaviour. It was also intended to demonstrate that studying a catalyst in a multistep flow system rather than studying a single reaction in isolation would lead to a greater understanding of how the catalyst would behave in a process wide environment and hence this system can be used to assess the industrial viability of a process and to identify any potential problems with the catalyst, which could assist in future catalyst design.

The case study chosen for this work was the multistep synthesis of benzylacetone (**4**) and 4-(4methoxyphenyl)butan-2-one (**4**) from benzyl alcohol (**1**) and 4-methoxybenzyl alcohol (**1**). The reaction chemistry is shown in Figure 3-1 and for clarity each species is assigned a number, as shown in Table 3-1, which is written directly after the species name. The desired reactions are:

- oxidation of benzyl alcohol (**1**) to benzaldehyde (**2**),
- aldol condensation of benzaldehyde (**2**) with acetone to form benzalacetone (**3**),
- reduction of benzalacetone (**3**) to the desired product benzylacetone (**4**).

There are also a number of undesired reactions which can take place. During the oxidation reaction the undesired side products (**2b-2e**) are formed due to disproportionation, hydrogenolysis and oxidation reactions [168]. During the aldol condensation reaction, (coupling reaction), the undesired aldol condensation of acetone and two benzaldehyde (**2**) molecules occurs to form dibenzalacetone (**3b**). Also over reduction of the final product, benzylacetone (**4**) to the alcohol 4-phenyl butan-2-ol (**5**) occurs. Therefore, this is a challenging multistep synthesis where the selectivites of each reaction must be kept high to ensure a high yield of the final product. The same reactions occur for the 4-methoxybenzyl alcohol (**1**) system, but with the methoxy functional group.

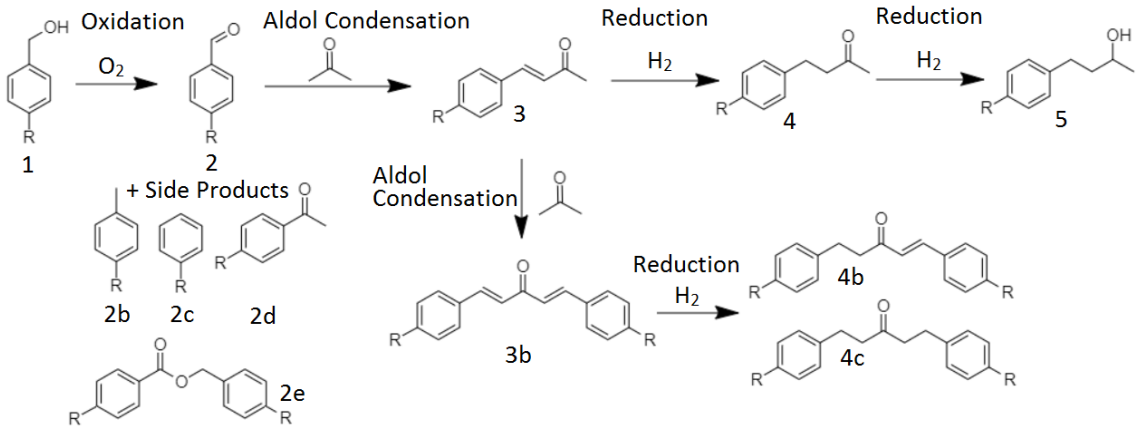

Figure 3-1 Reaction chemistry for the multistep synthesis of benzylacetone (R=H) and 4-(4-methoxyphenyl)butan-2-one (R=OCH_3).

Table 3-1 Species names for the benzyl alcohol (R=H) and 4-methoxybenzyl alcohol (R=OCH_3) systems.

Number	R=H	R=OCH_3
1	Benzyl Alcohol	4-Methoxybenzyl Alcohol
2	Benzaldehyde	4-Methoxybenzaldehyde
2b	Toluene	4-Methylanisole
2c	Benzene	Anisole
2d	Benzoic Acid	Anisic Acid
2e	Benzyl Benzoate	4-Methoxybenzyl-4-methoxybenzoate
3	Benzalacetone	4-(4-Methoxyphenyl)but-3-en-2-one
3b	Dibenzalacetone	1,5, Bis(4-methoxyphenyl)-penta1,4-den-3-one
4	Benzylacetone	4-(4-Methoxyphenyl)butan-2-one
4b	1,5-Diphenylpent-1-en-3-one	1,5-(4-Methoxy) diphenylpent-1-en-3-one
4c	1,5-Diphenylpentan-3-one	1,5-(4-Methoxy) diphenylpentan-3-one
5	4-Phenyl Butan-2-ol	4-4(Methoxyphenyl)butan-2-ol

This case study was chosen because the products have high commercial value as food additives, insect attractants and fragrances [23, 136] and because the multistep synthesis was recently demonstrated in batch cascade using Au-Pd supported nanoparticle catalysts [23] which was more selective and produced less waste than current commercial production methods using Friedel-Crafts alkylations [136, 208]. Therefore, this new synthesis route has significant industrial potential. Furthermore, this case study was chosen because two of the reaction steps, oxidation and reduction, are known to be fast dangerous reactions using flammable solvents with oxygen and hydrogen gas. Therefore, there is a strong motivation to move from batch to flow due to safety concerns and due to the potential benefits from increased rates of heat and mass transport.

3.2 Materials & Methods

3.2.1 Catalysts

The catalysts used in the batch study were AuPd nanoparticles supported on MgO or TiO_2, and the optimum catalyst was found to be AuPd/MgO [23]. However, it was not possible to use MgO supported catalysts in packed bed reactors. This is because to be used in a packed bed reactor, the catalyst powder must be pressed into a pellet and then ground and sieved to give a desired particle size. For micropacked bed reactors the particle diameter is typically between 40 and 100 µm. However, after this pelletisation procedure, during use in the packed bed it was found that the MgO particles did not retain their mechanical integrity and the particles in the packed bed broke into smaller ones leading to blockages during prolonged use. The instability of MgO particles is attributed to the hydroxylation of MgO to $Mg(OH)_2$ in the presence of water, which has been previously reported for this system [23, 209]. Unfortunately, this meant that it was not possible to use the MgO supported catalysts in the multistep flow system. This is because in a multistep flow system it is always preferable to use heterogeneous catalysts in packed bed reactors. Alternative flow reactor designs which enable the use of powders such as a cascade of CSTRs [56, 57, 210] or slurry flow reactors [58, 59] are considered too complex to use in a multistep flow system due to the increased likelihood of reactor clogging [107]. Therefore, only TiO_2 supported catalysts were available for use in this work as they were compatible with packed bed reactors and could easily be integrated into a multistep flow system.

In this work a 1 wt% 65:35 (weight ratio) Au:Pd/TiO_2 catalyst was used for the oxidation reaction, TiO_2 was used for the aldol condensation reaction and both 1 wt% Pt/TiO_2 and 1 wt% Pd/TiO_2 catalysts were used for the reduction reaction. All of these nanoparticle supported catalysts were obtained from the Prof Graham Hutchings research group at Cardiff University, the catalysts preparation methods are shown in Appendix A. A number of other catalysts have been reported in the literature to be very promising for these reactions. For example, for the aldol condensation reaction, recent research has shown that bifunctional catalysts which possess both acid and basic sites [211], metal oxides (MgO, ZrO_2 and TiO_2) [212-214], double layered hydroxides [215] and amine-functionalised SBA-15, ZrO_2 and TiO_2 [211] have all shown high activity. However, none of these catalysts were used in this work because it was intended only to use the nanoparticle supported catalysts from Cardiff which had previously been used in the batch cascade [23] to allow direct comparisons between batch and flow.

3.2.2 Reactor Design & Experimental Set-Up

When studying the reactions in isolation, all experiments were conducted in silicon-glass microreactors which were fabricated using photolithography, Deep Reactive Ion Etching (DRIE) and anodic bonding of the silicon and glass. The chosen microreactor design was one that was previously developed and used by the Gavriilidis research group [216]. The microreactor design consisted of a serpentine channel of dimensions 600 µm width, 300 µm height and 190 mm length with rectangular posts at the outlet to retain the solid catalyst, as shown in Figure 3-2. The silicon-glass reactor was heated using heating cartridges in a chuck enclosed in ceramic packaging for insulation, and the catalyst was loaded into the reactor by applying vacuum to the reactor outlet and introducing a known mass of catalyst through the reactor inlet. The reactors were weighed before and after loading to measure the mass of catalyst. However, there is expected to be some error associated with measuring the mass of the catalyst as the catalyst masses used were very small, typically 8 mg, and the mass balance used for this work only had 4 decimal places (readability of 0.1 mg) and therefore it cannot be expected to be highly accurate or precise for these small mases.

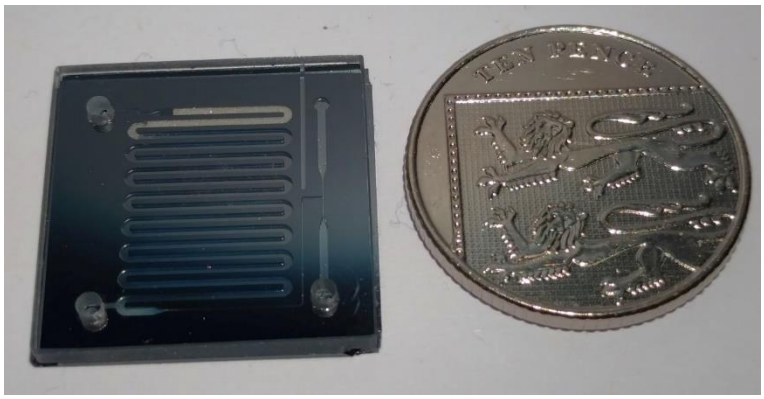

Figure 3-2 Photograph of the silicon-glass microreactor.

The experimental set up for studying the oxidation and reduction reactions in isolation is shown in Figure 3-3. Liquid feeds were introduced using stainless steel 8 mL syringes (Harvard Apparatus) and syringe pumps (Harvard Apparatus, Ph.D. Ultra). The gases were fed using mass flow controllers (Brooks 5850TR) and the pressure at the reactor outlet was controlled using a back pressure regulator (Swagelok KBP series, 250 PSIG). Calibration of equipment is shown in Appendix B. The gas and liquid feeds mixed at a T junction in the silicon-glass microreactor and formed gas liquid slug flow in the empty serpentine channel, which ensured that the liquid became saturated with the gas and that the reactants reached reaction temperature before reaching the packed bed. The liquid product was collected in a custom made PEEK collection vessel, which separated the liquid from the gas via gravity and had a needle valve at its base to allow the removal of liquid product for sampling.

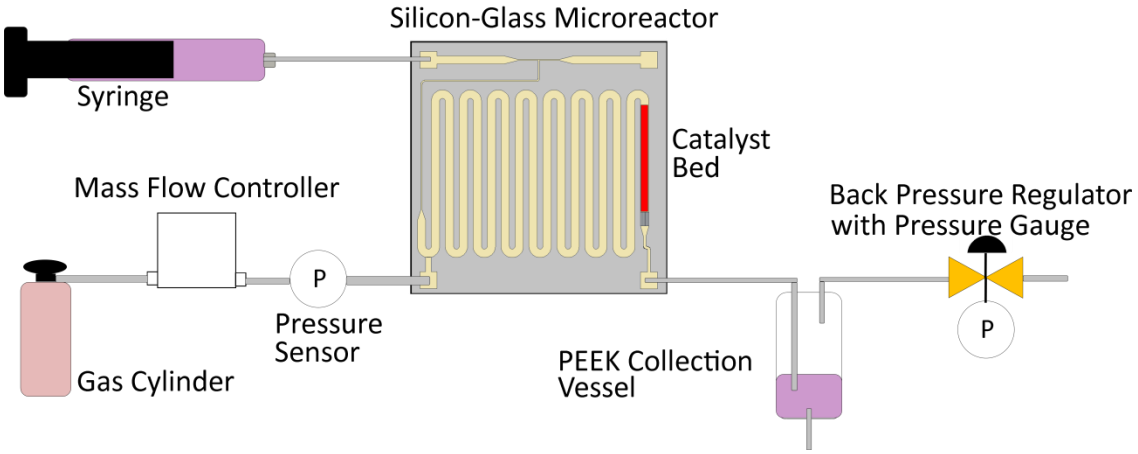

Figure 3-3 Experimental set-up for gas-liquid reactions (oxidation and reduction reactions) in a silicon-glass micropacked bed reactor.

For liquid only experiments (aldol condensation reaction), the same experimental set up was used except the gas inlet on the microreactor chip was closed and the system was pressurised with nitrogen gas flowing directly into the PEEK collection vessel, as shown in Figure 3-4.

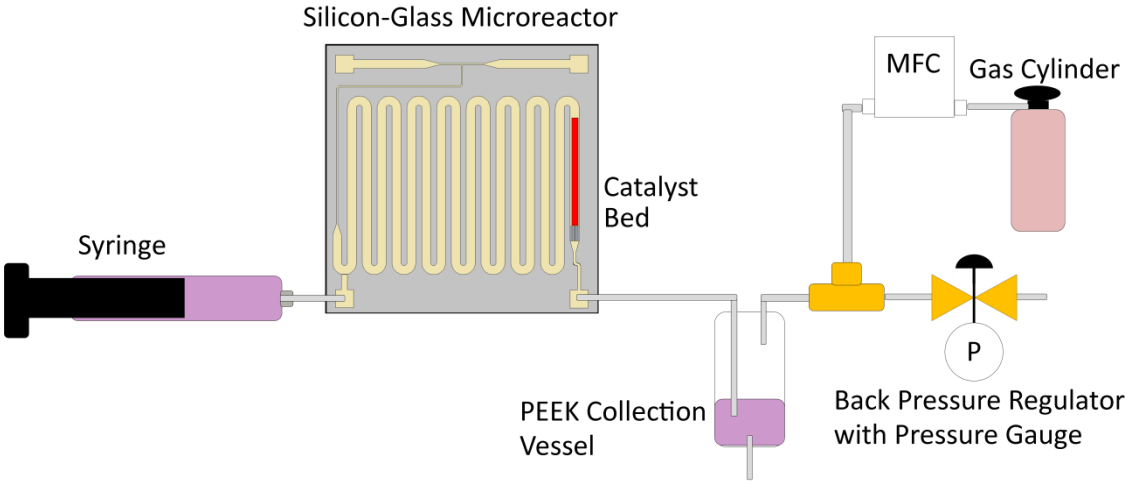

Figure 3-4 Experimental set-up for liquid phase reactions (aldol condensation reaction) in a silicon-glass micropacked bed reactor.

The liquid product was analysed off-line using gas chromatography (Agilent, 7820A) with a FID detector and an Agilent DB-624 capillary column, calibration details are included in Appendix B. Mesitylene was used as an internal standard to allow for volume change corrections associated with the generation of water and the loss of acetone through evaporation upon sample collection and depressurisation. A carbon balance where the concentration of the reactant in the feed was compared to the concentration of the reaction products in the outlet stream is shown in Eq (3-1), where C represents concentration (M) and p_i and f represent the stoichiometric coefficients of the i^{th} product species and the alcohol feed (f=1). For the benzylacetone system the

carbon balance closed to within 95% when studying reactions in isolation. All chemical species were from Sigma Aldrich and used without further purification.

$$Carbon\ Balance = \frac{C_{Reactant\ In} - \left(C_{Reactant\ Out} + \sum \frac{f}{p_i} * C_{i\ Product\ Out}\right)}{C_{Reactant\ In}} \quad (3\text{-}1)$$

Reactant feed conversion X, was calculated using Eq (3-2) and the selectivity S_i, using Eq (3-3). When studying reactions in isolation the average reaction rate, r_{av} (mol/s/g catalyst) was calculated according to Eq (3-4), where W is the catalyst mass (g) and υ is the inlet liquid flowrate (L/s). The reaction rate varies along the length of the packed bed, however this average reaction rate is still a useful quantity for comparison purposes. Where shown, error bars in graphs represent 1 standard deviation obtained from triplicate sampling.

$$X = \frac{C_{Reactant\ In} - C_{Reactant\ Out}}{C_{Reactant\ In}} \quad (3\text{-}2)$$

$$S_i = \frac{\frac{f}{p_i} * C_{Desired\ Product}}{C_{Reactant\ In} - C_{Reactant\ Out}} \quad (3\text{-}3)$$

$$r_{av} = \frac{(C_{Reactant\ In} - C_{Reactant\ Out})\upsilon}{W} \quad (3\text{-}4)$$

When studying the reactions in isolation, the aldol condensation and reduction catalysts (TiO_2 and Pd or Pt/TiO_2) were both observed to undergo considerable deactivation, with up to 50% loss in activity in 8 h of operation. For this reason fresh catalyst was used every day and a deactivation correction procedure was applied assuming linear deactivation, so that data collected near the end of the day could still be used. The deactivation correction procedure is shown in Appendix C.

3.2.3 Experimental Procedure

The aim of studying each reaction in isolation was to try and identify suitable operating conditions for each reaction and to investigate if the catalysts deactivated or were inhibited by any impurities that are likely to be produced in the system through undesired side reactions in the previous reactions.

3.2.3.1 Oxidation of Benzyl Alcohol

Benzyl alcohol (**1**) oxidation with molecular oxygen had already been studied extensively in the literature [13, 43, 216-222] in both solvent and solvent free conditions. The catalyst used in this work, $AuPd/TiO_2$ is one of the best catalysts for this reaction as it is highly active, with Turn Over Frequency (TOF) greater than 10,000 h^{-1} [221], reasonable selectivity [43] and its deactivation behaviour has been optimised [220]. Therefore, from the literature, suitable operating conditions for this reaction were

easily identified. It was known that reaction rate increased with temperature, but at the expense of falling selectivity to the desired benzaldehyde species. As such, a moderate temperature of 115°C was chosen as a compromise. The literature also indicated that the reaction rate and selectivity increased with oxygen availability, which could be controlled by pressure or gas-liquid ratio [43, 216, 221]. For this reason, a moderate pressure of 6 barg and large gas liquid ratios, typically 100 or greater by volumetric flowrate, were chosen for the oxidation reaction. However, this led to the requirement of separation of the oxygen gas downstream as it was not desired to allow the oxygen gas to flow into the reduction reactor where it would mix with hydrogen gas.

Due to the large amount of information obtained from the literature regarding benzyl alcohol (**1**) oxidation, only a small number of experiments were required to learn more about how the oxidation reaction would behave in the multistep flow system. There were two objectives in these experiments,

1. It was desired to identify if running the oxidation reaction in acetone solution instead of using pure alcohol would have a significant effect on the reaction. This is because acetone is needed in the second reaction (aldol condensation) and using pre mixed acetone from the very first reaction would eliminate the need for online mixing of liquid streams at the entrance to the second reaction which would considerably simplify the pressure and flow management in the multistep flow system. Further details on the pressure and flow management are provided in the next chapter.
2. As there was far less information about the oxidation of 4-methoxybenzyl alcohol (**1**) in the literature, it was necessary to run some experiments to check that 4-methoxybenzyl alcohol (**1**) oxidation behaved in a similar way as benzyl alcohol (**1**) oxidation.

3.2.3.2 Aldol Condensation of Benzaldehyde with Acetone

The catalyst used in this work for the aldol condensation reaction, TiO_2, is a suitable heterogeneous catalyst due to its weak acid base properties and furthermore it is cheap, readily available, and non-toxic [223]. Unfortunately, there was very little information available in the literature about the aldol condensation of benzaldehyde (**2**) or 4-methoxybenzaldehyde (**2**) with acetone using TiO_2 as a catalyst. Therefore, a large number of experiments were performed to screen variables including temperature, feed concentration, flowrate, catalyst type, particle size and catalyst contact time. The stability of the catalyst also needed to be assessed as deactivation and product inhibition is commonly a problem for aldol condensation reactions as the reaction products can undergo undesired subsequent carbon-carbon couplings into

larger molecules which adsorb onto the catalyst surface causing deactivation by fouling [224, 225]. Additionally, as this is the second reaction in the multistep system, it was necessary to study how the presence of undesired side products from the previous oxidation reaction (toluene (**2b**) and benzoic acid (**2d**)) as well as unreacted benzyl alcohol (**1**) would affect the reaction. In particular, water which is produced as a co-product in the oxidation reaction is known to deactivate and inhibit most heterogeneous aldol condensation catalysts [226-229].

3.2.3.3 Reduction of Benzalacetone

The reduction of benzalacetone (**3**) to benzylacetone (**4**) is typical of reduction reactions and the production of benzylacetone (**4**) is deemed quite straightforward as it is known that the reduction of the C=C double bond is far easier to achieve than the C=O double bond in the carbonyl group. The main concern is to avoid over reduction of the carbonyl group forming the alcohol, 4-phenyl butan-2-ol (**5**). Generally to avoid over reduction it is suggested to use a less active catalyst and to reduce hydrogen availability [230]. In this work Pd and Pt catalysts were used for the reduction reaction because a number of successful hydrogenation reactions with Pd and Pt catalysts in microreactors have been reported in the literature [105]. Due to the large amount of information available in the literature relating to reduction reactions using Pd and Pt catalysts, only a small number of experiments were needed to be conducted for the reduction reaction. The main experimental effort was spent on studying how the presence of unreacted reagents, co-products and undesired side products from the previous two reactions affected this reaction.

3.3 Results & Discussion

3.3.1 Oxidation of Benzyl Alcohol

To study the effect of using acetone as a solvent for the oxidation reaction, two experiments were designed, one using pure benzyl alcohol (**1**) and one using benzyl alcohol (**1**) in acetone solvent. The experiments were designed to have the same catalyst contact time per gram of benzyl alcohol (**1**) by using the same catalyst mass in both experiments and running one reaction at a flowrate of 10 µL/min pure benzyl alcohol (**1**) and the other at 44 µL/min of a 2.2 M benzyl alcohol (**1**) in acetone solution. Both experiments were performed at the same temperature (140 ^{o}C), pressure (6 barg) and catalyst mass (4 mg of 1 wt% AuPd/TiO_2) and both experiments resulted in similar conversion (57%) and selectivity (67%) indicating that acetone had no effect on the reaction. This result then enabled the use of premixed acetone and benzyl alcohol (**1**) feeds for the multistep system. As selectivity is known to increase with lower temperatures, in further experiments at 120 ^{o}C using 0.7 M and 3 M benzyl alcohol (**1**)

in acetone the selectivity could be increased to above 80% with selectivity being independent of the feed concentration.

The oxidation of 4-methoxybenzyl alcohol (**1**) was found to behave very similarly to the benzyl alcohol (**1**) oxidation, except that it was less selective to the desired 4-methoxybenzaldehyde product (**2**). At a temperature of 115 °C and a pressure of 6 barg the 4-methoxybenzyl alcohol (**1**) oxidation achieved 75% selectivity compared to the >85% that could be achieved with benzyl alcohol (**1**).

3.3.2 Aldol Condensation of Benzaldehyde and Acetone

By varying the flowrate, but keeping the catalyst contact time constant by changing the catalyst mass, it was found that the coupling reaction exhibited significant external mass transfer resistances at high temperatures but not at low temperatures. This is shown in Figure 3-5 where it can be observed that the rate of reaction increases with increasing liquid flowrate only for the high temperature experiments. This indicates that at low temperatures, the catalyst operates in the kinetic regime, but at high temperatures, the reaction becomes limited by external mass transfer. Note that all the data points corresponded to conversion of less than 40%, explaining why the catalyst contact time had a minimal effect on reaction rate.

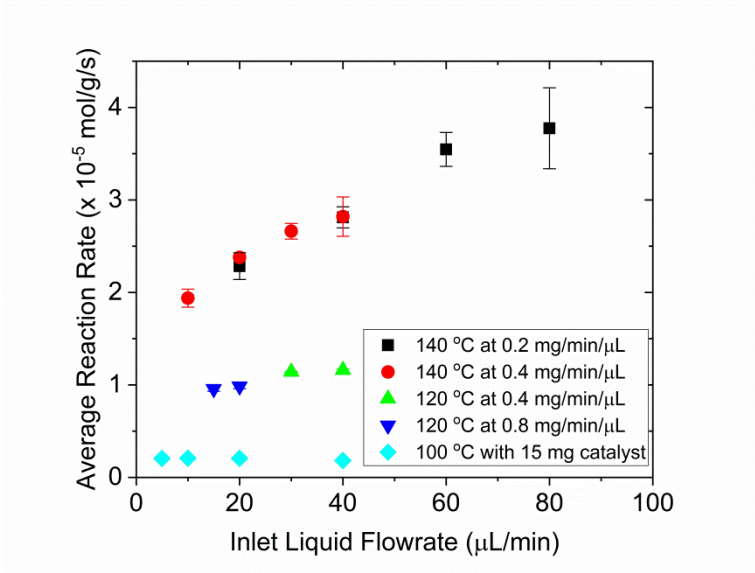

Figure 3-5 Average reaction rate (corrected for deactivation) against inlet liquid flowrate for the coupling reaction of benzaldehyde (**2**) with acetone. Experimental conditions were 6 barg, 2.2 M benzaldehyde (**2**) in acetone, 63-75 µm TiO_2 catalyst.

A set of experiments were then conducted at benzaldehyde (**2**) feed concentrations ranging from 1 to 3.5 mol/L in acetone solution at a constant flowrate of 10 µL/min. The results of these experiments were surprising, as it was expected that the reaction rate would increase with feed concentration. However, as shown in Figure 3-6, the reaction

rate appears to be zero order with respect to benzaldehyde (**2**) feed concentration in the high temperature external mass transfer regime, and negative order in the low temperature kinetic controlled regime. These results indicate at high temperatures that the reaction is not limited by the rate of external mass transfer of the reactant to the catalyst surface. Therefore, it was speculated that the external mass transfer resistances may be caused by the rate of removal of product from the catalyst surface into the bulk liquid phase.

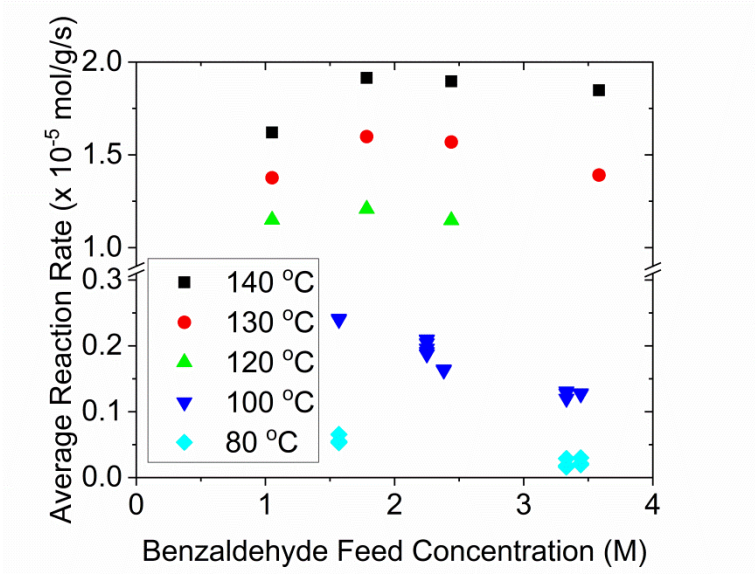

Figure 3-6 Average reaction rate (corrected for deactivation) against concentration of benzaldehyde (**2**) in the feed stream for the coupling reaction of benzaldehyde (**2**) with acetone. Experimental conditions were 6 barg, 10 µL/min liquid feed rate with 8 mg of 63-75 µm TiO_2 catalyst for 120-140 °C data, and up to 15 mg for 80 and 100 °C data.

To confirm the hypothesis that at high temperatures the reaction was limited by external mass transfer of the product benzalacetone (**3**) from the catalyst surface, a set of experiments was conducted with increasing amount of product in the feed along with the reactant. In all cases the reactant feed was held constant at 2.8 M benzaldehyde (**2**) in acetone, but increasing amounts of the product benzalacetone (**3**) and dibenzalacetone (**3b**) were added to the feed solution. The concentration of dibenzalacetone (**3b**) in the feed was approximately 20% of the concentration of benzalacetone (**3**) as the selectivity of this reaction was approximately 80%. The results of these experiments, shown in Figure 3-7, do confirm product inhibition, as the rate of reaction decreases with increasing product concentration in the feed. Therefore, it is concluded that at high temperatures, this reaction is limited by the rate of mass transfer of the product away from the catalyst surface.

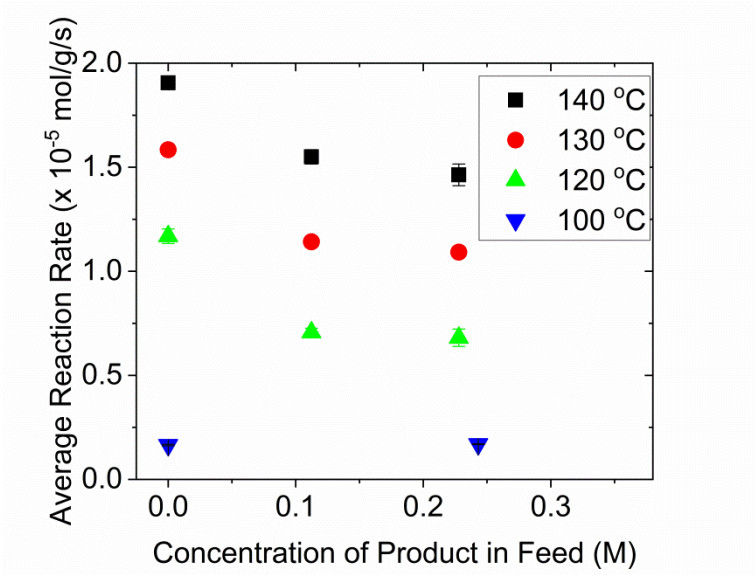

Figure 3-7 Average reaction rate (corrected for deactivation) against concentration of the product benzalacetone (**3**) in the feed stream for the coupling reaction of benzaldehyde (**2**) with acetone. Experimental conditions were 6 barg, 10 µL/min inlet liquid feed rate of approximately 2.8 M benzaldehyde (**2**) in acetone, 8 mg of 63-75 µm TiO_2 catalyst.

A similar form of product inhibition has also been reported in the literature for TiO_2 catalysed aldol condensation reactions, where it has been reported that the reaction is limited by low equilibrium conversions [212] and that the reaction products undergo further condensation reactions forming heavy molecular weight species that adsorb on the catalyst leading to catalyst deactivation [212, 214]. In the literature it has been reported that both the equilibrium limitation and deactivation problem can be overcome by immediately reducing the products [212]. As the final step of the multistep synthesis in this work is a reduction reaction, this strategy to increase reaction rate and deactivation appeared very attractive. For this reason it was attempted to conduct both the aldol condensation and reduction reactions in the same reactor over a Pd/TiO_2 catalyst, using the gas liquid experimental set up, shown in Figure 3-3, (note that using nanoparticle supported catalysts was not found to affect the aldol condensation reaction compared to just using TiO_2, as shown in Appendix C). Unfortunately, it was found that the rate of the coupling reaction dropped significantly in the presence of hydrogen gas, as shown in Figure 3-8, and deactivation still occurred so there was no benefit in conducting both reactions in the same reactor. Interestingly, a drop in the reaction rate was also observed if nitrogen gas was used in this reactor, or if some of the acetone was allowed to evaporate and form two phase gas liquid flow. Similarly, when the oxidation reaction was carried out with premixed benzyl alcohol and acetone feed over a $AuPd/TiO_2$ packed bed, the conversion to benzalacetone (**3**) was less than 2% despite the fact that the oxidation conversion is high (60%) so that there is a significant amount of benzaldehyde and acetone reagents for the aldol condensation

reaction to occur. Therefore, it was concluded that the aldol condensation reaction only performed well in liquid phase reactors, and when any type of gas phase was introduced the reaction rate would drop. This was possibly because the gas phase would occupy volume in the reactor and hence reduce the residence time of the liquid in the reactor.

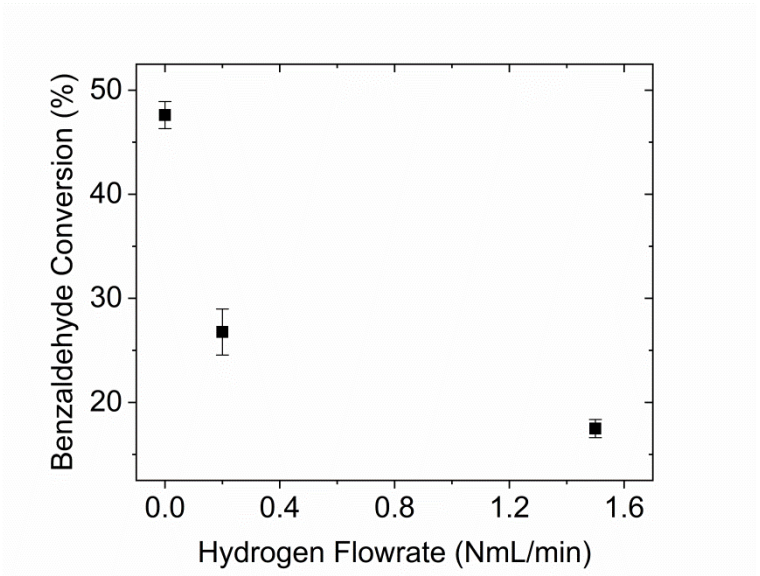

Figure 3-8 Benzaldehyde (**2**) conversion (corrected for deactivation) against hydrogen flowrate when the aldol condensation and reduction reactions were conducted together in the same packed bed. Experimental conditions were 140 °C, 6 barg, 10 µL/min of 2.1 M benzaldehyde (**2**) in acetone, 8.1 mg of 63-75 µm Pd/TiO_2.

The aldol condensation reaction produced two products, the desired benzalacetone (**3**) and the undesired dibenzalacetone (**3b**). The selectivity of the reaction was not observed to vary with the flowrate, indicating it was not strongly influenced by external mass transfer. Instead selectivity was observed to decrease with increasing temperature, as shown in Figure 3-9.

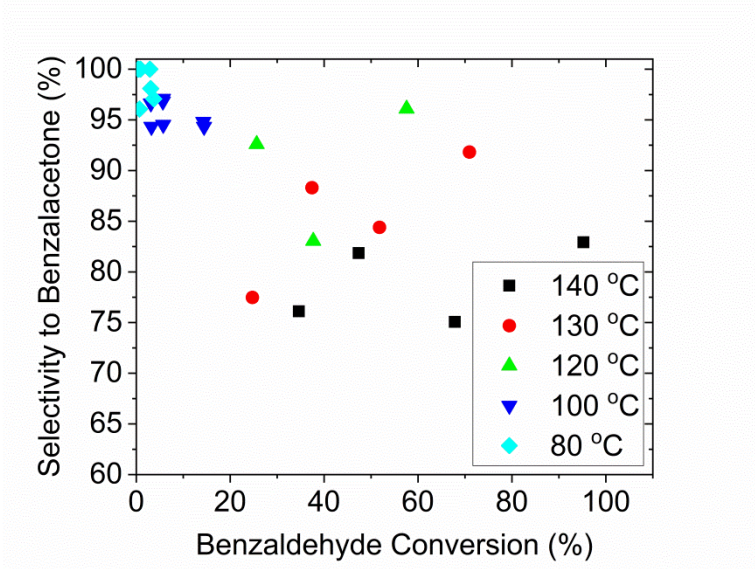

Figure 3-9 Selectivity to benzalacetone (**3**) against benzaldehyde (**2**) conversion for the coupling reaction of benzaldehyde (**2**) with acetone at five different temperatures. The data are from the same set of experiments as Figure 3-6.

In order to determine if there were also internal mass transfer resistances in this reaction, experiments were conducted with three different particle sizes, 63-75, 75-90 and 90-120 µm. The results shown in Figure 3-10, indicate the presence of only minor internal mass transfer resistances as the rate of reaction rate did not increase significantly with decreasing particle size.

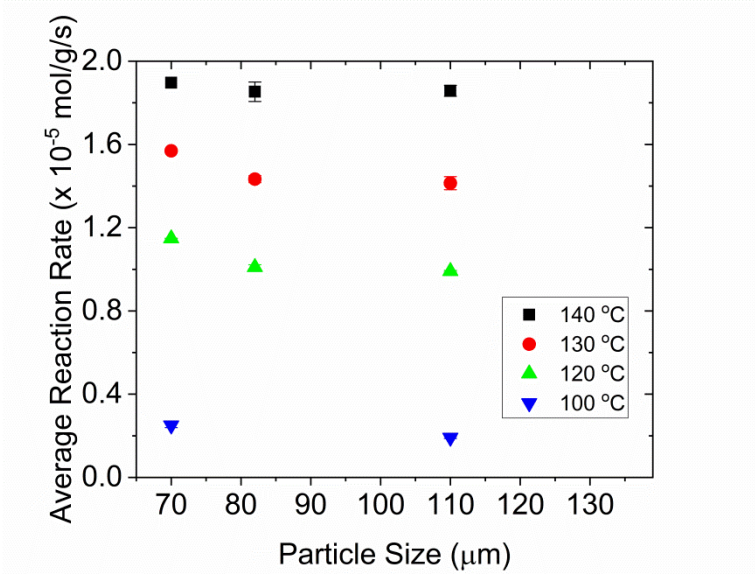

Figure 3-10 Average reaction rate (corrected for deactivation) against particle size (µm) 63-75, 75-90 and 90-120 µm, for the coupling reaction of benzaldehyde (**2**) with acetone. Experimental conditions were 6 barg, 10 µL/min inlet liquid flowrate of approximately 3 M benzaldehyde (**2**) feed, 8 mg of TiO_2.

Having studied how the coupling reaction of benzaldehyde (**2**) and acetone occurred when pure feeds were used, it was then necessary to study how it would be affected by

the presence of the likely impurities from the oxidation reaction (unreacted benzyl alcohol (**1**), toluene (**2b**) and water).

First the effect of water in the feed stream was investigated by using two syringe pumps, one with the benzaldehyde (**2**) feed in acetone solution, and the other with deionised water. The feed and water stream were mixed at a T-junction before entering the microreactor and the concentration of water could be controlled by varying the flowrate ratios. The results shown in Figure 3-11 show that a small amount of water, up to 1.5 wt % can be tolerated without any catalyst inhibition, but that a sharp decrease in reaction rate occurs as the water concentration reached 2.75%. Almost complete inhibition of the reaction was observed when larger concentrations of water (20 wt%) were used. This result confirmed reports in the literature that indicated that many heterogeneous aldol condensation catalysts are inhibited by water [226-229].

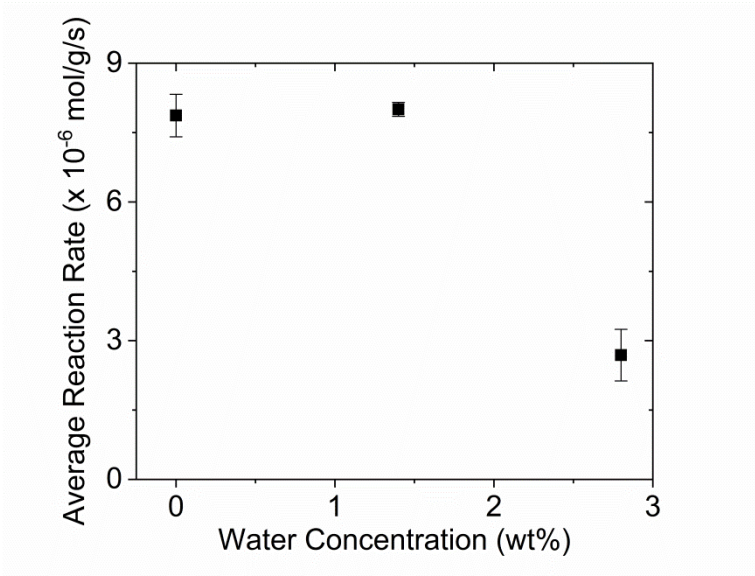

Figure 3-11 Average reaction rate against water concentration in the feed stream for the coupling reaction of benzaldehyde (**2**) with acetone. Experimental conditions were 130 °C, 6 barg, 20 µL/min inlet flowrate of 2.3 M benzaldehyde (**2**) in acetone, 11.4 mg of 63-75 µm TiO_2.

A second experiment was then conducted to investigate if any of the organic species from the oxidation reaction would inhibit the aldol condensation reaction. The two species that are most likely to be present in high concentrations are benzyl alcohol (**1**) (unreacted feed) and toluene (**2b**) (the major undesired side product of the oxidation reaction), so 0.3 M of each of these compounds were added to the benzaldehyde (**2**) acetone feed. The reaction was then run at 130 °C, with a liquid flowrate of 10 µL/min with 4.6 mg of TiO_2 catalyst and the same level of conversion was attained (approximately 50%) as when the reaction was run without the impurities added to the feed. However, later on it was found that very low concentrations of benzoic acid (**2d**)

of just 0.03 M would inhibit this reaction. This was found by accident, as some auto-oxidation of benzaldehyde (**2**) to benzoic acid (**2d**) had occurred in the benzaldehyde (**2**) reagent bottle, resulting in the experimental feed to consist of 0.03 M benzoic acid (**2d**) as well as the intended 1.05 M of benzaldehyde (**2**). It was found that benzoic acid (**2d**) contaminated feed had significantly lower rates of reaction than the previous experiments, as shown in Figure 3-12. As the production of small amounts of benzoic acid (**2d**) is expected in the oxidation reaction (even if the reaction conditions were tuned to try and avoid its formation), it was concluded that some organic species inhibition of the aldol condensation reaction would be expected during the multistep flow system.

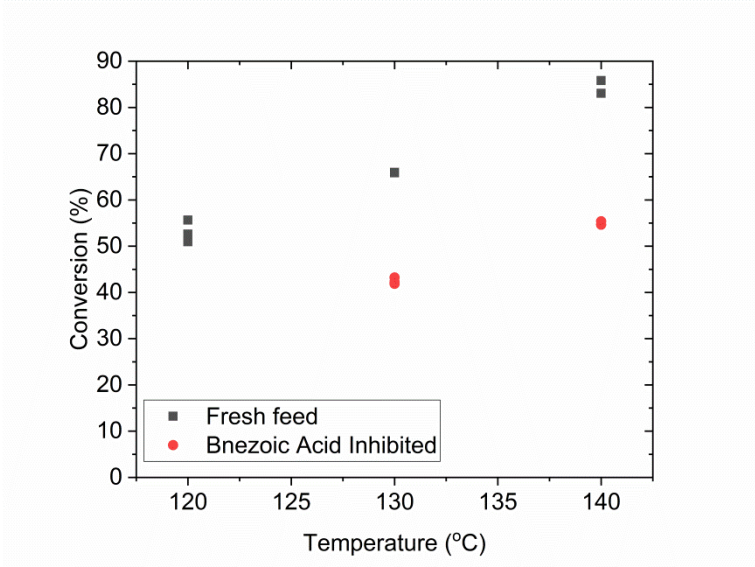

Figure 3-12 The conversion of benzaldehyde (**2**) during the aldol condensation reaction when a fresh feed is used and when an old feed contaminated with 0.03 M benzoic acid (**2d**) is used. Reaction conditions are 10 µL/min of 1.06 M benzaldehyde (**2**) with 8.1 mg of 63-75 µm TiO_2 catalyst.

3.3.3 Reduction of Benzalacetone

The reduction of benzalacetone (**3**) to benzylacetone (**4**) using a 1 wt% Pd/TiO_2 catalyst was studied using the gas liquid experiment set-up shown in Figure 3-3. The reaction was first studied using pure feed (benzalacetone (**3**) in acetone) and varying the temperature, liquid flowrate, hydrogen gas flowrate, feed concentration and particle size. Overall the rate of reaction was found to be very high with approximately 90% selectivity to the desired product benzylacetone (**4**).

An investigation of external mass transfer resistances was conducted by varying the gas and liquid flowrates. The effect of liquid flowrate was examined by increasing the liquid flowrate while keeping all other parameters fixed. The results shown in Figure 3-13 a, indicate that the liquid flowrate had negligible impact on the rate of reaction. In

contrast, in Figure 3-13 b, the flowrate of hydrogen gas was shown to increase conversion before plateauing, possibly when the hydrogen flowrate reached a critical value to keep the bulk liquid saturated for the given reaction conditions.

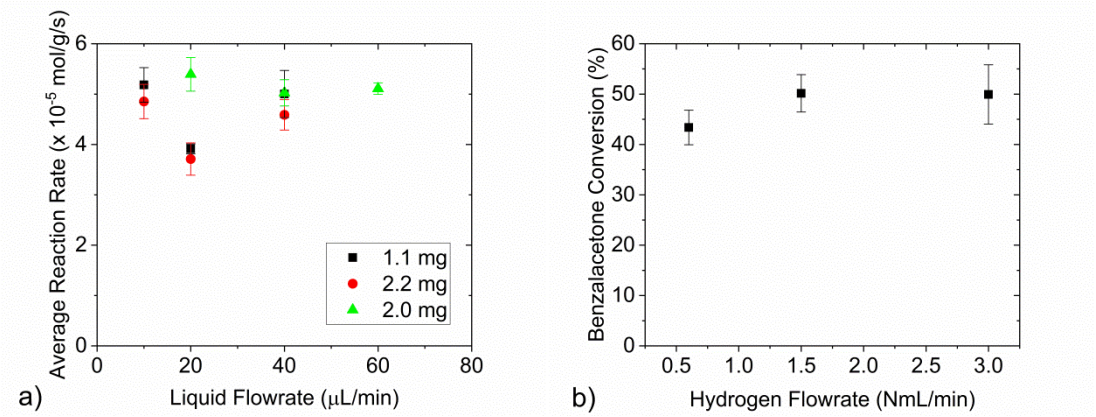

Figure 3-13 a) Average reaction rate (corrected for deactivation) of the reduction reaction against inlet liquid flowrate. b) Conversion of benzalacetone (**3**) (corrected for deactivation) against gas flowrate. Experimental conditions were 80 °C, 6 barg, approximately 1.4 M feed of benzalacetone (**3**), approximately 2 mg of 63-75 µm Pd/TiO_2. a) Gas flowrate was 1.5 NmL/min and b) liquid flowrate was 10 µL/min.

The internal mass transfer resistances were investigated by running the same experimental condition with a range of different particle sizes, 53-63, 63-75 and 90-120 µm. The results of these experiments, shown in Figure 3-14, indicate the presence of internal mass transfer resistances, as the rate of reaction dropped with increasing particle size.

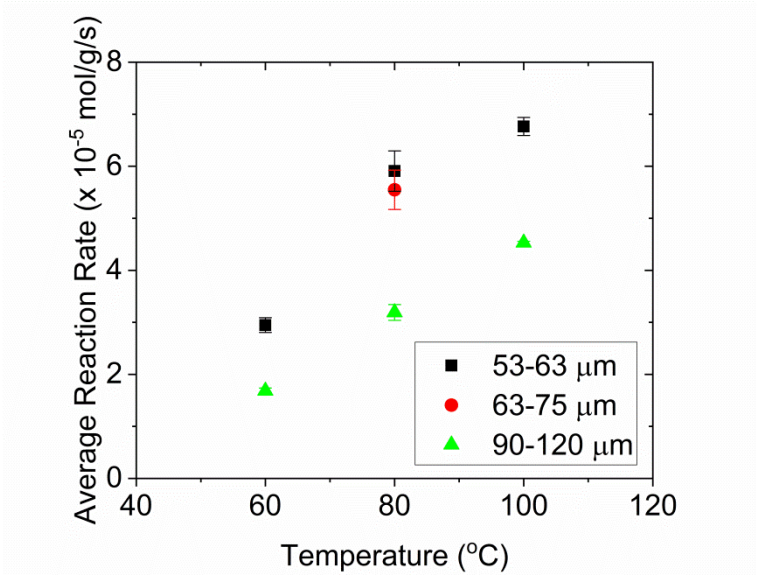

Figure 3-14 Average reaction rate (corrected for deactivation) of the reduction reaction against temperature. Experimental conditions were 6 barg, 10 µL/min inlet liquid flowrate of a 1.3 M benzalacetone (**3**) solution, 1.5 NmL/min hydrogen flowrate, approximately 2 mg of Pd/TiO_2 of different particle sizes.

The reaction rate also increased with pressure as shown in Figure 3-15, due to increased hydrogen solubility in the liquid phase.

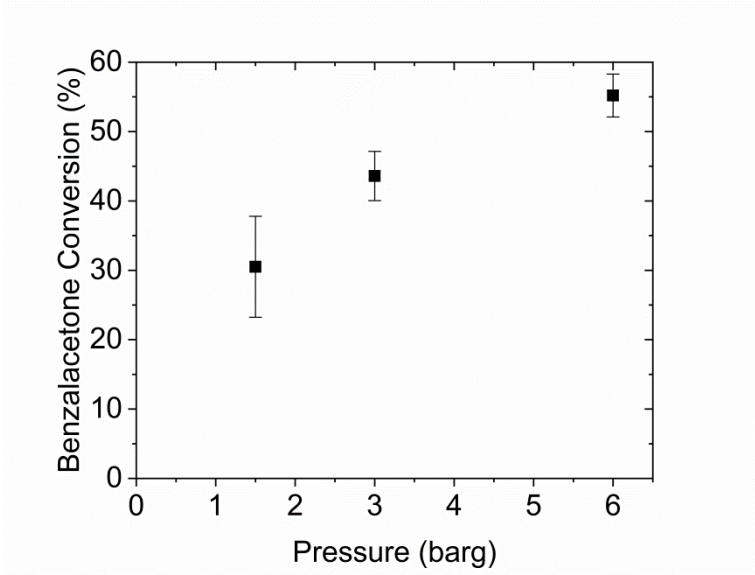

Figure 3-15 Conversion of benzalacetone (**3**) (corrected for deactivation) during the reduction reaction against pressure. Experimental conditions were 80 °C, 10 µL/min of 1.37 M feed, 1.5 NmL/min hydrogen gas flowrate, approximately 2 mg of 63-75 µm 1 wt% Pd/TiO_2.

Reaction rate also increased with benzalacetone (**3**) feed concentration and temperature, as shown in Figure 3-16a. Interestingly, selectivity was not strongly influenced by temperature, as shown in Figure 3-16b or by other variables including pressure or hydrogen gas flowrate. Importantly, the selectivity to the final desired product, benzylacetone (**4**) was very high, at approximately 90% and very little over reduction to 4-phenyl butan-2-ol (**5**) was observed.

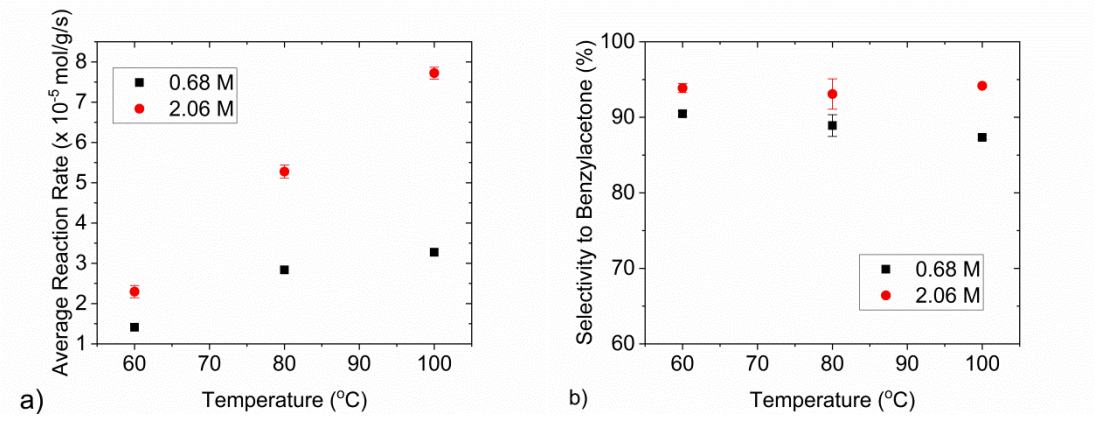

Figure 3-16 a) Average reaction rate (corrected for deactivation) of the reduction reaction against temperature. b) Selectivity against temperature. Experimental conditions were 6 barg, 10 µL/min liquid feed, 1.5 NmL/min hydrogen gas flowrate, approximately 2 mg of 63-75 µm 1 wt% Pd/TiO_2.

In order to investigate the possibility of inhibition of the reduction reaction due to unreacted reagents and side products from the previous oxidation and coupling reactions, the reduction reaction was run in isolation where known amounts of impurities were added to the inlet liquid feed stream. The results of these experiments are shown in Figure 3-17 where it is observed that many of the species do in fact inhibit the reaction. Additionally it was observed that this reaction was also inhibited by water, which is produced as a co-product in both the oxidation and aldol condensation reactions. Therefore, for the multistep flow system it may be required to use a greater mass of catalyst to compensate for the inhibition from organic species.

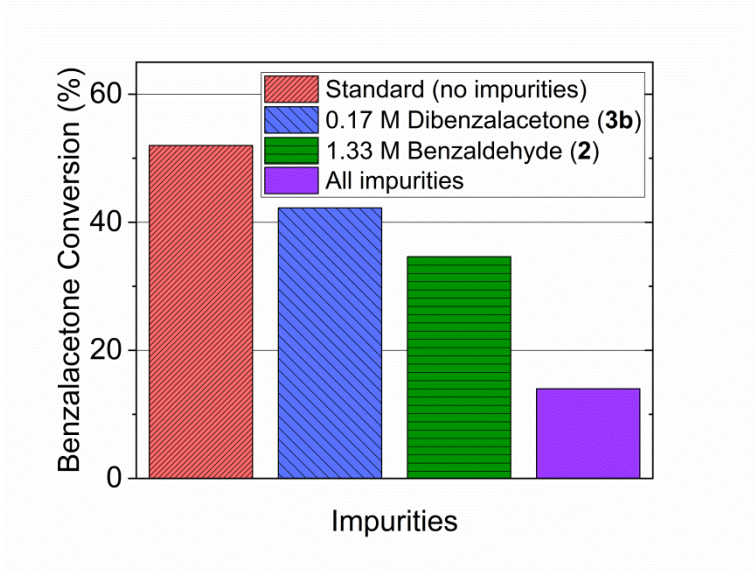

Figure 3-17 Conversion of benzalacetone (**3**) during the reduction reaction when pure feed was used (standard) and when various reaction products and by-products were added. Experimental conditions were 80 °C, 6 barg, 10 µL/min inlet liquid flow of 1.35 M benzalacetone in acetone, 1.5 NmL/min H_2 flow, 2 mg of 1 wt% Pd/TiO_2 catalyst of particle size 63-75 µm. "All impurities" refers to 0.5 M benzaldehyde (**2**), 0.05 M dibenzalacetone (**3b**), 0.43 M benzyl alcohol (**1**) and 0.04 M benzoic acid (**2d**).

After studying the 1 wt% Pd/TiO_2 catalyst, it was decided to also investigate a 1 wt% Pt/TiO_2 catalyst to check if it suffered from the same problems with water and organic species inhibition. Unfortunately, the 1 wt% Pt/TiO_2 catalyst was also inhibited by water and organic species, however at the reaction condition of 80 °C, 6 barg, 1.5 NmL/min hydrogen flow and 10 µL/min liquid flowrate, the Pt/TiO_2 catalyst displayed higher activity (92% conversion compared to 78%) and higher selectivity (95 compared to 85%) than the Pd/TiO_2, and as such it was used in all subsequent experiments for the multistep system.

3.4 Conclusions

By studying the three reactions in isolation it was possible to identify suitable operating conditions for each reaction to achieve high selectivity and conversion in the multistep

flow system. Overall it was observed that the oxidation and reduction reactions both had a fast reaction rate making it relatively easy to achieve high conversion. Furthermore, selectivites of 80% and 90% could be achieved for the oxidation and reduction reactions respectively. In contrast the aldol condensation reaction was found to be a bottleneck in this system, as its reaction rate without any impurities in the feed was only $1.5*10^{-5}$ mol g^{-1} s^{-1}, approximately an order of magnitude lower than that of the oxidation or reduction reactions. The aldol condensation reaction also could not be integrated with either the oxidation or reduction reactions, as it was shown that the aldol condensation reaction rate dropped significantly in the presence of gas flow. For this reason, oxygen gas separation will be needed immediately after the oxidation reaction in the multistep flow system, to maintain a reasonable reaction rate in the aldol condensation reaction. Finally, the reaction rate of the aldol condensation reaction was found to be further inhibited in the presence of water, an unavoidable co-product from the oxidation reaction and by benzoic acid, an undesired side product in the oxidation reaction. Similarly the reduction reaction was also found to be inhibited by water and organic side products, although as the reduction reaction is much greater than the aldol condensation this is not as great a concern. Overall the problem of water and side product inhibition for the aldol condensation reaction appears to be the greatest challenge in developing this multistep flow system.

4 Multistep Flow Synthesis: Process Integration

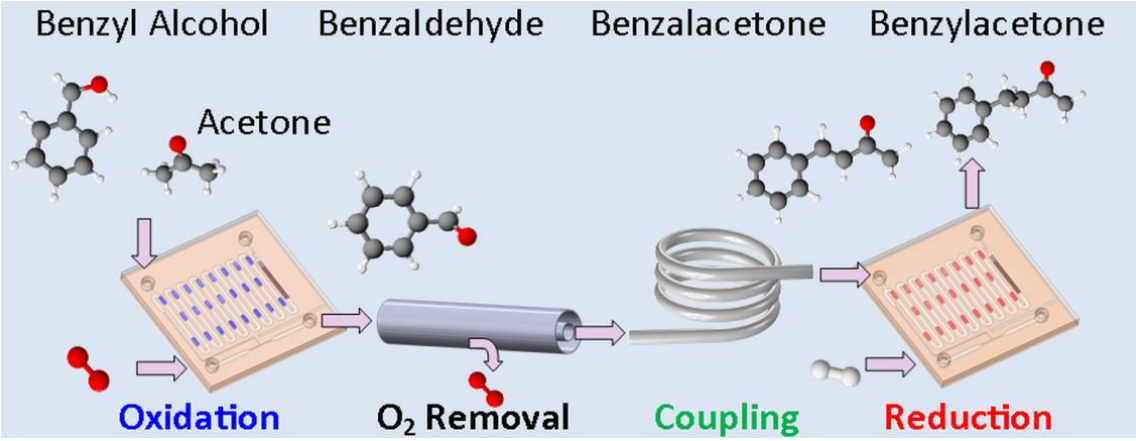

Abstract

A multistep flow system was developed involving three reactions and a gas liquid separation step that achieved maximum yields of 56% benzylacetone and 48% 4-(4-methoxyphenyl)butan-2-one from benzyl alcohol and 4-methoxybenzyl alcohol respectively. The multistep flow system identified the aldol condensation reaction as the major bottleneck in this system, and demonstrated the many problems associated with the TiO_2 catalyst used for this reaction including its low reaction rate, water inhibition and product inhibition, which restricted the system to operate with dilute feeds to keep the concentration of inhibiting species as low as possible. Modest process intensification was obtained compared to the previously reported batch system, as demonstrated by the use of lower catalyst contact times and increased space time yields. However, a major drawback of the multistep flow system was that it was not possible to use MgO supported catalysts in micropacked bed reactors due to its unsuitable mechanical properties. MgO supported catalysts were previously shown to be the optimal catalyst in the batch study, and the TiO_2 catalysts which were used in the flow system were not able to match the high yield of 63% 4-(4-methoxyphenyl)butan-2-one achieved in batch. Despite this restriction, the multistep flow system is considered to have greater potential for future improvement as each of the catalysts can be replaced individually until an optimum combination of catalysts is identified. In comparison, this is much harder to achieve in batch as all catalysts must be in the same pot and must not negatively interfere with each other.

The contents of this chapter have been published in
C. Waldron, E. Cao, S. Cattaneo, G.L. Brett, P.J. Miedziak, G. Wu, M. Sankar, G.J. Hutchings and A. Gavriilidis, “Three step synthesis of benzylacetone and 4-(4-methoxyphenyl)butan-2-one in flow using micropacked bed reactors”. *Chemical Engineering Journal,* 2019, **377**, 119976. https://doi.org/10.1016/j.cej.2018.09.137

4.1 Introduction

Using the information gained from studying the reactions in isolation a plan for the multistep flow synthesis of benzylacetone (**4**) and 4-(4methoxyphenyl)butan-2-one (**4**) was developed which involved oxygen gas separation directly after the oxidation reactor and then using a large mass of catalyst for the aldol condensation reaction to compensate for its low rate of reaction and its water and side product inhibition. The multistep flow system was operated at a variety of different feed concentrations and catalyst contact times and comparisons are then made between the multistep flow synthesis and the batch cascade synthesis [23] in order to identify which system provides greater advantages for both process intensification and for studying catalyst behaviour.

4.2 Materials & Methods

The experimental set-up for the multistep flow system (or telescoped flow system) is shown in Figure 4-1, where the reactors were connected in series with a tube-in-tube membrane separator immediately after the oxidation reactor to remove the oxygen gas. The oxidation and reduction reactions were conducted in the same silicon glass microreactors as in the previous chapter. However, the aldol condensation reaction was conducted in a tube capillary reactor as it was desired to use a catalyst mass which was greater than the maximum capacity of the silicon glass microreactors (approximately 40 mg of TiO_2). This large catalyst mass was required due to the low reaction rate of the aldol condensation reaction and to compensate for the expected reaction inhibition due to water and organic impurities. The tube reactor consisted of PTFE tubing with 1.587 mm O.D. and 1 mm I.D. (VICI Jour). The catalyst was retained in the tubing by use of a nickel mesh (Tecan, UK) of 25 µm thickness and 25 µm diameter holes which was held in place with compressive force between a PEEK union (Upchurch) and a PEEK ferrule (Upchurch). The tube reactor was heated by submerging it in an oil bath.

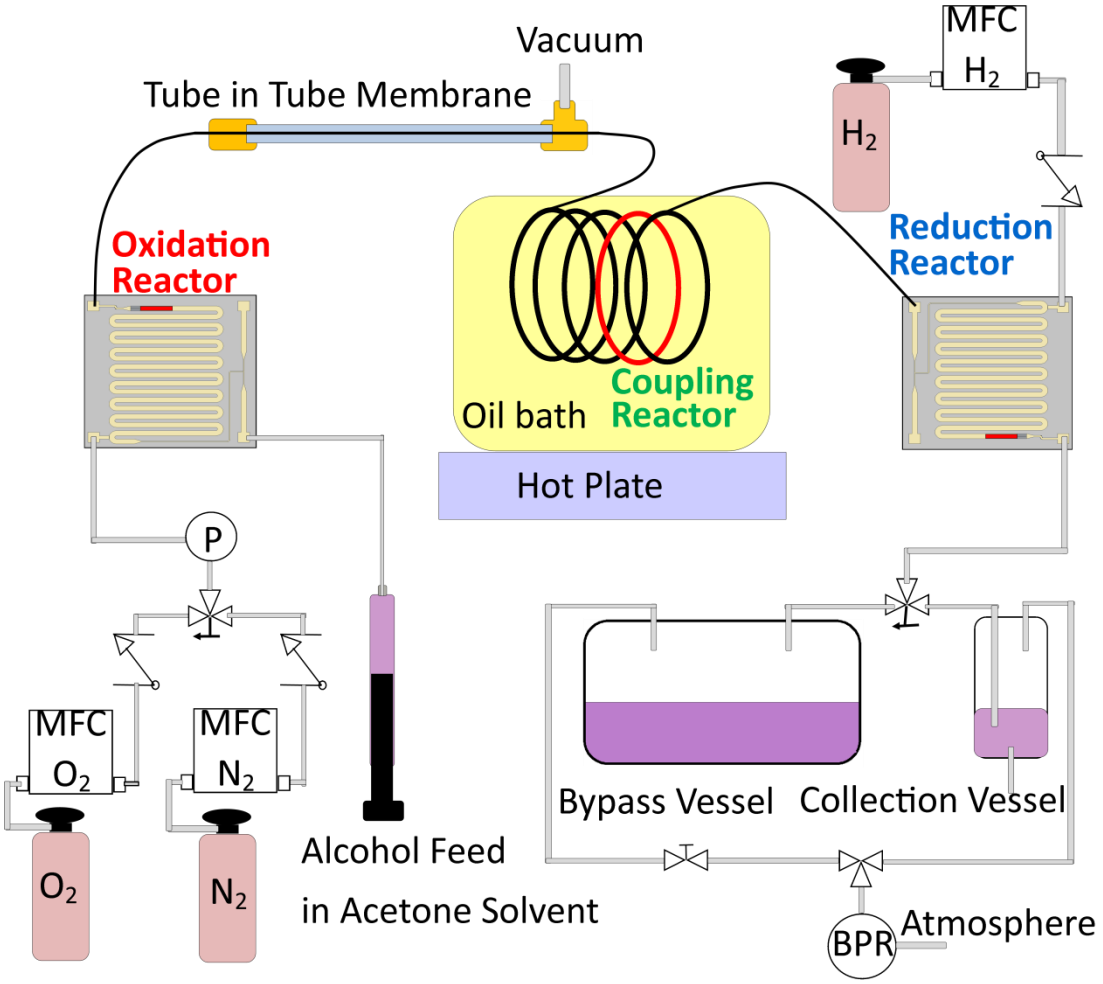

Figure 4-1 Experimental set-up for the multistep synthesis of benzylacetone (**4**) and 4-(4-methoxyphenyl)butan-2-one (**4**).

The membrane separator consisted of a 65 cm long Teflon AF-2400 tubular membrane (Biogeneral, U.S.) of I.D. 0.8 mm and thickness 0.1 mm within a 3.175 mm O.D., 2.4 mm I.D. PTFE tube (VICI Jour). The tube-in-tube membrane device operated with the gas-liquid flow in the inner tube at 6 bar pressure while the outer tube was connected to a vacuum pump (KNF labs) providing -500 mbar vacuum. The area, A (m^2), of tubular membrane required to separate the oxygen gas was calculated using Eq (4-1).

$$A = \frac{J_{O_2}\,\delta}{\Delta P\ \mathrm{K}} \qquad (4\text{-}1)$$

Where J_{O_2} (m^3/s) is the volumetric flowrate of oxygen gas to be separated, δ (m) is the thickness of the membrane, K is the membrane permeability ($m^2\ Pa^{-1}\ s^{-1}$) and ΔP (Pa) is the transmembrane pressure difference. It can then be observed that the area of membrane required to separate the gas varies with the pressure in the system. Therefore, if the multistep flow system experiences pressure changes, due to changing the gas or liquid flowrates, the area of membrane required changes. It was originally intended to use pure benzyl alcohol (**1**) for the oxidation reaction, followed by oxygen

gas separation and then mixing the separated liquid stream with acetone just before the aldol condensation reaction. However, it was found that this configuration led to pressure oscillations, leading to a non-stable operation of the membrane. Therefore, to simplify the flow management of this system, premixed benzyl alcohol (**1**) and acetone were used from the very beginning, eliminating the need for online mixing which led to pressure and flow oscillations.

In the multistep flow system, samples were collected from the outlet of the third reactor, the reduction reactor. In order to collect the sample from the system which was held at 6 barg, while causing as little disturbance to the system pressure as possible, a product collection system was created with a collection vessel and a bypass vessel, as shown in Figure 4-1. The liquid product was then analysed offline using GC as in the previous chapter. When studying the reactions in isolation, the carbon balance was shown to close to within 95%, however for the multistep flow system the carbon balance only closed to within 70-90% due to the formation of side products which the GC was not calibrated for, such as species 4b and 4c. The yield of the reaction to each species *i*, Y_i, represents the fraction of the reagent that forms species *i*, and it was calculated according to Eq (4-2) which takes into account the reaction stoichiometry. The catalyst contact time in the flow was calculated by dividing the catalyst mass, W, by the mass flowrate of alcohol as shown in Eq (4-3). Often comparisons are made between the catalyst contact time used in the flow system and the batch cascade system [23]. In the batch system the catalyst contact time was calculated by dividing the product of reaction time *t* and catalyst mass by the mass of alcohol in the reactor, which is given by the product of the reactor volume *V*, feed concentration and molecular weight of the feed alcohol $MW_{Reactant}$, as shown in Eq (4-4).

$$Y_i = \frac{C_{i\,Out} * \frac{f}{p_i}}{C_{Reactant\,In}} \tag{4-2}$$

$$Flow\ Catalyst\ Contact\ Time = \frac{W}{\upsilon * MW_{Reactant} * C_{Reactant}} \tag{4-3}$$

$$Batch\ Catalyst\ Contact\ Time = \frac{t * W}{V * MW_{Reactant} * C_{Reactant}} \tag{4-4}$$

The multistep flow system was then conducted using a variety of different feed concentrations and catalyst contact times for both the benzyl alcohol (**1**) and 4-methoxylbeznyl alcohol (**1**) systems. The standard operating conditions used, which were identified by previously studying the reactions in isolation were 115 °C, 130 °C and 120 °C for the oxidation, coupling and reduction reactions, 2 NmL/min oxygen gas flowrate and 1.5 NmL/min hydrogen flowrate with the system back pressure regulator

set to 5 barg. The catalysts used were 1 wt% AuPd/TiO_2, anatase TiO_2 and 1 wt% Pt/TiO_2.

4.3 Results & Discussion

4.3.1 Effect of Alcohol Feed Concentration

It was found that the yield of the desired product (**4**) of the telescoped flow system decreased significantly with increasing feed concentration, as shown in Figure 4-2 and Figure 4-3 for the benzyl alcohol (**1**) and 4-methoxybenzyl alcohol (**1**) systems respectively. While this drop in yield was partly due to the decreasing catalyst contact time for all reactions, the most significant cause was proposed to be the water inhibition of the aldol condensation reaction. This conclusion was reached because studies of the aldol condensation reaction in isolation, shown in the previous chapter, found that water concentration of just 2.75 wt% resulted in a 50% drop in activity. Therefore, in the multistep flow system where water is a co-product in the oxidation reaction, which is operating at nearly 100% conversion, the amount of water in the system is proportional to the initial feed concentration of alcohol in the system. It can be calculated that a feed concentration of just 1.3 M benzyl alcohol (**1**) would produce the 2.75 wt% water necessary for water inhibition to reduce the rate of reaction by 50%. This suggests that the low yields in the 1.83 M and 3.06 M experiments in Figure 4-2 can be mostly attributed to water inhibition rather than the decreasing catalyst contact times. An unexpected result shown in Figure 4-2 was the large amount of unreacted benzyl alcohol (**1**) in the final product of the multistep flow system, which increased with increasing feed concentration. This was unexpected because when the oxidation reaction was conducted in isolation at these operation conditions, conversion of nearly 100% was obtained. Furthermore, as the oxidation reaction was the first reaction in the multistep series, there could not be any problems with catalyst inhibition due to water or organic species from a previous reaction. It was later shown that the oxidation reaction was actually operating at near 100% conversion in all cases with high selectivity to benzaldehyde (**2**), however due to the low performance of the water inhibited aldol condensation reaction, significant amounts of benzaldehyde (**2**) were unreacted and passed directly on to the reduction reactor where they were converted back to benzyl alcohol (**1**), making it appear that the oxidation reaction was not performing well, which was not the case. This was later demonstrated by running the 3.06 M feed concentration experiment with nitrogen gas in the reduction reactor instead of hydrogen gas in order to turn off the reduction reaction. When the reduction reaction was stopped the amount of unreacted benzyl alcohol (**1**) then dropped to almost zero and the yield of unreacted benzaldehyde (**2**) rose dramatically to 70%, as shown in Figure 4-2.

While in the previous chapter, the reduction reaction was also shown to be inhibited by water and organic side products, this was not found to be a problem in the multistep flow system because the rate of the reduction reaction was sufficiently high that high conversion could be obtained even with some inhibition occurring. This can be observed in Figure 4-2 as there is very little unreacted benzalacetone (**3**) present for any experiment conducted.

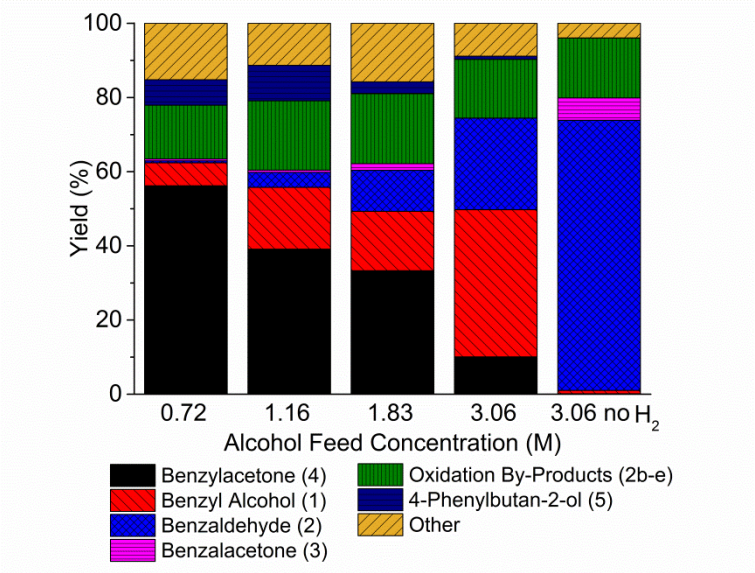

Figure 4-2 Yield of reaction products from the multistep flow synthesis of benzylacetone (**4**) in flow at four different inlet concentrations of benzyl alcohol (**1**), and from an experiment where no hydrogen gas was used (to prevent the reduction reaction). The standard experimental conditions of temperatures, pressure and gas flows were used. The mass of oxidation and reduction catalysts were approximately 10 mg for all experiments. The inlet liquid flowrate and coupling catalyst mass varied for different experiments to keep the coupling catalyst contact time to a similar value between experiments; the coupling catalyst mass was approximately 250 mg for the 0.72 M and 1.16 M experiments and 150 mg for the 1.83 M and 3.06 M experiments, while the inlet liquid flowrate was 40 µL/min, 40 µL/min, 10 µL/min and 20 µL/min for the 0.72 M, 1.16 M, 1.83 M and 3.06 M experiments respectively.

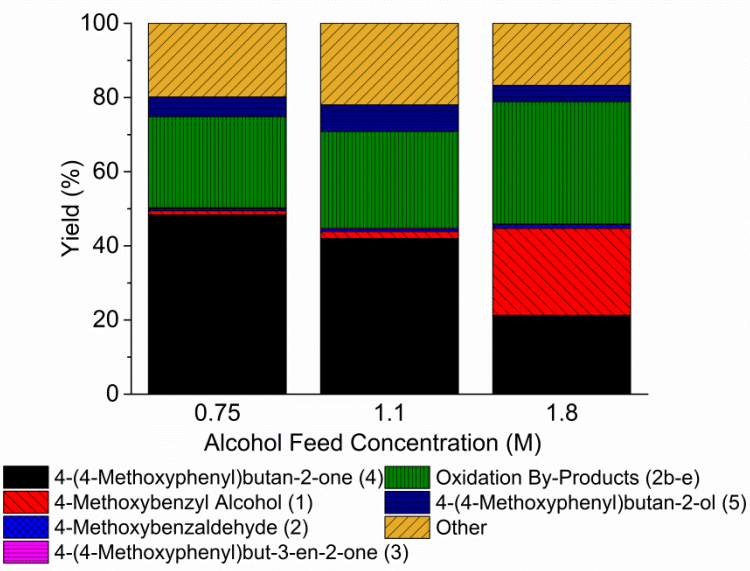

Figure 4-3 Yield of reaction products from the multistep flow synthesis of 4-(4-methoxyphenyl)butan-2-one (**4**) in flow at three different inlet concentrations of 4-methoxybenzyl alcohol (**1**). The liquid flowrate was 10 µL/min and the standard experimental conditions for temperatures, pressure and gas flowrates were used with 10 mg, 150 mg and 10 mg of catalysts for the oxidation, coupling and reduction reactions respectively.

Overall the aldol condensation reaction presented the greatest challenge in this system, as the water inhibition of the aldol condensation reaction resulted in the requirement of using dilute feed concentrations of less than 1.3 M as well as using large amounts of TiO_2 catalyst to try and achieve a high conversion of benzaldehyde (**2**) to benzalacetone (**3**). However, while the problem of low reaction rates and low conversion could be overcome by using dilute feeds and large masses of catalyst. The biggest barrier to achieving high yield was in the non-perfect selectivity of each reaction. It can be observed in Figure 4-2 that approximately 20% of the yield is lost to oxidation side products, and the “other” group, which represents approx. 10-15% of the yield, is suspected to be species 4b and 4c which are the reduced forms of dibenzalacetone (3b) which is the undesired side product of the aldol condensation reaction. Finally another 5% of yield is lost to the over reduction of the final product. These fractions observed in the multistep system are similar to the selectivites that were observed when studying the reactions in isolation, approximately 80%, 80% and 90% for the oxidation, aldol condensation and reduction reactions respectively.

4.3.2 Effect of Catalyst Contact Time

The effect of catalyst contact time was investigated for both the benzylacetone and the 4-(4-methoxyphenyl)butan-2-one system by changing the inlet liquid feed flowrate while keeping all other conditions constant. The results in Figure 4-4 for the 4-(4-methoxyphenyl)butan-2-one system, show the expected trend that at lower catalyst contact times the yield of the desired product decreases. Again the drop in yield is

attributed to the low performance of the aldol condensation reaction as demonstrated by the large amount of unreacted 4-methoxybenzaldehyde (**2**). Note that the presence of 4-methoxybenzyl alcohol (**1**) in the product is not due to low performance of the oxidation reaction, but instead due to the low performance of the aldol condensation reaction leading to unreacted 4-methoxybenzaldehyde (**2**) being converted back into 4-methoxybenzyl alcohol (**1**) in the reduction reactor. This is known because when the oxidation reaction was carried out at similar conditions or even with a lower catalyst contact time than that used in the telescoped system (9.4 mg of 1 wt% $AuPd/TiO_2$ at 115 ^{o}C, 2 NmL/min O_2 flowrate, 20 µL/min liquid flowrate of 0.96 M 4-methoxybenzyl alcohol feed at 6 bar back pressure) greater than 95% conversion was achieved. The same trend was observed for the benzylacetone system, where the aldol condensation reaction began to limit the overall system performance as the catalyst contact time was reduced, as shown in Figure 4-5.

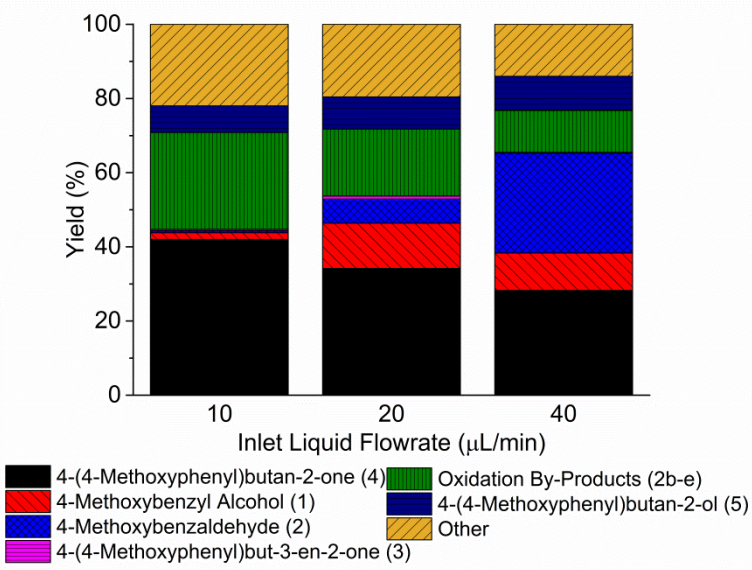

Figure 4-4 Yield for the 4-(4-methoxyphenyl)butan-2-one (**4**) system at three different inlet liquid flowrates using a 1.1 M feed of 4-methoxybenzyl alcohol (**1**). The standard experimental conditions for temperatures, pressure and gas flowrates were used with 10 mg, 149 mg and 11 mg of catalysts for the oxidation, coupling and reduction reactions respectively.

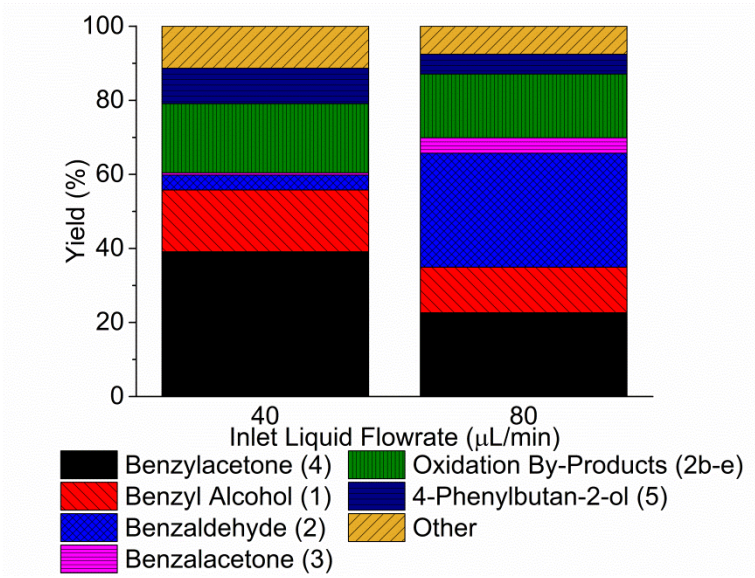

Figure 4-5 Yield for the benzylacetone (**4**) system at two different inlet liquid flowrates using a 1.15 M feed of benzyl alcohol (**1**). Standard reaction conditions for temperature, pressure and gas flowrates were used with 14 mg, 270 mg and 14.6 mg of catalysts for the oxidation, coupling and reduction reactions respectively.

It is clear from these results that the aldol condensation reaction was bottleneck of this system, as its reaction rate was approximately an order of magnitude lower than that of the oxidation or reduction reactions, and because it was strongly inhibited by water and benzoic acid which were co and by products of the previous reaction. It was attempted to overcome this problem by using very large amounts of catalyst (up to 250 mg, compared to approximately 10 mg for the oxidation and reduction reactions), however this was only partially successful. Furthermore, it is clear that the aldol condensation catalyst used in this work, TiO_2, was not particularly suited for this system for two major reasons.

1. For the aldol condensation reaction of benzaldehyde (**2**) to benzalacetone (**3**) using TiO_2 as the catalyst, the reaction was shown to be inhibited by the product. This is of immediate concern as in a multistep flow system it is desired to operate at as high conversions as possible. However, with this catalyst, due to product inhibition, it will be difficult to achieve high conversions except at low feed concentrations to keep the product concentration low.
2. This reaction was found to exhibit external mass transfer resistances at high temperatures. Therefore to maximise the rate of reaction, it is necessary to use high flowrates. However, at the same time it has been shown that to achieve high conversion it is necessary to use high catalyst contact times, hence it is necessary to use large masses of catalyst to maintain the high catalyst contact time at high flowrates. However, using high flowrates through a large packed bed leads to significant pressure drops and significantly increases the likelihood

of clogging the reactor. In this work when a flowrate of 40 µL/min was used through a 250 mg packed bed, a pressure drop greater than 1 bar was observed and the reactor clogged on more than 1 occasion forcing the experiment to end. Therefore, it can be observed that the optimum operating conditions for this catalyst of high flowrate and large catalyst masses are not practical due to the risk of clogging.

4.3.3 Comparison between Batch and Flow Operation

Having studied the multistep flow system, the best operating conditions for attaining high yields to the desired product were found to use low feed concentrations as this minimised water and side product inhibition. The best results obtained from the flow system are compared against the batch cascade [23] in Figure 4-6. It is observed that for the benzyl alcohol system that the flow synthesis achieved much higher yields of the desired product compared to the batch system, 56% compared to 8%. For the 4-methoxybenzyl alcohol (**1**) system, when comparing the flow result to the batch result when the TiO_2 catalyst was used, the flow system again attains higher yields of the desired product, 48% compared to 41%. This increase in yield is attributed to the greater flexibility of the telescoped flow system being able to perform each reaction in a separate reactor, allowing the choice of different catalysts and operating condition for each reaction.

However, for the 4-methoxybenzyl alcohol (**1**) system the best result obtained in batch actually used the MgO supported catalysts and achieved a much higher yield of the desired product than the best yield obtained in flow with the TiO_2 supported catalysts, 63% compared to 48% as shown in Figure 4-6. The poorer performance in the flow system was largely because the AuPd/TiO_2 catalyst which was used in flow, was not able to achieve the high selectivity in the oxidation reaction that the AuPd/MgO catalyst was able to achieve in batch. Unfortunately, it was not possible to use the MgO support in micropacked bed reactors, as the support particles broke into smaller particles and clogged the reactors. This demonstrates a drawback of current telescoped flow systems, in that the catalyst must be compatible with packed beds as current slurry reactors which retain the slurry in the reactor (via filtration at the reactor exit) are not reliable enough to integrate with a telescoped system. However, it is expected that the multistep system could be improved in future work, in particular if a more active aldol condensation catalyst was found. This represents one of the greatest advantages of the multistep flow system over the batch system, in that it is possible to replace the catalyst of each reaction independently without having to worry about how that would affect the other reactions. In comparison in the batch system it is very difficult to change the catalyst or add additional catalysts because as everything is in one pot, the

new catalyst must be compatible with all reactions and operate at the same reaction conditions. Therefore, the batch cascade synthesis presents a very challenging design problem with many constraints, but by swapping to flow many of these constraints are removed.

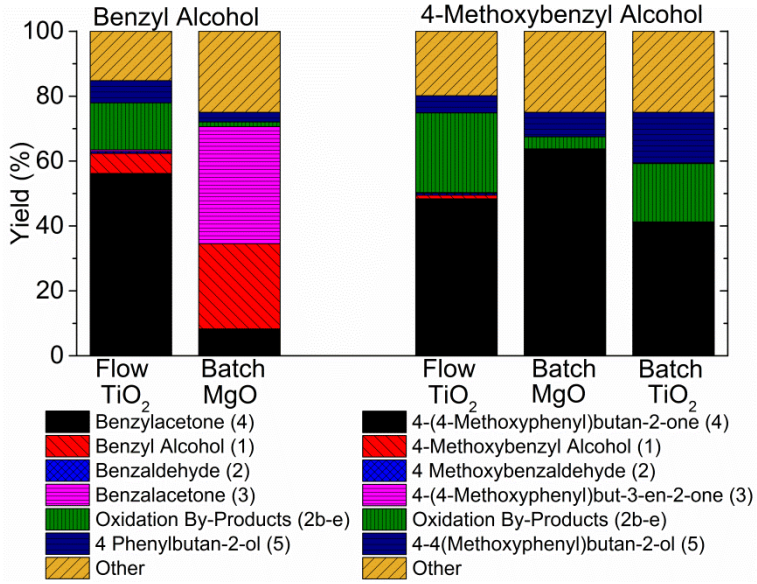

Figure 4-6 Yields of the benzylacetone (**4**) and 4-(4-methoxyphenyl)butan-2-one (**4**) systems for both the one-pot and flow experiments. In flow, only TiO_2 supported catalysts were used but in batch TiO_2 or MgO were used. The flow data is from the most dilute experiments conducted (0.72 M benzyl alcohol (**1**), 0.75 M 4-methoxybenzyl alcohol (**1**)) which produced the highest yield of the desired product. Both flow systems were run at the standard temperatures, pressure and gas flows. The benzyl alcohol (**1**) flow system had a liquid flowrate of 40 µL/min and 10.4 mg, 223 mg and 12.0 mg of catalysts for the oxidation, coupling and reduction reactions respectively. The methoxybenzyl alcohol (**1**) flow system had a flowrate of 10 µL/min and 10.1 mg, 152 mg and 9.5 mg of catalysts for the oxidation, coupling and reduction reactions respectively. Data for the one-pot experiments was taken from [39]. The batch experiments used 500 mg of 1 wt% AuPd/supported catalysts at 5 barg for 22 h and with feed concentration approximately 0.9 M, the reaction temperature was 75 ^{o}C for the TiO_2 support and 125 ^{o}C for the MgO support experiments.

In addition to comparing the batch and flow systems in terms of yield to the desired product, it is also possible to compare their catalyst requirements and productivity. It is noteworthy that the multistep flow system allowed for the replacement of significant amounts of the expensive nanoparticle supported catalysts with the cheaper TiO_2 catalyst. To process a similar amount (0.01 moles) of either feed alcohol, the batch system used 500 mg of AuPd supported catalyst, while the flow system used only 20 mg nanoparticle supported catalysts (approximately 10 mg of AuPd/TiO_2 and 10 mg of Pt/TiO_2) and 150-250 mg of the cheap anatase TiO_2. Additionally, although the catalyst contact time per gram of alcohol varied in the flow experiments due to the range of inlet liquid flowrates, feed concentrations and catalyst masses used, the experiments still suggest that the catalyst was being used more efficiently in flow than in batch. For the

flow experiments shown in Figure 4-6, which were conducted at dilute conditions but produced the maximum yield, the catalyst contact times were only 55 h $mg_{catalyst}/g_{alcohol}$ and 65 h $mg_{catalyst}/g_{alcohol}$ for the oxidation and reduction reactions and 1,190 h $mg_{catalyst}/g_{alcohol}$ for the coupling reaction. In comparison, in the one-pot system the catalyst contact time was 8,460 h $mg_{catalyst}/g_{alcohol}$. Thus, the total amount of catalysts utilised in the benzyl alcohol multistep flow system was approximately 6.5 times lower than in the one-pot system. For the 4-methoxybenzyl alcohol system the same comparisons are harder to make, as the batch reaction reached completion before the end of the 22 h, so it is unclear what time to use when calculating the catalyst contact time.

The batch and flow systems can also be compared in terms of their space time yield, which is the moles of product produced per unit time per unit reactor volume. For the batch system the space time yield is calculated using the 22 h batch duration and using the volume of the liquid in the reactor, 10.3 mL, as the volume of the reactor. The amount of product produced in batch is calculated using the known amount of alcohol in the batch (0.01 moles of benzyl alcohol and 0.009 moles of 4-methoxybenzylalcohol) and the reported conversions and product selectivity. For the flow system the rate of product produced is the alcohol feed concentration multiplied by the liquid flowrate multiplied by the product yield. The reactor volume used for the flow space time yield calculation is the combined volume of the two silicon glass microreactors (0.034 mL each) and the tube reactor (0.39 mL). For the benzyl alcohol system the space time yield of the flow system is 2.1 mol/h/L which is three orders of magnitude greater than the batch space time yield of only 0.0037 mol/h/L. For the 4-methoxybenzyl alcohol system the flow space time yield was 0.47 mol/h/L whereas in batch the space time yield using MgO and TiO_2 catalysts supports were only 0.026 and 0.017 mol/h/L respectively. The much higher space time yield in flow indicates a much higher reactor productivity level, demonstrating the advantages of flow reactors.

4.3.4 Catalyst Deactivation

Deactivation was found to be a serious problem in the batch cascade study, where reusing catalyst from one batch to the next led to a fall in conversion from 100% to 46% after a single use in hydrogen atmosphere and from 96% to 0% in nitrogen atmosphere [23]. Similarly, in this multistep flow system deactivation was also found to be a significant problem. Deactivation of up to 50% in 8 h of operation was observed when studying the coupling and reduction reactions in isolation. The problem of using deactivating catalysts in multistep flow systems could be partially overcome by using an excess of catalyst. This was demonstrated for the benzylacetone multistep flow system, as the yield of benzylacetone remained stable after 6.5 h of continuous operation, as shown in Figure 4-7. While the duration of this flow experiment (6.5 h) is

far shorter than the batch (22 h), the amount of alcohol processed is comparable, hence showing that the effect of deactivation in flow was reduced. Despite the relative stability of the system over the 6.5 h experiment, catalysts with higher stability would be needed for industrial application.

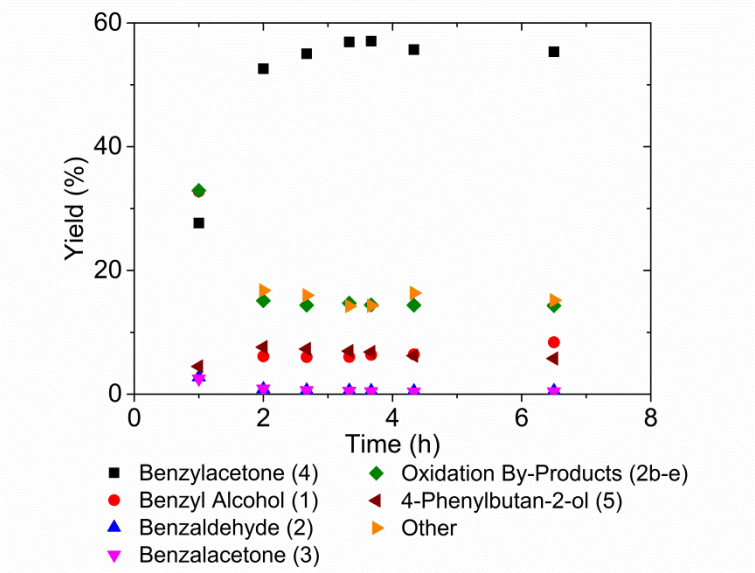

Figure 4-7 Deactivation study for the benzylacetone (**4**) multistep flow system, showing yield of various products against operation time. The standard experimental conditions of temperatures, pressure and gas flowrates were used with 10.4 mg, 223 mg and 12.1 mg of oxidation, coupling and reduction catalysts respectively and an inlet liquid flowrate of 40 µL/min of 0.7 M benzyl alcohol (**1**) in acetone.

4.4 Conclusions

The multistep synthesis of benzylacetone (**4**) and 4-(4-methoxyphenyl)butan-2-one (**4**) using AuPd, Pd and Pt supported catalysts was successfully converted from batch cascade to a multistep flow system demonstrating both the advantages and challenges of flow systems. The most critical advantage of the telescoped flow system compared to the batch cascade was the ability to separate the three reactions, oxidation, coupling and reduction, hence allowing more freedom to choose different catalysts and operating conditions without the necessity of finding a compromise among reactions. In this case this freedom enabled process intensification, reducing catalyst contact requirements by a factor of 6.5 for the benzylacetone (**4**) system and increasing the reactor space time yield by more than an order of magnitude. Furthermore, it allowed the replacement of significant amounts of expensive nanoparticle supported catalysts with cheaper anatase TiO_2 catalyst. Additionally, the flow system attained higher yields of benzylacetone compared to the batch system (56% vs 8%), and when both systems were compared using TiO_2 catalysts, the flow system attained a higher yield of 4-(4-methoxyphenyl) butan-2-one (**4**) (48% compared to 41%). However, the drawback of the telescoped flow system was that it was not possible to use the optimal MgO

supported catalysts found in the batch study, due to the unsuitable mechanical properties of MgO for micropacked bed operation. Therefore, the flow system was restricted to using only TiO_2 catalysts resulting in the flow system not being able to achieve the highest yield to 4-(4-methoxyphenyl) butan-2-one (**4**) of 63%, which was achieved in batch with the MgO supported catalyst. While in this work the selection of catalysts for the telescoped flow system was restricted to those used in batch to focus on the effect of reactor configuration (batch vs flow), it is expected that the performance of the telescoped flow system could be improved if the choice of catalysts is extended beyond the nanoparticle supported catalysts previously used in the batch system. This would be taking full advantage of the telescoped flow system's extended design space and may overcome some of the challenges encountered in this work, including water and product inhibition. The multistep flow system was also successfully used to study the catalysts in this reaction, as it helped to identify that both the aldol condensation and reduction reactions were inhibited by water and organic species, and it showed the major limitations of the aldol condensation reaction including its low reaction rate and product inhibition.

5 Rapid Kinetic Modelling: Online MBDoE for Sequential Steady-State Experiments Applied to Homogenous Esterification Reaction

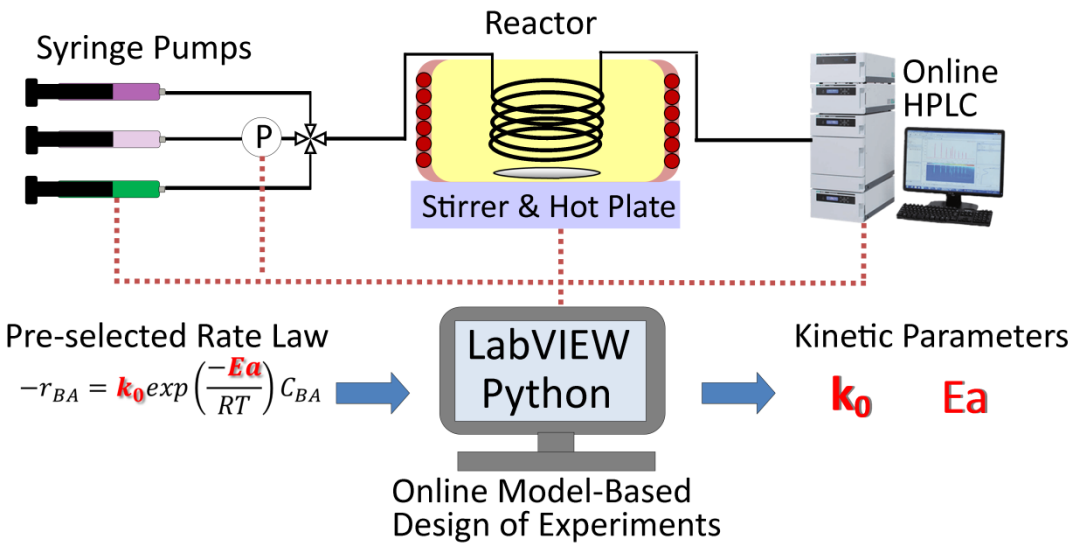

Abstract

An automated microreactor platform was developed that was able to conduct kinetic experiments without user supervision. The automated platform utilised online HPLC to measure the concentration of the product stream and if a model structure was provided by a user, the system would perform online parameter estimation. The platform could either conduct a list of steady-state experiments supplied by the user in advance, or the platform could design steady-state experiments using online D and E-optimal MBDoE. The automated system was demonstrated for the esterification of benzoic acid and ethanol using a sulfuric acid catalyst, where campaigns of 8 experiments designed by a full factorial were compared against 8 experiments designed by online MBDoE. The reaction was found to be first order with respect to benzoic acid, and it was shown that online MBDoE led to significantly more precise estimates of the kinetic parameters than the factorial experiments.

The contents of this chapter have been published in
C. Waldron, A. Pankajakshan, M. Quaglio, E. Cao, F. Galvanin and A. Gavriilidis, “An autonomous microreactor platform for the rapid identification of kinetic models”. *Reaction Chemistry & Engineering,* 2019, **4**, 1623-1636.

5.1 Introduction

The aim of this work is to develop an autonomous reactor platform which utilises MBDoE for rapid kinetic studies. The reactor platform should be flexible so that it can conduct both steady-state and transient kinetic experiments, and also so that it can be used for a wide variety of reactions. As described in the literature review in Chapter 2, a similar reactor platform has already been demonstrated for homogenous reactions [14, 41], so it is desired to go beyond the current state of the art by applying this system to more challenging heterogeneous reactions. However, before beginning with very difficult heterogeneous reactions, the automated reactor platform was first developed and tested using a simple case study, the homogenous esterification of benzoic acid and ethanol using sulfuric acid as a catalyst. This case study reaction is studied using both sequential steady-state experiments, which are presented in this chapter, and using transient experiments which are discussed in the following chapter.

5.2 Materials & Methods

5.2.1 Experimental Set-Up

The homogenous esterification of benzoic acid and ethanol with a sulfuric acid catalyst, shown in Eq (5-1), was chosen as a case study reaction due to its simplicity as there are no known side reactions and the rate of reaction is extremely slow at room temperature, so the reaction can be stopped by cooling without requiring chemical quenching [231].

$$Benzoic\ Acid + Ethanol \rightleftarrows Ethyl\ Benzoate + Water \qquad (5\text{-}1)$$

The experimental set-up is shown in Figure 5-1 and included a reactor which was a 2 m long, 250 µm internal diameter (i.d.) PEEK tube (Agilent) placed in a stirred oil bath heated by a rope heater (OMEGALUX FGR 6 foot length, 250 W). The reaction was shown not to occur without the presence of the sulfuric acid catalyst so it was possible to mix the benzoic acid and ethanol in 5 ml glass syringes (5 mL mid pressure, Cetoni) before use. Two syringes filled with different concentrations of benzoic acid in ethanol (0.85 and 1.65 M) were used to allow control of the feed concentration at any value between these two concentrations by adjusting the relative flowrates of the syringe pumps (neMESYS, low pressure module, Cetoni). The sulfuric acid concentration was kept constant at 0.163 M in the reactor by pumping a 1.63 M sulphuric acid in water solution at a flowrate 10% of the value of the total inlet flowrate. The reagents were mixed at a PEEK four-way junction with a 0.5 mm through-hole (UpChurch) before reaching the oil bath. Due to the low boiling point of ethanol and the high reaction temperatures required to produce a reasonable rate of reaction, the system was

pressurised to 6 barg to keep the reactants in the liquid phase for temperatures up to 140 °C. This was achieved by pressurising the product collection vessel with nitrogen gas from a mass flow controller (SLA mass flow controller, Brooks) and using a back-pressure regulator (Swagelok K series, 250 psig) set to the desired pressure. A pressure sensor (Honeywell 40PC, 250 psig) was connected inline with the pressure vessel to provide an accurate pressure reading of the back-pressure and a second pressure sensor (Zaiput Hastelloy, 300 psi, ≈10 µL dead volume) was placed inline in the low concentration benzoic acid line to measure the upstream pressure and hence the pressure drop, which was typically <0.2 bar. The product collection vessel consisted of a centrifuge tube (Corning 50 mL) with a custom made PEEK holder with three ports designed to withstand high pressure. Calibration of the equipment is shown in Appendix B.

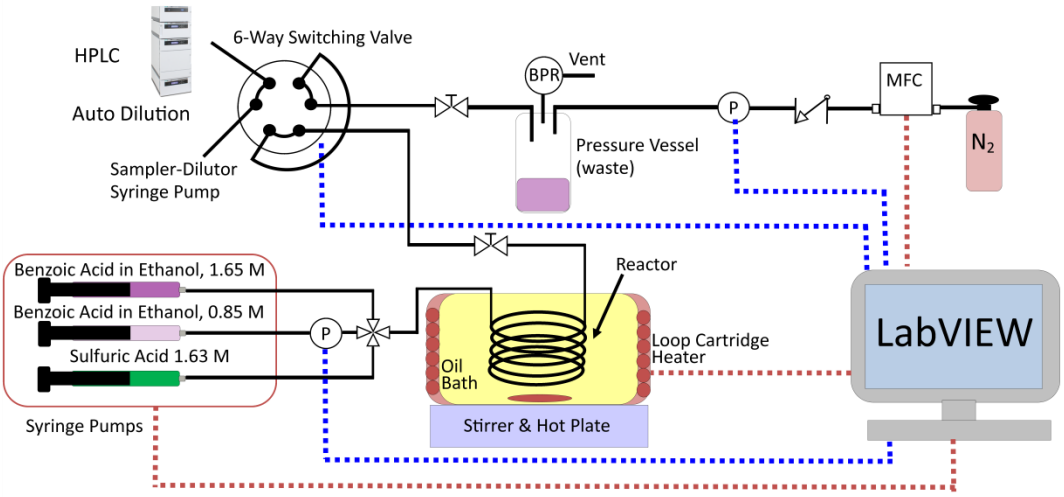

Figure 5-1 Experimental set-up for the esterification of benzoic acid with ethanol using sulfuric acid as a homogenous catalyst. Red dashed lines indicate LabVIEW controls the equipment, blue dashed lines indicate LabVIEW reads the measurement from the equipment.

The reactor outlet was connected to the 6-way switching valve of an automatic sampler-dilutor (Syrris, Asia Sampler and Dilutor), which was connected to a HPLC (Jasco LC-4000) for online concentration measurement. The sampler-dilutor had a 10 µL sample loop and a large dilution factor of 250 was used to protect the column from the sulfuric acid. The HPLC column was a 250 mm long, 4.6 mm i.d. ODS hypersil column with 5 µm particle size (Thermo Fisher Scientific). The HPLC method used 1.25 mL/min of mobile phase consisting of 40% water and 60% acetonitrile by volume and the analysis lasted 7 min. The oven was held constant at 30 °C and a UV detector at 274 nm was used for quantification of the benzoic acid and ethyl benzoate concentrations, the calibrations are shown in Appendix B. The standard deviation of the

measurement error was found from repeated identical experiments to be 0.03 M for the benzoic acid concentration and 0.0165 M for the ethyl benzoate concentration. These standard deviations were used in the constant variance model for both parameter estimation and MBDoE. The measurement error was attributed to the combination of errors in the HPLC and the sampler-dilutor.

The hydrodynamic and heat transfer characteristics of the tubular reactor were studied before beginning the kinetic experiments. Full details are shown in Appendix D, however the major findings were that the small tubing diameter resulted in approximately plug flow behaviour with very fast rates of heat transfer. Hence the reactor could be modelled as a PFR, and the reactor volume could be defined as the volume of tubing submerged in the oil bath, as it was shown that the reaction fluid changes from room temperature to reaction temperature and vice versa, very quickly at the point where the reactor tubing enters and leaves the oil bath.

5.2.2 Kinetic Models

The reactor in this work was modelled as an ideal isothermal plug flow reactor. The steady-state reactor equation is shown below

$$\frac{dC_{BA}}{dV} = \frac{r_{BA}}{\nu} \tag{5-2}$$

where C_{BA} is the benzoic acid concentration (M), V is the reactor volume (L), ν is volumetric flowrate (L s^{-1}) and r_{BA} (mol L^{-1} s^{-1}) is reaction rate. Appropriate rate laws for this reaction are then obtained from the literature. Due to the large excess of ethanol used (molar ratio greater than 9:1) the reverse reaction was assumed to be negligible. Additionally, as the excess ethanol concentration can be considered constant, the ethanol dependence in the rate law was lumped with the pre-exponential factor, hence the rate laws were functions of temperature and benzoic acid only [231]. Thus, only two different irreversible kinetic rate laws were proposed, as shown in Eq (5-3) and (5-4).

$$r_{BA} = -kC_{BA} \tag{5-3}$$

$$r_{BA} = -kC_{BA}{}^{2} \tag{5-4}$$

where k is the temperature dependent rate constant described by the Arrhenius equation, Eq (5-5), where k_0 is the pre-exponential factor (units are either s^{-1} or L mol^{-1} s^{-1} depending on if the reaction is 1st or 2nd order), E_a, is the activation energy (J/mol), R is the universal gas constant (J mol^{-1} K^{-1}) and T is temperature (K).

$$k = k_0 exp\left(\frac{-E_a}{R * T}\right) \tag{5-5}$$

However, it is known that the Arrhenius equation often leads to very high correlation between the pre-exponential factor and activation energy and that this makes parameter estimation and MBDoE very difficult [232]. Therefore, instead the rate constant *k* is described in the reparameterised form [233] shown below

$$k = exp\left(-KP1 - \frac{KP2 * 10000}{R} * \left[\frac{1}{T} - \frac{1}{T_M}\right]\right) \quad (5\text{-}6)$$

where T_M is the mean temperature 378.15 K, which was the average of the maximum and minimum temperature values, and *KP1* (dimensionless) and *KP2* (J/mol) are the kinetic parameters to be estimated. The Arrhenius pre-exponential factor, k_0, and activation energy, E_a can be calculated from the estimated parameters *KP1* and *KP2* according to Eq (5-7) and (5-8).

$$k_0 = exp\left(-KP1 + \frac{KP2 * 10000}{R * T_M}\right) \quad (5\text{-}7)$$

$$E_a = KP2 * 10000 \quad (5\text{-}8)$$

5.2.3 Experimental Protocols

Four campaigns of steady-state experiments were conducted by the automated system. The first campaign was a set of 8 steady-state experiments designed by the factorial method, and the second campaign was an identical copy of the first to test the reproducibility of the system. The third and fourth campaigns were a set of 8 steady-state experiments designed by online MBDoE for improved parameter precision using the D and E-optimal criteria. In all campaigns the three design variables were the reaction temperature, the inlet liquid flowrate and the benzoic acid feed concentration. The system pressure of 6 bar and the sulfuric acid concentration of 0.163 M were held constant for all experiments. The experimental duration for each individual experiment within a campaign was 60 min for the factorial campaign and 65 min for the MBDoE campaigns. Therefore, a campaign would take approximately 8 h to complete. The experimental duration was chosen to be long enough to ensure the reactor reached steady-state and that the HPLC would obtain a steady-state measurement before the end of each experiment. The HPLC was set to measure the reactor outlet every 7 min, however at the end of each individual experiment, only the most recent measurement was taken as the corresponding steady-state measurement for that experimental condition. The other measurements were not used by the online system, but if needed, they could be viewed by the user after the experiment was completed.

The factorial campaign design was a full factorial at two levels for the three variables. The low and high values for the factorial campaign were 120 and 140 °C for

temperature, 10 and 20 µL/min for inlet liquid flowrate and 1 and 1.5 M benzoic acid feed concentration. Starting with the second experiment, the automated system performed online parameter estimation after each successive experiment was completed, including reporting confidence intervals and t-values for each estimated parameter and testing the model adequacy with the χ^2 test. In order to conduct online parameter estimates a pre-selected kinetic model is needed, initially the first order model shown in Eq (5-3) was assumed to be true, however the data analysis could be repeated offline after the experiments were completed with any other candidate model.

In order to conduct a campaign of experiments designed by MBDoE it is first necessary to choose a model structure and to obtain an initial estimate for the parameter values. In this work, the model structure chosen was the steady-state PFR model in Eq (5-2) combined with a first order rate law, Eq (5-3). This model structure was chosen based on the results of the factorial campaign which will be discussed later. This demonstrates one of the drawbacks of MBDoE, that it is required to know the model structure in advance. However, often this can be obtained from the literature or from performing a few factorial experiments, or even experiments designed by MBDoE for model discrimination. MBDoE algorithms require an initial estimate for the parameter values. However, in order to allow as fair a comparison of the Factorial and MBDoE campaigns as possible, it was not desired to use the final parameter estimates from the steady-state campaign to be the initial parameter estimate for the MBDoE campaign. For this reason, the first two experiments of the MBDoE campaign were pre-selected by the user in advance. The two experiments chosen were two of the factorial experiments, the first being 140 ^{o}C, 20 µL/min, 1.5 M benzoic acid feed concentration and the second being 120 ^{o}C, 10 µL/min, 1 M benzoic acid feed concentration. Only after conducting these two experiments would the autonomous system perform online parameter estimation and then use the obtained parameter estimates to conduct either D or E-optimal MBDoE to design the next experiment. Therefore, the two MBDoE campaigns each consisted of two pre-selected experiments followed by 6 experiments designed by sequential MBDoE. The allowed range for each of the three design variables (temperature, flowrate and benzoic acid feed concentration) were 70-140 ^{o}C, 7.5-30 µL/min and 0.9-1.55 M.

5.2.4 Selection of Optimisation Algorithms

In order to conduct online parameter estimation it was necessary to maximise the loglikelihood function shown in Eq (2-6). This was done by minimising the negative of the loglikelihood function using the Nelder-Mead simplex algorithm in the SciPy Python package. The initial guesses for the parameter values *KP1* and *KP2* required by this

algorithm were 8.97 and 7.6 based on some initial experiments. The Nelder-Mead method is a local optimisation algorithm which uses the direct search method, meaning it does not need to compute the values of derivatives [173]. This algorithm was chosen because it does not need to compute derivatives or Hessians which can be computationally expensive and because it gave reliably good results when used offline. The default SciPy convergence criteria for the Nelder-Mead algorithm were used, which were that the difference between the optimised parameter values in the final iteration and the previous iteration must be less than 0.0001 and also that the function value in the final iteration and the previous iteration must be less than 0.0001. The SciPy default settings for the maximum number of iterations is 200 times the number of variables to be optimised, so for this case study with 2 parameters to be optimised the maximum number of iterations was 400. In the online parameter estimation code this limit was increased to 2,000 however this was later found to be unnecessary as typically less than 50 iterations were required before the optimiser met the convergence criteria and terminated. The Nelder-Mead optimiser with the previously described settings was used for all parameter estimation problems in this thesis.

MBDoE was conducted by minimising either the determinant or the largest eigen value of the expected covariance matrix, shown in Eq 2-18. In all cases in this thesis the MBDoE optimisation problem was solved using the SLSQP (Sequential Least Squares Programming) algorithm which is a gradient based method that can handle constraints. This algorithm was chosen as MBDoE is a constrained optimisation problem where the optimised experimental conditions must be within an allowed range. To prevent getting stuck in a local optimum, 10,000 randomly generated designs uniformly spread over the allowable design space were screened, and the best design was used as the initial guess for the SLSQP optimiser. The value of 10,000 was chosen as it was a sufficiently large value to cover the entire three-dimensional design space (temperature, flowrate and feed concentration), but it was not so large that it led to large computational times which would be undesirable in an online system. For the SLSQP optimiser the convergence criterion was changed from its default value of 1E-6 to 1E-20 and the maximum number of iterations was increased from 100 to 10,000. While decreasing the convergence tolerance from its default value of 1E-6 did improve the performance of the optimiser, choosing a value of 1E-20 was later shown to be excessive and a value of 1E-10 may have been more appropriate as it gave almost identical results as the 1E-20 setting. However, even with the very small convergence criterion of 1E-20, it was shown that the optimiser would successfully terminate within 50 iterations and that the code would take approximately 1 minute to run which was acceptable for the online system.

5.2.5 Automation

The autonomous platform was developed using a combination of LabVIEW (National Instruments) and Python, where LabVIEW was used to control lab equipment and monitor process values and Python was used to perform online parameter estimation, online MBDoE and also reading and writing the experimental results to Excel files. The advantage of using LabVIEW is that many commercial manufacturers of lab equipment make instrument drivers specifically for LabVIEW. Therefore, LabVIEW and its large collection of instrument drivers enable the quick integration of multiple pieces of equipment. A detailed description of how the LabVIEW code worked is provided in Appendix D, including its use of online parameter estimation, MBDoE and its various safety shutdown features.

One of the common problems of autonomous systems is that they are task-specific and that small changes in the experimental set-up require significant work to update the system. This can lead to situations where it is faster to conduct experiments manually than to develop automation algorithms for each new version of an experimental set-up [32]. However, the LabVIEW code developed can be used with different equipment types, allowing this platform to be used for numerous reaction systems with only minor changes to the LabVIEW code. For example, without changing any LabVIEW code it is possible to replace the rope heater oil bath with a cartridge heater typically used to heat silicon-glass or glass microreactors. Additionally, with some simple changes to the LabVIEW code it is possible to incorporate different analysis methods, such as online Raman, UV or IR spectroscopy if such equipment were available. Therefore, the same LabVIEW code developed here is also used in Chapters 7 and 8 and is also being used for future projects by the Gavriilidis' research group.

5.3 Results & Discussion

5.3.1 Factorial Experiments

The results of the two identical Steady-State Factorial campaigns (shown graphically in Figure 5-2 and numerically in Table 5-1) showed that the system behaved well with high reproducibility. It was also shown that the mole balance always closed to within 5%, where the mole balance was calculated according to Eq (5-9) as the difference in the total outlet and inlet concentrations divided by the inlet concentration.

$$Mole\ Balance\ \% = 100 * \frac{C_{BA,in} - C_{BA,out} - C_{EB,out}}{C_{BA,in}} \qquad (5\text{-}9)$$

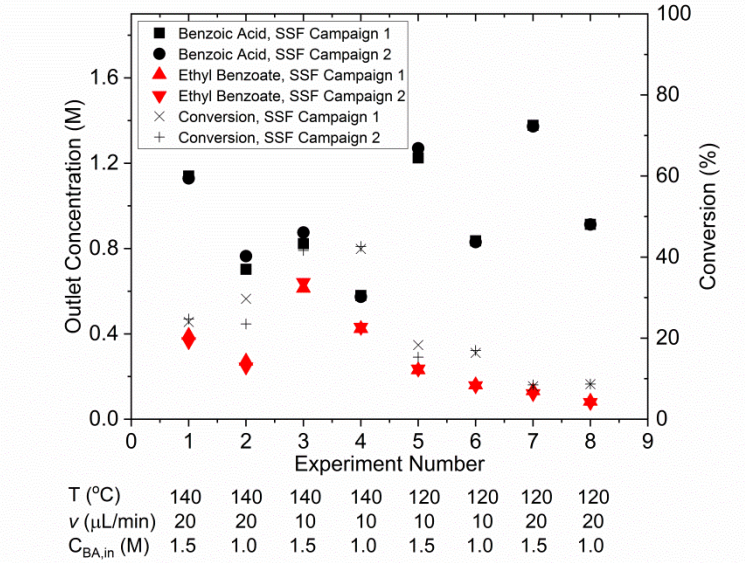

Figure 5-2 Outlet concentrations of benzoic acid and ethyl benzoate and benzoic acid conversion for the two identical Steady-State Factorial (SSF) campaigns, each consisting of 8 steady-state experiments.

Table 5-1 Experimental conditions, benzoic acid conversion, outlet concentrations of benzoic acid (BA) and ethyl benzoate (EB) and mole balance for the Steady-State Factorial campaign 1 (SSF 1) and 2 (SSF 2).

Exp	Temp.	Flowrate	Feed Conc. BA	Conversion		Outlet Conc. BA		Outlet Conc. EB		Mole Balance	
	°C	µL/min	M	%	%	M	M	M	M	%	%
				SSF 1	SSF 2	SSF 1	SSF 2	SSF 1	SSF 2	SSF 1	SSF 2
1	140.0	20	1.5	24.0	24.7	1.14	1.13	0.39	0.36	-2.0	0.7
2	140.0	20	1.0	30.0	23.0	0.70	0.77	0.27	0.25	3.0	-2.0
3	140.0	10	1.5	45.3	41.3	0.82	0.88	0.61	0.64	4.7	-1.3
4	140.0	10	1.0	42.0	43.0	0.58	0.57	0.42	0.43	0.0	0.0
5	120.0	10	1.5	18.0	15.3	1.23	1.27	0.23	0.24	2.7	-0.7
6	120.0	10	1.0	16.0	17.0	0.84	0.83	0.16	0.16	0.0	1.0
7	120.0	20	1.5	8.0	8.7	1.38	1.37	0.13	0.12	-0.7	0.7
8	120.0	20	1.0	9.0	9.0	0.91	0.91	0.08	0.08	1.0	1.0

In order to identify the appropriate rate law from the two candidate models described in Eq (5-3) and (5-4), the χ^2 data fitting test was applied to the data obtained from the factorial campaigns for both models. The results of the χ^2 test are shown in Table 5-2, where it is observed that Eq (5-4), which has 2nd order kinetics with respect to benzoic acid, must be rejected.

Table 5-2 Data fitting results for two candidate kinetic models using experimental data from the two identical Steady-State Factorial campaigns.

Eq	Model	X^2 (X^2 ref = 43.7)	Result
(5-3)	$r = kC_{BA}$	16.2	Possible model
(5-4)	$r = kC_{BA}{}^2$	156	Reject model

As only a single candidate model remained after the initial factorial screening, it was not necessary to conduct further experiments designed by MBDoE algorithms for model discrimination [38]. The estimated parameter values of *KP1* and *KP2* obtained from a single campaign of 8 experiments designed by the Steady-State Factorial campaigns were 9.11 and 7.98. These estimates correspond to a pre-exponential of 11.65×10^6 s^{-1} and activation energy of 79.8 kJ/mol. In the literature the activation energy for this reaction has been reported as 80.5 kJ/mol [231], which is in agreement with our results.

5.3.2 MBDoE Experiments

The experimental conditions designed by the two steady-state MBDoE campaigns, D and E-optimal, are shown in Figure 5-3 and numerically in Table 5-3 and Table 5-4.

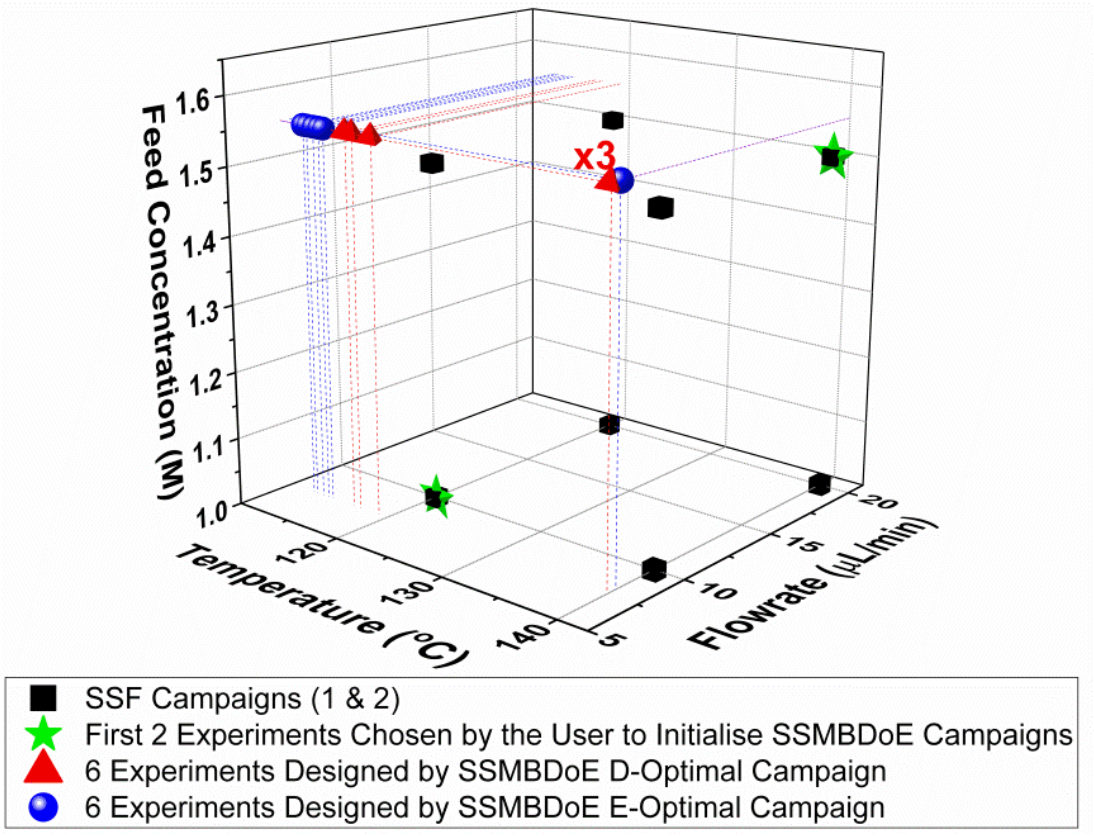

Figure 5-3 Experimental conditions utilised by the Steady-State Factorial (SSF) and Steady-State MBDoE (SSMBDoE) campaigns.

Table 5-3 Experimental conditions, benzoic acid conversion, outlet concentrations of benzoic acid (BA) and ethyl benzoate (EB), kinetic parameter estimates and statistics for the Steady-State MBDoE D-Optimal campaign.

Exp	Temp.	Flowrate	Feed Conc. BA	Conversion	Outlet Conc. BA	Outlet Conc. EB	KP1	KP2	X^2	X^2 ref
	°C	µL/min	M	%	M	M				
1	140.0	20	1.5	22.7	1.16	0.36	-	-	-	-
2	120.0	10	1.0	15.0	0.85	0.16	9.10	7.80	0.43	8.76
3	119.1	7.5	1.55	16.8	1.29	0.30	9.16	7.99	1.60	12.8
4	140.0	7.5	1.55	50.3	0.77	0.83	9.19	8.26	4.49	16.2
5	116.6	7.5	1.55	14.2	1.33	0.26	9.17	8.20	5.82	19.5
6	140.0	7.5	1.55	50.3	0.77	0.81	9.17	8.15	6.70	22.6
7	117.3	7.5	1.55	14.2	1.33	0.28	9.16	8.13	9.98	25.5
8	140.0	7.5	1.55	51.0	0.76	0.82	9.16	8.14	10.9	28.4

Table 5-4 Experimental conditions, benzoic acid conversion, outlet concentrations of benzoic acid (BA) and ethyl benzoate (EB), kinetic parameter estimates and statistics for the Steady-State MBDoE E-Optimal campaign.

Exp	Temp.	Flowrate	Feed Conc. BA	Conversion	Outlet Conc. BA	Outlet Conc. EB	KP1	KP2	X^2	X^2 ref
	°C	µL/min	M	%	M	M				
1	140.0	20	1.5	22.0	1.17	0.37				
2	120.0	10	1.0	14.0	0.86	0.16	9.16	8.13	1.52	8.76
3	112.8	7.5	1.55	11.6	1.37	0.21	9.17	8.19	2.23	12.8
4	112.4	7.5	1.55	12.3	1.36	0.20	9.17	8.19	2.26	16.2
5	140.0	7.95	1.55	47.7	0.81	0.78	9.17	8.11	3.82	19.5
6	114.4	7.5	1.55	12.3	1.36	0.23	9.16	8.09	5.01	22.6
7	113.4	7.5	1.55	12.9	1.35	0.21	9.16	8.10	5.16	25.5
8	114.0	7.5	1.55	12.3	1.36	0.22	9.17	8.12	6.23	28.4

After the initial two experiments chosen by the user to be the opposite corners of the previously used factorial design space, the autonomous platform executed MBDoE algorithms to design each experiment sequentially, using the information gathered from previous experiments. It is observed that the MBDoE algorithms always designed

experiments with the maximum feed concentration of benzoic acid (1.55 M) and minimum flowrate (7.5 µL/min). The optimum temperature for experiments was found to alternate between the maximum temperature allowed of 140 °C and lower temperatures in the range 110 to 120 °C. For the D-optimal campaign the MBDoE algorithm choose to run the exact same experimental conditions (140 °C, 7.5 µL/min, 1.55 M) three times, whereas the E-optimal campaign only designed one experiment at this condition and placed the other five designed experiments in the low temperature region. The E-optimum campaign explored lower temperatures than the D-optimum, possibly because the wider temperature range explored helped to reduce correlation between the two parameters.

The parameter estimates and the associated statistics (including t-values, confidence intervals and χ^2 tests) from the Steady-State Factorial and the Steady-State MBDoE experiments are compared in Table 5-5. All parameter estimates and associated statistics in this chapter and in the rest of this thesis were computed using Python and were separately confirmed using the gPROMs Model Builder software (PSE). The parameter estimates are similar for all campaigns, however the 95% confidence intervals are substantially smaller and the t-values substantially larger for the MBDoE campaigns. This demonstrates the benefits of online MBDoE for identifying kinetic models. As there are only two parameters in this model it is also possible to show these results graphically in the form of confidence ellipsoids in Figure 5-4, where we can observe that both the Steady-State MBDoE campaigns produce confidence ellipsoids which are much smaller than the Steady-State Factorial campaigns. Similarly, it is observed that the E-optimal campaign produces a shorter (but "fatter") confidence ellipsoid than the D-optimal campaign, as the E-optimal campaign aims to minimise the length of the longest axis of the confidence ellipsoid.

Table 5-5 Parameter estimates and statistics obtained from the Steady-State Factorial (SSF) and the Steady-State MBDoE (SSMBDoE) campaigns.

Campaign	KP1 ± 95% Confidence Interval	KP2 ± 95% Confidence Interval	KP1 95% t-value	KP2 95% t-value	t ref	χ^2	χ^2 ref	k_0 (s^{-1})	E_a (kJ/mol)
SSF 1	9.06 ± 0.19	7.84 ± 0.75	48.0	10.5	1.76	14.9	23.7	$7.8*10^6$	78.4
SSF 2	9.11 ± 0.19	7.98 ± 0.77	46.9	10.4	1.76	0.98	23.7	$11.7*10^6$	79.8
SSMBDoE D-optimal	9.17 ± 0.12	8.15 ± 0.46	79.1	17.6	1.76	10.6	23.7	$18.8*10^6$	81.5
SSMBDoE E-optimal	9.17 ± 0.10	8.12 ± 0.43	95.5	18.8	1.76	6.1	23.7	$17.1*10^6$	81.2

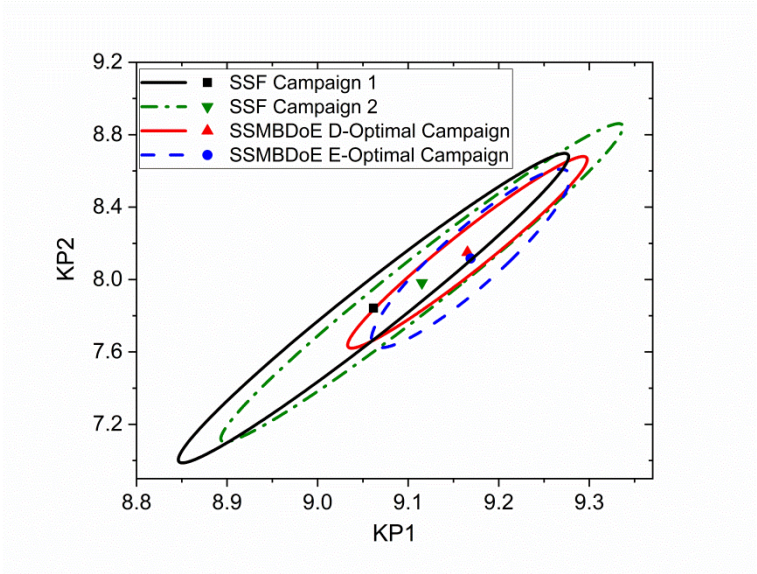

Figure 5-4 Statistical certainty of the parameters KP1 and KP2 for the Steady-State Factorial (SSF) and Steady-State MBDoE (SSMBDoE) D and E-Optimal campaigns, as illustrated by the 95% confidence ellipsoids.

Additionally, Figure 5-5 shows the diminishing return on conducting multiple experiments. For both the Steady-State Factorial and the Steady-State MBDoE campaigns, after conducting five experiments, the determinant of the covariance matrix (directly proportional to the volume of the confidence ellipsoid) did not get much smaller with further experiments in the allowable design space.

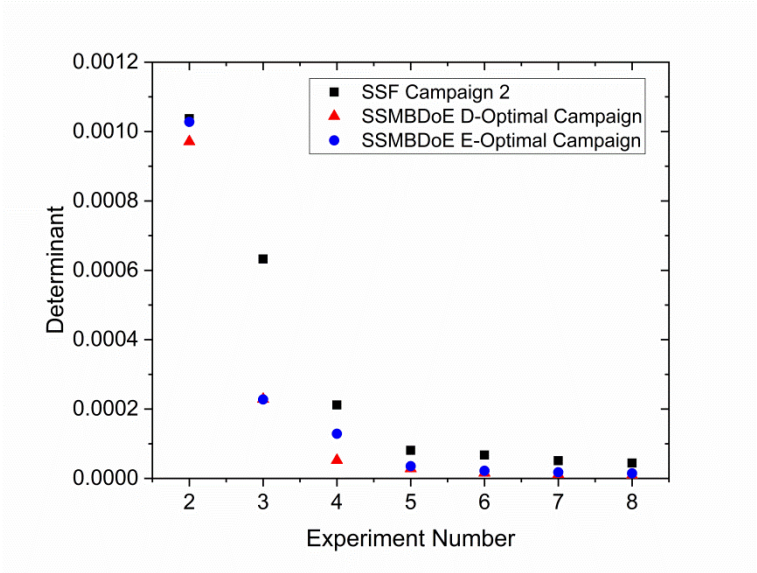

Figure 5-5 Determinant of the covariance matrix against number of experiments conducted for the Steady-State Factorial (SSF) and the Steady-State MBDoE (SSMBDoE) D and E-Optimal campaigns.

The occurrence of repeated experiments designed by MBDoE methods for improved parameter precision may appear surprising at first as it intuitively appears that more information can be gathered by studying a wider design space, however the occurrence of replicates is well documented in the literature [233-235]. This is because MBDoE for improved parameter precision is not trying to find the domain in which the model is valid. Instead MBDoE for improved parameter precision assumes that the chosen model is the "true" model. In this situation with 100% certainty in the model in all locations of the design space, it is more useful for obtaining precise parameter estimates to repeatedly conduct experiments in a highly informative region instead of conducting experiments spread across a wide but lowly informative design space. This concept can be easily explained using the simple example of a linear model with one control variable x, and one parameter to be estimated, a.

$$y = a * x \tag{5-10}$$

In this case it is obvious that if the measurement y, has a fixed measurement error, that the optimum experimental value to identify a with the highest precision is the maximum value of x. Therefore, with any number of experiments, in order to get the most precise estimate for the parameter a it is always best to repeatedly run at the maximum value of x.

The only situation where studying a wide range of conditions would be preferable to repeatedly running the same high information experiment, is if there is a low confidence in the model structure. In such a situation it would be better to design experiments with factorial methods, or using robust MBDoE methods which take into consideration parameter uncertainty [191-193], or to use experiments designed by MBDoE for model discrimination to identify a model with greater confidence before progressing to MBDoE for improved parameter precision.

5.4 Conclusions

In this work an autonomous microreactor platform for the rapid identification of reaction kinetics has been developed. This platform combines the advantages of flow microreactors, online analysis and automation to create a lab tool that can save researchers time and resources. Using the case study of esterification of benzoic acid and ethanol with homogenous sulfuric acid catalyst, the platform was tested to conduct unsupervised campaigns of 8 experiments designed by the full factorial method, and by D and E-optimal MBDoE for improved parameter precision. All experimental campaigns required only 8 h of operation and successfully estimated the kinetic parameters. It was shown that online MBDoE led to considerably more precise parameter estimates than a

campaign of factorial experiments, hence demonstrating the considerable advantage of MBDoE in rapid kinetic model identification. However, the MBDoE experiments were found to be clustered in a very small area of the experimental design space, which can result in making it difficult to test the validity of a model. Therefore, this offers a clear warning that MBDoE should only be used when there is already high confidence in the model, especially because experiments designed by MBDoE with an incorrect model, or with the correct model but with poor parameter estimates, can result in non-optimum experimental designs which lead to the generation of very little information.

6 Rapid Kinetic Modelling: Offline MBDoE for Transient Experiments, Applied to Homogenous Esterification Reaction

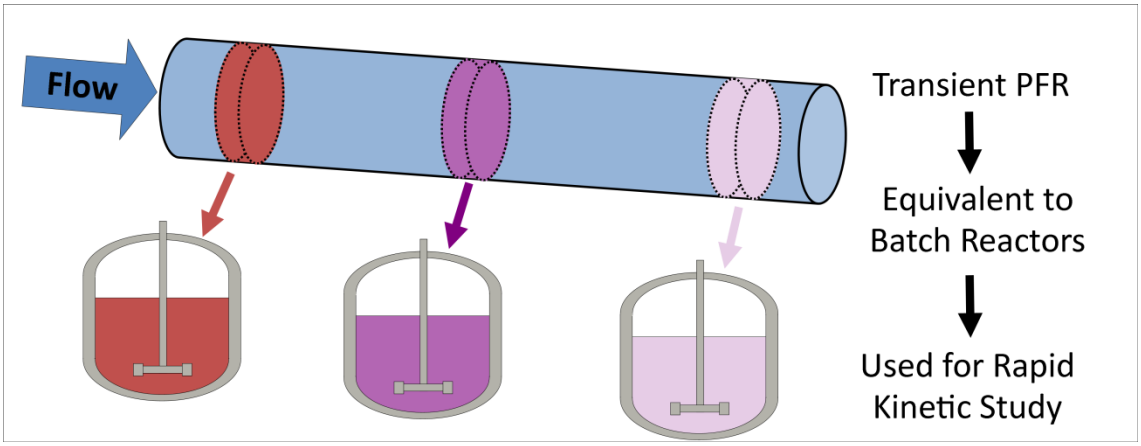

Abstract

For the case study of benzoic acid and ethanol esterification, transient experiments allowed the estimation of kinetic parameters in just 2 h compared to the 8 h required if steady-state experiments were used. The parameter estimates from the steady-state and transient experiments were in agreement with each other and could successfully be used to predict reactor behaviour. Offline MBDoE was found to be necessary for the design of transient multi variable ramp experiments, as this experiment design was very non-intuitive. Additionally, when offline MBDoE was used the precision of the parameter estimates obtained from the multivariate ramp experiment was similar to the precision obtained from the campaigns of steady-state experiments which required 8 h of operation. Ramping only flowrate required two experiments to be conducted at different temperatures to allow the estimation of the kinetic parameters. Therefore, ramping temperature and flowrate simultaneously offered considerable benefits as only one experiment was required. However, ramping temperature, flowrate and concentration simultaneously offered no additional benefit for this case study, as it was always preferable to use high feed concentrations.

The contents of this chapter have been accepted for publication
C. Waldron, A. Pankajakshan, M. Quaglio, E. Cao, F. Galvanin and A. Gavriilidis, “Model-Based Design of Transient Flow Experiments for the Identification of Kinetic Parameters”. *Reaction Chemistry & Engineering,* 2019.

6.1 Introduction

In the previous chapter, it was shown that the online design of sequential steady-state experiments using MBDoE for improved parameter precision was very successful for the rapid identification of kinetic models. However, while the steady-state experiments led to the identification of very precise parameter estimates, the experimental campaign took a long time, requiring 8 h of operation. The major bottleneck in these steady-state experiments is that it is required to wait for long periods of time for the reactor to reach steady-state for each experimental condition. Therefore, the objective of this chapter is to use transient experiments combined with offline MBDoE to obtain highly precise parameter estimates in a much shorter amount of time as it is no longer required to wait for the reactor to reach steady-state.

A common method of operating transient flow reactors for kinetic studies is to ramp control variables such as flowrate [12, 34, 36] or temperature [174, 175] and monitoring the outlet concentration. Note that ramping the flowrate to a Plug Flow Reactor (PFR) is mathematically equivalent to running a batch reactor. To explore an even greater range of conditions in a single experiment it is also possible to ramp multiple control variables simultaneously [33, 37]. Alternative methods of running transient flow reactors include introducing step changes to the PFR, however this is more difficult to achieve experimentally, as it is often not physically possible to achieve perfect step changes in many variables such as temperature or flowrate [176]. Using sinusoidal input profiles has also been investigated, but this led to experimental difficulties and did not offer any substantial benefits compared to linear ramps [37]. Therefore, in this work only the ramp style transient PFR experiment will be considered as it is the easiest transient protocol to implement experimentally. Furthermore, the kinetic behaviour of a PFR under transient ramp conditions can be modelled using a system of ODEs rather than PDEs. This feature typically results in a reduction of computational power required to identify kinetics from transient experiments [33] and it simplifies the MBDoE optimisation problem.

Transient flow reactors have already been successfully applied to a number of kinetic studies for homogenous reactions [12, 33-35, 176], for gas liquid reactions [134] and for gas phase catalytic reactions [175]. However, recent work has shown that the design of the ramp transient experiment is crucial for producing highly informative data and that a good design is not intuitive, especially for experiments where multiple variables are ramped simultaneously [33]. Therefore, there is a clear need for MBDoE techniques to assist in this challenging experiment design. When designing a ramp transient experiment the researcher must choose the initial value for all variables of

interest (most commonly flowrate, feed concentration, temperature) and also choose the ramp rate for each variable. The simplest transient experiments to design are the single variable ramps, such as where only flowrate [12, 34, 36] or temperature [134] are ramped while other variables are held constant. Here, it is only necessary to choose the upper and lower limit of the ramped variable which sets how much of the design space is explored, and to choose the ramp rate, which decides the experiment duration and the number of data points obtained. However, when choosing the values of the other variables which are not ramped, the constant variables, researchers often resort to standard factorial design of experiments (or fractional designs and similar methods), which may result in requiring a large number of experiments [12, 34, 36]. For situations where multiple variables are ramped simultaneously [33], the experimental design becomes more difficult. While intuitively a researcher might choose initial values and ramp rates so that over the course of the experiment a wide range of flowrates, feed concentrations and temperatures were studied, this often can lead to a low information experiment. The challenge in designing ramp transient experiments is demonstrated in the literature as trial and error is often required to obtain satisfactory experiment designs [33]. To address this challenge, in this chapter MBDoE for improved parameter precision is applied to design ramp transient PFR experiments for both single variable ramps and multi variable ramps, and these results are compared against traditional methods of experiment design using researcher intuition. While MBDoE has previously been applied to transient flow experiments, this was for the purposes of model discrimination [35] and to the best of the author's knowledge MBDoE has not been applied to transient microreactors for the purpose of precise estimation of the kinetic parameters.

6.2 Materials & Methods

6.2.1 Reaction & Experimental Set-Up

The same reaction that was previously used in Chapter 5, the esterification of benzoic acid and ethanol using a sulfuric acid catalyst, shown in Eq (6-1), is used again in this Chapter.

$$Benzoic\ Acid + Ethanol \rightleftarrows Ethyl\ Benzoate + Water \qquad (6\text{-}1)$$

The focus of the work in this chapter is precise parameter estimation, not model discrimination (although similar MBDoE techniques could be used for the design of transient experiments for model discrimination). Therefore, using the results of the previous chapter, it is assumed that the reaction rate r_{BA}, can be modelled as a first order reaction with respect to benzoic acid, as shown in Eq (6-2)

$$r_{BA} = -kC_{BA} \tag{6-2}$$

where C_{BA} is the concentration of benzoic acid and k is the pre-exponential factor which is described in the re-parameterised form shown in Eq (6-3)

$$k = exp\left(-KP1 - \frac{KP2 * 10000}{R} * \left[\frac{1}{T} - \frac{1}{T_M}\right]\right) \tag{6-3}$$

where *KP1* and *KP2* are the kinetic parameters to be estimated, *R* is the universal gas constant (J/mol K), *T* is reaction temperature (K) and T_M is the mean temperature 378.15 K, chosen as the average value between the maximum and minimum temperatures used in this work.

The same experimental set up that was used in the previous chapter for steady-state experiments is used again in this chapter for transient experiments, and is shown again in Figure 6-1. For transient experiments it is preferable to have the measurement directly at the reactor exit, however if this is not possible, then the volume of tubing between the reactor outlet and the measurement location must be accurately known. In this work the HPLC instrument is connected to the reactor outlet by a section of tubing of volume 44.2 µL, while the reactor volume is known to be 98.17 µL. The sampling frequency of the HPLC is the same as in the previous chapter, which is every 7 min and the standard deviation of the measurement error is again assumed to be 0.03 M and 0.0165 M for benzoic acid and ethyl benzoate concentrations.

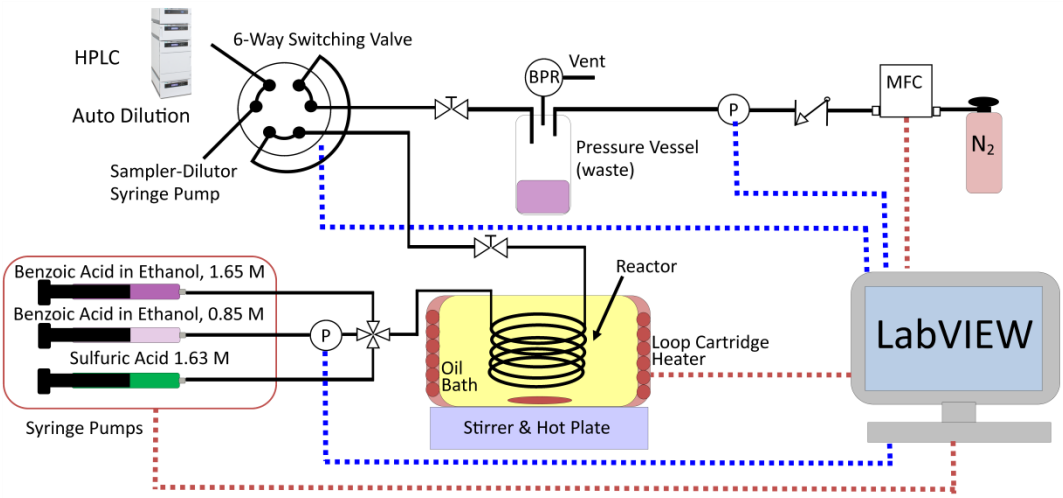

Figure 6-1 Experimental set-up for the esterification of benzoic acid with ethanol using sulfuric acid as a homogenous catalyst. Red dashed lines indicate LabVIEW controls the equipment, blue dashed lines indicate LabVIEW reads the measurement from the equipment.

As in the previous chapter for steady-state experiments, in this work with transient experiments there are three experimental design variables, flowrate, temperature and

benzoic acid feed concentration. The system pressure is kept constant at 6 barg and the sulfuric acid concentration is kept constant at 0.163 M.

Three types of ramp transient experiments were studied.

- **Ramp F** experiments where only flowrate is ramped while temperature and feed concentration are kept constant.
- **Ramp FT** experiments where both flowrate and temperature are ramped while feed concentration is kept constant.
- **Ramp FTC** experiments where temperature, flowrate and feed concentration are all ramped.

In each case, it is desired to use the experimental data from a single experiment type to estimate the kinetic parameters *KP1* and *KP2* for this esterification reaction. Therefore, it is possible to compare the experiment types to identify how much additional information can be obtained by allowing additional control variables to be ramped simultaneously. Note that for the **Ramp FT** and **Ramp FTC** experiments only a single experiment is required to estimate kinetic parameters, but that for the **Ramp F** experiment, as temperature is kept constant it is required to run 2 experiments at different temperatures to estimate the 2 kinetic parameters.

6.2.2 Modelling Transient PFRs

A transient PFR can be modelled using the reactor design equation for an ideal PFR, shown in Eq (6-4)

$$\frac{\partial C_{BA}}{\partial t} = -\nu \frac{\partial C_{BA}}{\partial V} + r_{BA} \tag{6-4}$$

where C_{BA} is the benzoic acid concentration (M), t is time (min), V is the reactor volume (L), ν is volumetric flowrate (L min^{-1}) and r_{BA} (mol L^{-1} min^{-1}) is reaction rate. This equation can be used for any type of transient experiment including experiments which use ramps, step changes or any other time dependent profile for one of the input control variables.

For ramp transient experiments it is possible to model the transient PFR without using a PDE by instead modelling the system as a series of hypothetical batch reactors, each of which can be modelled using the ideal batch reactor equation, Eq (6-5), which is a simple ODE where τ is the reactor residence time (min) [33]. This approach is taking advantage of the fact that each section of flow in a PFR can be viewed as an independent batch reactor, as shown in Figure 6-2. The time dependence of the PDE is still maintained in the system of ODEs as the residence time and initial conditions of the batch reactor (temperature and concentration) are functions of time, as will be discussed in the following section. Modelling the transient experiment as a system of

ODEs instead of as a PDE offers the advantage that the ODE solvers from the open source SciPy package in Python can be used to perform parameter estimation and MBDoE. This then opens the possibility of extending this work to perform online MBDoE of transient experiments using the LabVIEW and Python codes that were already developed in the previous chapter.

$$\frac{dC_{BA}}{d\tau} = r_{BA} \tag{6-5}$$

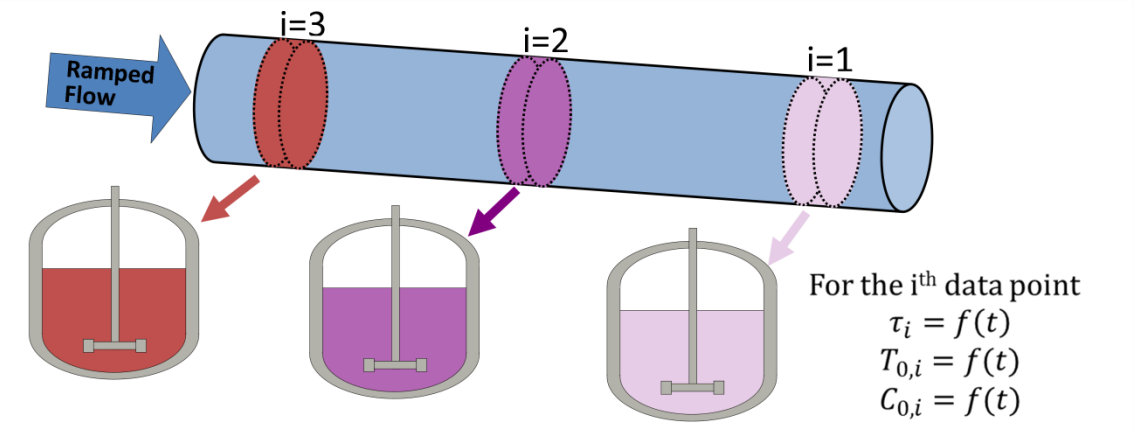

Figure 6-2 Ramped PFR modelled as a series of hypothetical batch reactors.

For isothermal experiments, where only flowrate is ramped, a single transient experiment can be viewed as being equivalent to a single batch experiment. This is shown graphically in Figure 6-3 where the measurement time of each data point from the transient flow reactor in Figure 6-3 a, is converted to an equivalent residence time in the hypothetical batch reactor in Figure 6-3 b.

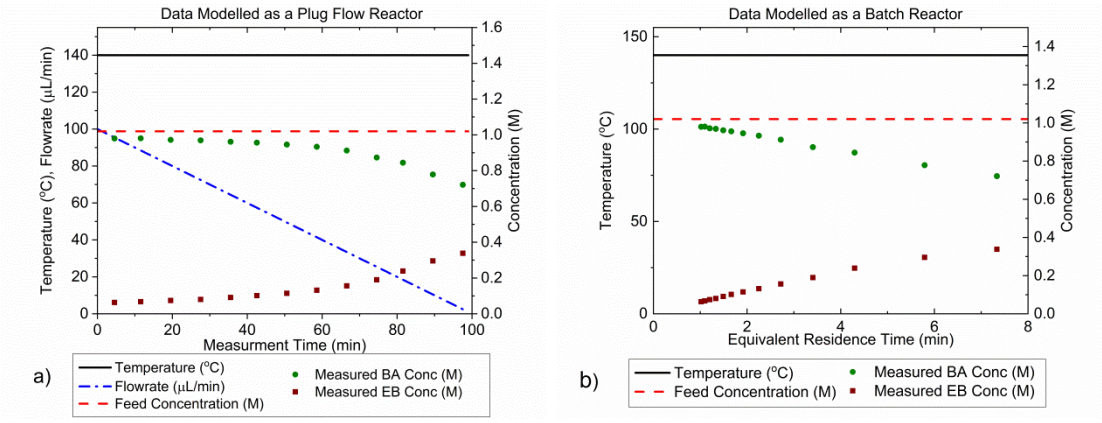

Figure 6-3 PFR data when flowrate is ramped and all other variables are held constant shown when modelled a) as a transient PFR and b) as a hypothetical batch reactor.

However, if temperature or feed concentration is simultaneously ramped with flowrate, than a single transient experiment is instead viewed as a collection of independent

batch reactors which all have their own unique initial conditions, this is demonstrated in Figure 6-4.

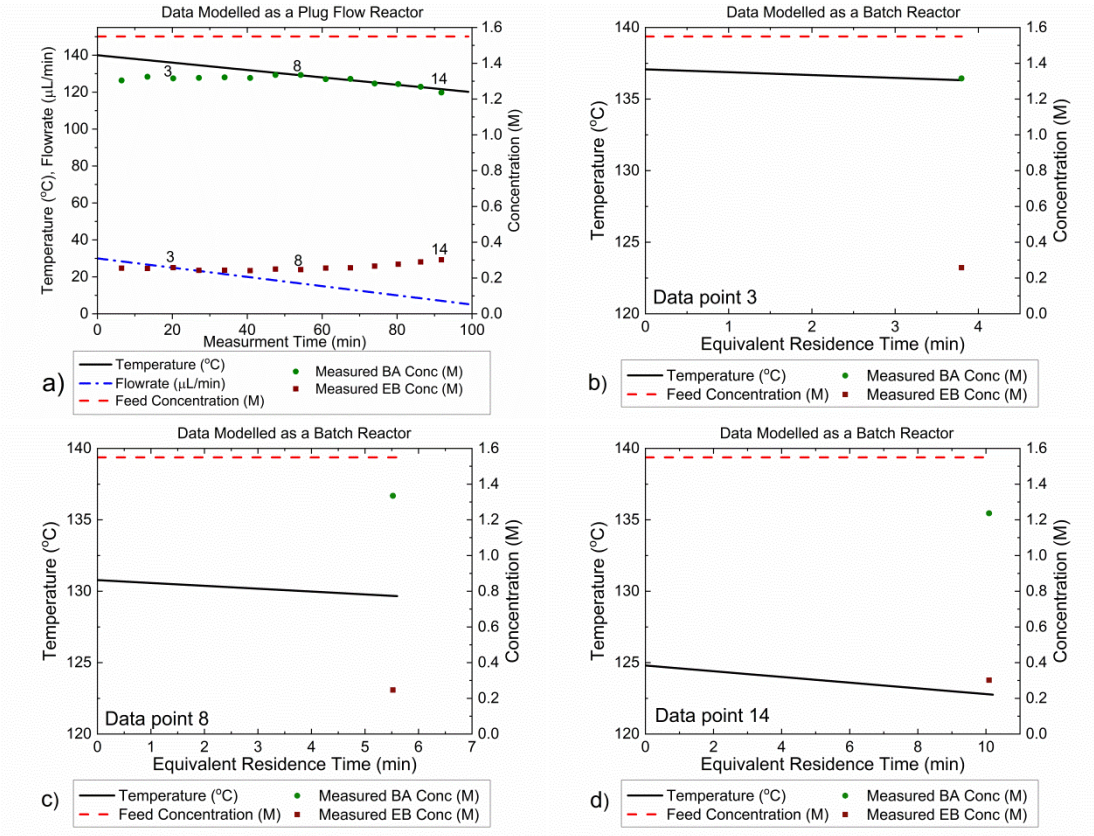

Figure 6-4 PFR data when flowrate and temperature are ramped simultaneously when modelled a) as a transient PFR and b) as a hypothetical batch reactor (shown for the 3rd, 8th and 14th data points in figures b, c and d respectively).

The initial temperature in the i[th] hypothetical batch reactor, $T_{i,0}$, is found from Eq (6-6), where T_0 is the initial temperature of the transient experiment, α_T is the temperature ramp rate and t_{In} is the time the sample entered the reactor (min). An equivalent equation for the initial concentration in the i[th] hypothetical batch reactor $C_{i,0}$ (M), is shown in Eq (6-7) where C_0 is the initial concentration (M) in the transient experiment and α_C is the concentration ramp rate (M/min).

$$T_{i,0} = T_0 - \alpha_T * t_{In} \quad (6\text{-}6)$$

$$C_{i,0} = C_0 - \alpha_C * t_{In} \quad (6\text{-}7)$$

In order to model a transient PFR as a series of batch reactors it is necessary to calculate the residence time each sample spent in the reactor. This can be calculated by subtracting the time the sample left the reactor, t_L (min), from the time the sample entered the reactor, t_{In} (min).

$$\tau = t_L - t_{In} \quad (6\text{-}8)$$

However, only the measurement time, t_M (min), of each sample is known from the time stamp of the HPLC result file. It is important to note that the measurement time is not the same as the time the sample left the reactor, t_L, because the HPLC measurement is not taken directly at the reactor outlet, as there is a section of tubing of dead volume V_d (µL) between the reactor outlet and the HPLC sample loop. Therefore for every sample there is a measurement time, t_M, a time the sample left the reactor, t_L, and a time the sample entered the reactor, t_{In}.

For ramp transient experiments, both the time the sample entered and left the reactor can be easily calculated for each corresponding measurement time. This is demonstrated in the following equations for the time the sample left the reactor, t_L, however the same method is used to calculate the time the sample entered the reactor, t_{In}.

First the known dead volume, V_{dead}, (the volume between the reactor outlet and the HPLC measurement point) is related to the integral of the volumetric flowrate v, from the time the sample left the reactor to the time the sample was measured by the HPLC.

$$V_{dead} = \int_{t_L}^{t_M} v\, dt \tag{6-9}$$

In all ramp transient experiments, the volumetric flowrate is expressed according to Eq (6-10)

$$v = v_0 - \alpha_V t \tag{6-10}$$

where v_0 is the initial volumetric flowrate (µL/min) at the beginning of the experiment, α_V is the ramp rate (µL/min^2) and t is the time passed since the start of the experiment (min). Substituting Eq (6-10) into Eq (6-9) and integrating leads to the quadratic equation

$$\left(\frac{1}{2}\alpha_V\right) t_L^2 - (v_o) t_L + \left(v_0 t_M - \frac{1}{2}\alpha_V t_M^2 - V_{dead}\right) = 0 \tag{6-11}$$

Solving this equation leads to only one physically meaningful solution shown in Eq (6-12).

$$t_L = \frac{v_o - \sqrt{v_o^2 - 2\alpha_V * (v_o t_M - 0.5 * \alpha_V t_M^2 - V_{dead})}}{\alpha_V} \tag{6-12}$$

The time the sample entered the reactor, t_{In}, is also calculated using Eq (6-12) except the volume term is changed from the dead volume V_{dead}, to the sum of the dead volume, V_{dead}, and reactor volume, V_{rxr}.

6.2.3 Experimental Design, Intuitive and MBDoE

One of the major objectives of this work is to use MBDoE to design ramp transient experiments and to compare these experiments to intuitively designed experiments to identify how beneficial it is to use MBDoE. Here experimental design refers to choosing the initial values (T_0, v_0, C_0) and ramp rates ($\alpha_T, \alpha_v, \alpha_C$) for the three control variables. The allowed ranges for each of the design variables are shown in Table 6-1. Additionally there are three further constraints

- The experimental duration is limited to a maximum of 100 min.
- The flowrate can never drop below 5 µL/min as such a low flowrate would not adequately refill the HPLC sample loop between measurements leading to measurement errors.
- All variables must be ramped from an initial high value, downwards. For flowrate this is important as before the experiment can begin, the experiment must reach steady-state at the initial condition, so a fast initial flowrate minimises this initial waiting period.

Table 6-1 Allowed range of the design variables, initial flowrate (v_0),flowrate ramp rate (α_V), initial feed concentration (C_0), feed concentration ramp rate (α_C), initial temperature (T_0), temperature ramp rate (α_T).

Variable	v_o (µL/min)	α_V (µL min^{-2})	C_0 (M)	α_C (M/min)	T_0 (°C)	α_T (°C/min)
Range	7.5 - 100	10^{-5} - 1.25	0.9 - 1.55	10^{-6} – 0.01	70 - 140	0 - 3

Intuitive design

For the intuitively designed experiments the experimental design rational was to try and cover as wide a section of the design space as possible, which is a common strategy in black box experimental design where wide spacing is often encouraged in factorial designs [236]. Therefore, the ramped variables in intuitively designed transient experiments would start at a very high value, and then be ramped down at a sufficient rate so that they would reach a low value by the end of the 100 min experiment, and hence have explored a very wide section of the design space.

MBDoE design

In this case study, the design vector **φ** for the **Ramp F** experiment consists of 8 variables ($T1_0$, $v1_0$, $\alpha 1_v$, $C1_0$ and $T2_0$, $v2_0$, $\alpha 1_v$, $C2_0$) while the **Ramp FT** and **Ramp FTC** design vectors consist of only 5 ($T_0, \alpha_T, v_0, \alpha_v, C_0$) and 6 ($T_0, \alpha_T, v_0, \alpha_v, C_0, \alpha_C$), variables respectively. The values for the experimental design vector are then

calculated offline using D-optimal MBDoE to minimise the expected covariance matrix for the designed experiment. The parameter estimates obtained from the factorial campaign of steady-state experiments in the previous chapter, 9.12 (-) and 7.98 (J/mol), are used as the initial parameter estimates required by MBDoE. It is worth highlighting that these initial estimates for the parameters *KP1* and *KP2* used in the MBDoE design are quite good, which assists the MBDoE in designing the optimum experiment. In other situations where there is large uncertainty in the parameter values, MBDoE may lead to suboptimal designs. In these situations it may be more appropriate to use robust MBDoE techniques [191-193]. However, simulations shown in Appendix E demonstrate that for this case study, even if the initial estimate for the parameters are poor that the MBDoE designs are still far superior to intuitively designed experiments in terms of the precision of parameter estimates obtained. Therefore, there is still considerable value in this technique even when only poor or uncertain parameter estimates are available.

In this chapter, each experiment was designed as if no previous experiments had been conducted, so that there was no prior covariance term when calculating the expected covariance matrix in the MBDoE optimisation problem, as shown in Eq (6-13).

$$\mathbf{V}_{\boldsymbol{\theta},\mathbf{expected}}(\boldsymbol{\varphi}) = \left[\sum_{\mathrm{i}=1}^{N_{new}} \mathbf{H}_{\mathbf{expected,i}}(\boldsymbol{\varphi})\right]^{-1} \tag{6-13}$$

where $\mathbf{V}_{\boldsymbol{\theta},\mathbf{expected}}$ is the expected covariance matrix, $\mathbf{H}_{\mathbf{expected,i}}$, is the Fisher Information matrix of the ith transient experiment to be designed, and N_{new} is the number of transient experiments to be planned, which is 1 for **Ramp FT** and **Ramp FTC** experiments, and 2 for the **Ramp F** experiment. The optimisation problem is solved with the SLSQP (Sequential Least Squares Programming) algorithm in Python, where the initial guess for the design vector was chosen as the best result from screening 10,000 design vectors randomly distributed across the experimental design space, this helps prevent the optimiser getting stuck in a local optimum.

6.3 Results & Discussion

6.3.1 Ramp F experiments

The intuitive and MBDoE designs for the **Ramp F** experiments are shown in Table 6-2 and in Figure 6-5. It can be observed that the intuitive designed experiments explored a wide range of reaction conditions including high and low temperatures (140 and 120 ^{o}C) and concentrations (1.02 and 1.5 M). Additionally, the intuitive flowrate profile chosen, which was used for both experiments, resulted in the flowrate varying from 100 to 5 µL/min during the transient experiment, ensuring a wide range of residence times

would be observed. In comparison the MBDoE designed experiments were found to have quite low flowrates, of less than 30 µL/min, and both experiments used the same high feed concentration of 1.55 M. This indicates that the MBDoE experiment explored a much smaller portion of the experimental design space than the intuitive design. This shows the tendency of MBDoE designs to study a small section of the design space which carries the highest information, instead of studying a wide range of the design space. This is a similar trend as what occurred for the steady-state experiments.

Table 6-2 Intuitive and MBDoE designs for the **Ramp F** experiment.

Experiment	v_o (µL/min)	α_V (µL/min^2)	C (M)	T (°C)
Ramp F Intuitive Design 1	100	1	1.50	120
Ramp F Intuitive Design 2	100	1	1.02	140
Ramp F MBDoE 1	29.8	0.253	1.55	119.0
Ramp F MBDoE 2	9.13	0.043	1.55	139.4

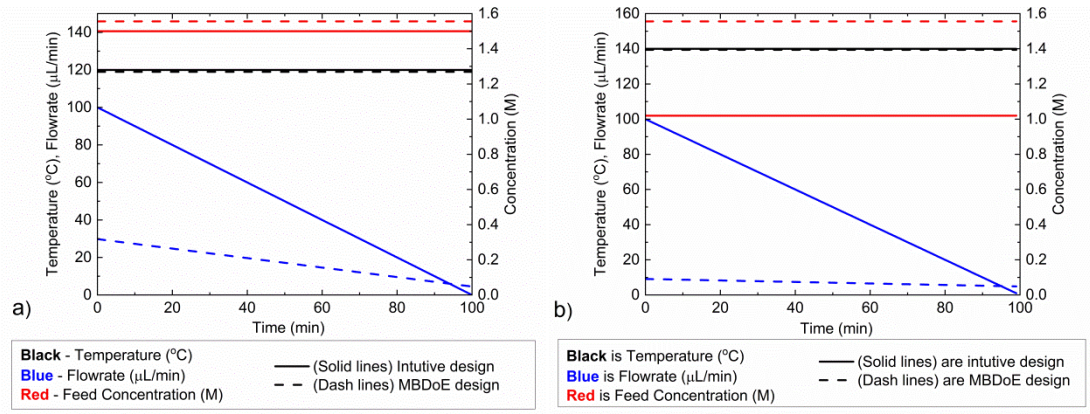

Figure 6-5 Control variable profiles designed by the intuitive method and by MBDoE for a) the first and b) the second **Ramp F** experiment.

The raw data from the four **Ramp F** experiments conducted are shown in Appendix E. Using the raw data to conduct parameter estimation, it was found that the MBDoE designed experiments led to significantly more precise estimates as shown by the 95% confidence ellipsoid plot in Figure 6-6.

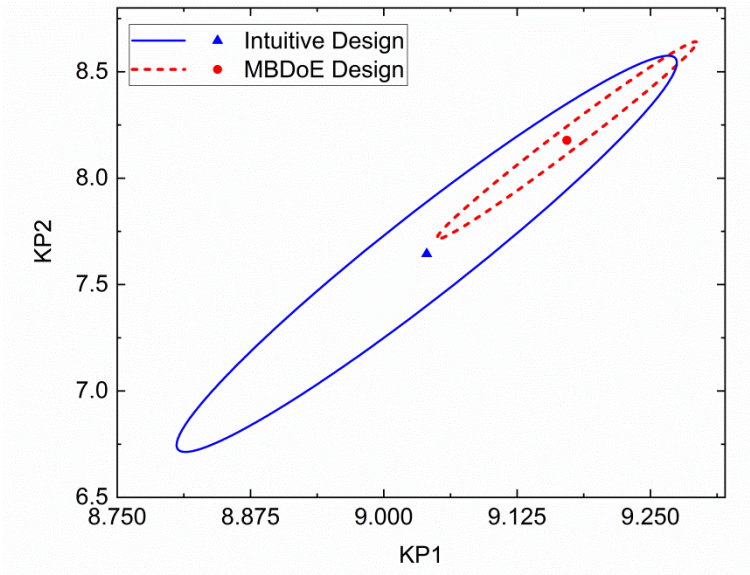

Figure 6-6 95% Confidence ellipsoids comparing the statistical certainty of the kinetic parameters *KP*1 and *KP2* between the MBDoE and intuitive **Ramp F** experiments.

6.3.2 Ramp FT experiments

The intuitive and MBDoE designs for the **Ramp FT** experiments can be observed and compared in Table 6-3 and Figure 6-7. The intuitive design again tried to cover a wide area of the design space, using flowrates that vary from 100 to 5 µL/min and temperatures that range from 140 to 90 °C. The feed concentration for the intuitive design was held constant at 1.5 M. In comparison it is observed that MBDoE designed a very similar temperature profile and fixed benzoic acid feed concentration profile as the intuitive design. However, the MBDoE flow profile was dramatically different, only exploring a small region of low flowrates, with the initial flowrate being only 10.1 µL/min and a slow ramp rate of just 0.05 µL/min^2.

Table 6-3 Values of the control variables for the intuitive and MBDoE **Ramp FT** experiments.

Experiment	v_o (µL/min)	α_V (µL/min^2)	C (M)	T_0 (°C)	α_T (°C/min)
Intuitive Design	100	1	1.50	140	0.5
MBDoE Design	10.1	0.05	1.55	139.2	0.537

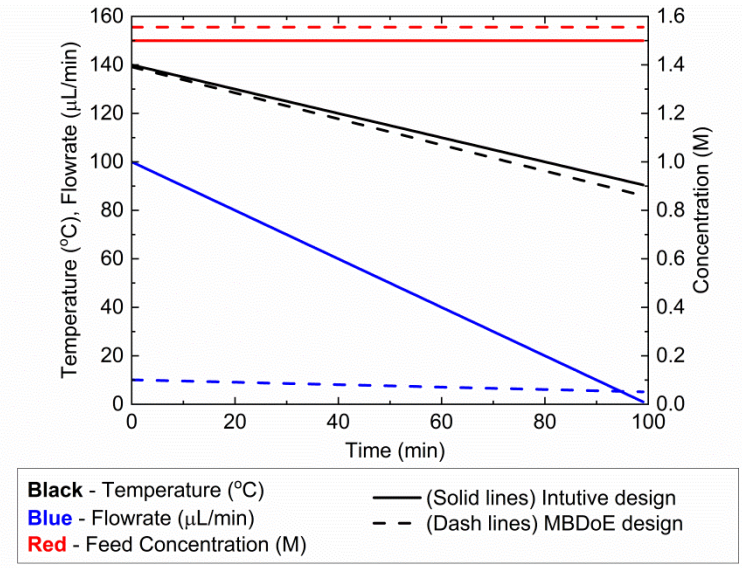

Figure 6-7 Control variable profiles designed by the intuitive method and by MBDoE for the **Ramp FT** experiments.

Despite some similarities in the experimental design, the MBDoE designed experiment was found to give much more precise parameter estimates than the intuitive design as shown in Figure 6-8 by the smaller 95% confidence ellipsoid. The very large difference in the size of the confidence ellipsoids highlights how difficult it is to intuitively design a multi-variate ramp transient experiment, and demonstrates the need for MBDoE approaches for their design. In this particular case, it is speculated that the intuitive designed experiment design is poor due to the low conversions attained, which were always less than 6% as shown in the raw data section in Appendix E. Therefore, it was difficult to estimate the kinetic parameters, as the reaction was never allowed to progress to significant levels and because the concentration change between the feed and the outlet value (typically less than 0.1 M) was only slightly larger than the measurement error (0.03 and 0.0165 M). In contrast the MBDoE designed experiment explored conditions that led to much higher conversions of up to 20% as shown in Appendix E.

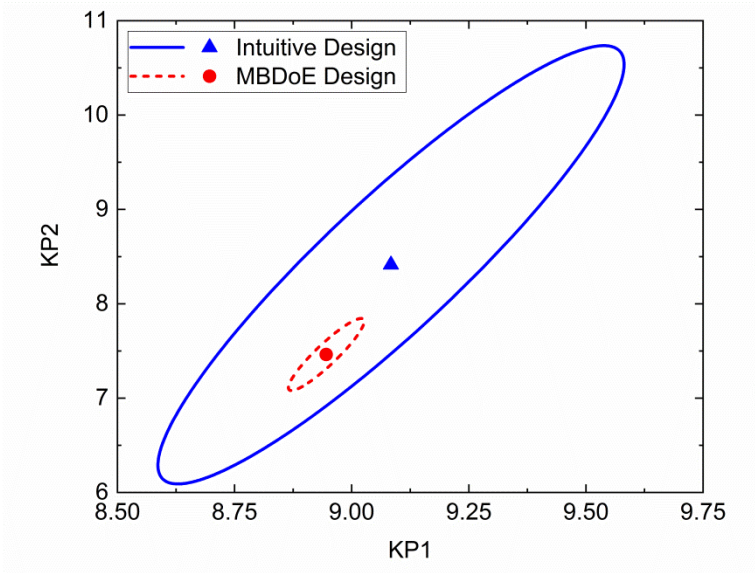

Figure 6-8 95% Confidence ellipsoids comparing the statistical certainty of the kinetic parameters *KP*1 and *KP2* between the MBDoE and intuitive **Ramp FT** experiments.

6.3.3 Ramp FTC experiments

The final experiment was intended to ramp flowrate, temperature and inlet concentration all simultaneously. However, the MBDoE algorithm designed a single experiment where initial inlet concentration was almost the maximum at 1.54 M, but the ramp rate in concentration was the minimum possible, 10^{-6} M/min, which in terms of actually running this experiment in the automated system, resulted in a constant concentration experiment (concentration varied from 1.54 to 1.5399 M). Therefore, it was concluded that ramping concentration offered no added value to this case study, as it was preferable to run at maximum concentration. It was considered that allowing concentration to be ramped in the MBDoE algorithm, just added an unnecessary extra design variable which made the optimisation more challenging. For these reasons the experiment was not conducted, however for other experimental systems ramping all three variables may present interesting opportunities to get very precise parameter estimates. Additionally, for this case study, if the objective was model discrimination between zero, first and second order rate laws, it is quite likely that allowing the feed concentration to vary would significantly improve the discriminating power of the experiment.

6.3.4 Comparison of Parameter Estimates

The kinetics of benzoic acid and ethanol esterification using a sulfuric acid catalyst has been thoroughly examined using both steady-state and transient experiments, which were both designed by traditional methods such as factorial approaches and researcher intuition as well as by MBDoE. In order to demonstrate that the parameter estimates from the various experiments are all consistent a 95% confidence plot of the

parameter estimates from all experiments is shown in Figure 6-9, where it can be observed that all of the confidence ellipsoids overlap except for the **Ramp FT** MBDoE designed transient experiment. The cause of this outlier could be some unknown disturbance in the **Ramp FT** experiment or else it could suggest that the modelling assumptions are wrong, for example that the true model is not first order or that the measurement error is not randomly distributed with a mean of 0 and a constant standard deviation. However, as the parameter estimates are still very close this is not a major problem, nor does it undermine the result here which shows the considerable advantages of MBDoE design for transient experiments.

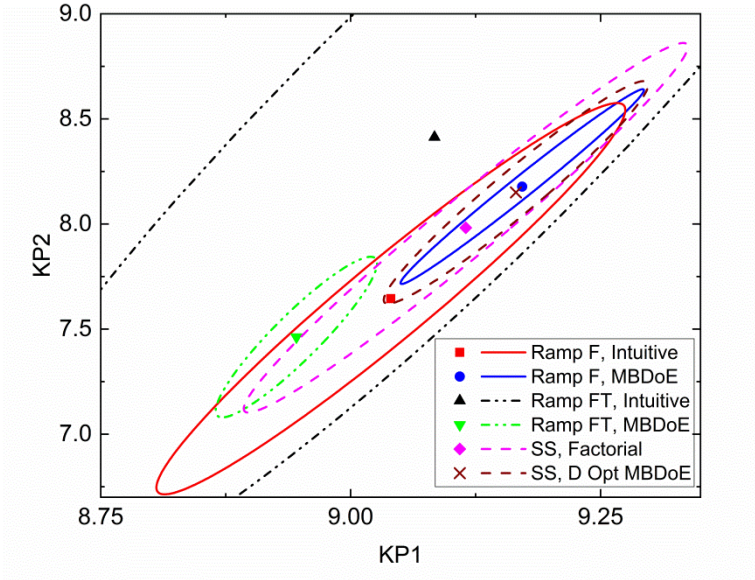

Figure 6-9 95% Confidence ellipsoids comparing the statistical certainty of the kinetic parameters *KP*1 and *KP2* obtained from both steady-state (SS) experiments and transient experiments.

Additionally, one of the major objectives of this work was to highlight the time savings achieved by transient experiments compared to steady-state experiments. All of the steady-state experiment campaigns in this work took 8 h of operation, while the transient experiments are observed to be much faster as the **Ramp F** transient experiments required 4 h (as 2 experiments conducted at different temperatures are required), and the **Ramp FT** experiments required only 2 h. It is worth highlighting that the **Ramp FT** MBDoE designed experiment, where both temperature and flowrate were ramped simultaneously, produces one of the smallest confidence ellipsoids, comparable with those ellipsoids generated from campaigns of 8 steady-state experiments which were also designed using MBDoE. This demonstrates the value of MBDoE designed transient experiments as the experiment which takes only 2 h, produces parameter estimates with similar levels of precision as experiments which take 4 h (isothermal transient experiments) or 8 h (steady-state campaigns), provided

that good initial guesses for the parameter values are available either from previous experiments or from values found in the literature.

When the re-parameterised kinetic parameters *KP1* and *KP2* are converted back to the original Arrhenius constants of pre-exponential factor (*A*) and activation energy (*Ea*), the parameter estimates, which previously were all very similar in value, spread much further apart. This is shown in Table 6-4 where the maximum and minimum pre-exponential factor estimates are $2.65*10^6$ and $45.2*10^6$ s^{-1}, even though the reparametrized parameters were very similar in value at 8.95 and 9.25. This large difference in pre-exponential factor estimates is due to the exponential transformation between the two parameterisations, and the high correlation between the pre-exponential factor and activation energy.

Table 6-4 Maximum Likelihood Estimates and 95% confidence intervals for the parameter values *KP1* and *KP2*, and their corresponding values in the original Arrhenius equation, *A* and *Ea*, for all steady-state and transient experiments.

Experiment	Experiment Duration (h)	*KP1* ± 95% CI	*KP2* ± 95% CI	A $*10^6$ (s^{-1})	Ea (kJ/mol)	χ^2 / χ^2_{ref}
Ramp F, MBDoE	4	9.17 ± 0.10	8.18 ± 0.38	20.6	81.8	9.80/72.1
Ramp F, Intuitive	4	9.03 ± 0.18	7.63 ± 0.76	4.15	76.3	25.9/67.5
Ramp FT, MBDoE	2	8.95 ± 0.07	7.46 ± 0.32	2.65	74.6	13.2/38.9
Ramp FT, Intuitive	2	9.06 ± 0.40	8.36 ± 1.97	41.0	83.6	4.77/31.4
SS, Factorial 1	8	9.06 ± 0.19	7.84 ± 0.75	7.80	78.4	14.9/23.7
SS, Factorial 2	8	9.11 ± 0.19	7.98 ± 0.77	11.7	79.8	0.98/23.7
SS, D Opt	8	9.17 ± 0.12	8.15 ± 0.46	18.8	81.5	10.6/23.7
SS, E Opt	8	9.17 ± 0.10	8.12 ± 0.43	17.1	81.2	6.10/23.7

Finally as the work to this point has been focused on parameter precision, it is shown here that the parameter estimates can also be used to accurately predict the outlet concentration for this reaction. This is demonstrated in Figure 6-10, which shows all three of the MBDoE designed transient experiments conducted in this work (Figure 6-10 a and b are the **Ramp F** experiments, while Figure 6-10 c is the **Ramp FT** experiment), where the experimental measurements are shown beside the simulated concentration profile created with various parameter estimates that were from both steady-state and transient experiments. All of the predicted concentration profiles are quite similar, as their parameter estimates were similar, and they accurately predict the reaction performance. In particular, it is worth highlighting that the parameter estimates obtained from the steady-state experiments are capable of accurately predicting the reaction performance of transient experiments.

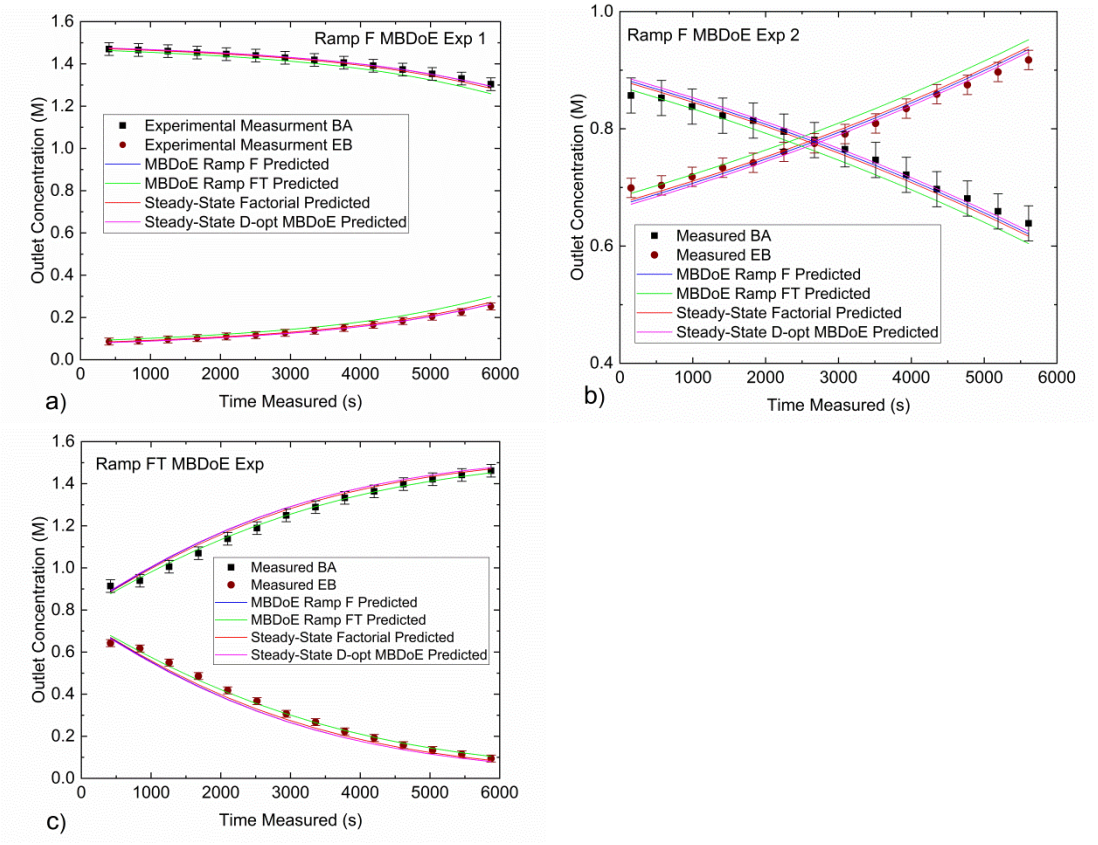

Figure 6-10 Experimentally measured outlet concentrations for the Ramp F experiments (a and b) the Ramp FT experiment (c), compared against predicted values based on the parameter estimates obtained from different experiments in this work.

6.4 Conclusions

The automated reactor platform developed in this work was shown to be able to conduct transient experiments, and the kinetic parameters obtained were consistent with the previous parameter estimates obtained from steady-state experiments. It was demonstrated that transient experiments offered the fastest way to identify kinetic parameters. When flowrate and temperature were ramped simultaneously, parameter estimates could be obtained in less than 2 h, whereas 8 h were required for a campaign of steady-state experiments. Furthermore, even faster and more efficient experiments could have been achieved if the analysis equipment used in this work were faster. Here a HPLC was used with a sampling time of 7 minutes, however if a spectroscopic method were used which could produce data more quickly it is expected that the experiments could be completed more than ten times faster, as the time limiting step would then be set by the temperature controller response time rather than the analysis equipment.

In comparing whether steady-state or transient experiments are superior for kinetic studies, the answer is dependent on the relevant time scales for the reactor to reach a new steady-state compared to the time scale of the analysis method. In cases where

the analysis time is significantly less than the time required for the reactor to reach steady-state, there is an advantage in using transient experiments for saving time and reagents. Therefore, if the analysis method is fast (spectroscopic methods), or the reactor residence time is long, conducting a large number of transient experiments would be preferable to running steady-state campaigns. In contrast, if the analysis method is long (GC or HPLC with long method times) compared to the reactor residence time, then a campaign of steady-state experiments may be preferable. However, it is also necessary to highlight that transient experiments can only be applied to systems which exhibit near instantaneous responses to changes in the process conditions. Some catalysts, such as the Fischer-Tropsch catalysts are known to have an induction time for the catalyst to come into equilibrium with changing process conditions [174]. If this induction time is significant compared to the ramp rate of the experiment, transient methods would lead to erroneous results. However, there are many catalysts which do exhibit fast responses to changing process conditions, such as oxidation of carbon monoxide and steam reforming of methanol, both of which were successfully studied using temperature ramped transient experiments [175]. Therefore, the application of transient experiments is most suited to non-catalytic reactions and systems with catalysts that are stable (non or very slowly deactivating) and equilibrate sufficiently quickly with their environment. Another requirement for transient flow experiments are that the reactor hydrodynamics are well characterised, ideally plug flow behaviour with no dead volumes between the reactor outlet and sampling location.

This work showed that the efficient design of transient experiments is non-intuitive, particularly when multiple variables are ramped simultaneously and hence that MBDoE is a particularly useful tool in this area. It was shown that intuitive designs which attempted to cover a wide region of the design space led to low information experiments and low precision parameter estimates whereas MBDoE designed transient experiments explored a very narrow range of the design space which carried greater information. However, one limitation to keep in mind for all MBDoE methods is that it is necessary to assume a suitable model structure in advance along with some initial estimates for all the model parameters. In most cases it is possible to make such assumptions based on information from the literature or researcher experience with similar reactions. If MBDoE is applied with an incorrect model structure or particularly poor parameter estimates, there is no guarantee that that the designed experiment will provide highly informative data, although similarly there is no guarantee that an intuitive design will provide highly informative data either. Generally, if there is high confidence in the model structure, but low confidence in the parameter estimates, it is still advised

to use MBDoE for improved parameter precision to design a sequence of transient experiments. This strategy benefits from the fact that as each experiment is conducted, the parameter estimates become more precise, so that the following MBDoE design becomes more effective. If however, there is low confidence in the model structure, MBDoE for improved parameter precision should not be used. If there is low confidence in the model because there are two or more candidate models available, transient experiments could be designed using MBDoE for model discrimination. Alternatively, if there is no suitable model structure available, the best option is to use traditionally designed transient experiments to span as much of the design space as possible. This can be used as a starting point to collect kinetic data, before proposing new candidate models and eventually being able to use the more efficient MBDoE techniques for transient experiment design.

7 Rapid Kinetic Modelling: Online MBDoE for Sequential Steady-State Experiments, Applied to Heterogeneous Esterification Reaction

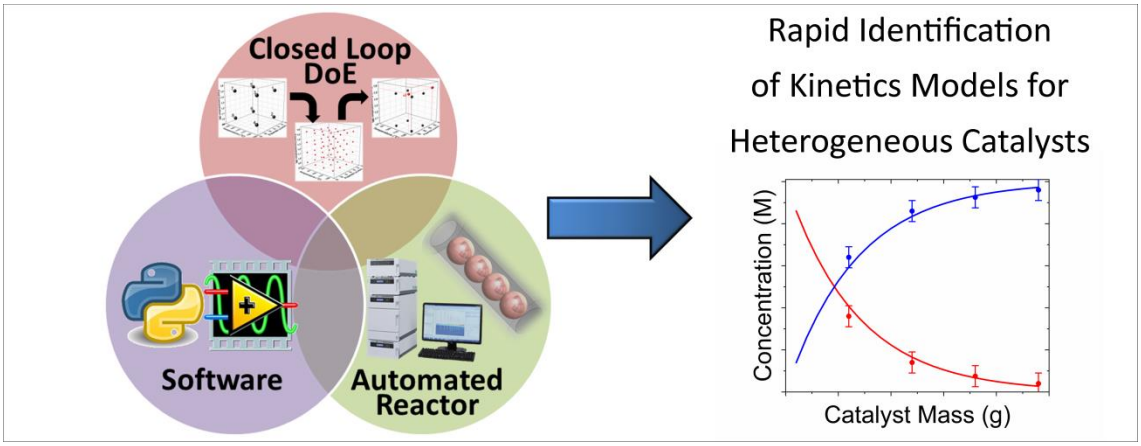

Abstract

The automated reactor platform successfully identified a practical kinetic model for the heterogeneous catalytic reaction of benzoic acid and ethanol esterification using an Amberlyst-15 catalyst in a string reactor configuration. In order to ensure that the automated reactor platform was being used in the most efficient way possible, a 5 step methodology was developed with the aim of identifying a practical kinetic model with the minimum number of experiments. This included i) initial screening using traditional factorial designed steady-state experiments, ii) proposing and testing candidate kinetic models, iii) performing an identifiability analysis to reject models whose model parameters cannot be estimated for a given experimental budget, iv) performing online Model-Based Design of Experiments (MBDoE) for model discrimination to identify the best model from a list of candidates and v) performing online MBDoE for improving parameter precision for the chosen model. This methodology, combined with the reactor platform which conducted all kinetic experiments unattended, reduces the number of experiments and time required to identify kinetic models, significantly increasing lab productivity.

The contents of this chapter have been accepted for publication
C. Waldron, A. Pankajakshan, M. Quaglio, E. Cao, F. Galvanin and A. Gavriilidis, “Closed Loop Model-Based Design of Experiments for Kinetic Model Discrimination and Parameter Estimation: Benzoic Acid Esterification on Heterogeneous Catalyst”. *Industrial & Engineering Chemistry Research,* 2019.

7.1 Introduction

In the previous two chapters MBDoE techniques for improved parameter precision were successfully implemented using the automated flow system to rapidly identify a kinetic model of a homogenous reaction. However, this study did not fully address several of the challenges in designing efficient kinetic experiments, including how to design the initial experiments when very little information is known about the system, how to design experiments for model discrimination and whether it is best to pursue a complicated model with many highly correlated parameters that is believed to be the true model, or whether it is better to instead focus on simpler approximated models. Additionally, the main objective of this thesis was to develop a platform to study heterogeneous catalysts, which is much more difficult than studying homogenous systems due to the increased number of phenomena occurring including external and internal mass transfer, adsorption and desorption on the active site, surface reaction and possibly catalyst deactivation or non-ideal reactor effects. Therefore, the objective of this chapter is to develop a general methodology for experimental design which covers all stages of kinetic modelling, from initial experiments, practical identifiability checks to the application of online MBDoE for model discrimination and parameter precision, and to apply this methodology using the automated reactor system to a heterogeneous catalytic reaction. While there exist a number of automated heterogeneous flow reactors with online analysis in the literature [16, 18, 32], to the best of the author's knowledge no one has ever applied online MBDoE to speed up the identification of kinetic models involving heterogeneous catalysts. The esterification of benzoic acid and ethanol using the heterogeneous catalyst Amberlyst-15 is chosen as the case study for this work because this reaction is already well understood from the previous chapters. Furthermore, Amberlyst-15 is a commercial catalyst that is known to be stable, hence avoiding problems of deactivation.

7.2 Materials & Methods

7.2.1 Reaction and Candidate Models

The case study for this work was the esterification of benzoic acid and ethanol using Amberlyst-15 catalyst, as shown in Eq (7-1).

$$Benzoic\ Acid + Ethanol \rightleftarrows Ethyl\ Benzoate + Water \qquad (7\text{-}1)$$

Based on kinetic studies in the literature for similar esterification reactions [237, 238], a number of candidate kinetic models are assumed for this reaction, including simple power law models (M1) and Langmuir Hinshelwood models at various levels of complexity (M2, M3 and M4). Due to the large excess of ethanol used (molar ratio greater than 9:1), the reverse reaction is considered to be negligible [231].

$$r'_{BA} = -kC_{BA}C_{EtOH} \quad \text{(M1)}$$

$$r'_{BA} = \frac{-kC_{BA}C_{EtOH}}{(1 + K_W C_W)^2} \quad \text{(M2)}$$

$$r'_{BA} = \frac{-kC_{BA}C_{EtOH}}{(1 + K_W C_W + K_{EtOH}C_{EtOH})^2} \quad \text{(M3)}$$

$$r'_{BA} = \frac{-kC_{BA}C_{EtOH}}{(1 + K_{BA}C_{BA} + K_{EtOH}C_{EtOH} + K_W C_W + K_{EB}C_{EB})^2} \quad \text{(M4)}$$

In these kinetic models the terms K_{BA}, K_{EtOH}, K_W and K_{EB} are the adsorption terms for each species, which are parameters to be estimated. In all cases the rate constant, *k*, is expressed in the re-parameterised Arrhenius form with two parameters *KP1* and *KP2* as shown in Eq (7-2), as this reduces correlation between the pre-exponential factor and the activation energy [233]. Here, *T* is temperature (K), and T_M is the mean temperature of 378.15 K, calculated as the average value of the upper and lower temperature limits for this experiment.

$$k = exp\left(-KP1 - \frac{KP2 * 10000}{R} * \left[\frac{1}{T} - \frac{1}{T_M}\right]\right) \quad \text{(7-2)}$$

When proposing simplified versions of the Langmuir Hinshelwood model (M2 and M3), the adsorption terms for benzoic acid and ethyl benzoate were the first to be neglected as the literature reports that the these adsorption terms are less significant than the more polar water and ethanol species [237, 238]. When developing a further simplified model (M2) the ethanol adsorption term was also removed from the model, because as the concentration of ethanol was in excess, it would be approximately constant.

7.2.2 Experimental Set-Up

The reaction is conducted in a string reactor of internal diameter 1 mm packed with particles of average size 825 µm as shown in Figure 7-1. The motivation behind this reactor design are shown in Appendix F.

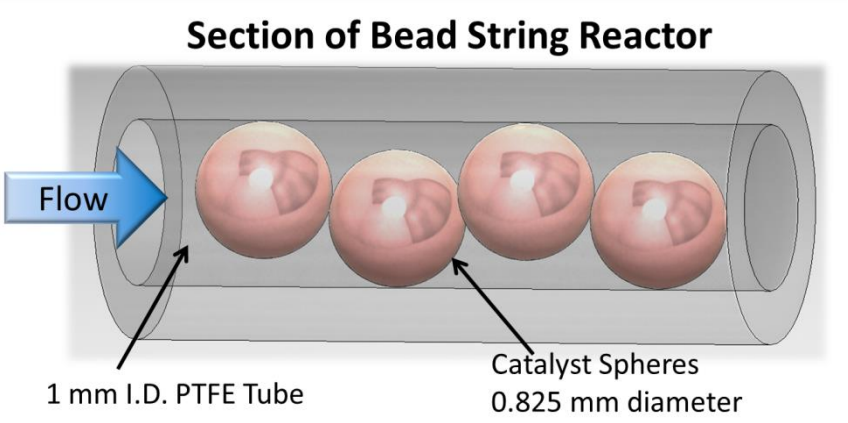

Figure 7-1 A section of the bead string reactor showing the PTFE tubing with 1 mm inner diameter, filled with 0.825 mm diameter Amberlyst-15 spheres.

Before conducting kinetic experiments, it was first necessary to characterise the string reactor's hydrodynamic and mass transfer properties. This was done by performing a residence time distribution study, a liquid solid mass transfer study and by analysing internal mass transfer using the Weisz-Prater criterion, all of which are shown in detail in Appendix F. The key findings were that it was reasonable to model this reactor as a plug flow reactor and to ignore external mass transfer resistances. The Amberlyst-15 catalyst had a hierarchical structure, where the large macro spheres of diameters ranging from 0.35 mm to 1.18 mm are composed of a porous network of agglomerates of randomly packed gel microspheres where each microsphere has a gel porosity [239, 240]. It was shown in Appendix F with the Weisz-Prater criterion, that there are no internal resistances within the large macro sphere, so the rate of reaction does not vary with the size of the Amberlyst-15 particle used. However, Pöpken et al reported that if the Amberlyst-15 particles are ground in a mill, and a sieve fraction of less than 63 μm is used, that the rate of reaction doubles [241]. Pöpken et al do not present this as evidence of internal mass transfer resistances in the macro sphere, as they also report that the reaction rate is independent of the sieve fraction of Amberlyst-15 particles used. Instead they attribute this to a "mass transfer limitation, which is only of importance when the catalyst is subjected to grinding or abrasion", which implies that they are breaking the microspheres and hence increasing the surface area of microspheres in the catalyst. This result suggests that there are internal mass transfer resistances in the microspheres. Therefore, due to presence of internal mass transfer resistances in the microspheres all of the kinetic data generated in this work is from the mass transfer limited regime and all rate laws and activation energies reported in this paper are apparent rate laws and apparent activation energies. However, the presence of this internal mass transfer resistance has limited relevance to industry where the catalyst is always used in the sphere form without grinding or abrasion. Therefore, the apparent model developed in this chapter is still of value.

Based on these findings, the string reactor is modelled using the steady-state ideal plug flow equation as shown in Eq (7-3), where W is the catalyst mass (g), r'_{BA} is the rate of reaction of benzoic acid (mol g^{-1} s^{-1}) and v is the inlet liquid flowrate (L/s).

$$\frac{dC_{BA}}{dW} = \frac{r'_{BA}}{v} \tag{7-3}$$

The kinetic experiments were conducted by the autonomous reactor platform shown in Figure 7-2, which was previously used for the homogenous esterification of benzoic acid with sulfuric acid catalyst. The updated experimental set-up consisted of four 5 mL glass syringes (Cetoni) being driven by a syringe pump (neMESYS low pressure module, Cetoni) where two syringes were filled with a low concentration benzoic acid in

ethanol solution (0.85 M) and the other two syringes were filled with high concentration benzoic acid in ethanol (1.65 M). Each pair of syringes was connected by a T-junction (UpChurch) and the fluids were mixed at a Y-junction (UpChurch) before entering the string reactor. As in the previous work, here there are three design variables temperature, flowrate and feed concentration. Temperature varies from 80 to 120 ^{o}C, which is the maximum operating temperature of the Amberlyst-15 catalyst, while the flowrate ranges from 15-60 µL/min and the benzoic acid feed concentration varies from 0.95 – 1.55 M. The other experimental details are the same as that described in chapter 5, including the online analysis of the reactor product with HPLC.

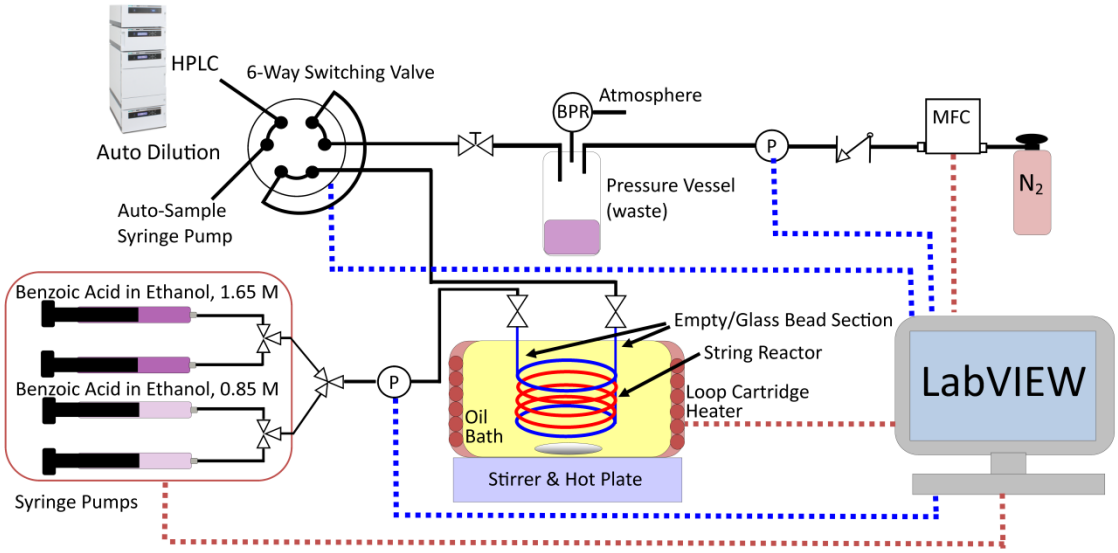

Figure 7-2 Autonomous reactor platform used for the esterification of benzoic acid and ethanol using Amberlyst-15 as a heterogeneous catalyst in a string reactor. Red dashed lines indicate LabVIEW controls the equipment, blue dashed lines indicate LabVIEW reads the measurement from the equipment.

7.2.3 Experimental Design Procedure

A generalised methodology for designing efficient kinetic experiments was developed to cover all stages of kinetic studies modelling, this is shown in Figure 7-3 and described in detail below.

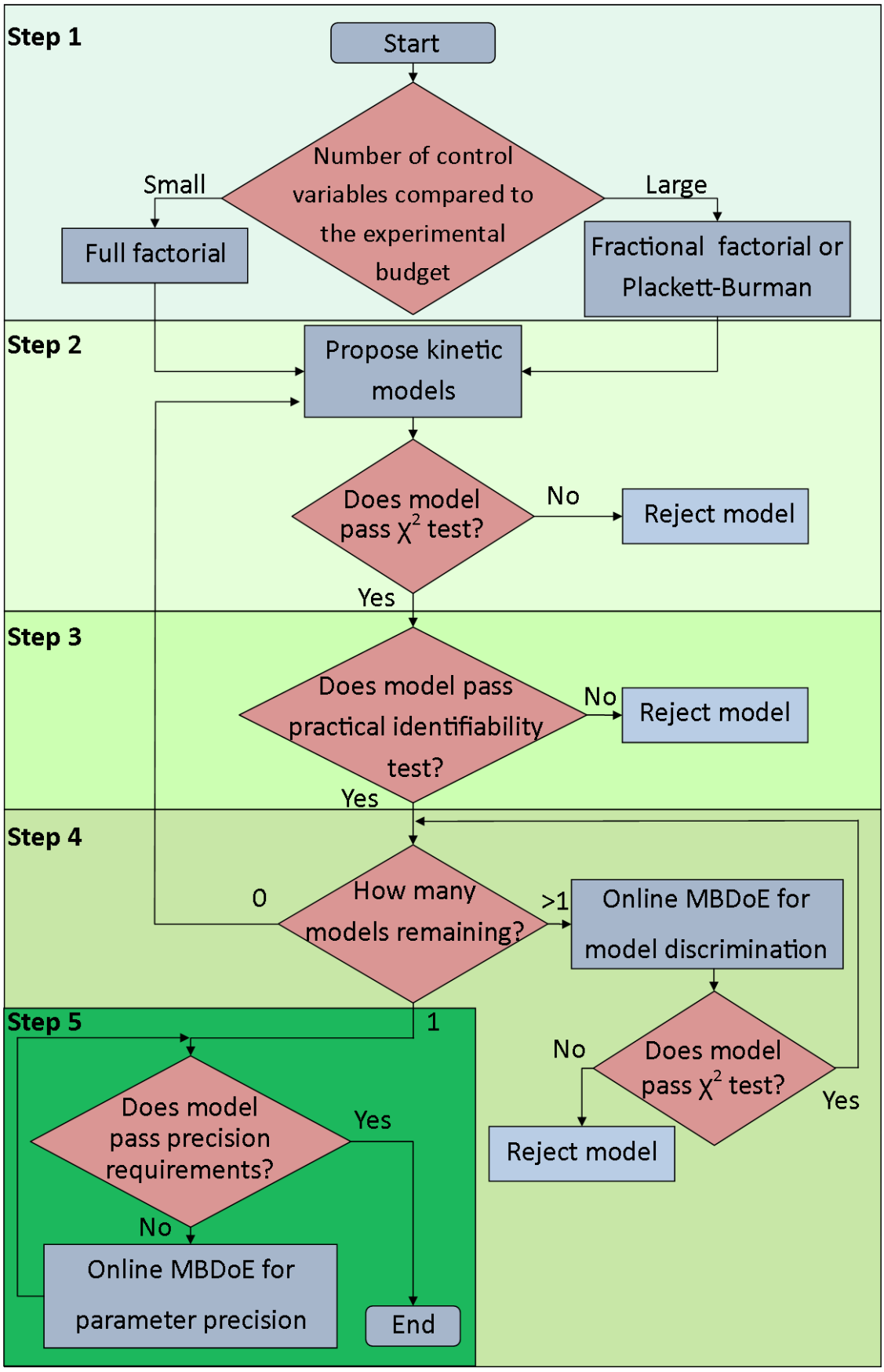

Figure 7-3 Flowchart showing the experimental methodology that can be applied to any general kinetic study.

Step 1. Factorial Screening & Catalyst Stability Check. In some cases if there is prior information available from the literature, so that candidate kinetic models are available, it may be most efficient to begin with MBDoE experiments designed for model discrimination or improved parameter precision and then continue on to step 2. However, if there is no prior information about the reaction and there are no candidate kinetic models (which is assumed to be the case for this work), then the best start is to perform a traditional design of experiment technique [242]. In this case, where there are only three control variables (temperature, flowrate and feed concentration), it is reasonable to carry out a full factorial design at two levels, consisting of 8 steady-state experiments. Here, the levels for each variable were 100 ^{o}C and 120 ^{o}C, 20 µL/min and 40 µL/min and 1 M and 1.5 M benzoic acid feed concentration. However, in more general cases, if there were a larger number of control variables a fractional factorial or Plackett-Burman design could be used [242]. The automated reaction platform can then be used to carry out the corresponding experiments, as it can conduct a list of experiments given in advance by the user. In addition to the factorial screening, in order to check the stability of the catalyst, the 1st experiment conducted every day was repeated at the end of the day. Furthermore a new reactor was packed at the beginning of every day.

Step 2. Propose and Test Candidate Rate Laws. Candidate kinetic models can be proposed and tested against the initial experimental data collected from the factorial campaign. Any candidate model that fails the 95% χ^2 test, or has a parameter estimate whose entire 95% confidence interval is not realistic (e.g. negative activation energies), is rejected. All other models proceed to the next step.

Step 3. Practical Model Identifiability for a Given Experimental Budget. Model identifiability is a property of the model which describes if a model's parameters can be uniquely estimated; this depends on the model structure and the experimental data available [243]. Identifiability analysis [244] can be broadly divided into structural and practical identifiability. Structural identifiability analysis can be conducted by examining the model's equations and this is independent of experimental data, whereas practical identifiability, which is the focus of this work, examines if a model's parameters are identifiable with a given experimental data set. Generally, as the number of parameters in a model increase, the model gains improved data fitting capabilities at the cost of the parameter uncertainty becoming increasingly large (reduced identifiability). For a structurally identifiable model, parameter uncertainty normally reduces as more experiments are conducted.

A simulated practical identifiability test is simple to perform, a researcher with knowledge of the experimental system needs to decide what the allowable experimental design space is (the upper and lower limits for all experimental variables), what experimental measurements can be taken and what the expected measurement error for these measurements is. Then the experimental budget, the maximum number of experiments that can be performed, must be decided based on time and resource constraints. As practical identifiability is affected by the parameter values, a set of parameter values need to be chosen to be the true model parameters, an estimate for these values can be taken from the literature or from researcher experience. If there is very little confidence in these parameter estimates, the entire practical model identifiability analysis can be repeated numerous times with different parameter estimates. Finally all of the experiments in the experimental budget must be designed and then simulated with the model parameters. Randomly distributed measurement noise, equal to the expected level of measurement error in the real experiments, should be added to the simulated model predictions. These simulated data points are then called the practical identifiability simulated data set, and they are used for parameter estimation. The predicted t-values for each of the estimated parameters should then be computed and compared to the reference t-value. If the t-values for all of the parameters exceed the reference value, the model is declared practically identifiable for that experimental system and budget, for the assumed true parameter values. If however, one or more parameters fails the t-test, then the model is declared practically unidentifiable for that combination of experimental set up, budget and parameter values. However, as the experimental design dramatically affects model identifiability it may be possible that the candidate model is identifiable with improved experimental design. Normally to minimise computational effort the first experiment design used for practical identifiability tests is a factorial or latin hypercube design. However, if these strategies fail, then sequential MBDoE for improved parameter precision should be employed. This method is more computationally expensive, especially if there is a large experimental budget, so for that reason it may not be the immediate choice of experimental design. If the model still fails the practical identifiability test with the improved experimental design, than the model is declared practically unidentifiable. This procedure is shown in Figure 7-4.

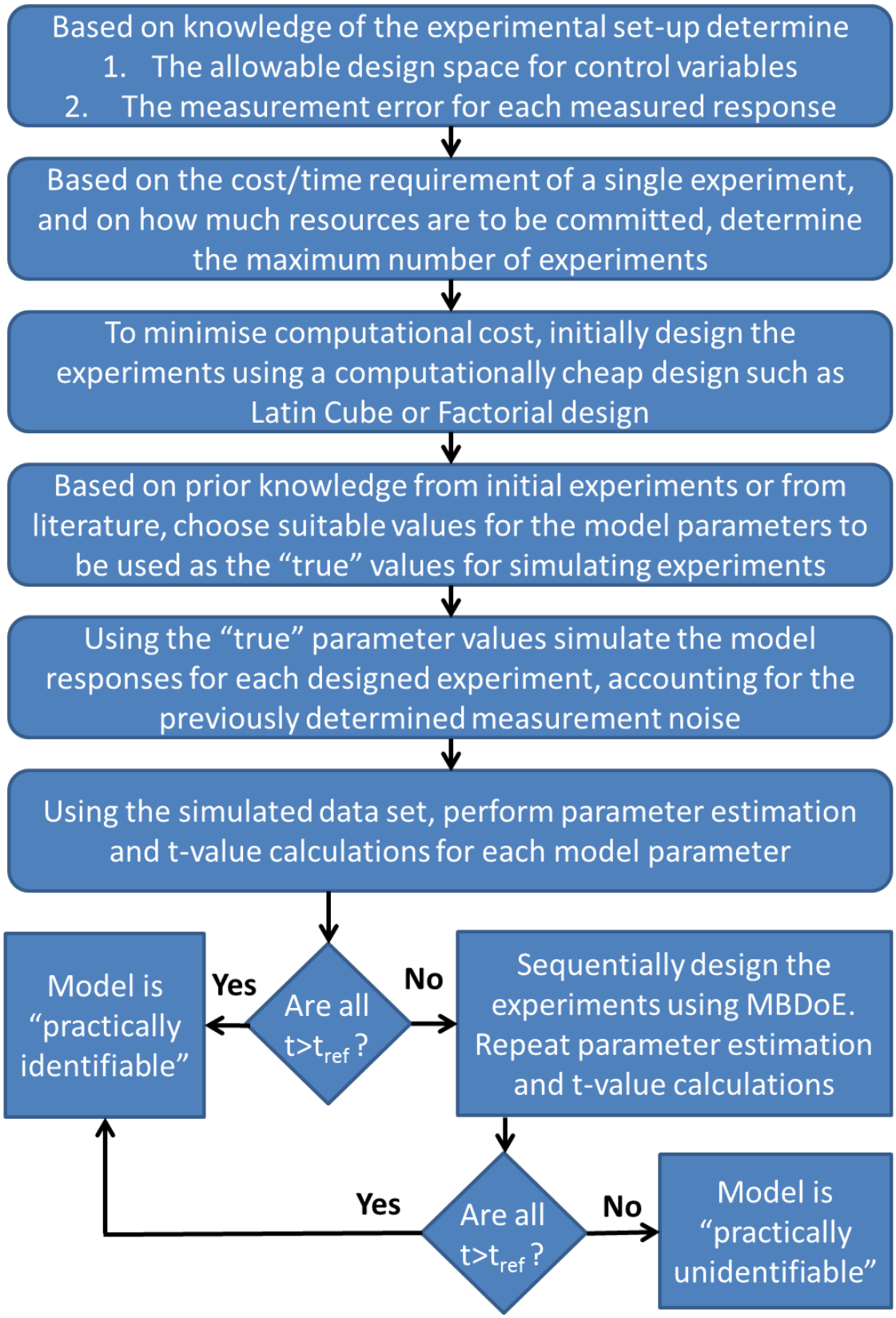

Figure 7-4 Flow chart demonstrating the steps in testing the practical identifiability of a single candidate model for a given experimental budget. This procedure should be repeated for each candidate model.

The simulated practical identifiability test described in Figure 7-4 was conducted for each of the candidate rate laws. In this case, the design space was defined as 80–120

^{o}C, 15–60 µL/min and 0.9-1.55 M, and then the maximum experimental budget was set at 64 experiments. The parameter values used to simulate the experiments were the estimates obtained from performing parameter estimation with the experimental data from step 1. Normally distributed noise with standard deviations equal to the level expected in the real experimental set-up was added to all simulated experiments. To increase computational efficiency, the practical identifiability of all models were initially tested against 64 experiments designed using a four level factorial design. However, if any model was deemed practically unidentifiable after this test (if one of the parameters failed the t-test), the procedure was repeated where the 8 actually conducted experiments from step 1 are used, followed by 56 simulated experiments sequentially designed by D- or E-optimal MBDoE. If a kinetic model failed the practical identifiability test at this point, the model was rejected.

Step 4. Online MBDoE for Model Discrimination. In order to identify the correct model from all the other candidate models that both fit the preliminary data and pass the practical model identifiability test, experiments should be conducted using online MBDoE for model discrimination. This is facilitated by the autonomous reactor platform, which is capable of performing online MBDoE for model discrimination between candidate models using the method proposed by Buzzi-Ferraris (see section 2.3.3 for further details) [38, 177]. Multiple experiments are conducted until all but one model is rejected for failing the 95% χ^2 test. When only a single model remains which passes the 95% χ^2 test, this is considered the correct kinetic model structure and it is brought forward to step 5. If it is not possible to distinguish between two or more models after a large number of discriminating experiments, it may be because the model uncertainty is too large and hence experiments have very little discriminating power. In this case it may be more useful to conduct a small number of experiments targeted at improved parameter precision for one of the candidate models, so that the model uncertainties can be reduced, hence making discrimination easier. If this does not work, the models may be too similar to distinguish for the given design space and the given level of experimental error. In this case, one of the models is chosen and brought forward to step 5. Alternatively if all models fail the χ^2 test it may be necessary to develop new models. It may be that all of the suitable models are rejected in the practical identifiability test. If this is the case, it is suggested to increase the maximum experimental budget to try and assist more models getting through the practical identifiability test.

Step 5. Online MBDoE for Improved Parameter Precision. With the single chosen model, experiments are now designed using online D-optimal MBDoE for improved parameter precision (see section 2.3.3 for further details). These experiments can be

conducted autonomously by the reactor platform and hence new experiments can be continuously conducted until a desired level of parameter precision is achieved, at which point the model is considered identified.

Note that the experimental system is capable of automatically performing all of the experimental steps in this methodology, steps 1, 4 and 5. However, the system does not automatically switch from one step to another. In the case of the factorial experiments in step 1, the platform will automatically stop once the final pre-defined experiment is finished, but for steps 4 and 5 where experiments are designed online by MBDoE, the system will run an infinite number of experiments unless the user intervenes and stops the experiments. Therefore, the user must manually select when to swap from discriminating experiments to parameter precision experiments. This decision is aided by the parameter statistics displayed on the LabVIEW user interface, which are automatically updated with each successive experiment.

7.3 Results & Discussion

Step 1. Factorial Screening & Catalyst Stability Check. The first kinetic experiments conducted were a campaign of 8 experiments designed by the factorial method. The experimental conditions are shown in Figure 7-5a, while the outlet concentrations are shown in Figure 7-5b, and are also reported in Table 7-5 at the end of the results section. In order to assess the stability of the catalyst, after the 8 experiments were completed, a 9th experiment was run at the same conditions as the first experiment. As shown in Figure 7-5b, the outlet concentration of the first and ninth experiment are approximately the same indicating that the catalyst is stable and no deactivation is present.

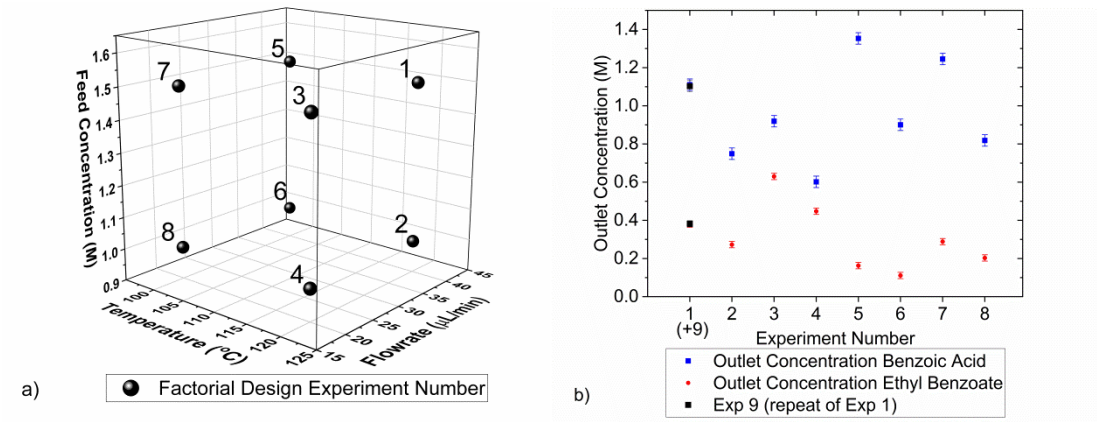

Figure 7-5 a) The experimental conditions of the 8 steady-state experiments designed by the factorial method. b) the outlet concentrations measured from these experiments.

Step 2. Propose and Test Candidate Rate Laws. The parameter estimates and 95% χ^2 values are reported in Table 7-1 for each reaction model considered and it can be observed that all models pass the 95% χ^2 test after the initial 8 experiments. Therefore all models are brought forward to step 3.

Table 7-1 The χ^2 values and parameter estimates obtained for each model after parameter estimation with the experimental data from the campaign of 8 factorial designed experiments.

Model	Reaction Rate Law	χ^2	χ^2ref	Parameters ± 95% Conf. Interval	Action
M1	$r'_{BA} = kC_{BA}C_{EtOH}$	10.5	23.7	*KP1* = 16.7 ± 0.07 *KP2* = 5.93 ± 0.60	Accept
M2	$r'_{BA} = \frac{kC_{BA}C_{EtOH}}{(1+K_WC_W)^2}$	7.34	22.4	*KP1* = 16.7 ± 0.14 *KP2* = 6.40 ± 0.90 K_W = 0.28 ± 0.39	Accept
M3	$r'_{BA} = \frac{kC_{BA}C_{EtOH}}{(1+K_WC_W+K_{EtOH}C_{EtOH})^2}$	6.41	21.0	*KP1* = 15.3 ± 4.49 *KP2* = 6.57 ± 1.02 K_W = 0.81 ± 2.57 K_{EtOH} = 0.06 ± 0.28	Accept
M4	$\frac{kC_{BA}C_{EtOH}}{(1+K_{BA}C_{BA}+K_{EtOH}C_{EtOH}+K_WC_W+K_{EB}C_{EB})^2}$	6.40	18.3	*KP1* = 13.4 ± 67.1 *KP2* = 6.57 ± 1.21 K_W = 0.82 ± 3048 K_{EtOH} = 0.25 ±10.0 K_{BA} = 0.16 ±6.11 K_{EB} = 1.49 ± 3060	Accept

Step 3. Practical Model Identifiability for a Given Experimental Budget. The experimental conditions designed from the four level factorial design are shown in Figure 7-6. The results of these simulated experiments show that model M3 and M4, which are Langmuir Hinshelwood type models with 4 and 6 parameters, are practically unidentifiable for a campaign of 64 factorial designed experiments, as the predicted t-values for the adsorption parameters are below the t-reference value, as shown in Table 7-2.

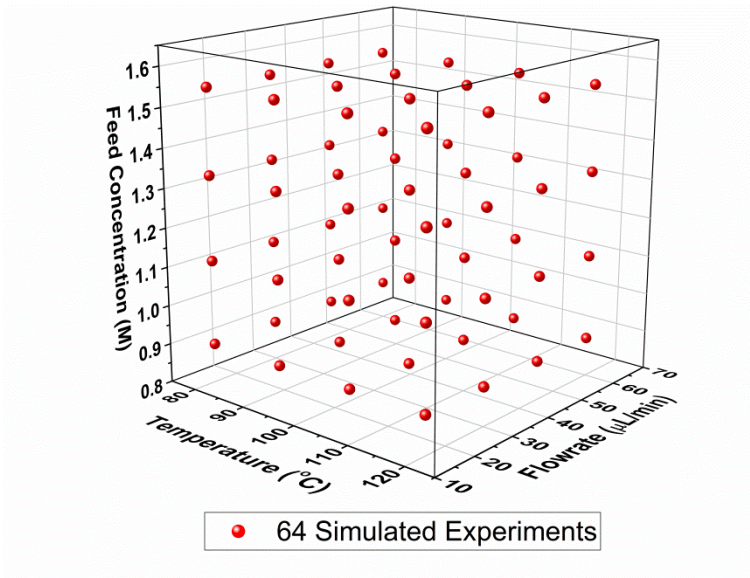

Figure 7-6 Experimental conditions for the simulated experiments for the practical model identifiability test in Step 3, designed by the factorial method.

Table 7-2 The predicted t-values for the parameters in each model estimated after parameter estimation with the data set obtained from the simulated campaign of 64 experiments designed by a four level factorial campaign.

	Reaction Rate Law	Predicted t-values (reference = 1.657)						Action
		KP1	*KP2*	K_W	K_{EtOH}	K_{BA}	K_{EB}	
M1	$kC_{BA}C_{EtOH}$	681	26.6	/	/	/	/	Accept
M2	$\frac{kC_{BA}C_{EB}}{(1+K_WC_W)^2}$	326	22.0	1.95	/	/	/	Accept
M3	$\frac{kC_{BA}C_{EB}}{(1+K_WC_W+K_{EtOH}C_{EtOH})^2}$	8.83	21.4	0.63	0.34	/	/	Reject
M4	$\frac{kC_{BA}C_{EB}}{(1+K_{BA}C_{BA}+K_{EtOH}C_{EtOH}+K_WC_W+K_{EB}C_E}$	0.87	19.6	0.02	0.10	0.10	-0.01	Reject

For model M3, which failed the factorial designed practical identifiability test, the practical identifiability was then repeated with MBDoE to improve the predicted t-values. This was not done for model M4, as model M4 was not even close to being practically identifiable for this experimental budget and design space. The designed experiments are shown in Figure 7-7 a and b for D and E-optimal designs, and the parameter statistics show that the model was still unidentifiable despite some improvements in the predicted t-values, as shown in Table 7-3. Therefore both model M3 and M4 were rejected due to them being practically unidentifiable and only models M1 and M2 were brought forward to step 4. This is not an unusual result, as the estimation of all of the adsorption terms in the Langmuir Hinshelwood equation is frequently so difficult that the use of simplified Langmuir Hinshelwood rate laws is common in the literature [237]. Furthermore, in the cases where studies report kinetic

parameters for the full Langmuir-Hinshelwood rate law, they usually just report parameter values without confidence intervals or t-values [238], therefore it is possible that these estimated values are actually estimated poorly with large confidence intervals.

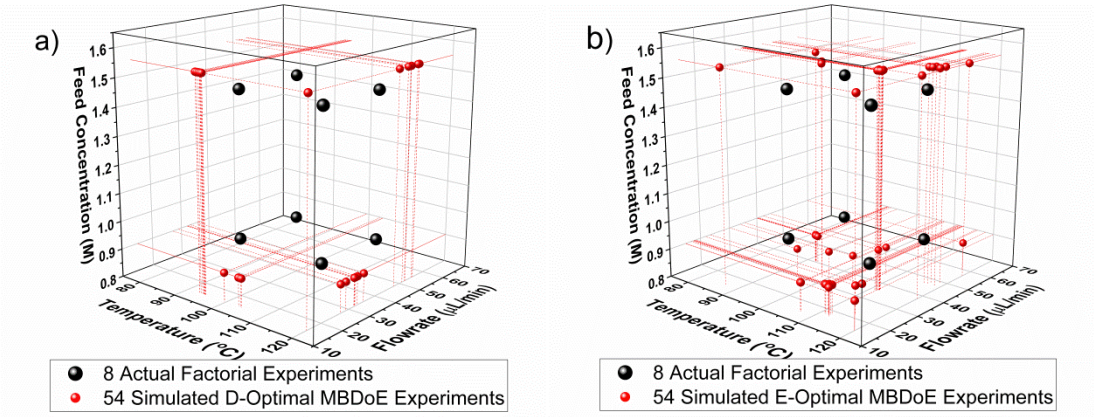

Figure 7-7 Experimental conditions of the 54 simulated experiments sequentially designed by a) D-optimal MBDoE and b) E-optimal MBDoE, for testing practical identifiability of model M3.

Table 7-3 Predicted t-values for the parameters in each model, as estimated after performing parameter estimation with the data set of 64 simulated experiments designed by D- and E-optimal MBDoE applied to model M3.

Model	Design Method	t-value *KP1*	t-value *KP2*	t-value K_W	t-value K_{EtOH}	t-value ref	Action
M3	4 Level Factorial	8.80	21.4	0.63	0.34	1.66	Reject
M3	D-Opt MBDoE	5.80	33.8	0.60	0.51	1.66	Reject
M3	E-Opt MBDoE	9.03	16.3	0.77	0.63	1.66	Reject

The practical identifiability step is important as time is not wasted pursuing models that are not identifiable with the available experimental set-up and experimental budget. Therefore, rather than pursuing a model which may be the true mechanistic model, such as the 6 parameter Langmuir Hinshelwood model M4, instead resources are better spent obtaining a practical model such as the simplified 3 parameter Langmuir Hinshelwood model M2, that can describe the reaction behaviour in the allowable design space. While it can be argued that simplified models will behave poorly when extrapolated outside of the design space they were developed in, this is also the case for true models if their parameters are estimated poorly. Furthermore, while simplified model structures give less mechanistic information about the behaviour of the catalyst, they can still be used for reactor design and process control, as long as the process conditions are within the domain of model validity. Therefore, in many industrial applications a simplified model could be sufficient.

Step 4. Online MBDoE for Model Discrimination. The number of candidate models is now reduced to 2 after models M3 and M4 were rejected for being practically non-identifiable for this experimental set-up and budget. In order to distinguish between the remaining two models, model M1 and model M2, a campaign of online experiments designed by the Buzzi-Ferraris method of MBDoE for model discrimination [38, 177] was conducted using the autonomous reactor platform. The initial 8 experiments from the factorial campaign were used as preliminary information when designing discriminating experiments. The designed experimental conditions are shown in Figure 7-8, and they are reported along with the measured outlet concentrations in Table 7-5 at the end of the results section. The statistics after each experiment are shown in Table 7-4, where it can be seen that model M1 can be rejected after just 1 discriminating experiment as it failed the 95% χ^2 test. However, the automated system did not have a stop condition to automatically detect when to stop performing model discrimination and when to perform MBDoE for parameter precision. Therefore, three more experiments for model discrimination were designed online and executed before the user intervened and changed the design criteria to MBDoE for parameter precision with model M2.

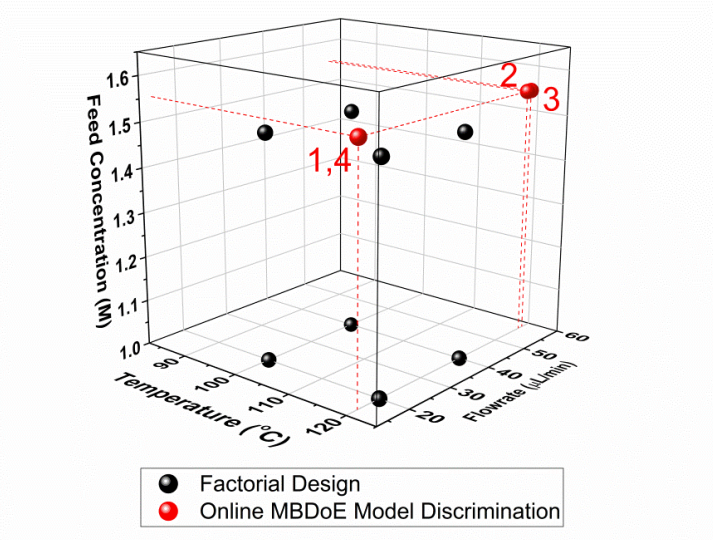

Figure 7-8 Experimental conditions of the MBDOE designed discriminating experiments during Step 4. Numbers indicate the order in which experiments were conducted.

Table 7-4 The χ^2 values obtained by online parameter estimation conducted after each successive model discrimination experiment designed by MBDoE as part of Step 4.

Experiments Conducted	Model M1 χ^2/χ^2ref	Model M2 χ^2/χ^2ref	Action
8 Factorial	10.5/23.7	7.34/22.4	Accept Both Models
8 Factorial + MD1	35.4/26.3	13.5/25.0	Reject Model 1
8 Factorial + MD2	37.6/28.9	17.9/27.6	Reject Model 1
8 Factorial + MD3	41.9/31.4	24.2/30.1	Reject Model 1
8 Factorial + MD4	54.7/33.9	26.9/32.7	Reject Model 1

Interestingly, it is observed that after the 4th discriminating experiment, all the parameters in model M2 passed the t-test, as shown in Table 7-5 (highlighted in red and green). This is significant as passing the t-test for all parameters is frequently used as the criterion for identifying a model and ending the experiments.

Step 5. Online MBDoE for Improved Parameter Precision. The single candidate model, M2, which was both practically identifiable and capable of fitting all the experimental data collected, was already identified in the model discrimination stage, as all the parameters passed the t-test. However, in order to improve the confidence in which the parameters are known, and to hence improve model prediction certainty, a campaign of online MBDoE experiments for improved parameter precision using the D-optimal criterion was performed by the autonomous reactor platform. The experimental measurements from the 8 factorial experiments and the 4 discriminating experiments were provided to the MBDoE algorithm to give prior information about the system. The experimental conditions designed by the MBDoE algorithm are shown in Figure 7-9, and are reported in Table 7-5. The automated system was stopped by user intervention at the end of a working day, when it had designed and performed 8 experiments.

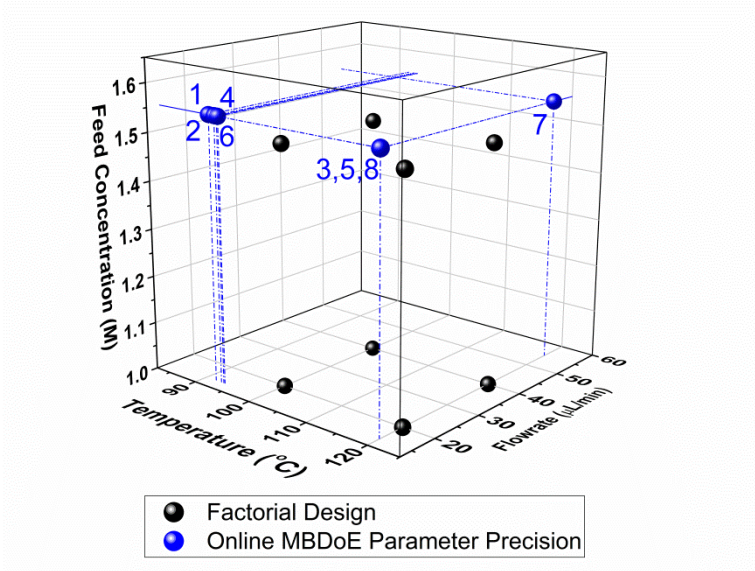

Figure 7-9 Experimental conditions of the D-optimal MBDOE designed experiments for improved parameter precision during Step 5. Numbers indicate the order in which experiments were conducted.

The parameter statistics after these 8 experiments, were found to have improved significantly compared to their values at the end of the model discriminating experiments, with the confidence intervals for parameters *KP1*, *KP2* and K_W being reduced from 0.11, 0.74 and 0.25 to 0.08, 0.45 and 0.2. At this point, the model is declared to be well identified with acceptable confidence intervals and no further experiments were considered necessary.

The final parameter estimates for *KP1*, *KP2* and K_W are converted back to the original form of the Arrhenius equation and the final rate expression is shown in Eq (7-4) where the pre-exponential factor k_0 was 185.3 $L^2\ g^{-1}\ s^{-1}\ mol^{-1}$, the apparent activation energy *Ea* was 68.8 kJ/mol and the adsorption constant of water K_W was 0.53 L/mol. In comparison with the literature, Pipus et al, reported a similar activation energy of 69.1 ± 0.5 kJ/mol [231]. Further comparisons of the model parameters cannot be made as Pipus et al used a different model structure, they reported that the reaction could be modelled as second-order with respect to benzoic acid without any adsorption terms.

$$r'_{BA} = \frac{185.3 * exp\left(-\frac{68800}{RT}\right) * C_{BA}C_{EtOH}}{(1 + 0.53C_W)^2} \tag{7-4}$$

The adequacy of the model developed in this work is demonstrated by passing the 95% χ^2 test and the parity plot in Figure 7-10.

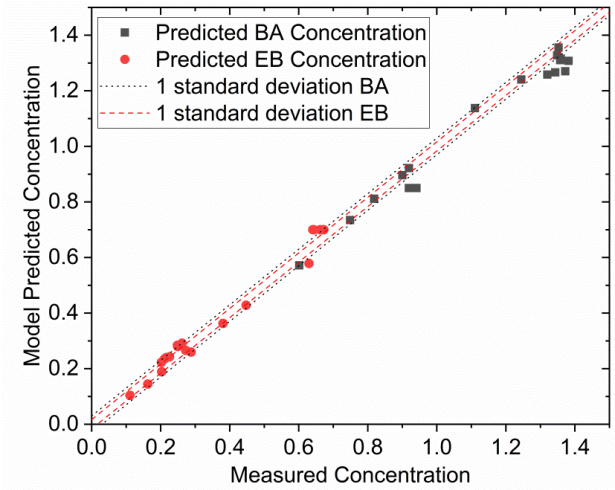

Figure 7-10 Parity plot for the model predicted and experimentally measured concentrations of benzoic acid and ethyl benzoate.

It can be shown that the model prediction uncertainty decreased significantly after conducting the 8 MBDoE experiments for improved parameter precision, as shown in Figure 7-11. The model uncertainty figures were created by randomly drawing 10,000 parameter sets from a multivariate normal distribution function, with the MLE values $\hat{\boldsymbol{\theta}}$, and the covariance matrix $\mathbf{V_\theta}$. Each of these 10,000 parameter sets were then used to simulate the reactor at a range of reaction conditions and the model predicted responses were recorded. The model prediction responses were then used to create the observed frequency distributions in Figure 7-11, which shows the model prediction uncertainty. If even smaller confidence intervals were required it would be possible to continue performing further experiments designed by MBDoE, however the expected gain in information with further experiments is expected to be diminishing, unless changes to the experimental procedure allowed an exploration of a wider design space.

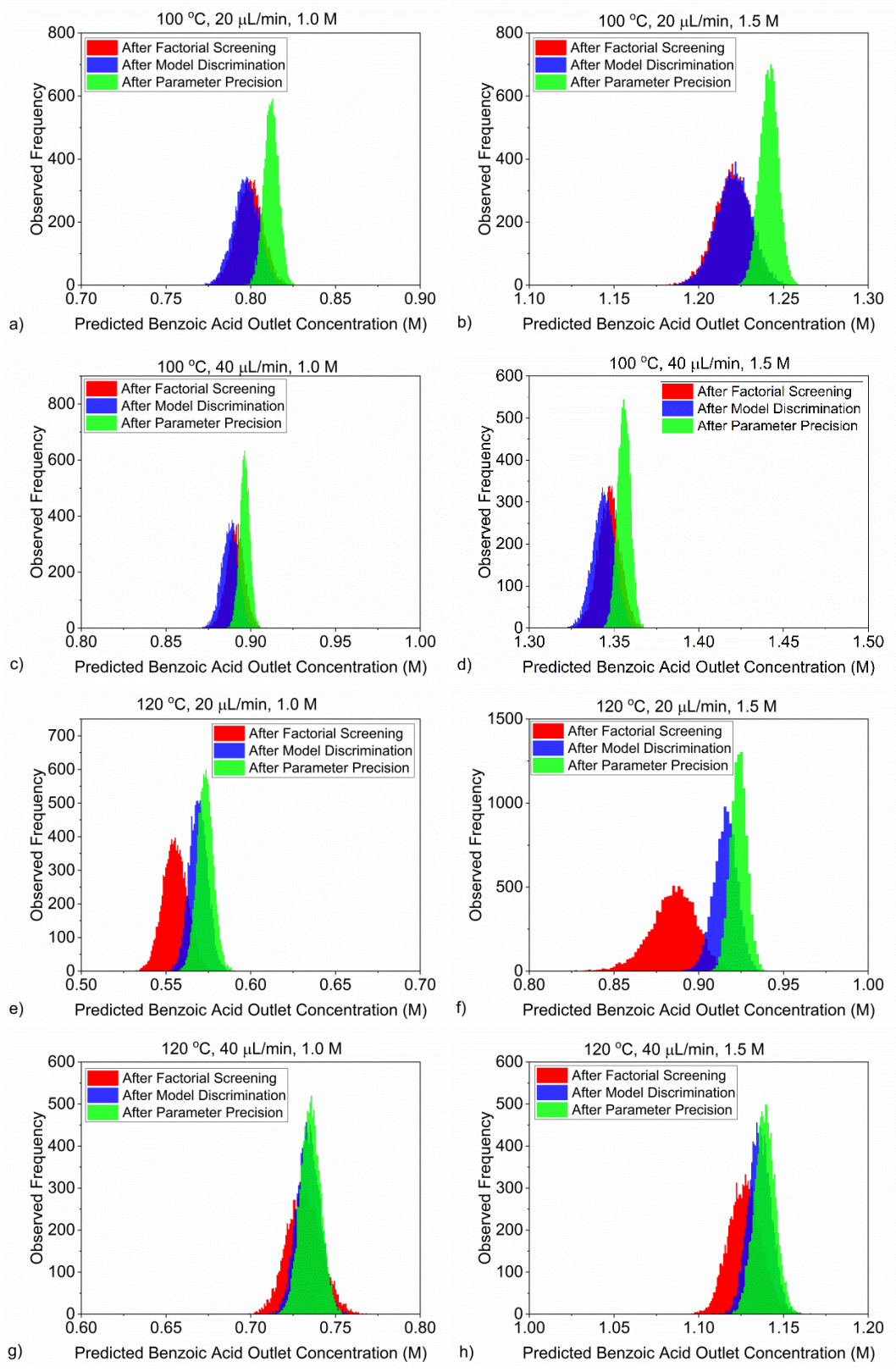

Figure 7-11 Model prediction for model M2 at a reaction temperature of 120 °C, an inlet flowrate of 20 µL/min and a feed concentration of 1.5 M benzoic acid and 0.1156 g of Amberlyst-15 catalyst after the factorial (Step 1), model discrimination (Step 4) and parameter precision campaigns (Step 5).

Table 7-5 Experimental conditions, measured outlet concentrations and parameter statistics (for model M2) for all experiments conducted (including 8 factorial experiments, 4 MBDoE for model discrimination experiments and 8 MBDoE for parameter precision.

Exp.	Temp.	Flowrate	Conc.	Cat. diameter	Cat. mass	BAC	EBC	KP1	KP2	K_W	KP1 95%CI	KP2 95%CI	K_W 95%CI	KP1 t-value	KP2 t-value	K_W t-value	t-ref	X^2	X^2 ref
	°C	µL/min	M	µm	g	M	M												
F1	120.00	40.00	1.50	950	0.1156	1.111	0.381												
F2	120.00	40.00	1.00	950	0.1156	0.749	0.273												
F3	120.00	20.00	1.50	950	0.1156	0.920	0.630												
F4	120.00	20.00	1.00	950	0.1156	0.602	0.448												
F5	100.00	40.00	1.50	950	0.1156	1.353	0.163												
F6	100.00	40.00	1.00	950	0.1156	0.901	0.111												
F7	100.00	20.00	1.50	950	0.1156	1.245	0.288												
F8	100.00	20.00	1.00	950	0.1156	0.819	0.203	16.65	6.40	0.28	0.14	0.90	0.39	116.60	7.15	**0.71**	1.77	7.34	22.36
MD1	120.00	15.00	1.55	825	0.1014	0.919	0.641	16.56	6.76	0.62	0.14	0.94	0.40	115.60	7.20	**1.55**	1.75	13.46	25.00
MD2	120.00	56.86	1.55	825	0.1014	1.343	0.249	16.60	6.45	0.47	0.12	0.80	0.30	139.00	8.07	**1.57**	1.74	17.90	27.59
MD3	120.00	57.93	1.55	825	0.1014	1.372	0.249	16.62	6.28	0.40	0.11	0.73	0.26	154.00	8.59	**1.56**	1.73	24.21	30.14
MD4	120.00	15.00	1.55	825	0.1014	0.930	0.644	16.60	6.33	0.48	0.11	0.74	0.25	156.13	8.60	**1.94**	1.72	26.89	32.67
PP1	91.68	15.00	1.55	825	0.1043	1.349	0.202	16.63	6.61	0.50	0.10	0.61	0.25	164.87	10.87	2.02	1.71	28.59	35.17
PP2	92.68	15.00	1.55	825	0.1043	1.359	0.211	16.64	6.77	0.51	0.10	0.55	0.25	169.56	12.36	2.07	1.71	30.43	37.65
PP3	120.00	15.00	1.55	825	0.1043	0.937	0.673	16.63	6.78	0.53	0.10	0.54	0.23	174.59	12.45	2.27	1.70	33.58	40.11
PP4	93.13	15.00	1.55	825	0.1043	1.358	0.216	16.64	6.88	0.53	0.09	0.51	0.23	178.06	13.54	2.29	1.70	34.95	42.56
PP5	120.00	15.00	1.55	825	0.1043	0.941	0.670	16.64	6.89	0.55	0.09	0.51	0.22	180.92	13.59	2.44	1.70	38.40	44.99
PP6	93.35	15.00	1.55	825	0.1043	1.382	0.226	16.64	6.95	0.55	0.09	0.48	0.22	183.55	14.43	2.46	1.69	41.85	47.40
PP7	120.00	54.96	1.55	825	0.1043	1.320	0.262	16.66	6.87	0.51	0.08	0.45	0.20	201.04	15.30	2.54	1.69	43.93	49.80
PP8	120.00	15.00	1.55	825	0.1043	0.928	0.662	16.66	6.88	0.53	0.08	0.45	0.20	202.81	15.32	2.66	1.69	45.63	52.19

7.4 Conclusions

A five step methodology was developed to offer a systematic way to identify practical kinetic models with the minimum number of experiments. In this case the 5-step methodology was conducted using a string reactor and the automated reactor platform, which led to the identification of a simplified 3-parameter Langmuir Hinshelwood model as the most appropriate kinetic model for the esterification of benzoic acid and ethanol using an Amberlyst-15 catalyst. The adequacy of the model was validated using the χ^2 test and a parity plot. The number of experiments required were minimised by using online MBDoE for model discrimination and improved parameter precision, and by using practical identifiability tests to prevent resources being wasted pursuing non identifiable models. Using the automated system offered considerable time savings with all of the kinetic experiments in this work being completed in just three days.

8 Rapid Kinetic Modelling: Automated Kinetic Study of HMF Oxidation in Micropacked Bed Reactor

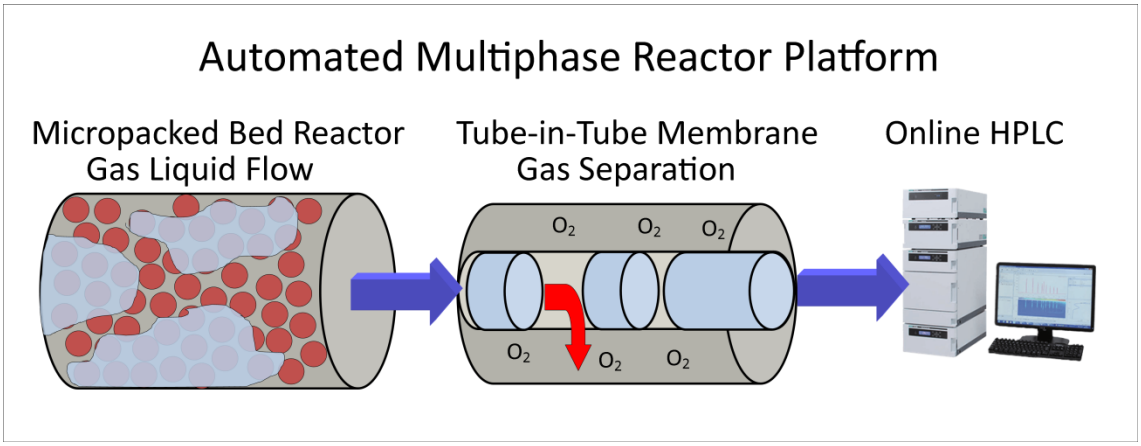

Abstract

An automated reactor platform was developed that was capable of performing the three step oxidation of HMF to FDCA in a micropacked bed reactor with gas liquid flow without user supervision. The automated system included online gas liquid separation and online HPLC analysis of the liquid product. This automated system was successfully used to screen five different Au and AuPd/TiO_2 catalysts in the presence of NaOH. It was observed that only the Au/TiO_2 catalysts underwent reversible deactivation at low temperatures of 60 ^oC, and that the AuPd/TiO_2 catalysts were most active and selective to FDCA. A factorial campaign of experiments using a AuPd/TiO_2 catalyst was conducted without user supervision to study the effect of temperature, catalyst mass, NaOH concentration and oxygen concentration. The oxidation of HMF was found to occur by three sequential oxidation reactions, oxidising HMF to HFCA to FCA and finally to FDCA. It was shown that oxygen concentration increased the rate of all reactions, while the NaOH concentration only significantly increased the rate of FCA oxidation. Maximum yields of FDCA were obtained at 100 ^oC, as further increases in temperature led to excessive degradation of the HMF feed. The factorial experiments were found to have low reproducibility and a difference in activity was observed between reactor packings. The cause of these errors was unknown but it speculated to be caused by errors in measuring the catalyst mass, non-reproducible reactor packing or differences in activity within the catalyst batch. These challenges prevented the identification of a single reliable kinetic model for this reaction.

8.1 Introduction

Up to this point in the thesis, an automated reactor platform capable of performing online MBDoE has been developed and demonstrated on simple case study reactions, the homogenous and heterogeneous esterification of benzoic acid and ethanol. Therefore, the final part of this thesis is to apply this reactor platform to a much more challenging and industrially interesting reaction, the aerobic oxidation of 5-hydroxymethylfurfural (HMF) to 2,5 furandicarboxylic acid (FDCA) in a micropacked bed reactor with gas liquid flow.

HMF is an important molecule obtained from biomass via acid dehydration of hexose, and it can be used to produce a wide variety of chemicals, polymers and biofuels [245-247]. The oxidation of HMF to FDCA was chosen as the case study for this work due to the potential of FDCA to produce polyethylene furanoate (PEF), a bioplastic which could replace fossil-based polyethylene terephthalate (PET) [245, 248, 249]. Furthermore, there has been significant research conducted on this reaction in batch [248, 250-255], but to the best of the author's knowledge it has not been conducted in flow. The production of FDCA from HMF is shown in Figure 8-1 [256], where it can be observed that the aldehyde and alcohol functional groups are progressively oxidised to produce 5-hydroxymethyl-2-furancarboxylic acid (HFCA), 5-formyl-2-furancarboxylic acid (FCA) and then 2,5-furandicarboxlyic acid (FDCA) [256].

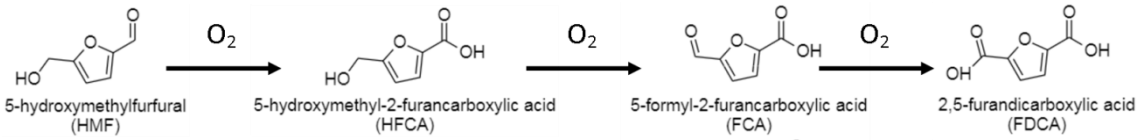

Figure 8-1 Reaction network for HMF oxidation.

The most promising catalysts reported in the literature for HMF oxidation to FDCA are supported noble metal nanoparticle catalysts [248, 250-255] in alkaline solutions, which can produce high yields of up to 99% under mild temperature and pressure conditions (65-130 ^{o}C, 10 bar air) [248]. For this reason, this reaction is studied using Au/TiO_2 and AuPd/TiO_2 catalysts. The challenges in this reaction include the degradation of HMF in the presence of base by ring opening reactions to form products such as levulinic and formic acids [248, 251, 252], reduced selectivity to FDCA at elevated temperatures above 80 ^{o}C [248], the requirement of low substrate to catalyst ratios [248, 251] and poor catalyst stability [248, 251]. The reaction pathway and mechanism for HMF oxidation to FDCA vary depending on what catalyst and base are used [253, 254, 257]. For Au and Pt supported nanoparticles in alkaline environment, the expected reaction mechanism, developed through isotype labelling experiments [253, 256], involves oxidation of the HMF's aldehyde functional group through a two-step process forming a

geminal diol intermediate. The HMF's alcohol group is then oxidised to form an aldehyde, which is also oxidised via the geminal diol intermediate. In these mechanisms, oxygen acts only as an electron scavenger; while the oxygen required for the reaction is obtained from water [253, 256]. The base, typically NaOH, ensures that the products are removed from the catalyst surface and are soluble in the solvent [248]. The base is also necessary in the oxidation of the alcohol group, particularly for Au catalysts which are less active for alcohol group oxidation than Pt or Pd [256]. Despite these mechanistic studies, there are comparatively few kinetic studies, with some initial work conducted in batch suggesting that all the reactions are zero order with respect to the reactant and with respect to oxygen, but that the aldehyde oxidation steps are first order with respect to the base concentration [256]. The activation energy for HMF oxidation to HFCA, and for HFCA oxidation to FCA were reported to be 29.0 and 29.6 kJ/mol respectfully, but the final reaction, FCA oxidation to FDCA, which is known to be very fast compared to the other reactions, was not modelled. Therefore, it is the objective of this work to try and expand on this work to create a more detailed kinetic model for this reaction.

In addition to the complex chemistry of this reaction network, this case study is very challenging because it is a three-phase reaction in a micropacked bed reactor. Multiphase systems are much more difficult to automate than single phase systems because it is often required to separate the phases at the reactor outlet before conducting online analysis. For this reason, there exist only a small number of three phase automated systems with online analysis reported in the literature, such as the automation of a catalytic wall coated reactor with gas liquid flow using GC analysis of the liquid [32] and the automation of a micropacked bed reactor with inline FTIR analysis [172]. Furthermore, micropacked bed reactors are a particularly difficult reactor configuration to study [172]. In comparison to wall coated tube reactors, microreactors have considerably more complex hydrodynamic and mass transfer behaviour [6, 43, 62] and they are more prone to non-ideal reactor effects including channelling and non-reproducible reactor packing. A fully comprehensive model of a reaction in a micropacked bed reactor would include multiple flow regimes [43], liquid hold up, axial and radial dispersion [258], gas-liquid mass transfer, liquid-solid mass transfer, catalyst wetting and internal mass transfer resistances in the catalyst particle [259, 260]. Very often these models include many unknown reactor parameters including mass transfer coefficients, liquid hold up and axial dispersion coefficients resulting in it being impossible to simultaneously estimate the kinetic parameters and the reactor parameters [261, 262]. For these reasons, detailed kinetic studies in micropacked bed reactors, or lab scale trickle bed reactors are very challenging and

are quite rare. In some cases researchers prefer to study the kinetics of three phase reactions using powder catalysts in batch reactors and then validate the obtained kinetics in packed bed reactors [260, 263]. In other cases researchers avoid modelling the micropacked bed reactor at all, instead they check that the reactor is not limited by heat or mass transfer resistances and they operate in differential mode with conversion less than 10%. They can then calculate the rate of reaction as the rate of product formation divided by the mass of catalyst, and they can fit kinetic models directly to this rate data [29, 45, 264-266]. Alternatively, a common approach, and the approach used in this work, is to make a number of simplifying assumptions when modelling the reactor, and then to operate at only a single gas liquid flowrate so that greater focus can be directed towards the kinetics [168, 169, 267, 268].

8.2 Materials & Methods

8.2.1 Catalyst Details, Reactor Design and Experimental Set Up

The oxidation of HMF was studied using five different Au and AuPd catalysts supported on TiO_2. The details of all five catalysts are shown in Table 8-1, where it can be observed that in all cases the nanoparticle loading was 1 wt%. The catalyst were obtained from the group of Prof Hutchings in Cardiff and their synthesis procedures are shown in Appendix A. In all cases the catalyst sieve fraction used in the micropacked bed reactor was 63-75 µm.

Table 8-1 Catalyst batch details

Batch Number	Nanoparticle
1	1 wt% Au/TiO_2
2	1 wt% Au/TiO_2
3	1 wt% Au/TiO_2
4	1 wt% 50:50 $AuPd/TiO_2$
5	1 wt% 95:5 $AuPd/TiO_2$

The micropacked bed reactor used in this work consisted of an 18 cm long, 750 µm i.d. PFA tube (Upchurch Scientific) and a schematic of the reactor is shown in Figure 8-2. The catalyst was retained in the tube using a 25 µm pore size nickel mesh (Tecan, UK) which was held in place at the reactor outlet by compressive force between a PEEK ferrule (Upchurch Scientific) and a PEEK union (Upchurch Scientific). A section of 75 µm glass beads (Sigma Aldrich), approximately 5 cm in length, was placed before and after the catalyst section in the packed bed to ensure that the gas-liquid flow in the packed bed was fully established at the catalytic section. The length of the catalyst section varied from approximately 1 cm for 4 mg of catalyst to 3 cm for 13 mg of catalyst, resulting in a total packed bed length of approximately 12 cm. Unfortunately,

this was later shown to be a poor reactor design. The biggest problem was that it is very difficult to accurately measure such small catalyst masses and it is suspected that measurement errors in weighing the catalyst mass may have contributed to the non-reproducible results that will later be discussed. A second potential problem that was identified was the use of plastic tubing for the reactor. As plastic tubing can be bent, pinched and compressed, it is likely that the internal diameter of the reactor and hence the hydrodynamic behaviour and reactor performance may vary from reactor packing to reactor packing. Instead precision glass capillaries with a larger catalyst mass may have been a more appropriate reactor design.

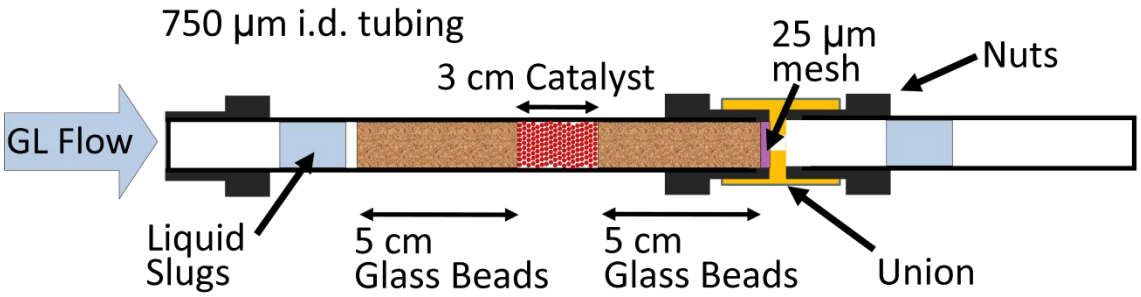

Figure 8-2 Tubular micropacked bed reactor for the HMF reaction.

The experimental set-up, shown in Figure 8-3, consisted of the same automated reactor platform and the same LabVIEW codes used in the previous work, but adapted for the requirements of the new reaction. The reactor was heated by submerging it in an oil bath and the reactor was assumed to behave as a plug flow reactor as residence time distribution studies in the literature for similar micropacked bed reactors observed only minor deviations from ideal plug flow [62, 269]. The liquid reagents, HMF and NaOH, could not be pre-mixed in a single syringe as HMF decomposes in the presence of bases [248, 251, 252]. Therefore a 0.1 M aqueous solution of HMF in water, and a 0.2 or 0.4 M aqueous solution of NaOH were separately prepared and fed to the reactor using two syringe pumps (neMESYS, low pressure module, Cetoni) with 5 mL glass syringes (5 mL mid pressure, Cetoni). As NaOH is very corrosive, it could not be loaded directly into the syringe. Instead the NaOH was loaded into a 7.5 m long, 1 mm i.d. PEEK tube, which was connected to a syringe filled with heptane. Therefore, the heptane syringe would push the desired flowrate of NaOH solution into the reactor. The gas feed to the reactor consisted of a mixture of oxygen and nitrogen delivered using mass flow controllers (Brooks 5850TR). The gas and liquid streams met at a T junction producing gas liquid slug flow before entering the reactor. The reactor outlet stream was connected to a tube-in-tube membrane where the gas would be removed and only the liquid would pass on to the 6-way switching valve of an automatic sampler-dilutor (Syrris, Asia Sampler and Dilutor) for online HPLC analysis. The tube-in-tube

membrane consisted of a 65 cm long Teflon AF-2400 tubular membrane (Biogeneral, U.S.) of i.d. 0.8 mm and thickness 0.1 mm, which was placed inside a PTFE tube of 2.4 mm i.d. (VICI Jour). The outlet of the 6-way switching valve was then connected to a waste pressure vessel consisting of centrifuge tube (Corning 50 mL) with a custom made PEEK holder with three ports designed to withstand high pressure. To facilitate gas separation in the membrane, the system pressure was maintained at 5 barg using a back-pressure regulator (Swagelok K series, 250 psig). Pressure sensors were placed on the gas inlet lines (Honeywell 40PC, 250 psig) so that the reactor inlet pressure (pressure sensors P2 and P3) and outlet pressure (pressure sensor P1) could be measured. Equipment calibrations are shown in Appendix B.

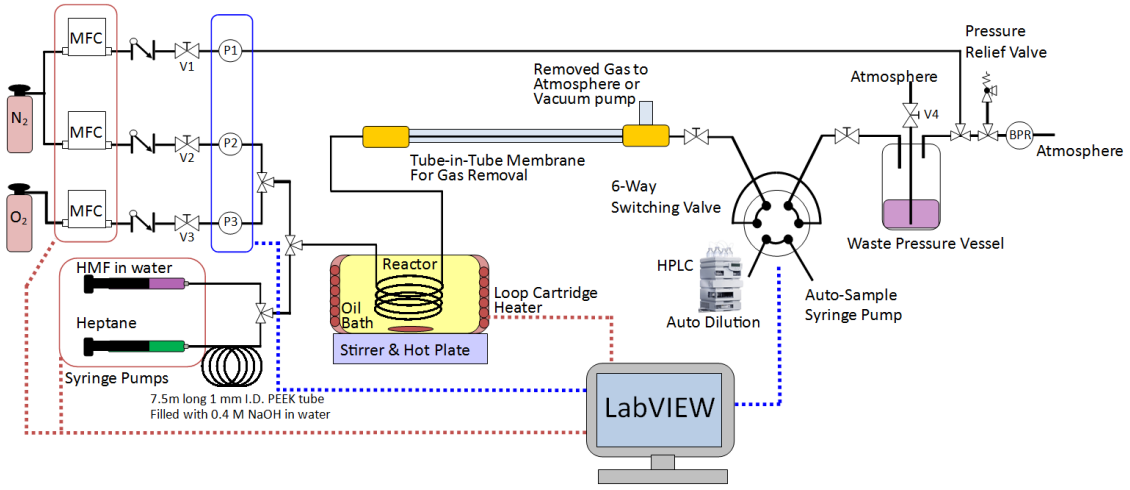

Figure 8-3 Experimental set-up up for the oxidation of HMF in a micropacked bed reactor. Red dashed lines indicate LabVIEW controls the equipment, blue dashed lines indicate LabVIEW reads the measurement from the equipment.

The online HPLC analysis method began with sample dilution by a factor of 20 with deionised water before injection into a MetaCard 67H (Agilent) column. The mobile phase was 0.01 M sulfuric acid aqueous solution pumped at a flowrate of 0.8 mL/min, while the column was maintained at 50 ^{o}C. The analysis time was 20 min and the UV detection at 210 nm was used for quantification of HMF, HFCA, FCA and FDCA (calibration shown in Appendix B). Minor peaks were observed in the HPLC chromatograph, due to HMF degradation and undesired side reactions [248, 251], however, these species could not be identified.

8.2.2 Experimental Protocol

Three types of experiments were conducted in this work, blank experiments to study the system behaviour without the catalyst, catalyst screening experiments to identify the most active and stable catalyst and finally a factorial campaign of experiments to generate the kinetic data required for model identification. In all cases the reactor was run in steady-state mode.

The blank experiments were conducted with empty reactors and with reactors loaded with TiO_2 without any supported metal nanoparticles to study HMF degradation and to confirm that the reaction does not occur without a catalyst.

The catalyst screening experiments consisted of running the reaction at 100 ^oC for 2 h, before dropping to 60 ^oC for 2 h and returning again to 100 ^oC, all while sampling every 20 min to check for the presence of deactivation. For these experiments the experimental conditions were a liquid flowrate of 20 µL/min, a gas flowrate of 2 NmL/min oxygen, a system pressure of 5 barg and approximately 8 mg of catalyst. The liquid feed was 50 mM HMF for all experiments and a 4:1 ratio of NaOH:HMF was used for three of the catalyst batches, but a ratio of just 2:1 was used for catalyst batches 2 and 3.

The kinetic study, conducted with the best catalyst selected from the screening study, consisted of running a factorial campaign of steady-state experiments at four temperature levels (60, 80, 100 and 120 ^oC), three catalyst masses (4, 8, 12 mg), two NaOH:HMF ratios (4:1 and 2:1) and two oxygen compositions of the feed gas (50% and 100% by mol) resulting in a total of 48 experiments. The system pressure was fixed at 5 barg, the feed concentration of HMF was 50 mM and the liquid and gas flowrates were 20 µL/min and 2 NmL/min. Each experiment was run for 80 min in order to collect triplicate sampling (at 40, 60 and 80 min of operation) and the measured steady-state outlet concentration was calculated as the average of the three measurements. For these factorial experiments, a single reactor would be packed and used for two days before being discarded. The reactor was left in oxygen only flow overnight at room temperature, and to check for catalyst deactivation, a reference experiment (80 ^oC, 2 NmL/min O_2 flowrate, 20 µL/min liquid flowrate) was run at the start and end of both days. As the reference experiment would be run four times for each reactor, the standard deviation of each reactor could be calculated from the 4 experiments. In total 6 reactors were used for the factorial study and the standard deviation of the experimental error was then estimated as the pooled standard deviation of all of the 6 reactors used. Due to the repetition of the standard condition, 71 experiments were conducted in this factorial campaign.

8.2.3 Reactor Model

The model developed to describe the oxidation of HMF in a micropacked bed reactor includes three oxidation reactions in series as shown in Eq (8-1) to (8-3). The product FDCA has two acid functional groups, and as the reaction is conducted in basic environment, the products exist as anions and OH^- ions are consumed in reactions (8-1) and (8-3) as each acidic group is formed [248]. Because NaOH is a strong base,

it completely dissociates in water such that the concentration of OH^- ions equals the concentration of NaOH.

$$HMF + \frac{1}{2}O_2 + OH^- \rightarrow HFCA^- + H_2O \quad (8\text{-}1)$$

$$HFCA^- + \frac{1}{2}O_2 \rightarrow FCA^- + H_2O \quad (8\text{-}2)$$

$$FCA^- + \frac{1}{2}O_2 + OH^- \rightarrow FDCA^{2-} + H_2O \quad (8\text{-}3)$$

Rather than using Langmuir Hinshelwood rate laws which would introduce a large number of kinetic parameters, each reaction is modelled with a simple power law to try and improve the identifiability of the model parameters, as shown in Eq (8-4) to (8-6). The reactions were originally assumed to be first order with respect to oxygen, base and substrate concentration, however when trying to fit the experimental data and perform parameter estimation different reaction orders were considered.

$$-r'_{HMF} = k_{HMF}C_{HMF}C_{O_2}C_{NaOH} \quad (8\text{-}4)$$

$$-r'_{HFCA} = k_{HFCA}C_{HFCA}C_{O_2}C_{NaOH} \quad (8\text{-}5)$$

$$-r'_{FCA} = k_{FCA}C_{FCA}C_{O_2}C_{NaOH} \quad (8\text{-}6)$$

In the rate law equations, r'_j is the rate of the j[th] reaction, C is concentration, $C_{O_2}$is the dissolved concentration of oxygen, C_{NaOH} is the concentration of base and k_j is the reaction rate constant for reaction j, described here using the reparameterised form of the Arrhenius equation to reduce parameter correlation, where T_M, the mean temperature has a value of 353.15 K.

$$k_j = exp\left(-KP1_j - \frac{KP2_j * 10000}{R} * \left[\frac{1}{T} - \frac{1}{T_M}\right]\right) \quad (8\text{-}7)$$

The net rate of reaction for each species i is given by

$$r'_i = \sum_{j=1}^{N_{rxn}} \alpha_{ij} r'_j \quad (8\text{-}8)$$

where α_{ij} is the stoichiometric coefficient of the i[th] species in the j[th] reaction.

The reactor is modelled using the ideal plug flow reactor assumption. Mass balances are written for the liquid phase but not the gas or solid phases, hence this is a pseudohomogenous model as if the reaction occurred in the liquid phase. The liquid phase mass balances are shown in Eq (8-9) and (8-10) below. Liquid-solid and internal mass transfer resistances were both neglected and these assumptions will be examined later with experimental data.

$$\frac{dC_{i,L}}{dW} = \frac{r_i'}{v} \tag{8-9}$$

where $C_{i,L}$ is the concentration of species i (M) in the liquid, W is the catalyst mass (mg), r_i' is the net rate of reaction of species i (mol min^{-1} mg^{-1}), v is the liquid flowrate (L/min). The mole balance for the concentration of dissolved oxygen also includes a term for the mass transfer of oxygen from the gas to the liquid phase as shown below.

$$\frac{dC_{O_2,L}}{dW} = \frac{r_{O_2}' + \frac{k_{GL}a}{\rho_b}\left(C_{O_2,L}^* - C_{O_2,L}\right)}{v} \tag{8-10}$$

where $C_{O_2,L}$ is the concentration of dissolved oxygen in the liquid (M), k_{GL} is the gas-liquid mass transfer coefficient (m/min), a is the specific gas-liquid interfacial area per volume of reactor (m^{-1}), ρ_b is the bulk catalyst density (mg/L) and $C_{O_2,L}^*$ is the saturation concentration of oxygen in water (M). The saturation oxygen concentration in water is calculated using Eq (8-11) [270].

$$C_{O_2,L}^* = P_{O_2} exp\left(\frac{0.046T^2 + 203.35T * \ln\left(\frac{T}{298}\right) - (299.378 + 0.092T) * (T - 298) - 20.591 * 10^3}{8.3144T}\right) \tag{8-11}$$

where $P_{O_2}$is the oxygen partial pressure in atm and T is the temperature in Kelvin. This equation is valid for temperatures and pressures ranging from 273-620 K and 1-60 atm, and is therefore more suitable than the commonly used Henry's law equation which is not meant to be extrapolated to the high temperatures (>100 ^oC) needed in this work [271].

For the experimental conditions used in this work, the maximum oxygen consumption which would occur if all of the HMF was converted to FDCA is only 3.6% of the oxygen supplied to the reactor. Therefore, it can be approximated that the concentration of oxygen in the gas phase is constant and the gas phase material balance is not used in the model.

The gas-liquid mass transfer coefficient k_{GL}, and the specific gas-liquid interfacial area per volume of reactor a, are lumped together and treated as a single variable $k_{GL}a$ (min^{-1}). As an approximation that may be valid over the small temperature range used in this work it is assumed that the mass transfer coefficient $k_{GL}a$ varies linearly with temperature. The value of the mass transfer coefficient at any temperature can be then be computed with respect to its value at a reference temperature T_M.

$$k_{GL}a = k_{GL}a_{T_M}\frac{T}{T_M} \tag{8-12}$$

The value of the mass transfer coefficient at the reference temperature $k_{GL}a_{T_M}$, is treated as a parameter to be estimated, so there are 7 parameters in total in this model, 6 kinetic parameters and 1 mass transfer parameter.

8.3 Results and Discussion

8.3.1 Blank Experiments

A blank experiment conducted with an empty reactor at 20 µL/min liquid flowrate of concentration 50 mM HMF and 200 mM NaOH, 2 NmL/min pure oxygen gas flowrate, 5 barg and at 60 °C showed that a negligible amount of HMF was consumed and no products were detected by the HPLC. However, when the reaction temperature was increased to 100 °C, 10% of the HMF feed was found to be consumed and the HPLC detected several unknown peaks. This result was expected as HMF degradation behaviour is known to be promoted at high temperature and high base conditions [248]. Further blank experiments in a reactor packed with 12 mg of TiO_2 (without any metal nanoparticles) conducted at 100 °C showed an increased consumption of HMF of up to 20% and a greater number of unknown peaks being detected by the HPLC. However, little to no formation of HFCA, FCA and FDCA was observed in this experiment, showing that TiO_2 on its own, is not a catalyst for the desired reactions.

One consequence of HMF degradation is that the mole balance will not close for this reaction under the conditions of high temperature and high base concentration. This is because the HPLC is not calibrated for the HMF degradation products. In several of the following figures, the difference between the inlet concentration and the total measured outlet concentration is calculated and labelled as “Side Products”, however, it is expected that this is predominately due to HMF degradation rather than to any other unknown reactions.

8.3.2 Catalyst Screening

Before the reaction was automated some initial experiments conducted with offline sample collection and analysis showed that catalyst batch 1 (1wt% Au/TiO_2) suffered from reversible deactivation only at low temperatures. This is shown in Figure 8-4 for an experiment conducted with 4.2 mg of catalyst, at 20 µL/min liquid flowrate of feed concentration 52.5 mM HMF and 4:1 NaOH to HMF ratio, 2 NmL/min oxygen gas flowrate at 1.5 barg system pressure. It can be observed that the concentration of unreacted HMF (orange) increases with prolonged time on stream at low temperatures, and that this deactivation is reversible as high temperature operation appears to regenerate the catalyst. These initial results led to the design of the full catalyst screening study using the automated system.

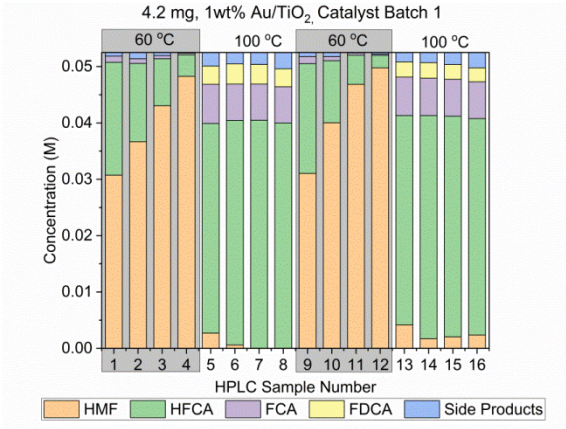

Figure 8-4 Reactor outlet concentrations obtained from the deactivation study using 4.2 mg of the 1 wt% Au/TiO_2 catalyst from batch 1. The experiments were conducted at 20 µL/min liquid flowrate, 2 NmL/min gas flowrate, 52.25 mM HMF feed concentration, 200 mM NaOH feed concentration conducted at 1.6 barg using offline sampling at 30 min intervals. The temperature was alternated between 60 and 100 °C at 2 h intervals.

In the automated deactivation study, the activity and stability of each catalyst batch was tested by running the reactor with each catalyst at 100 °C for 2 h, then at 60 °C for 2 h, before returning to 100 °C for 2 h. A sample was taken by the HPLC every 20 min, resulting in 6 data points per experimental condition. It is expected that the reactor should reach steady-state within 30 min, so the 2 h duration for each experimental condition is sufficient to ensure the observation of steady-state reactor behaviour. The results of the screening experiments, shown in Figure 8-5, indicated that all of the Au/TiO_2 catalysts were stable at high temperatures but reversibly deactivated under low temperature conditions. This is particularly visible in Figure 8-5 a, where during the 60 °C operating conditions the concentration of unreacted HMF in the outlet stream is increasing with time. This deactivation behaviour suggests adsorption of some species on the catalyst surface is blocking active sites, but that the species are only weakly adsorbed and are removed at higher temperatures. In comparison no deactivation was observed for either of the $AuPd/TiO_2$ catalysts during the low temperature experiment, as shown in Figure 8-5 d and e, although this may just be because these catalysts appeared to be much more active for the oxidation of HMF, resulting in almost 100% HMF conversion. Therefore, the same deactivation may be occurring, but it may not be visible at this high level of conversion. The 1 wt% 50:50 $AuPd/TiO_2$ catalyst was found to produce more FDCA than the 1 wt% 95:5 $AuPd/TiO_2$ catalyst and it also appeared to be more stable, as the steady-state outlet concentrations during the 100 °C experiment conditions were approximately equal before and after the 60 °C experiment, unlike the 95:5 $AuPd/TiO_2$ catalyst whose performance varied throughout the experiment. Therefore, the 1 wt% 50:50 $AuPd/TiO_2$ catalyst was chosen due to its superior activity and stability to be used for the kinetic experiments. Note that two of the experiments (b and c, both 1 wt% Au/TiO_2 catalysts) were run at reduced base concentration and this

reduced the amount of HMF degradation observed, which is in agreement with previous reports in the literature [252].

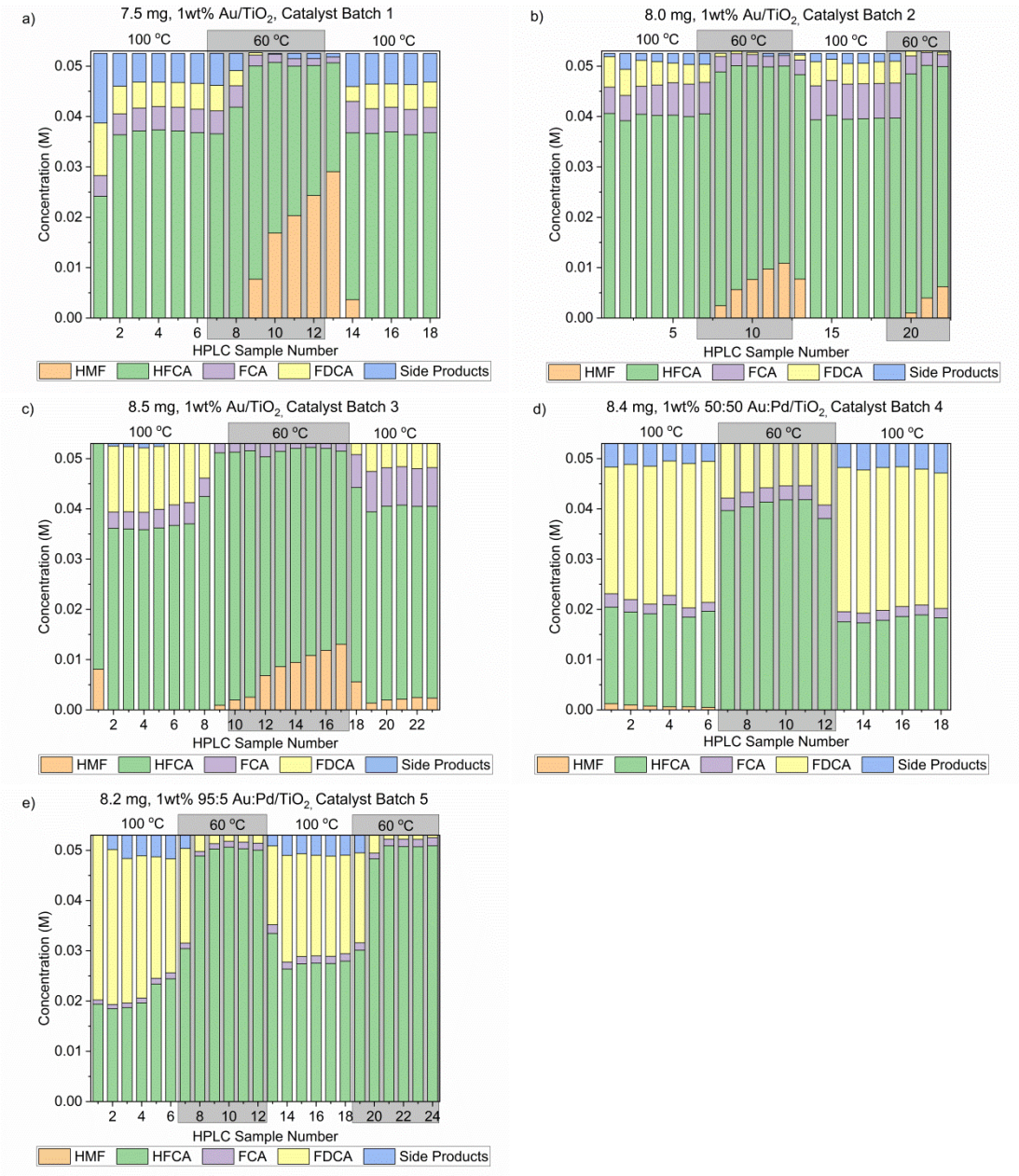

Figure 8-5 Reactor outlet concentrations from the catalyst screening experiments for the 5 catalyst batches. The temperature was cycled between 100 and 60 °C, maintaining each temperature for 2 h. The samples collected during the 60 °C experiment are shown in the grey highlighted section. The experimental conditions were a concentration of 52.5 mM HMF, 200 mM NaOH (100 mM for experiments b and c), 20µL/min liquid flowrate, 2 NmL/min oxygen flowrate and 5 barg system pressure.

8.3.3 Factorial Campaign

8.3.3.1 Reproducibility and Estimating Experimental Error from Factorial Campaign

Using catalyst batch 4 (1 wt% 50:50 AuPd/TiO_2) the factorial campaign was conducted at 4 temperatures, 3 catalyst masses, 2 NaOH:HMF ratios and 2 oxygen feed concentrations, resulting in 48 combinations of experimental conditions. This work was conducted in 6 different reactors, where each reactor was run for two days before both the catalyst and the reactor tubing were discarded. A reference condition (80 ^{o}C, 2 NmL/min O_2 flowrate, 20 µL/min liquid flowrate) was run at the start and end of each day for each reactor, resulting in 4 experiments to assess the reproducibility of each reactor. Note that even though all 6 reactors were operating at the same reference condition of temperature and flowrates, each reactor has its own catalyst mass and NaOH:HMF ratio, therefore the results are not expected to be the same between reactors, however the 4 repeated experiments within each reactor should be identical. The results of these reference condition experiments are shown in Figure 8-6, where it can be observed that the reproducibility is quite poor. It should be noted that the catalyst does not appear to be deactivating, as in some cases the amount of FDCA produced increases with time on stream. The cause of the poor reproducibility within each reactor is not clear, as it cannot be related to errors in measuring the catalyst mass. Instead it could be due to unstable catalyst behaviour, or due to changes in the reactor packing over time, particularly overnight when the system is depressurised and liquid flow is stopped.

In order to quantify the experimental error for each reactor, the standard deviation of the 4 experiments conducted at the same reference condition was taken for each chemical species, this is shown in Table 8-2. It can be observed that the standard deviation of the experimental error varied from reactor to reactor, therefore in order to get an overall standard deviation for each chemical species, the pooled standard deviation was calculated as 2.44, 3.38, 1.74 and 3.29 mM for HMF, HFCA, FCA and FDCA respectively. In comparison, the average standard deviation of the triplicate measurements in each experiment was only 0.57 mM. This indicates that most of the experimental error comes from the catalyst behaviour changing slowly over the 2 days of experiments rather than from HPLC measurement errors or from sudden changes in catalyst behaviour within the 80 min experiment duration.

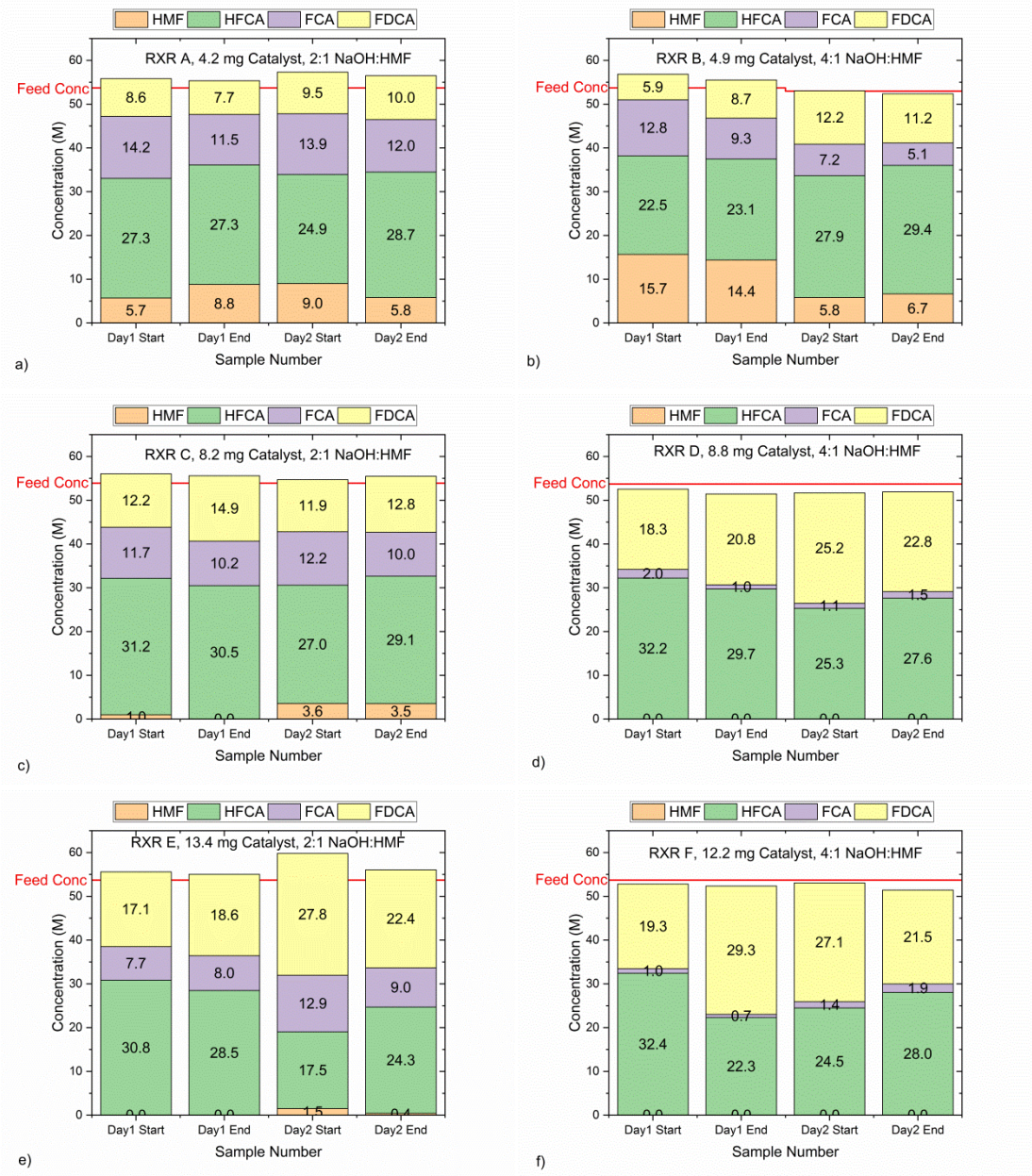

Figure 8-6 Reference condition (80 °C, 20 µL/min liquid flowrate of approx. 50 mM HMF feed, 2 NmL/min oxygen gas flow at 5 barg pressure) for the 6 reactors used in the factorial study showing the average (from triplicate measurements) outlet concentration at the start and end of the days the reactor was used. The reactor was left running in oxygen only flow overnight between the two days.

Table 8-2 Standard deviation of the HPLC measurements for each species, for each reactor conducted at the reference condition.

Reactor	Mass mg	NaOH:HMF	HMF mM	HFCA mM	FCA mM	FDCA mM
A	4.2	2:1	1.83	1.60	1.38	1.07
B	4.9	4:1	5.36	2.56	3.08	3.36
C	8.2	2:1	1.79	1.75	1.15	1.36
D	8.8	4:1	0.00	2.96	0.44	2.94
E	13.4	2:1	0.64	5.34	2.23	4.56
F	12.2	4:1	0.00	4.39	0.51	4.61
Pooled Standard Deviation			**2.44**	**3.38**	**1.74**	**3.29**

8.3.3.2 Mole Balance

The mole balance from the factorial experiments was found to be strongly dependent on temperature and NaOH:HMF ratio, as shown in Figure 8-7. This was expected due to the degradation of HMF to non-detectable side products at high temperatures and high base ratios [248]. As the degradation of HMF is not included in the kinetic model, for the purposes of kinetic modelling it was necessary to exclude the data collected at 120 °C, and also the data at 100 °C with a 4:1 NaOH:HMF ratio, as the mole balance did not close to within 95%. A small section of the data was found to have a measured outlet concentration of more than 105% of the feed concentration, this was caused by a small leak in the NaOH syringe in that particular experiment, resulting in a lower NaOH flowrate and hence a higher HMF inlet concentration, this data was also excluded from the kinetic modelling. In total from the 71 experiments, 21 experiments were excluded due to HMF degradation and 4 experiments were excluded due to the syringe leak.

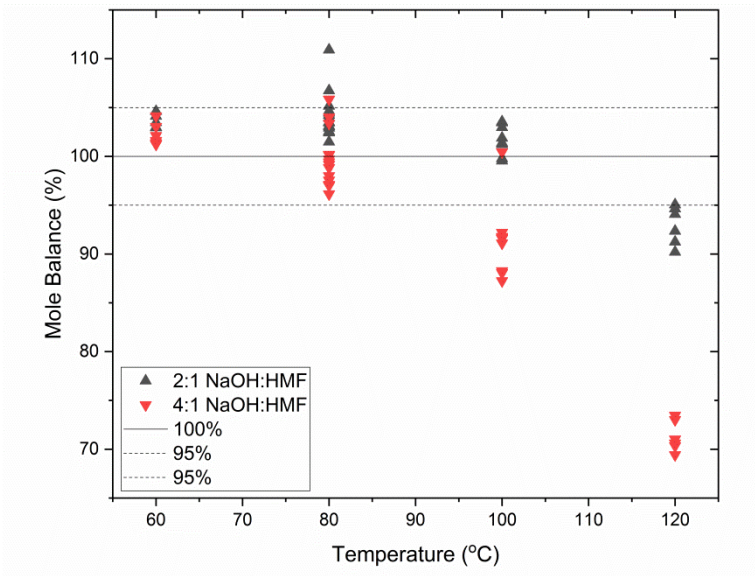

Figure 8-7 Mole balance for all of the factorial experiments as a function of temperature and NaOH:HMF ratio.

8.3.3.3 Trends from the Factorial Experiments

The results of all the factorial experiments are shown in Appendix G, as concentration profiles along the length of the packed bed for each combination of temperature, oxygen feed concentration and NaOH:HMF ratio. As the gas and liquid flowrates were held constant for all experiments, the catalyst contact time only varies with catalyst mass.

The factorial experiments allowed the effect of temperature, oxygen composition and NaOH:HMF ratio to be observed. The temperature effect is shown in Figure 8-8 a-h, which shows the concentration of the reactant HMF and the final product FDCA along the length of the packed bed at different temperatures. From these figures it is shown that near complete conversion of HMF was obtained at all temperatures if 8 mg of catalyst or more was used, however when only 4 mg of catalyst was used, HMF conversion increased with temperature. It was also shown that FDCA yield increased with temperature. However, at very high temperatures, FDCA yield was found to decrease due to increased degradation of HMF. This was most clearly observed for the 4:1 NaOH:HMF experiments, as shown in Figure 8-8 f and h, where the selectivity to FDCA was at the maximum at 100 ^{o}C.

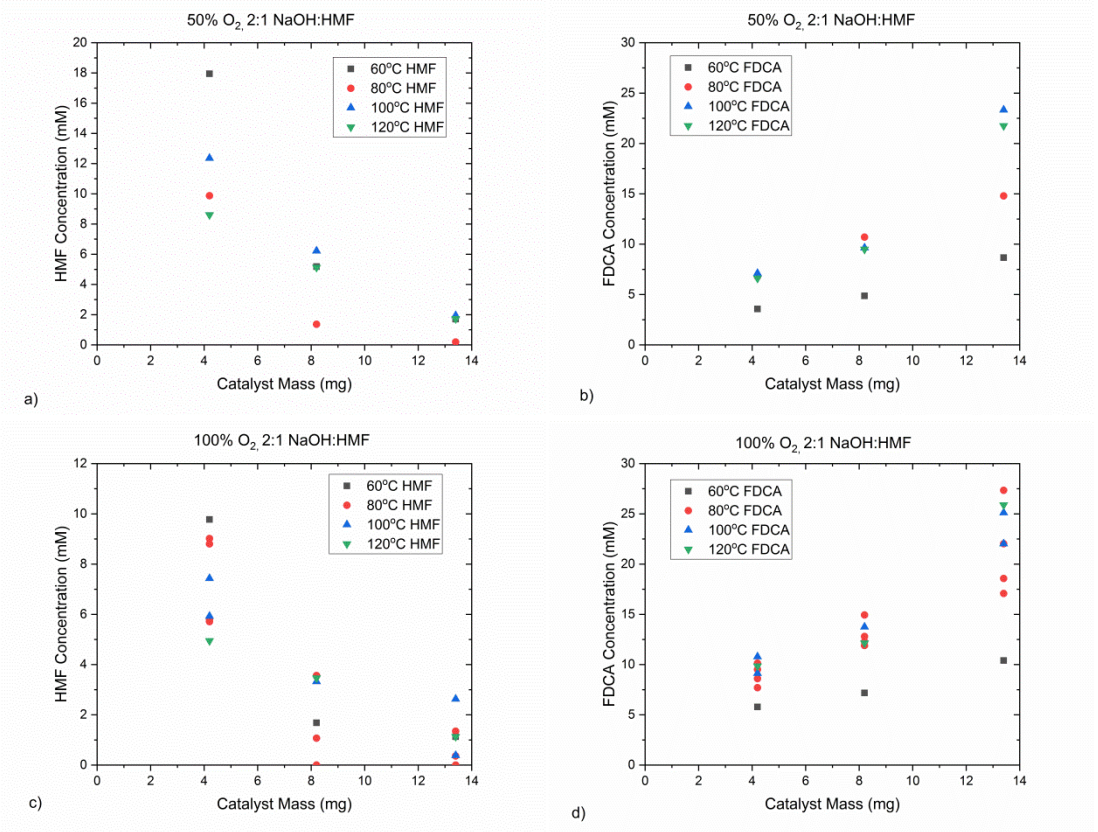

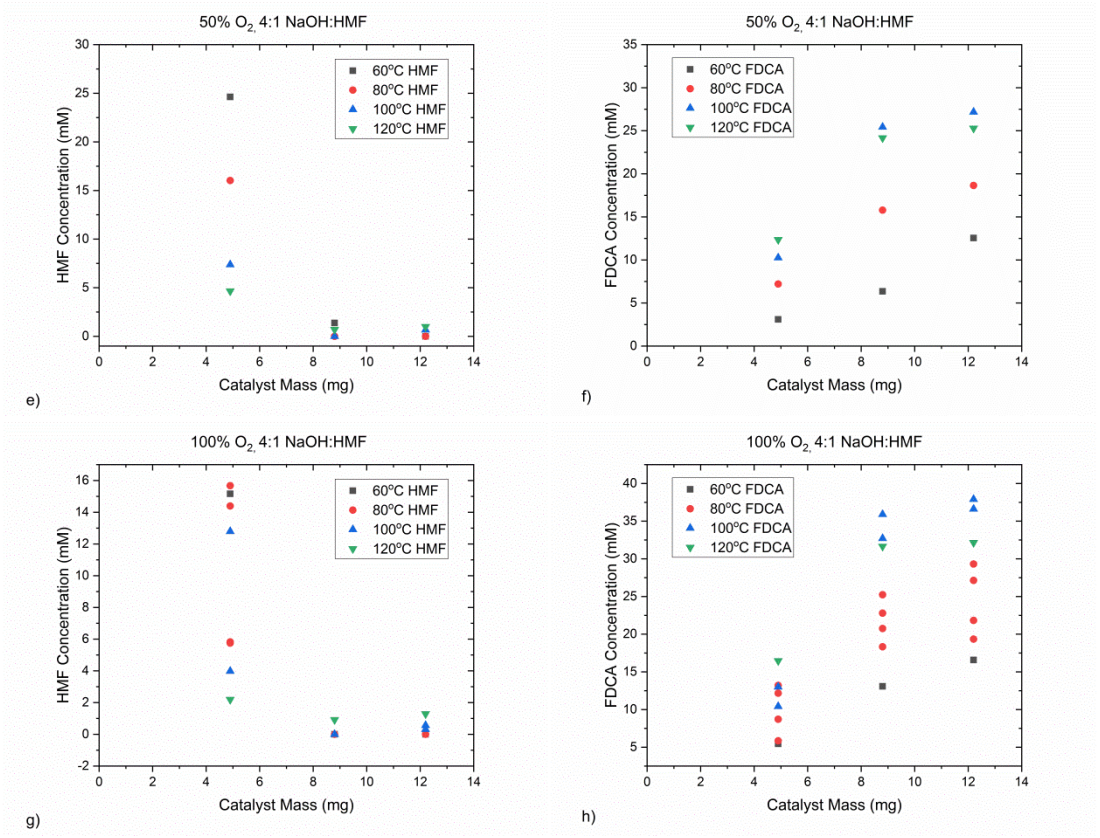

Figure 8-8 Reactor outlet concentration of HMF (figures a, c, e and g) and FDCA (figures b, d, f and h) along the length of the packed bed at different temperatures, for each experimental condition of NaOH:HMF ratio and oxygen composition studied.

Increasing oxygen was observed to slightly increase both the conversion of HMF and selectivity to FDCA, as shown for the representative conditions of 60 °C and 2:1 NaOH:HMF ratio in Figure 8-9. This small increase was expected as the literature reported that the rates of reaction are nearly zero order with respect to oxygen [256].

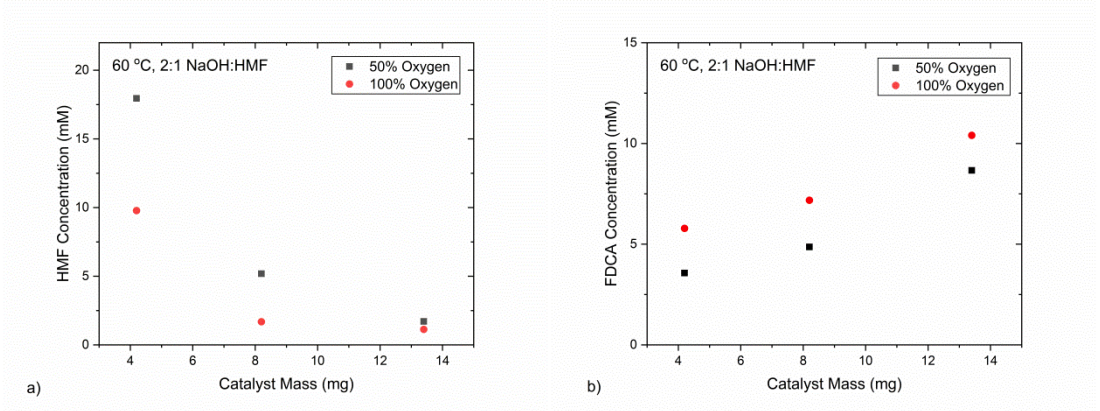

Figure 8-9 Reactor outlet concentration of HMF (a) and FDCA (b) along the length of the packed bed at 60 °C using a 2:1 NaOH: HMF ratio with 50 and 100 % oxygen gas composition.

The literature reports that the rate of the 1st and 3rd reactions, which are both oxidation of aldehyde groups, are dependent on the concentration of base, while the rate of the

2nd reaction, the oxidation of an alcohol functional group, is not dependent on base [256]. However, when examining the effect of base concentration from the experiments conducted, there does not appear to be a significant difference in the outlet concentration of HMF, as shown in Figure 8-10 a. This suggests that the rate of the first reaction is not strongly dependent on base concentration. In contrast the third reaction, is clearly shown to be promoted by higher concentrations of base, this is evident by the significantly lower concentration of FCA and higher concentrations of FDCA, shown in Figure 8-10 c and d.

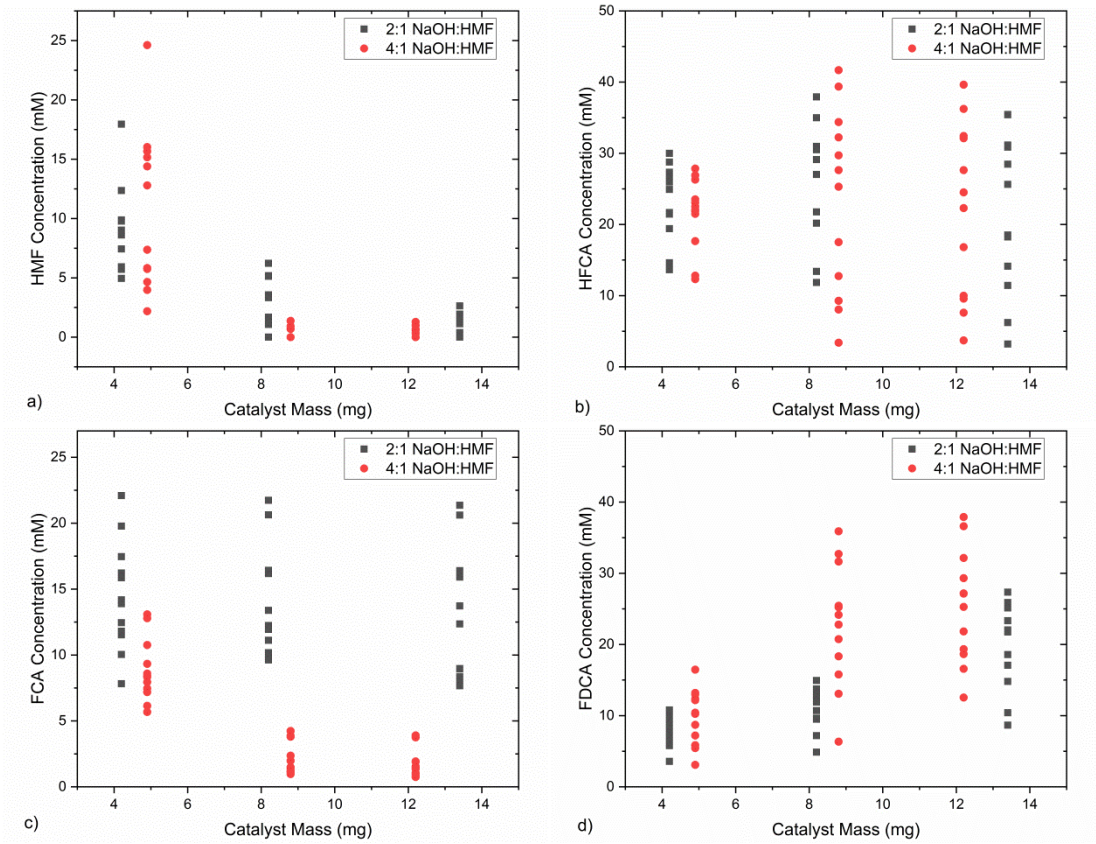

Figure 8-10 Reactor outlet concentration of HMF (a), HFCA (b), FCA (c) and FDCA (D) for all of the 71 factorial experiments split into two groups based on the NaOH:HMF ratio.

8.3.3.4 Mass Transfer Analysis from the Factorial Experiments

In this work there are three mass transfer steps, gas-liquid, liquid-solid and internal mass transfer. However, only the gas-liquid mass transfer step is included in the kinetic model, and the value of the mass transfer coefficient $k_{GL}a_{T_M}$ is treated as a parameter to be estimated. In order to justify neglecting both liquid-solid and internal mass transfer resistances the Mears and Weisz Prater criteria are used. It was shown that the rate of mass transfer of oxygen was more limiting than the rate of mass transfer of HMF. Therefore, the mass transfer resistance steps were evaluated on an oxygen basis.

The Mears criteria was calculated using Eq (8-13) with oxygen as the reactant.

$$\frac{-r'_{O_2}\rho_b Rn}{k_{LS}C_{O_2,b}} < 0.15 \tag{8-13}$$

where ρ_b is the bulk catalyst bed density (981 kg/m^3 based on the known mass of the catalyst and the measured volume of the packed bed), R is the particle radius (34.5 μm) and n is the reaction order (assumed to be 1). The observed average rate of reaction r'_{O_2}, is calculated for all 71 experiments conducted, however for the Mear's criteria, the fastest reaction rate of 3.5*10^{-6} mol g^{-1} s^{-1} (obtained from an experiment using 4.2 mg of catalyst at 100ºC) was used. The observed average reaction rate is calculated using Eq (8-14).

$$-r'_{O_2} = \frac{v(0.5 * C_{HFCA} + 1 * C_{FCA} + 1.5 * C_{FDCA})}{W} \tag{8-14}$$

The liquid-solid mass transfer coefficient k_{LS} needed to be estimated from the literature. Unfortunately, no k_{LS} values could be found in the literature for micropacked beds, only $k_{overall}a$ values were reported which were typically 10 s^{-1} [5]. It was then assumed that the $k_{LS}a$ value for this reactor would also be 10 s^{-1}. The specific surface area per volume of catalyst a, was calculated using Eq (8-15) to be 43,478 m^{-1} and then the k_{LS} value was estimated to be 2.3*10^{-4} m/s.

$$a = \frac{(4\pi r_c^2)\left(\frac{W}{\rho_c \frac{4}{3}\pi r_c^3}\right)}{\pi r_r^2 l_r} \tag{8-15}$$

The dissolved oxygen concentration in the bulk, $C_{O_2,b}$, was assumed to be the saturated oxygen concentration calculated using Eq (8-11), which in this temperature range was approximately 48 mM when pure oxygen feed was used, but only 24 mM when the gas feed was 50% oxygen and 50% nitrogen. Assuming the concentration of dissolved oxygen in the bulk is the saturated oxygen concentration value, is equivalent to assuming that the gas-liquid mass transfer is very fast. While this is not necessarily known in advance, as the gas-liquid mass transfer coefficient $k_{GL}a$ at the reference temperature is treated as a parameter to be estimated, it is still a reasonable assumption to make as very high $k_{GL}a$ values (10.2 s^{-1}) have been reported in the literature for other micropacked bed reactors [168].

Using all of these values, for the case of 50% oxygen gas feed, the Mear's criterion is calculated to be 0.22 which is greater than the criterion value of 0.15, indicating some external mass transfer resistances. However, when the gas feed is pure oxygen, the Mear's criterion is calculated to be 0.11, which is below the limit indicating negligible

mass transfer resistances. Therefore, external mass transfer is only significant for some of the experimental data collected. Considering that the rate of reaction used for these calculations was the fastest rate of reaction in the entire data set, it is likely that for most of the rest of the data, that external mass transfer resistances can be ignored.

The internal mass transfer resistances are assessed using the Weisz Prater criterion shown below

$$\frac{-r'_{O_2}\rho_c R^2}{D_{e,O_2}C_{O_2,S}} < 1 \tag{8-16}$$

where the rate of oxygen consumption, r'_{O_2} and catalyst particle radius R, have the same values as before of 3.5*10^{-6} mol g^{-1} s^{-1} and 34.5 µm. The catalyst particle density ρ_c is 1961 kg/m^3, and the concentration of oxygen at the catalyst surface $C_{O_2,S}$ is assumed to be the saturated oxygen concentration value (24 mM for the 50% oxygen feed and 48 mM for the pure oxygen gas feed). This is equivalent to assuming that the rate of oxygen transport from the gas to the bulk liquid, and also from the bulk liquid to the catalyst surface are both very fast, and in the absence of any reliable estimates for these mass transfer coefficients this is a reasonable assumption knowing that micropacked bed reactors provide high rates of mass transport. As the catalyst tortuosity, constriction factor and porosity are unknown, the effective diffusivity of oxygen, D_{e,O_2}, is estimated as 10% of the molecular oxygen diffusivity in water, D_{m,O_2} [272]. The molecular oxygen diffusivity in water is estimated using the Wilke-Chang equation at 80 °C.

$$D_{O_2} = \frac{7.4 * 10^{-8}(\varphi M_2)^{0.5}T}{\mu_2 V_1^{0.6}} \tag{8-17}$$

where φ is the empirical parameter of 2.6 for water [273], M_2 is the molecular weight of water, 18 g/mol, T is temperature, 353 K, μ_2 is the viscosity of water at 80 °C which is 0.355 cP and V_1 is the molar volume of oxygen, 25 cm^3/mol [273]. The molecular diffusivity at 80 °C is then estimated as 7.2*10^{-9} m^2/s, and the effective diffusivity is 7.2*10^{-10} m^2/s. Using all of these values the Weisz-Prater number is calculated to be 4.8 for 50% oxygen composition in the gas feed, and 2.4 for pure oxygen gas, both of these numbers are greater than 1, indicating significant internal mass transfer resistances for oxygen.

8.3.3.5 Kinetic Model Identification from the Factorial Experiments

The ideal reactor model previously described in Eq (8-9) and (8-10) which assumed a pseudohomogenous reaction in the liquid phase, and that liquid-solid and internal mass transfer resistances were negligible, was still used for apparent kinetic model

identification, even though the experimental data suggested that internal mass transfer resistances were not negligible. This was done in an effort to simplify the modelling procedure and because there was a lot of uncertainty for the required mass transfer coefficients. Therefore, the following kinetic results are apparent kinetics, not intrinsic kinetics, and they are of limited value for process design and scale up, as the equations obtained are not valid for reactors which use different catalyst particle sizes.

The experimental data from the factorial campaign was used without any outlier detection procedure, except for removing 21 data points which were conducted at high temperatures resulting in excessive HMF degradation (which was not included in the model), and 4 data points which were effected by a leaking syringe.

An effort was made to fit the experimental data using the rate laws shown in Eq (8-4) to (8-6), where all three of the reactions were first order with respect to oxygen, the base and the reagent. This was a 7 parameter model, including 6 kinetic parameters and 1 gas-liquid mass transfer parameter, $k_{GL}a_{T_M}$. However, these rate laws could not fit the data, as shown by the χ^2 value of 1,120 far exceeding the reference value of 209. To try and fit the data, different rate laws were needed. As it was still desired to use a simple power law model, it was originally intended to treat the reaction orders as additional parameters in the parameter estimation problem. However, this was not possible as it led to a large number of numerical challenges, and the estimated rate orders had very large confidence intervals, indicating that the order had not been precisely estimated. Therefore, different reaction orders were manually proposed, but none of them were capable of fitting the data. The best model proposed, in terms of the lowest χ^2 value, was developed based on the trends observed in the experimental data, and was named the “trend model”. It was shown that oxygen slightly increased the rate of all reactions, so all three reactions were made 0.2 order with respect to oxygen. Furthermore, only the third reaction was observed to be promoted by increasing base concentration, so only the third reaction was made first order with respect to the base, while the other 2 reactions were independent of the base, as shown below in Eq (8-18) to (8-20).

$$-r'_{HMF} = k_{HMF}\, C_{HMF}\, C_{O_2}^{0.2} \tag{8-18}$$

$$-r'_{HFCA} = k_{HFCA}\, C_{HFCA}\, C_{O_2}^{0.2} \tag{8-19}$$

$$-r'_{FCA} = k_{FCA}\; C_{FCA}\, C_{O_2}^{0.2}\, C_{NaOH} \tag{8-20}$$

This trend model still was unable to fit the data, as the χ^2 value of 595 was greater than the reference value of 209.

At this point, it was necessary to question if the problem with trying to fit this data was down to using incorrect modelling assumptions (due to using incorrect rate laws or due to neglecting internal mass transfer resistances etc.), or if it was due to errors in the data set. It was already shown in Figure 8-6 that the experimental data collected was not very reproducible as when a reactor was run for 2 days, the results from the 4 reference conditions studied were often substantially different. However, this error within the reactor cannot explain the modelling problems, as the experimental error used in calculating the parameter estimates and χ^2 value was calculated from these repeated reference conditions and hence was large enough to compensate for this poor reproducibility. However, a second source of error which is not accounted for in the standard deviation of the experimental error, could be differences in performance between the 6 reactors used. In order to test for differences in activity between reactors, a linear regression model was created where temperature, oxygen fraction, base concentration, catalyst mass and the reactor number the experiment was conducted in were all included as variables. The full details are included in Appendix G, however it showed that the reactor the experiment was conducted in was a significant variable, hence there was a difference in activity between reactors explaining the difficulty in fitting a single kinetic model to all the data collected. The cause of the different behaviour from reactor to reactor is unclear but it could be due to any of the following

- Errors in measuring the mass of catalyst in each reactor, especially considering that the small masses of catalyst used (4, 8 and 12 mg) were only slightly larger than the mass balance error of 0.1 mg.
- Differences in reactor packing which led to different amounts of liquid bypass or channelling from one reactor to the other.
- Variation in the activity within the catalyst batch.
- Variations in catalyst activity between reactors due to the different operating histories of each reactor.

Due to the difference in performance between reactors, an adapted method was required to obtain kinetic information from this data. It was decided to assume that the difference in activity between the reactors would only affect the pre exponential factor of the reaction rates but that the activation energy for each reaction would be constant in all reactors. Therefore, the pre exponential factors in each reactor were treated as different and independent parameters. In this way the number of parameters increased from 7 to 22 (the gas-liquid mass transfer coefficient, 3 activation energies, and 18 pre-exponential factors as each of the 6 reactors had their own pre-exponential factors for each of the 3 reactions).

This parameter estimation procedure was applied using both the first order model and the trend model. It was found in both cases that the models passed the χ^2 test, with the first order and trend models having χ^2 values of 173.8 and 116.5 respectively compared to the reference value of 192.7.

The large number of parameters used in these models led to a significant chance of overfitting the data. However, despite the large number, it was found that for both models, that the vast majority of model parameters are estimated precisely, in that they passed the 95% t-test. For the first order model, only 3 parameters did not pass the t-test, the activation energy of the third reaction, *KP2 RXN3* ,the gas-liquid mass transfer coefficient, $k_{GL}a_{T_M}$, and also the pre-exponential factor of the first reaction, *KP1 RXN1* for reactor F. In particular it was shown that the mass transfer coefficient was particularly poorly estimated, with an estimated value of 3924 ± 186,900 (min^{-1}). For the trend model, only 2 parameters did not pass the t-test, these were again the activation energy of the third reaction and the gas-liquid mass transfer coefficient. However, in this case the mass transfer coefficient was estimated as 89.2 ± 72 (min^{-1}). The parameter estimates for both models are shown in Figure 8-11 and numerical values are in Appendix G.

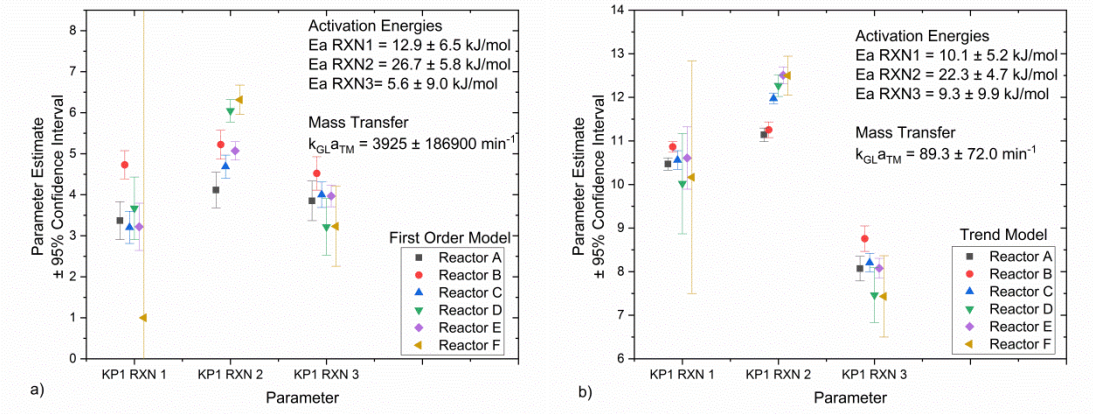

Figure 8-11 Parameter estimates for the 18 pre-exponential factors when a) the first order model shown in Eq (8-4) to (8-6) is used and when b) the trend model shown in Eq (8-18) to (8-20) is used.

In an effort to obtain more precise parameter estimates for the kinetic parameters, the mass transfer parameter, $k_{GL}a_{T_M}$, was fixed at a value of 612 min^{-1}, which was reported in the literature for a similar micropacked bed reactor [168]. The parameter estimation procedure was repeated for both models, however in both cases the parameter estimates did not change significantly and the identifiability of the third activation energy *KP2 RXN3* did not improve. It was shown for both models, that the dissolved oxygen concentration was almost equal to the saturated concentration along the entire length of the packed bed. Therefore, the model and the kinetic parameters are quite

insensitive to the value of the mass transfer coefficient, explaining why it is difficult to estimate the mass transfer parameter, further details are shown in Appendix G.

Overall the best model is probably the trend model because this model's rate laws capture the various trends which were observed in this work including how the base promoted mainly the third reaction and how oxygen slightly promoted all reactions. Unfortunately, it is not possible to say with any statistical certainty that this trend model is superior to the first order model, as both models pass the χ^2 test. The fact that two different models both pass the χ^2 test is due to the large experimental error in this work (due to the non-reproducible reactor behaviour) and also because of the large number of parameters used. Therefore, the experiments conducted have very little discriminating power. It was decided that due to the large experimental error and poor reproducibility between reactors, that there was little value in continuing the kinetic study. Therefore, after the factorial campaign the kinetic study was stopped and online MBDoE was not applied to this system.

8.4 Conclusions

The aerobic oxidation of HMF in a micropacked bed reactor was automated in a microreactor platform that included gas liquid separation and online analysis of the liquid product with HPLC. This automated platform was used to speed up catalyst screening and kinetic experiments. It was found that the most active and stable catalyst for the production of FDCA was 1 wt% 50:50 AuPd/TiO_2. In comparison, 1 wt% Au/TiO_2 catalysts were shown to be less active and underwent reversible deactivation at low reaction temperatures. A factorial campaign of experiments using the 1 wt% 50:50 AuPd/TiO_2 catalyst, showed that only the third reaction, the oxidation of FCA to FDCA was significantly promoted by the presence of increased base concentration, while all reactions showed a small increase in rate with increasing oxygen concentration. Maximum yields of FDCA were obtained at 100 ^oC, as further increases in temperature led to a reduction in FDCA yield due to increased degradation of HMF. The kinetic study encountered some considerable challenges including poor experiment reproducibility and significant differences in catalyst activity between the 6 reactors used in this work. The cause of these disturbances is unknown, but it could be due to errors in measuring the catalyst mass, non-reproducible reactor packing or non-uniformities within the catalyst batch. It was also found that internal mass transfer resistances were significant in this reaction, however this resistance was not included in the kinetic model so only apparent kinetics instead of intrinsic kinetic parameters were estimated. The best effort for identifying a kinetic model involved allowing each reactor to have its own set of pre-exponential factors, resulting in a 22 parameter

model. However, introducing so many parameters led to many candidate models passing the χ^2 test, and the high experimental error meant that the experiments had little distinguishing power to identify the correct model structure, hence a single reliable kinetic model was not identified.

Overall this was a challenging study involving complicated chemistry, a reactor with complex hydrodynamic and mass transfer behaviour, and a novel nanoparticle catalyst. While the principle aim of this project, to obtain a reliable intrinsic kinetic model, was not achieved, many useful achievements were made, including expanding the capabilities of the automated reactor to handle gas liquid systems and learning more about the oxidation of HMF with Au and AuPd/TiO_2 catalysts. In future, for applying the automated reactor platform to other challenging systems, greater care should be taken to ensure that the catalyst and reactor are reproducible (through repeated runs with different reactor packings) before beginning a factorial campaign.

9 Conclusions & Future Work

The objective of this thesis was to use microreactors to study catalysts in the most efficient way possible. This goal was pursued in two ways, first a multistep microreactor system was developed to study catalysts in a system wide environment and secondly, an automated microreactor platform was developed to rapidly identify kinetic models for catalytic reactions.

9.1 Multistep Flow Systems

A multistep flow system for the synthesis of benzylacetone and 4-(4-methoxyphenyl)butan-2-one was developed to allow the study of AuPd/TiO_2, Pd/TiO_2, Pt/TiO_2 and TiO_2 catalysts. The system was successfully used to identify a number of problems associated with these catalysts, the most important being water inhibition, deactivation and the low activity of the TiO_2 catalyst for the aldol condensation reaction, which was the second reaction in the multistep sequence. Due to the increased freedom offered by the multistep flow system to have different catalysts and different operating conditions for each reactor, some small increases in system performance were obtained in the flow system compared to a previously conducted batch cascade system using the same catalysts. These included decreasing the required catalysts contact times and increasing the yields of benzylacetone from 8% to 56% and of 4-(4-methoxyphenyl)butan-2-one from 41% to 48% when compared using the same TiO_2 catalysts. However, if in future the objective of this multistep flow system study is to create an optimised system for the synthesis of the final product, greater input from a chemist is required. In this work, when the TiO_2 aldol condensation catalyst was found to be unsuitable for this system, engineering solutions (using diluted feed) were found to work around this problem. However, in order to obtain an optimal solution, a chemist is needed to provide new catalysts in response to the various problems that are encountered.

In terms of developing improved multistep microreactor technology, a significant problem that was identified in this thesis was the over reliance of current multistep flow systems on packed bed reactors. As packed bed reactors require a minimum particle size to prevent excessive pressure drop and reactor clogging, it is not possible to use catalyst in powder form in these reactors. However, not all catalysts have the required mechanical properties to be converted from powder into catalyst pellets with the desired particle size by pelletisation, grinding and sieving. For the synthesis of 4-(4-methoxyphenyl)butan-2-one, it had previously been demonstrated that the optimal catalyst was AuPd/MgO, however the MgO support was not suitable for use in a micropacked bed reactor because MgO did not form mechanically stable catalyst

pellets after pelletising and grinding. For this reason the multistep flow system was restricted to the use of TiO_2 supported catalysts which were less optimum, and this contributed to the maximum yield of 4-(4-methoxyphenyl) butan-2-one of only 48% achieved by the multistep flow system with the TiO_2 catalysts compared to the 63% yield which was obtained in batch with the MgO catalyst. Therefore an area for future work would be in the development of improved slurry flow reactors that are capable of handling powder catalysts and which can be easily integrated into multistep flow systems. Note that these slurry flow reactors may need to operate as CSTRs or as slurry loop reactors as it is necessary to separate the catalyst from the outlet stream so that the catalyst is retained in the reactor, without flowing down to the next unit operation.

9.2 Rapid Kinetic Modelling

An automated flow reactor platform was developed for the objective of rapidly identifying kinetic models for heterogeneous catalytic reactions. This platform achieved many of its goals, as it was validated to be able to conduct online MBDoE for sequential steady-state experiments for both model discrimination and improved parameter precision, hence minimising the number of experiments required in kinetic studies. Additionally, a general methodology for conducting efficient kinetic studies was developed to maximise the benefit obtained from the automated reactor. This general methodology included aspects of traditional DoE for situations when there is very little prior knowledge, practical identifiability tests to prevent the wasting of resources pursuing non-identifiable models, and finally online MBDoE to minimise the number of experiments required to identify the correct model structure and to precisely estimate the model parameters.

In order to speed up experiments the automated platform was also shown to be able to conduct transient experiments, which are much faster at gathering kinetic data then sequential steady-state experiments. However, the transient experiments were only ever applied to a simple homogenous system and never demonstrated on heterogeneous catalytic systems, which was the aim of this project. It currently remains unclear if transient methods are a suitable kinetic technique for heterogeneous catalysis. This is because the transient methods require the catalysts to instantaneously respond to changing process conditions, however some heterogeneous catalytic reactions have been shown to have an induction period, hence these experiments would not be possible. One example of such a catalyst is the Fisher-Tropsch catalysts which are known to require time to come to chemical equilibrium with the feed stream [174]. Despite this challenge there are reports in the literature of the successful application of transient methods to gas phase catalytic reactions (oxidation

of carbon monoxide and steam reforming of methanol [175]. Therefore, the continued development of transient kinetic methods for heterogeneous catalyst applications remains a promising area of study.

The automated system was also shown to be very flexible as the same system and same LabVIEW codes was applied to two different reactions, the esterification of benzoic acid and ethanol, and the oxidation of HMF to FDCA in a micropacked bed reactor. This showed that the automated system, once developed, could be adapted easily and quickly from one system to another, which was important to demonstrate that the time saved from automating the experiments was greater than the time spent on developing the automated system.

The greatest failure of the automated system was that it was not able to obtain a reliable intrinsic kinetic model for the oxidation of HMF to FDCA, despite that the automated system was successfully adapted for multiphase systems. This failure was attributed to the poor reproducibility of the $AuPd/TiO_2$ catalyst and micropacked bed reactor used in the work. While a reliable kinetic model was not obtained and online MBDoE was not attempted for this complicated system, the automated system was still of great value for speeding up the kinetic experiments and significant amounts of valuable information were still obtained regarding HMF oxidation with Au and $AuPd/TiO_2$ catalysts. Additionally, the automated platform is still considered to be a very promising technology for future kinetic studies in both academia and industry. As the problem with the HMF case study was to do with the reproducibility of the reactor and the catalyst, rather than with some problem with the automated platform, there is no reason to believe that this automated system could not be applied in future to other challenging catalytic reactions. However, in future it should be checked that the experimental set-up gives reproducible results before beginning a factorial campaign of experiments. Additionally, in future, when selecting a new reaction system, it is recommended to begin by applying the automated system to less challenging systems than the oxidation of HMF, which combined complex chemistry, with a challenging reactor configuration and with a novel catalyst which had not been previously demonstrated to be reproducible. Therefore, more suitable future case studies should focus on either complicated chemistry in a simple reactor system (for example single phase flow in a packed bed instead of 2 phase flow), with a commercial catalyst, or else a complicated reactor system such as a micropacked bed reactor but with simple chemistry.

The automated system itself could also be improved in many ways. It is recommended to replace the syringe pumps with HPLC pumps as this would allow continuous

operation without having to stop to refill the syringe. While it was attempted to automate the refilling of the syringes by using 2 syringes for each feed stream along with non-return (check) valves, it was found that the non-return valves did not work for the low flowrates used in this work. Additionally, internal standards should be used in all feed streams to help reduce measurement error in the HPLC due to dilution errors and to detect errors in the mixing of reagent streams. Finally, new analytical equipment should be incorporated into the automated system. Adding online GC analysis would allow the study of many gas phase heterogeneous reactions, while adding spectroscopic analysis methods such as IR, Raman or UV-vis would dramatically reduce analysis time and lead to significant time savings. A variety of new algorithms could also be implemented on the automated system, including automated online outlier detection or more sophisticated forms of MBDoE, including joint MBDoE to find a trade-off between model exploration and exploitation, or robust MBDoE techniques [191, 192] which take into account the uncertainty in the parameter estimates in the experimental design.

One of the challenges encountered in this work when studying the kinetics of HMF in a micropacked bed reactor, was the lack of relevant mass transfer correlations in the literature for gas liquid flow in micropacked beds, for both gas-liquid mass transfer and liquid-solid mass transfer. As it is difficult to simultaneously estimate mass transfer parameters and kinetic parameters, it is suggested that a detailed characterisation of mass transfer in micropacked bed reactors is conducted under a wide range of flow rates and flow regimes. This information would then assist kinetic studies in the future. In order to conduct this mass transfer characterisation as efficiently as possible, it is recommended that the autonomous reactor platform and MBDoE algorithms developed in this thesis be applied to this challenge. Furthermore, the automated reactor platform and MBDoE algorithms developed in this work could be applied to a wide number of applications beyond the field of catalytic kinetic studies. For example, automated MBDoE could be applied to the development of first principle models for heat exchangers, absorption columns and many other unit operations within chemical engineering and beyond. Therefore, continued development of the automated system is considered a promising area for future work which would lead to significant savings of time and resources in lab based research.

10 References

1. Hagen, J., *Industrial catalysis: A practical approach*. 3 ed. 2015, Weinheim: John Wiley & Sons.
2. Chemistry_Growth_Strategy_Group, *Strategy for Delivering Chemistry-fuelled Growth of the UK Economy*. 2013: The Society of Chemical Industry Website.
3. International_Energy_Agency, International_Council_of_Chemical_Associations, and DECHEMA, *Technology Roadmap: Energy and GHG Reductions in the Chemical Industry via Catalytic Processes*. 2013.
4. European_Cluster_on_Catalysis, *Science and Technology Roadmap on Catalysis for Europe*. 2016.
5. Losey, M.W., M.A. Schmidt, and K.F. Jensen, *Microfabricated multiphase packed-bed reactors: Characterization of mass transfer and reactions.* Industrial & Engineering Chemistry Research, 2001. **40**(12): p. 2555-2562.
6. Zhang, J., A.R. Teixeira, and K.F. Jensen, *Automated measurements of gas-liquid mass transfer in micropacked bed reactors.* AIChE Journal, 2018. **64**(2): p. 564-570.
7. Tidona, B., et al., *Liquid-to-particle mass transfer in a micro packed bed reactor.* International Journal of Heat and Mass Transfer, 2012. **55**(4): p. 522-530.
8. Trachsel, F., C. Hutter, and P.R. von Rohr, *Transparent silicon/glass microreactor for high-pressure and high-temperature reactions.* Chemical Engineering Journal, 2008. **135, Supplement 1**: p. S309-S316.
9. Trachsel, F., et al., *Solid catalyzed hydrogenation in a Si/glass microreactor using supercritical CO_2 as the reaction solvent.* The Journal of Supercritical Fluids, 2009. **48**(2): p. 146-153.
10. Kockmann, N., et al., *Safety assessment in development and operation of modular continuous-flow processes.* Reaction Chemistry & Engineering, 2017. **2**(3): p. 258-280.
11. Al-Rifai, N., et al., *Microreaction technology aided catalytic process design.* Current Opinion in Chemical Engineering, 2013. **2**(3): p. 338-345.
12. Moore, J.S. and K.F. Jensen, *"Batch" kinetics in flow: online IR analysis and continuous control.* Angewandte Chemie International Edition, 2014. **53**(2): p. 470-473.
13. Cao, E., et al., *A micropacked-bed multi-reactor system with in situ Raman analysis for catalyst evaluation.* Catalysis Today, 2017. **283**: p. 195-201.
14. McMullen, J.P. and K.F. Jensen, *Rapid determination of reaction kinetics with an automated microfluidic system.* Organic Process Research & Development, 2011. **15**(2): p. 398-407.
15. Perera, D., et al., *A platform for automated nanomole-scale reaction screening and micromole-scale synthesis in flow.* Science, 2018. **359**(6374): p. 429-434.
16. Bédard, A.-C., et al., *Reconfigurable system for automated optimization of diverse chemical reactions.* Science, 2018. **361**(6408): p. 1220-1225.
17. Malig, T.C., et al., *Real-time HPLC-MS reaction progress monitoring using an automated analytical platform.* Reaction Chemistry & Engineering, 2017. **2**: p. 309-314.
18. Gross, E., et al., *In situ IR and X-ray high spatial-resolution microspectroscopy measurements of multistep organic transformation in flow microreactor catalyzed by Au nanoclusters.* Journal of the American Chemical Society, 2014. **136**(9): p. 3624.
19. Sagmeister, P., et al., *Laboratory of the future: a modular flow platform with multiple integrated PAT tools for multistep reactions.* Reaction Chemistry & Engineering, 2019.
20. Adamo, A., et al., *On-Demand Continuous-Flow Production of Pharmaceuticals in a Compact, Reconfigurable System.* Science, 2016. **352**(6281): p. 61-67.
21. Gürsel, I.V., N. Kockmann, and V. Hessel, *Fluidic separation in microstructured devices–Concepts and their Integration into process flow networks.* Chemical Engineering Science, 2017. **169**(21): p. 3-17.

22. Kenig, E.Y., et al., *Micro-separation of fluid systems: A state-of-the-art review.* Separation and Purification Technology, 2013. **120**: p. 245-264.
23. Morad, M., et al., *Multifunctional Supported Bimetallic Catalysts for a Cascade Reaction with Hydrogen Auto Transfer: Synthesis of 4-Phenylbutan-2-ones from 4-Methoxybenzyl Alcohols.* Catalysis Science & Technology, 2017. **7**(9): p. 1928-1936.
24. Blackmond, D.G., *Kinetic profiling of catalytic organic reactions as a mechanistic tool.* Journal of the American Chemical Society, 2015. **137**(34): p. 10852-10866.
25. Franceschini, G. and S. Macchietto, *Model-based design of experiments for parameter precision: State of the art.* Chemical Engineering Science, 2008. **63**(19): p. 4846-4872.
26. Blackmond, D.G., *Reaction progress kinetic analysis: a powerful methodology for mechanistic studies of complex catalytic reactions.* Angewandte Chemie International Edition, 2005. **44**(28): p. 4302-4320.
27. Schmidt, O.P., et al., *Kinetic Analysis of Catalytic Organic Reactions Using a Temperature Scanning Protocol.* ChemCatChem.
28. Salmi, T., et al., *Microreactors as tools in kinetic investigations: Ethylene oxide formation on silver catalyst.* Chemical Engineering Science, 2013. **87**: p. 306-314.
29. Tadepalli, S. and A. Lawal, *The Catalytic Hydrogenation of Aromatic Nitro Ketone in a Microreactor: Reactor Performance and Kinetic Studies.* International Journal of Chemical Reactor Engineering, 2009. **6**(1): p. 1542-6580.
30. Hessel, V., *Novel process windows–gate to maximizing process intensification via flow chemistry.* Chemical Engineering & Technology: Industrial Chemistry-Plant Equipment-Process Engineering-Biotechnology, 2009. **32**(11): p. 1655-1681.
31. Tidona, B., A. Urakawa, and P. Rudolf von Rohr, *High pressure plant for heterogeneous catalytic CO_2 hydrogenation reactions in a continuous flow microreactor.* Chemical Engineering and Processing: Process Intensification, 2013. **65**: p. 53-57.
32. Cherkasov, N., et al., *OpenFlowChem–a platform for quick, robust and flexible automation and self-optimisation of flow chemistry.* Reaction Chemistry & Engineering, 2018. **3**: p. 769-780.
33. Aroh, K.C. and K.F. Jensen, *Efficient kinetic experiments in continuous flow microreactors.* Reaction Chemistry & Engineering, 2018. **3**: p. 94-101.
34. Hone, C.A., et al., *Rapid multistep kinetic model generation from transient flow data.* Reaction Chemistry & Engineering, 2017. **2**(2): p. 103-108.
35. Schaber, S.D., et al., *Design, execution, and analysis of time-varying experiments for model discrimination and parameter estimation in microreactors.* Organic Process Research & Development, 2014. **18**(11): p. 1461-1467.
36. Hone, C.A., et al., *Definitive screening designs for multistep kinetic models in flow.* Reaction Chemistry & Engineering, 2019.
37. Wyvratt, B.M., J.P. McMullen, and S.T. Grosser, *Multidimensional dynamic experiments for data-rich process development of reactions in flow.* Reaction Chemistry & Engineering, 2019.
38. Buzzi-Ferraris, G., et al., *Sequential experimental design for model discrimination in the case of multiple responses.* Chemical Engineering Science, 1984. **39**(1): p. 81-85.
39. Echtermeyer, A., et al., *Self-optimisation and model-based design of experiments for developing a C–H activation flow process.* Beilstein Journal of Organic Chemistry, 2017. **13**: p. 150-163.
40. Cruz Bournazou, M., et al., *Online optimal experimental re-design in robotic parallel fed-batch cultivation facilities.* Biotechnology and bioengineering, 2017. **114**(3): p. 610-619.
41. Reizman, B.J. and K.F. Jensen, *An automated continuous-flow platform for the estimation of multistep reaction kinetics.* Organic Process Research & Development, 2012. **16**(11): p. 1770-1782.

42. Alsolami, B.H., et al., *Catalyst Performance Testing in Multiphase Systems: Implications of Using Small Catalyst Particles in Hydrodesulfurization.* Industrial & Engineering Chemistry Research, 2013. **52**(26): p. 9069-9085.
43. Al-Rifai, N., et al., *Hydrodynamic Effects on Three Phase Micro-packed Bed Reactor Performance – Gold–Palladium Catalysed Benzyl Alcohol Oxidation.* Chemical Engineering Science, 2016. **149**: p. 129-142.
44. Yang, C., et al., *Catalytic hydrogenation of N-4-nitrophenyl nicotinamide in a micro-packed bed reactor.* Green Chemistry, 2018. **20**(4): p. 886-893.
45. Joshi, N. and A. Lawal, *Hydrodeoxygenation of 4-propylguaiacol (2-methoxy-4-propylphenol) in a microreactor: performance and kinetic studies.* Industrial & Engineering Chemistry Research, 2013. **52**(11): p. 4049-4058.
46. Moonen, R., et al., *Performance testing of hydrodesulphurization catalysts using a single pellet string reactor.* Chemical Engineering & Technology, 2017. **40**(11): p. 2025-2034.
47. Müller, A., et al., *Evaluation of reactor concepts for the continuous production of fine chemicals using the selective hydrogenation of cinnamaldehyde over palladium catalysts.* Catalysis Today, 2015. **241**: p. 214-220.
48. Kallinikos, L.E. and N.G. Papayannakos, *Intensification of hydrodesulphurization process with a structured bed spiral mini-reactor.* Chemical Engineering and Processing: Process Intensification, 2010. **49**(10): p. 1025-1030.
49. Bauer, T. and S. Haase, *Comparison of structured trickle-bed and monolithic reactors in Pd-catalyzed hydrogenation of alpha-methylstyrene.* Chemical Engineering Journal, 2011. **169**(1-3): p. 263-269.
50. Jähnisch, K., et al., *Chemistry in Microstructured Reactors.* Angewandte Chemie International Edition, 2004. **43**(4): p. 406-446.
51. Pennemann, H. and G. Kolb, *Review: Microstructured reactors as efficient tool for the operation of selective oxidation reactions.* Catalysis Today, 2016. **278, Part 1**: p. 3-21.
52. Cherkasov, N., Y. Bai, and E. Rebrov, *Process Intensification of Alkynol Semihydrogenation in a Tube Reactor Coated with a Pd/ZnO Catalyst.* Catalysts, 2017. **7**(12): p. 358.
53. Galvanin, F., et al., *A joint model-based experimental design approach for the identification of kinetic models in continuous flow laboratory reactors.* Computers & Chemical Engineering, 2016. **95**: p. 202-215.
54. Görke, O., P. Pfeifer, and K. Schubert, *Kinetic study of ethanol reforming in a microreactor.* Applied Catalysis A: General, 2009. **360**(2): p. 232-241.
55. Benzinger, W., A. Wenka, and R. Dittmeyer, *Kinetic modelling of the SO_2-oxidation with Pt in a microstructured reactor.* Applied Catalysis A: General, 2011. **397**(1–2): p. 209-217.
56. Chapman, M.R., et al., *Simple and Versatile Laboratory Scale CSTR for Multiphasic Continuous-Flow Chemistry and Long Residence Times.* Organic Process Research & Development, 2017. **21**(9): p. 1294-1301.
57. Mo, Y. and K.F. Jensen, *A Miniature CSTR Cascade for Continuous Flow of Reactions Containing Solids.* Reaction Chemistry & Engineering, 2016. **1**(5): p. 501-507.
58. Sedelmeier, J.r., et al., *KMnO4-Mediated Oxidation as a Continuous Flow Process.* Organic letters, 2010. **12**(16): p. 3618-3621.
59. Hartman, R.L., et al., *Overcoming the Challenges of Solid Bridging and Constriction during Pd-Catalyzed C− N Bond Formation in Microreactors.* Organic Process Research & Development, 2010. **14**(6): p. 1347-1357.
60. Enache, D.I., et al., *The hydrogenation of isophorone to trimethyl cyclohexanone using the downflow single capillary reactor.* Catalysis today, 2005. **105**(3-4): p. 569-573.
61. Pollington, S.D., et al., *Enhanced selective glycerol oxidation in multiphase structured reactors.* Catalysis Today, 2009. **145**(1-2): p. 169-175.

62. Zhang, J., et al., *Hydrodynamics of gas-liquid flow in micro-packed beds: pressure drop, liquid holdup and two-phase model.* AIChE Journal, 2017. **63**(10): p. 6494-4704.
63. Márquez, N., et al., *Dispersion and Holdup in Multiphase Packed Bed Microreactors.* Chemical Engineering & Technology, 2008. **31**(8): p. 1130-1139.
64. Faridkhou, A. and F. Larachi, *Hydrodynamics of Gas–Liquid Cocurrent Flows in Micropacked Beds—Wall Visualization Study.* Industrial & Engineering Chemistry Research, 2012. **51**(50): p. 16495-16504.
65. Faridkhou, A., J.-N. Tourvieille, and F. Larachi, *Reactions, hydrodynamics and mass transfer in micro-packed beds—Overview and new mass transfer data.* Chemical Engineering and Processing: Process Intensification, 2016. **110**: p. 80-96.
66. Faridkhou, A., M. Hamidipour, and F. Larachi, *Hydrodynamics of gas–liquid micro-fixed beds – Measurement approaches and technical challenges.* Chemical Engineering Journal, 2013. **223**: p. 425-435.
67. Faridkhou, A. and F. Larachi, *Two-phase flow hydrodynamic study in micro-packed beds – Effect of bed geometry and particle size.* Chemical Engineering and Processing: Process Intensification, 2014. **78**: p. 27-36.
68. Márquez, N., et al., *Transient Behavior and Stability in Miniaturized Multiphase Packed Bed Reactors.* Industrial & Engineering Chemistry Research, 2010. **49**(3): p. 1033-1040.
69. Márquez, N., et al., *Volatile tracer dispersion in multi-phase packed beds.* Chemical Engineering Science, 2010. **65**(13): p. 3972-3985.
70. Inoue, T., M.A. Schmidt, and K.F. Jensen, *Microfabricated Multiphase Reactors for the Direct Synthesis of Hydrogen Peroxide from Hydrogen and Oxygen.* Industrial & Engineering Chemistry Research, 2007. **46**(4): p. 1153-1160.
71. Liebner, C., et al., *Are Micro Reactors Inherently Safe? An Investigation of Gas Phase Explosion Propagation Limits on Ethene Mixtures.* Process Safety and Environmental Protection, 2012. **90**(2): p. 77-82.
72. Chan, K.L.A., et al., *Rapid prototyping of microfluidic devices for integrating with FT-IR spectroscopic imaging.* Lab on a Chip, 2010. **10**(16): p. 2170.
73. Moore, J.S. and K.F. Jensen, *Automated multitrajectory method for reaction optimization in a microfluidic system using online IR analysis.* Organic Process Research & Development, 2012. **16**(8): p. 1409-1415.
74. Skilton, R.A., et al., *Real-Time Feedback Control Using Online Attenuated Total Reflection Fourier Transform Infrared (ATR FT-IR) Spectroscopy for Continuous Flow Optimization and Process Knowledge.* Applied Spectroscopy, 2013. **67**(10): p. 1127-1131.
75. Silverwood, I.P., et al., *Towards microfluidic reactors for in situ synchrotron infrared studies.* Review of Scientific Instruments, 2016. **87**(2): p. 024101.
76. Perro, A., et al., *Combining microfluidics and FT-IR spectroscopy: towards spatially resolved information on chemical processes.* Reaction Chemistry & Engineering, 2016.
77. Roberto, M.F., et al., *Integration of Continuous Flow Reactors and Online Raman Spectroscopy for Process Optimization.* Journal of Pharmaceutical Innovation, 2012. **7**(2): p. 69-75.
78. Figueroa, S.J.A., et al., *Innovative insights in a plug flow microreactor for operando X-ray studies.* Journal of Applied Crystallography, 2013. **46**(5): p. 1523-1527.
79. Koch, K., et al., *Optimizing the Deprotection of the Amine Protecting p-Methoxyphenyl Group in an Automated Microreactor Platform.* Organic Process Research & Development, 2009. **13**(5): p. 1003-1006.
80. Reizman, B.J. and K.F. Jensen, *Feedback in Flow for Accelerated Reaction Development.* Accounts of Chemical Research, 2016. **49**(9): p. 1786-1796.
81. Reizman, B.J., et al., *Suzuki-Miyaura cross-coupling optimization enabled by automated feedback.* Reaction Chemistry & Engineering, 2016. **1**(6): p. 658-666.

82. Walsh, B., et al., *The automation of continuous reactions in supercritical CO_2: the acid-catalysed etherification of short chain alcohols.* Green Chemistry, 2005. **7**(6): p. 456-463.
83. Fitzpatrick, D.E., C. Battilocchio, and S.V. Ley, *A novel internet-based reaction monitoring, control and autonomous self-optimization platform for chemical synthesis.* Organic Process Research & Development, 2015. **20**(2): p. 386-394.
84. Holmes, N., et al., *Online quantitative mass spectrometry for the rapid adaptive optimisation of automated flow reactors.* Reaction Chemistry & Engineering, 2016. **1**(1): p. 96-100.
85. Dou, J., et al., *Operando chemistry of catalyst surfaces during catalysis.* Chemical Society Reviews, 2017. **46**(7): p. 2001-2027.
86. Meunier, F.C., *The design and testing of kinetically-appropriate operando spectroscopic cells for investigating heterogeneous catalytic reactions.* Chemical Society Reviews, 2010. **39**(12): p. 4602-4614.
87. Fabry, D.C., E. Sugiono, and M. Rueping, *Online monitoring and analysis for autonomous continuous flow self-optimizing reactor systems.* Reaction Chemistry & Engineering, 2016. **1**(2): p. 129-133.
88. McMullen, J.P. and K.F. Jensen, *Integrated Microreactors for Reaction Automation: New Approaches to Reaction Development*, in *Annu. Rev. Anal. Chem.* 2010. p. 19-42.
89. Goodell, J.R., et al., *Development of an automated microfluidic reaction platform for multidimensional screening: reaction discovery employing bicyclo [3.2. 1] octanoid scaffolds.* The Journal of Organic Chemistry, 2009. **74**(16): p. 6169-6180.
90. Reizman, B.J. and K.F. Jensen, *Simultaneous solvent screening and reaction optimization in microliter slugs.* Chemical Communications, 2015. **51**(68): p. 13290-13293.
91. Mills, P.L. and J.F. Nicole, *Multiple automated reactor systems (MARS). 1. A novel reactor system for detailed testing of gas-phase heterogeneous oxidation catalysts.* Industrial & Engineering Chemistry Research, 2005. **44**(16): p. 6435-6452.
92. McMullen, J.P. and K.F. Jensen, *An automated microfluidic system for online optimization in chemical synthesis.* Organic Process Research & Development, 2010. **14**(5): p. 1169-1176.
93. Sans, V., et al., *A self optimizing synthetic organic reactor system using real-time in-line NMR spectroscopy.* Chemical Science, 2015. **6**(2): p. 1258-1264.
94. Parrott, A.J., et al., *Self-optimizing continuous reactions in supercritical carbon dioxide.* Angewandte Chemie International Edition, 2011. **50**(16): p. 3788-3792.
95. McMullen, J.P., et al., *An integrated microreactor system for self-optimization of a heck reaction: From micro-to mesoscale flow systems.* Angewandte Chemie International Edition, 2010. **49**(39): p. 7076-7080.
96. Vieira, R.A., et al., *Closed-loop composition and molecular weight control of a copolymer latex using near-infrared spectroscopy.* Industrial & Engineering Chemistry Research, 2002. **41**(12): p. 2915-2930.
97. Jumbam, D.N., et al., *The effect of self-optimisation targets on the methylation of alcohols using dimethyl carbonate in supercritical CO2.* Journal of Flow Chemistry, 2012. **2**(1): p. 24-27.
98. Cortés-Borda, D., et al., *Optimizing the Heck–Matsuda reaction in flow with a constraint-adapted direct search algorithm.* Organic Process Research & Development, 2016. **20**(11): p. 1979-1987.
99. Houben, C., et al., *Closed-loop multitarget optimization for discovery of new emulsion polymerization recipes.* Organic Process Research & Development, 2015. **19**(8): p. 1049-1053.
100. Sans, V. and L. Cronin, *Towards dial-a-molecule by integrating continuous flow, analytics and self-optimisation.* Chemical Society Reviews, 2016. **45**(8): p. 2032-2043.

101. Mateos, C., M.J. Nieves-Remacha, and J.A. Rincón, *Automated platforms for reaction self-optimization in flow.* Reaction Chemistry & Engineering, 2019.
102. Schotten, C., et al., *A machine-assisted approach for the preparation of follow-on pharmaceutical compound libraries.* Reaction Chemistry & Engineering, 2018. **3**(2): p. 210-215.
103. Venkatasubramanian, V., *The promise of artificial intelligence in chemical engineering: Is it here, finally?* AIChE Journal, 2019. **65**(2): p. 466-478.
104. Ley, S.V., et al., *Organic Synthesis: March of the Machines.* Angewandte Chemie International Edition, 2015. **54**(11): p. 3449-3464.
105. Kobayashi, J., et al., *A microfluidic device for conducting gas-liquid-solid hydrogenation reactions.* Science, 2004. **304**(5675): p. 1305-1308.
106. Yoshida, J., A. Nagaki, and T. Yamada, *Flash Chemistry: Fast Chemical Synthesis by Using Microreactors.* Chemistry – A European Journal, 2008. **14**(25): p. 7450-7459.
107. Jensen, K.F., *Flow Chemistry—Microreaction technology comes of age.* AIChE Journal, 2017. **63**(3): p. 858-869.
108. Jensen, K.F., B.J. Reizman, and S.G. Newman, *Tools for chemical synthesis in microsystems.* Lab on a Chip, 2014. **14**(17): p. 3206-3212.
109. Yao, X., et al., *Review of the applications of microreactors.* Renewable and Sustainable Energy Reviews, 2015. **47**: p. 519-539.
110. Elvira, K., et al., *The past, present and potential for microfluidic reactor technology in chemical synthesis.* Nature Chemistry, 2013. **5**: p. 905-15.
111. Kiwi-Minsker, L. and A. Renken, *Microstructured reactors for catalytic reactions.* Catalysis Today, 2005. **110**(1–2): p. 2-14.
112. Roberge, D.M., et al., *Microreactor technology: a revolution for the fine chemical and pharmaceutical industries?* Chemical Engineering & Technology: Industrial Chemistry-Plant Equipment-Process Engineering-Biotechnology, 2005. **28**(3): p. 318-323.
113. Poe, S.L., et al., *Solving the Clogging Problem: Precipitate-Forming Reactions in Flow.* Angewandte Chemie International Edition, 2006. **45**(10): p. 1544-1548.
114. Horie, T., et al., *Photodimerization of Maleic Anhydride in a Microreactor Without Clogging.* Organic Process Research & Development, 2010. **14**(2): p. 405-410.
115. Wada, Y., M.A. Schmidt, and K.F. Jensen, *Flow Distribution and Ozonolysis in Gas−Liquid Multichannel Microreactors.* Industrial & Engineering Chemistry Research, 2006. **45**(24): p. 8036-8042.
116. Lévesque, F. and P.H. Seeberger, *Continuous-Flow Synthesis of the Anti-Malaria Drug Artemisinin.* Angewandte Chemie International Edition, 2012. **51**(7): p. 1706-1709.
117. Correia, C.A., et al., *A Concise Flow Synthesis of Efavirenz.* Angewandte Chemie International Edition, 2015. **54**(16): p. 4945-4948.
118. Cole, K.P., et al., *Kilogram-scale prexasertib monolactate monohydrate synthesis under continuous-flow CGMP conditions.* Science, 2017. **356**(6343): p. 1144-1150.
119. FiercePharma. *FDA Urges Companies to get on Board with Continuous Manufacturing*. 2016; Available from: https://www.fiercepharma.com/manufacturing/fda-urges-companies-to-get-on-board-continuous-manufacturing.
120. Kahn, J., *FDA supports critical research to spur innovation for continuous manufacturing technology to support and advance drug and biologics development*. 2018: https://www.fda.gov/NewsEvents/Newsroom/FDAInBrief/ucm615431.htm.
121. Lee, S.L., et al., *Modernizing Pharmaceutical Manufacturing: from Batch to Continuous Production.* Journal of Pharmaceutical Innovation, 2015. **10**(3): p. 191-199.
122. McGovern, S., et al., *Multiphase flow regimes for hydrogenation in a catalyst-trap microreactor.* Chemical Engineering Journal, 2008. **135, Supplement 1**: p. S229-S236.
123. Nuzhdin, A.L., et al., *Selective Liquid-Phase Hydrogenation of a Nitro Group in Substituted Nitrobenzenes over Au/Al2O3 Catalyst in a Packed-Bed Flow Reactor.* ChemPlusChem, 2015. **80**(12): p. 1741-1749.

124. Gavriilidis, A., et al., *Aerobic oxidations in flow: opportunities for the fine chemicals and pharmaceuticals industries.* Reaction Chemistry & Engineering, 2016. **1**(6): p. 595-612.
125. Maurya, R.A., et al., *Continuous in situ generation, separation, and reaction of diazomethane in a dual-channel microreactor.* Angewandte Chemie international edition, 2011. **50**(26): p. 5952-5955.
126. Singh, R., et al., *Recent advances for serial processes of hazardous chemicals in fully integrated microfluidic systems.* Korean Journal of Chemical Engineering, 2016. **33**(8): p. 2253-2267.
127. Mastronardi, F., B. Gutmann, and C.O. Kappe, *Continuous flow generation and reactions of anhydrous diazomethane using a teflon AF-2400 tube-in-tube reactor.* Organic letters, 2013. **15**(21): p. 5590-5593.
128. Sankar, G., E. Cao, and A. Gavriilidis, *A microstructured reactor based in situ cell for the study of catalysts by X-ray absorption spectroscopy under operating conditions.* Catalysis Today, 2007. **125**(1–2): p. 24-28.
129. Baier, S., et al., *Lithographically fabricated silicon microreactor for in situ characterization of heterogeneous catalysts—Enabling correlative characterization techniques.* Review of Scientific Instruments, 2015. **86**(6): p. 065101.
130. Li, Y., et al., *Complex structural dynamics of nanocatalysts revealed in Operando conditions by correlated imaging and spectroscopy probes.* Nature Communications, 2015. **6**: p. 7583.
131. Holmes, N., et al., *Self-optimisation of the final stage in the synthesis of EGFR kinase inhibitor AZD9291 using an automated flow reactor.* Reaction Chemistry & Engineering, 2016. **1**(4): p. 366-371.
132. Jeraal, M.I., et al., *Enhanced process development using automated continuous reactors by self-optimisation algorithms and statistical empirical modelling.* Tetrahedron, 2018. **74**(25): p. 3158-3164.
133. Schweidtmann, A.M., et al., *Machine learning meets continuous flow chemistry: Automated optimization towards the Pareto front of multiple objectives.* Chemical Engineering Journal, 2018. **352**: p. 277-282.
134. Moore, J.S., C.D. Smith, and K.F. Jensen, *Kinetics analysis and automated online screening of aminocarbonylation of aryl halides in flow.* Reaction Chemistry & Engineering, 2016. **1**(3): p. 272-279.
135. Sheldon, R.A., *Fundamentals of Green Chemistry: Efficiency in Reaction Design.* Chemical Society Reviews, 2012. **41**(4): p. 1437-1451.
136. Climent, M.J., et al., *New One-Pot Multistep Process with Multifunctional Catalysts: Decreasing the E factor in the Synthesis of Fine Chemicals.* Green Chemistry, 2010. **12**(1): p. 99-107.
137. Grondal, C., M. Jeanty, and D. Enders, *Organocatalytic Cascade Reactions as a New Tool in Total Synthesis.* Nature Chemistry, 2010. **2**(3): p. 167-178.
138. Pieber, B., K. Gilmore, and P.H. Seeberger, *Integrated Flow Processing—Challenges in Continuous Multistep Synthesis.* Journal of Flow Chemistry, 2017: p. 1-8.
139. Jeena, V. and R.S. Robinson, *Recent developments in one-pot tandem oxidation process coupling reactions.* RSC Advances, 2014. **4**(77): p. 40720-40739.
140. Fogg, D.E. and E.N. dos Santos, *Tandem catalysis: a taxonomy and illustrative review.* Coordination Chemistry Reviews, 2004. **248**(21): p. 2365-2379.
141. Masson, G., *Catalytic Cascade Reactions. Edited by Peng-Fei Xu and Wei Wang.* Angewandte Chemie International Edition, 2014. **53**(50): p. 13656-13657.
142. Climent, M.J., A. Corma, and S. Iborra, *Mono-and Multisite Solid Catalysts in Cascade Reactions for Chemical Process Intensification.* ChemSusChem, 2009. **2**(6): p. 500-506.
143. Climent, M.J., et al., *Heterogeneous Catalysis for Tandem Reactions.* ACS Catalysis, 2014. **4**(3): p. 870-891.
144. Wang, K. and G. Luo, *Microflow extraction: A review of recent development.* Chemical Engineering Science, 2017. **169**: p. 18-33.

145. Noël, T., et al., *Suzuki–Miyaura Cross-Coupling Reactions in Flow: Multistep Synthesis Enabled by a Microfluidic Extraction.* Angewandte Chemie International Edition, 2011. **50**(26): p. 5943-5946.
146. Hartman, R.L., et al., *Multistep Microchemical Synthesis Enabled by Microfluidic Distillation.* Angewandte Chemie International Edition, 2010. **49**(5): p. 899-903.
147. Sahoo, H.R., J.G. Kralj, and K.F. Jensen, *Multistep Continuous-Flow Microchemical Synthesis Involving Multiple Reactions and Separations.* Angew Chem Int Ed Engl, 2007. **46**(30): p. 5704-8.
148. Seeberger, P.H., *Organic synthesis: Scavengers in full flow.* Nature Chemistry, 2009. **1**(4): p. 258-260.
149. Guan-Young, J., et al., *One-flow Syntheses of Diverse Heterocyclic Furan Chemicals Directly from Fructose via Tandem Transformation Platform.* NPG Asia Materials, 2015. **7**(4): p. e173.
150. Britton, J. and C.L. Raston, *Multi-Step Continuous-Flow Synthesis.* Chemical Society Reviews, 2017. **46**(5): p. 1250-1271.
151. Baumann, M. and I.R. Baxendale, *The Synthesis of Active Pharmaceutical Ingredients (APIs) using Continuous Flow Chemistry.* Beilstein Journal of Organic Chemistry, 2015. **11**: p. 1194.
152. Bogdan, A.R., et al., *The Continuous-Flow Synthesis of Ibuprofen.* Angewandte Chemie International Edition, 2009. **48**(45): p. 8547-8550.
153. Gutmann, B., D. Cantillo, and C.O. Kappe, *Continuous-Flow Technology—A Tool for the Safe Manufacturing of Active Pharmaceutical Ingredients.* Angewandte Chemie International Edition, 2015. **54**(23): p. 6688-6728.
154. Tsubogo, T., H. Oyamada, and S. Kobayashi, *Multistep Continuous Flow Synthesis of (R)-and (S)-Rolipram Using Heterogeneous Catalysts.* Nature, 2015. **520**(7547): p. 329-332.
155. Ghislieri, D., K. Gilmore, and P.H. Seeberger, *Chemical assembly systems: layered control for divergent, continuous, multistep syntheses of active pharmaceutical ingredients.* Angewandte Chemie International Edition, 2015. **54**(2): p. 678-682.
156. Murray, P.R., et al., *Continuous flow-processing of organometallic reagents using an advanced peristaltic pumping system and the telescoped flow synthesis of (E/Z)-tamoxifen.* Organic Process Research & Development, 2013. **17**(9): p. 1192-1208.
157. Snead, D.R. and T.F. Jamison, *A three-minute synthesis and purification of ibuprofen: Pushing the limits of continuous-flow processing.* Angewandte Chemie International Edition, 2015. **54**(3): p. 983-987.
158. Heider, P.L., et al., *Development of a multi-step synthesis and workup sequence for an integrated, continuous manufacturing process of a pharmaceutical.* Organic Process Research & Development, 2014. **18**(3): p. 402-409.
159. Zhang, P., M.G. Russell, and T.F. Jamison, *Continuous flow total synthesis of rufinamide.* Organic Process Research & Development, 2014. **18**(11): p. 1567-1570.
160. Mascia, S., et al., *End-to-end continuous manufacturing of pharmaceuticals: integrated synthesis, purification, and final dosage formation.* Angewandte Chemie International Edition, 2013. **52**(47): p. 12359-12363.
161. Bond, J.Q., et al., *Integrated Catalytic Conversion of γ-Valerolactone to Liquid Alkenes for Transportation Fuels.* Science, 2010. **327**(5969): p. 1110-1114.
162. Kunkes, E.L., et al., *Catalytic Conversion of Biomass to Monofunctional Hydrocarbons and Targeted Liquid-Fuel Classes.* Science, 2008. **322**(5900): p. 417.
163. Bogdan, A.R., et al., *High-Temperature Boc Deprotection in Flow and Its Application in Multistep Reaction Sequences.* Organic Letters, 2016. **18**(8): p. 1732-1735.
164. Cantillo, D., et al., *Continuous Flow Synthesis of a Key 1,4-Benzoxazinone Intermediate via a Nitration/Hydrogenation/Cyclization Sequence.* Organic Process Research & Development, 2017. **21**(1): p. 125-132.

165. Liu, X. and K.F. Jensen, *Multistep Synthesis of Amides from Alcohols and Amines in Continuous Flow Microreactor Systems using Oxygen and Urea Hydrogen Peroxide as Oxidants.* Green Chemistry, 2013. **15**(6): p. 1538-1541.
166. Ingham, R.J., et al., *A Systems Approach towards an Intelligent and Self-Controlling Platform for Integrated Continuous Reaction Sequences.* Angewandte Chemie International Edition, 2015. **54**(1): p. 144-148.
167. Nijhuis, T.A., et al., *The Direct Epoxidation of Propene in the Explosive Regime in a Microreactor. A Study into the Reaction Kinetics.* Industrial & Engineering Chemistry Research, 2010. **49**(21): p. 10479-10485.
168. Galvanin, F., et al., *Merging Information from Batch and Continuous Flow Experiments for the Identification of Kinetic Models of Benzyl Alcohol Oxidation over Au-Pd Catalyst.* Computer Aided Chemical Engineering, 2016. **38**: p. 961-966.
169. Voloshin, Y. and A. Lawal, *Overall kinetics of hydrogen peroxide formation by direct combination of H_2 and O_2 in a microreactor.* Chemical Engineering Science, 2010. **65**(2): p. 1028-1036.
170. Protasova, L.N., et al., *A kinetic study of the liquid-phase hydrogenation of citral on Au/TiO_2 and $Pt–Sn/TiO_2$ thin films in capillary microreactors.* Applied Catalysis A: General, 2011. **399**(1): p. 12-21.
171. Patel, D.C., et al., *Unattended reaction monitoring using an automated microfluidic sampler and on-line liquid chromatography.* Analytica Chimica Acta, 2018. **1004**: p. 32-39.
172. Fabry, D.C., et al., *Adaptive and automated system-optimization for heterogeneous flow-hydrogenation reactions.* Reaction Chemistry & Engineering, 2019.
173. Clayton, A.D., et al., *Algorithms for the Self-Optimisation of Chemical Reactions.* Reaction Chemistry & Engineering, 2019.
174. Wojciechowski, B., *The temperature scanning reactor I: Reactor types and modes of operation.* Catalysis Today, 1997. **36**(2): p. 167-190.
175. Wojciechowski, B., *The temperature scanning reactor: A kinetics instrument.* Chemical Engineering Communications, 2003. **190**(9): p. 1115-1131.
176. Mozharov, S., et al., *Improved method for kinetic studies in microreactors using flow manipulation and noninvasive Raman spectrometry.* Journal of the American Chemical Society, 2011. **133**(10): p. 3601-3608.
177. Buzzi-Ferraris, G. and P. Forzatti, *A new sequential experimental design procedure for discriminating among rival models.* Chemical Engineering Science, 1983. **38**(2): p. 225-232.
178. Hunter, W.G. and A.M. Reiner, *Designs for discriminating between two rival models.* Technometrics, 1965. **7**(3): p. 307-323.
179. Asprey, S. and S. Macchietto, *Statistical tools for optimal dynamic model building.* Computers & Chemical Engineering, 2000. **24**(2-7): p. 1261-1267.
180. Bard, Y., *Nonlinear Parameter Estimation*. 1974, New York: Academic Press.
181. Quaglio, M., et al., *An online reparametrisation approach for robust parameter estimation in automated model identification platforms.* Computers & Chemical Engineering, 2019. **124**: p. 270-284.
182. Box, G.E. and H. Lucas, *Design of experiments in non-linear situations.* Biometrika, 1959. **46**(1/2): p. 77-90.
183. Box, G.E. and W.G. Hunter, *The experimental study of physical mechanisms.* Technometrics, 1965. **7**(1): p. 23-42.
184. Draper, N.R. and W.G. Hunter, *Design of experiments for parameter estimation in multiresponse situations.* Biometrika, 1966. **53**(3-4): p. 525-533.
185. Box, G.E. and W.J. Hill, *Discrimination among mechanistic models.* Technometrics, 1967. **9**(1): p. 57-71.

186. Hill, W.J., W.G. Hunter, and D.W. Wichern, *A joint design criterion for the dual problem of model discrimination and parameter estimation.* Technometrics, 1968. **10**(1): p. 145-160.
187. Hunter, W.G., W.J. Hill, and T.L. Henson, *Designing experiments for precise estimation of all or some of the constants in a mechanistic model.* The Canadian Journal of Chemical Engineering, 1969. **47**(1): p. 76-80.
188. Bernaerts, K., K.J. Versyck, and J.F. Van Impe, *On the design of optimal dynamic experiments for parameter estimation of a Ratkowsky-type growth kinetics at suboptimal temperatures.* International Journal of Food Microbiology, 2000. **54**(1-2): p. 27-38.
189. Versyck, K., J. Claes, and J. Van Impe, *Optimal experimental design for practical identification of unstructured growth models.* Mathematics and Computers in Simulation, 1998. **46**(5-6): p. 621-629.
190. Shahmohammadi, A. and K.B. McAuley, *Sequential Model-Based A-and V-Optimal Design of Experiments for Building Fundamental Models of Pharmaceutical Production Processes.* Computers & Chemical Engineering, 2019.
191. Dette, H., et al., *Robust and efficient design of experiments for the Monod model.* Journal of Theoretical Biology, 2005. **234**(4): p. 537-550.
192. Dette, H., et al., *Maximin efficient design of experiment for exponential regression models.* Journal of Statistical Planning and Inference, 2006. **136**(12): p. 4397-4418.
193. Asprey, S. and S. Macchietto, *Designing robust optimal dynamic experiments.* Journal of Process Control, 2002. **12**(4): p. 545-556.
194. Berkholz, R., D. Röhlig, and R. Guthke, *Data and knowledge based experimental design for fermentation process optimization.* Enzyme and microbial technology, 2000. **27**(10): p. 784-788.
195. Franceschini, G. and S. Macchietto, *Novel anticorrelation criteria for model-based experiment design: Theory and formulations.* AIChE Journal, 2008. **54**(4): p. 1009-1024.
196. Franceschini, G. and S. Macchietto, *Anti-correlation approach to model-based experiment design: application to a biodiesel production process.* Industrial & Engineering Chemistry Research, 2008. **47**(7): p. 2331-2348.
197. Chen, B.H. and S.P. Asprey, *On the design of optimally informative dynamic experiments for model discrimination in multiresponse nonlinear situations.* Industrial & Engineering Chemistry Research, 2003. **42**(7): p. 1379-1390.
198. Espie, D. and S. Macchietto, *The optimal design of dynamic experiments.* AIChE Journal, 1989. **35**(2): p. 223-229.
199. Munack, A., *Optimal feeding strategy for identification of Monod-type models by fed-batch experiments*, in *Computer applications in fermentation technology: Modelling and control of biotechnological processes*. 1989, Springer. p. 195-204.
200. Munack, A. and C. Posten. *Design of optimal dynamical experiments for parameter estimation*. in *1989 American Control Conference*. 1989. IEEE.
201. Chakrabarty, A., G.T. Buzzard, and A.E. Rundell, *Model-based design of experiments for cellular processes.* Wiley Interdisciplinary Reviews: Systems Biology and Medicine, 2013. **5**(2): p. 181-203.
202. Galvanin, F., S. Macchietto, and F. Bezzo, *Model-based design of parallel experiments.* Industrial & Engineering Chemistry Research, 2007. **46**(3): p. 871-882.
203. Hunter, W. and R. Mezaki, *An experimental design strategy for distinguishing among rival mechanistic models an application to the catalytic hydrogenation of propylene.* The Canadian Journal of Chemical Engineering, 1967. **45**(4): p. 247-249.
204. Froment, G. and R. Mezaki, *Sequential discrimination and estimation procedures for rate modeling in heterogeneous catalysis.* Chemical Engineering Science, 1970. **25**(2): p. 293-301.

205. Dumez, F.J. and G.F. Froment, *Dehydrogenation of 1-butene into butadiene. Kinetics, catalyst coking, and reactor design.* Industrial & Engineering Chemistry Process Design and Development, 1976. **15**(2): p. 291-301.
206. Issanchou, S., P. Cognet, and M. Cabassud, *Sequential experimental design strategy for rapid kinetic modeling of chemical synthesis.* AIChE journal, 2005. **51**(6): p. 1773-1781.
207. Galvanin, F., M. Barolo, and F. Bezzo, *Online model-based redesign of experiments for parameter estimation in dynamic systems.* Industrial & Engineering Chemistry Research, 2009. **48**(9): p. 4415-4427.
208. Tateiwa, J.-i., et al., *Cation-Exchanged Montmorillonite-Catalyzed Facile Friedel-Crafts Alkylation of Hydroxy and Methoxy Aromatics with 4-Hydroxybutan-2-one to Produce Raspberry Ketone and Some Pharmaceutically Active Compounds.* The Journal of Organic Chemistry, 1994. **59**(20): p. 5901-5904.
209. Guadix-Montero, S., et al., *Deactivation studies of bimetallic AuPd nanoparticles supported on MgO during selective aerobic oxidation of alcohols.* Applied Catalysis A: General, 2017. **546**: p. 58-66.
210. Falß, S., et al., *A Continuous Process for Buchwald–Hartwig Amination at Micro-, Lab-, and Mesoscale using a Novel Reactor Concept.* Organic Process Research & Development, 2016. **20**(2): p. 558-567.
211. He, Y., et al., *Direct Aldol and Nitroaldol Condensation in an Aminosilane-Grafted Si/Zr/Ti Composite Hollow Fiber as a Heterogeneous Catalyst and Continuous-Flow Reactor.* Journal of Catalysis, 2016. **341**: p. 149-159.
212. Wang, S., K. Goulas, and E. Iglesia, *Condensation and Esterification Reactions of Alkanals, Alkanones, and Alkanols on TiO_2: Elementary Steps, Site Requirements, and Synergistic Effects of Bifunctional Strategies.* Journal of Catalysis, 2016. **340**: p. 302-320.
213. Fischer, A., et al., *High-Surface-Area TiO_2 and TiN as Catalysts for the C C Coupling of Alcohols and Ketones.* ChemSusChem, 2008. **1**(5): p. 444-449.
214. Rekoske, J.E. and M.A. Barteau, *Kinetics, Selectivity, and Deactivation in the Aldol Condensation of Acetaldehyde on Anatase Titanium Dioxide.* Industrial & Engineering Chemistry Research, 2011. **50**(1): p. 41-51.
215. Paterová, I., E. Vyskočilová, and L. Červený, *Two-Step Preparation of Benzylacetone.* Topics in Catalysis, 2012. **55**(11): p. 873-879.
216. Cao, E., et al., *Reaction and Raman Spectroscopic Studies of Alcohol Oxidation on Gold–Palladium Catalysts in Microstructured Reactors.* Chemical Engineering Journal, 2011. **167**(2–3): p. 734-743.
217. Ballarin, B., et al., *Supported Gold Nanoparticles for Alcohols Oxidation in Continuous-Flow Heterogeneous Systems.* ACS Sustainable Chemistry & Engineering, 2017. **5**(6): p. 4746-4756.
218. Alex, H., et al., *On the Selective Aerobic Oxidation of Benzyl Alcohol with Pd/Au-Nanoparticles in Batch and Flow.* Nanotechnology Reviews, 2014. **3**(1): p. 99-110.
219. Wu, G., et al., *Continuous Heterogeneously Catalyzed Oxidation of Benzyl Alcohol Using a Tube-in-Tube Membrane Microreactor.* Industrial & Engineering Chemistry Research, 2015. **54**(16): p. 4183-4189.
220. Al-Rifai, N., et al., *Deactivation Behavior of Supported Gold Palladium Nanoalloy Catalysts during the Selective Oxidation of Benzyl Alcohol in a Micropacked Bed Reactor.* Industrial & Engineering Chemistry Research, 2017. **56**(45): p. 12984-12993.
221. Cao, E., et al., *Selective Suppression of Disproportionation Reaction in Solvent-less Benzyl Alcohol Oxidation Catalysed by Supported Au–Pd Nanoparticles.* Catalysis Today, 2013. **203**: p. 146-152.
222. Morad, M., et al., *Solvent-free Aerobic Oxidation of Alcohols using Supported Gold Palladium Nanoalloys Prepared by a Modified Impregnation Method.* Catalysis Science & Technology, 2014. **4**(9): p. 3120-3128.

223. Zamora, M., et al., *Acetone gas phase condensation on alkaline metals doped TiO_2 sol–gel catalysts.* Applied Surface Science, 2005. **252**(3): p. 828-832.
224. Tanner, R., et al., *Aldol condensation reactions of acetone and formaldehyde over vanadium phosphate catalysts: Comments on the acid-base properties.* Physical Chemistry Chemical Physics, 2002. **4**(4): p. 688-695.
225. Herrmann, S. and E. Iglesia, *Elementary steps in acetone condensation reactions catalyzed by aluminosilicates with diverse void structures.* Journal of Catalysis, 2017. **346**: p. 134-153.
226. Ai, M., *Vapor-phase aldol condensation of formaldehyde with acetic acid on V_2O_5 · P_2O_5 catalysts.* Journal of Catalysis, 1987. **107**(1): p. 210-208.
227. Ai, M., *Vapor-Phase Aldol Condensation of Formaldehyde with Propionic Acid on Vanadium Pentoxide—Phosphorus Pentoxide.* Applied Catalysis, 1988. **36**: p. 221-230.
228. Ai, M., *Reaction of propionic acid with methylal over vanadium-silicon-phosphorus oxide.* Applied Catalysis, 1990. **63**(1): p. 365-373.
229. Tai, J. and R.J. Davis, *Synthesis of methacrylic acid by aldol condensation of propionic acid with formaldehyde over acid–base bifunctional catalysts.* Catalysis Today, 2007. **123**(1–4): p. 42-49.
230. Augustine, R.L., *Selective heterogeneously catalyzed hydrogenations.* Catalysis Today, 1997. **37**(4): p. 419-440.
231. Pipus, G., I. Plazl, and T. Koloini, *Esterification of benzoic acid in microwave tubular flow reactor.* Chemical Engineering Journal, 2000. **76**(3): p. 239-245.
232. Agarwal, A.K. and M.L. Brisk, *Sequential experimental design for precise parameter estimation. 1. Use of reparameterization.* Industrial & Engineering Chemistry Process Design and Development, 1985. **24**(1): p. 203-207.
233. Buzzi-Ferraris, G. and F. Manenti, *Kinetic models analysis.* Chemical Engineering Science, 2009. **64**(5): p. 1061-1074.
234. Box, M., *The occurrence of replications in optimal designs of experiments to estimate parameters in non-linear models.* Journal of the Royal Statistical Society. Series B (Methodological), 1968. **30**(2): p. 290-302.
235. Atkinson, A.C. and W.G. Hunter, *The design of experiments for parameter estimation.* Technometrics, 1968. **10**(2): p. 271-289.
236. Devore, J.L., *Probability and Statistics for Engineering and the Sciences*. 2011: Cengage learning.
237. Pereira, C.S.M., et al., *Thermodynamic equilibrium and reaction kinetics for the esterification of lactic acid with ethanol catalyzed by acid ion-exchange resin.* Industrial & Engineering Chemistry Research, 2008. **47**(5): p. 1453-1463.
238. Lee, M.-J., P.-L. Chou, and H.-M. Lin, *Kinetics of synthesis and hydrolysis of ethyl benzoate over Amberlyst 39.* Industrial & Engineering Chemistry Research, 2005. **44**(4): p. 725-732.
239. Kun, K.A. and R. Kunin. *The pore structure of macroreticular ion exchange resins*. in *Journal of Polymer Science Part C: Polymer Symposia*. 1967. Wiley Online Library.
240. Kunin, R., et al., *Characterization of Amberlyst 15.* Industrial & Engineering Chemistry Product Research and Development, 1962. **1**(2): p. 140-144.
241. Pöpken, T., L. Götze, and J. Gmehling, *Reaction kinetics and chemical equilibrium of homogeneously and heterogeneously catalyzed acetic acid esterification with methanol and methyl acetate hydrolysis.* Industrial & Engineering Chemistry Research, 2000. **39**(7): p. 2601-2611.
242. Antony, J., *Design of Experiments for Engineers and Scientists*. 2 ed. 2014, Amsterdam: Elsevier Science.
243. Söderström, T. and P. Stoica, *System Identification*. 1988: Prentice-Hall, Inc.
244. Guillaume, J.H., et al., *Introductory overview of identifiability analysis: A guide to evaluating whether you have the right type of data for your modeling purpose.* Environmental Modelling & Software, 2019.

245. Sheldon, R.A., *Green and sustainable manufacture of chemicals from biomass: state of the art.* Green Chemistry, 2014. **16**(3): p. 950-963.
246. Moreau, C., M.N. Belgacem, and A. Gandini, *Recent catalytic advances in the chemistry of substituted furans from carbohydrates and in the ensuing polymers.* Topics in Catalysis, 2004. **27**(1-4): p. 11-30.
247. Bozell, J.J. and G.R. Petersen, *Technology development for the production of biobased products from biorefinery carbohydrates—the US Department of Energy's "Top 10" revisited.* Green Chemistry, 2010. **12**(4): p. 539-554.
248. Casanova, O., S. Iborra, and A. Corma, *Biomass into chemicals: aerobic oxidation of 5-hydroxymethyl-2-furfural into 2, 5-furandicarboxylic acid with gold nanoparticle catalysts.* ChemSusChem: Chemistry & Sustainability Energy & Materials, 2009. **2**(12): p. 1138-1144.
249. Sousa, A.F., et al., *Biobased polyesters and other polymers from 2, 5-furandicarboxylic acid: a tribute to furan excellency.* Polymer Chemistry, 2015. **6**(33): p. 5961-5983.
250. Albonetti, S., et al., *Selective oxidation of 5-hydroxymethyl-2-furfural over TiO_2-supported gold–copper catalysts prepared from preformed nanoparticles: Effect of Au/Cu ratio.* Catalysis Today, 2012. **195**(1): p. 120-126.
251. Pasini, T., et al., *Selective oxidation of 5-hydroxymethyl-2-furfural using supported gold–copper nanoparticles.* Green chemistry, 2011. **13**(8): p. 2091-2099.
252. Davis, S.E., et al., *Oxidation of 5-hydroxymethylfurfural over supported Pt, Pd and Au catalysts.* Catalysis Today, 2011. **160**(1): p. 55-60.
253. Davis, S.E., B.N. Zope, and R.J. Davis, *On the mechanism of selective oxidation of 5-hydroxymethylfurfural to 2, 5-furandicarboxylic acid over supported Pt and Au catalysts.* Green chemistry, 2012. **14**(1): p. 143-147.
254. Rass, H.A., N. Essayem, and M. Besson, *Selective aqueous phase oxidation of 5-hydroxymethylfurfural to 2, 5-furandicarboxylic acid over Pt/C catalysts: influence of the base and effect of bismuth promotion.* Green Chemistry, 2013. **15**(8): p. 2240-2251.
255. Vuyyuru, K.R. and P. Strasser, *Oxidation of biomass derived 5-hydroxymethylfurfural using heterogeneous and electrochemical catalysis.* Catalysis Today, 2012. **195**(1): p. 144-154.
256. Davis, S.E., et al., *Kinetics and mechanism of 5-hydroxymethylfurfural oxidation and their implications for catalyst development.* Journal of Molecular Catalysis A: Chemical, 2014. **388**: p. 123-132.
257. Siankevich, S., et al., *A novel platinum nanocatalyst for the oxidation of 5-Hydroxymethylfurfural into 2, 5-Furandicarboxylic acid under mild conditions.* Journal of Catalysis, 2014. **315**: p. 67-74.
258. Moulijn, J.A., M. Makkee, and R.J. Berger, *Catalyst testing in multiphase micro-packed-bed reactors; criterion for radial mass transport.* Catalysis Today, 2016. **259, Part 2**: p. 354-359.
259. Kilpiö, T., et al., *Design and modeling of laboratory scale three-phase fixed bed reactors.* Physical Sciences Reviews, 2016. **1**(3).
260. Russo, V., et al., *Dynamic non-isothermal trickle bed reactor with both internal diffusion and heat conduction: Sugar hydrogenation as a case study.* Chemical Engineering Research and Design, 2015. **102**: p. 171-185.
261. Kilpiö, T., et al., *Modeling of a Three-Phase Continuously Operating Isothermal Packed-Bed Reactor: Kinetics, Mass-Transfer, and Dispersion Effects in the Hydrogenation of Citral.* Industrial & Engineering Chemistry Research, 2012. **51**(26): p. 8858-8866.
262. Kilpiö, T., et al., *Modeling of Direct Synthesis of Hydrogen Peroxide in a Packed-Bed Reactor.* Industrial & Engineering Chemistry Research, 2012. **51**(41): p. 13366-13378.
263. Nijhuis, T., F. Dautzenberg, and J. Moulijn, *Modeling of monolithic and trickle-bed reactors for the hydrogenation of styrene.* Chemical Engineering Science, 2003. **58**(7): p. 1113-1124.

264. Tadepalli, S., R. Halder, and A. Lawal, *Catalytic hydrogenation of o-nitroanisole in a microreactor: Reactor performance and kinetic studies.* Chemical Engineering Science, 2007. **62**(10): p. 2663-2678.
265. Voloshin, Y., J. Manganaro, and A. Lawal, *Kinetics and mechanism of decomposition of hydrogen peroxide over Pd/SiO_2 catalyst.* Industrial & Engineering Chemistry Research, 2008. **47**(21): p. 8119-8125.
266. Voloshin, Y., R. Halder, and A. Lawal, *Kinetics of hydrogen peroxide synthesis by direct combination of H_2 and O_2 in a microreactor.* Catalysis Today, 2007. **125**(1-2): p. 40-47.
267. Tadepalli, S., D. Qian, and A. Lawal, *Comparison of performance of microreactor and semi-batch reactor for catalytic hydrogenation of o-nitroanisole.* Catalysis Today, 2007. **125**(1–2): p. 64-73.
268. Bellos, G.D. and N.G. Papayannakos, *The use of a three phase microreactor to investigate HDS kinetics.* Catalysis Today, 2003. **79-80**: p. 349-355.
269. van Herk, D., et al., *Scaling down trickle bed reactors.* Catalysis Today, 2005. **106**(1–4): p. 227-232.
270. Tromans, D., *Temperature and pressure dependent solubility of oxygen in water: a thermodynamic analysis.* Hydrometallurgy, 1998. **48**(3): p. 327-342.
271. Smith, F.L. and A.H. Harvey, *Avoid common pitfalls when using Henry's law.* Chemical Engineering Progress, 2007. **103**(9): p. 33-39.
272. Fogler, H.S., *Elements of Chemical Reaction Engineering, 5th edn.* 2016: Boston : Prentice Hall.
273. Cussler, E.L., *Diffusion: Mass Transfer in Fluid Systems*. 2009, New York: Cambridge University Press.
274. Dimitratos, N., et al., *Solvent-free oxidation of benzyl alcohol using Au–Pd catalysts prepared by sol immobilisation.* Physical Chemistry Chemical Physics, 2009. **11**(25): p. 5142-5153.
275. Dortmund_Data_Bank. *Density of Ethanol*. 2019; Available from: http://www.ddbst.com/en/EED/PCP/DEN_C11.php.
276. Dortmund_Data_Bank. *Dynamic Viscosity of Ethanol*. 2018; Available from: http://www.ddbst.com/en/EED/PCP/VIS_C11.php.
277. Dortmund_Data_Bank. *Liquid Dynamic Viscosity-Calculation by Vogel Equation*. 2019; Available from: http://ddbonline.ddbst.de/VogelCalculation/VogelCalculationCGI.exe.
278. Levenspiel, O., *Chemical Reaction Engineering, 3rd edn.* 1999, New York: Wiley.
279. Sinnott, R.K., *CHAPTER 12 - Heat-transfer Equipment*, in *Coulson and Richardson's Chemical Engineering, 2nd edn.*, R.K. Sinnott, Editor. 1993, Pergamon: Amsterdam. p. 565-702.
280. Domalski, E.S. and E.D. Hearing, *Condensed Phase Heat Capacity Data*, in *NIST Chemistry WebBook, NIST Standard Reference Database Number 69*, P.J. Linstrom and W.G. Mallard, Editors. 2018, National Institute of Standards and Technology: Gaithersburg MD, 20899.
281. Serth, R.W. and T. Lestina, *Process Heat Transfer : Principles and Applications, 2nd edn.* Process Heat Transfer - Principles Applications and Rules of Thumb, ed. T. Lestina. 2014, Oxford: Academic Press.
282. Theodore, L., *Heat Transfer Applications for the Practicing Engineer*. 2011, Hoboken, NJ: John Wiley & Sons.
283. EngineeringToolBox. *Thermal Conductivites for Some Common Liquids*. 2018; Available from: https://www.engineeringtoolbox.com/thermal-conductivity-liquids-d_1260.html.
284. Cheng, N.-S., *Formula for the viscosity of a glycerol–water mixture.* Industrial & Engineering Chemistry Research, 2008. **47**(9): p. 3285-3288.
285. Righetti, M., G. Salvetti, and E. Tombari, *Heat capacity of glycerol from 298 to 383 K.* Thermochimica acta, 1998. **316**(2): p. 193-195.

286. Bergman, T.L., et al., *Fundamentals of Heat and Mass Transfer*. 2011, Hoboken, NJ: John Wiley & Sons.
287. Tang, D., et al., *Axial Dispersion and Wall Effects in Narrow Fixed Bed Reactors: A Comparative Study Based on RTD and NMR Measurements.* Chemical Engineering & Technology, 2004. **27**(8): p. 866-873.
288. Sie, S. and R. Krishna, *Process development and scale up: III. Scale-up and scale-down of trickle bed processes.* Reviews in Chemical Engineering, 1998. **14**(3): p. 203-252.
289. Kallinikos, L.E. and N.G. Papayannakos, *Fluid dynamic characteristics of a structured bed spiral mini-reactor.* Chemical Engineering Science, 2007. **62**(21): p. 5979-5988.
290. Kallinikos, L.E. and N.G. Papayannakos, *Operation of a miniscale string bed reactor in spiral form at hydrotreatment conditions.* Industrial & Engineering Chemistry Research, 2007. **46**(17): p. 5531-5535.
291. Gierman, H., *Design of laboratory hydrotreating reactors: scaling down of trickle-flow reactors.* Applied Catalysis, 1988. **43**(2): p. 277-286.
292. Heibel, A.K., et al., *Liquid residence time distribution in the film flow monolith reactor.* AIChE journal, 2005. **51**(1): p. 122-133.
293. Cantu-Perez, A., S. Barrass, and A. Gavriilidis, *Residence time distributions in microchannels: Comparison between channels with herringbone structures and a rectangular channel.* Chemical Engineering Journal, 2010. **160**(3): p. 834-844.
294. Bošković, D. and S. Loebbecke, *Modelling of the residence time distribution in micromixers.* Chemical Engineering Journal, 2008. **135, Supplement 1**: p. S138-S146.
295. Hipolito, A., et al., *Single pellet string reactor for intensification of catalyst testing in gas/liquid/solid configuration.* Oil & Gas Science and Technology–Revue d'IFP Energies nouvelles, 2010. **65**(5): p. 689-701.
296. Gruber, R. and T. Melin, *Mixed convection in the copper dissolution technique of studying mass transfer.* International Journal of Heat and Mass Transfer, 2003. **46**(13): p. 2403-2413.
297. Wakao, N. and T. Funazkri, *Effect of fluid dispersion coefficients on particle-to-fluid mass transfer coefficients in packed beds: correlation of Sherwood numbers.* Chemical Engineering Science, 1978. **33**(10): p. 1375-1384.
298. Sederman, A., P. Alexander, and L. Gladden, *Structure of packed beds probed by magnetic resonance imaging.* Powder Technology, 2001. **117**(3): p. 255-269.
299. Liu, W.-T. and C.-S. Tan, *Liquid-phase esterification of propionic acid with n-butanol.* Industrial & Engineering Chemistry Research, 2001. **40**(15): p. 3281-3286.
300. Zhang, Y., L. Ma, and J. Yang, *Kinetics of esterification of lactic acid with ethanol catalyzed by cation-exchange resins.* Reactive and Functional Polymers, 2004. **61**(1): p. 101-114.
301. Delgado, P., M.T. Sanz, and S. Beltrán, *Kinetic study for esterification of lactic acid with ethanol and hydrolysis of ethyl lactate using an ion-exchange resin catalyst.* Chemical Engineering Journal, 2007. **126**(2-3): p. 111-118.

Appendix A: Catalyst Preparation Methods

All of the metal nanoparticle supported catalysts used in this thesis were synthesised by the research group of Prof Graham Hutchings in Cardiff University.

A.1 Catalysts used in Multistep Flow Synthesis, Chapters 3 & 4

Three nanoparticle supported catalysts were used in the multistep flow synthesis chapters, 1 wt% 65:35 (weight ratio) Au:Pd/TiO_2, 1 wt% Pd/TiO_2 and 1 wt% Pt/TiO_2. The 1 wt% 65:35 Au:Pd/TiO_2 catalyst was prepared by a modified impregnation method, where a round bottom flask was charged with $HAuCl_4$ (0.53 mL, 12.25 mgAu/mL), $PdCl_2$ dissolved in 0.58 M HCl (0.97 mL, 6 mgPd/mL) and water (13.5 mL) following a method described in previously published work [220]. The monometallic 1 wt% Pd/TiO_2 and 1 wt% Pt/TiO_2 catalysts were prepared by impregnation, where the metal salt $PdCl_2$ or $PtCl_2$ was dissolved in a small amount of water, to which TiO_2 was added. The slurry was stirred and heated until a paste was formed, then dried (110 °C, 16 h) and later calcined at 400 °C for 3 h. For all the supported nanoparticle catalysts used, the TiO_2 support was P25 TiO_2 (Evonik).

In addition to nanoparticle supported catalysts, for the aldol condensation reaction TiO_2 on its own without any nanoparticles was used as a catalyst. For this reaction two different types of TiO_2 were used. Initially a 21 nm particle size nanopowder (Sigma Aldrich, 99.5% pure, 75% anatase and 25% rutile) was used. However, after studying the coupling reaction in isolation it was found that pure anatase TiO_2 was more active and subsequently for all multistep flow experiments a 31 nm nanopowder anatase TiO_2 was used (Alfa Aesar).

All of the catalysts used in this study were obtained from Cardiff in powder form and were then pelletised with 4,000 N force using a pellet press, ground and sieved to give the appropriate particle size range, ranging from 63-120 µm. Typically the proportion of catalyst attaining the desired sieve fraction was 10-20%. BET studies showed only a small reduction in surface area, from 58.7 m^2/g to 53.65 m^2/g after pelletisation.

A.2 Catalysts used in HMF Oxidation, Chapter 8

The Au/TiO_2 catalysts used for HMF oxidation were prepared by the sol immobilisation technique reported in the literature [274]. This method involved adding a 1 wt. % solution of PVA to aqueous $HAuCl_4$ solution under vigorous stirring before adding freshly prepared $NaBH_4$ and then immobilising on the TiO_2 support followed by washing and drying overnight at 120 ^oC.

Appendix B: Calibrations

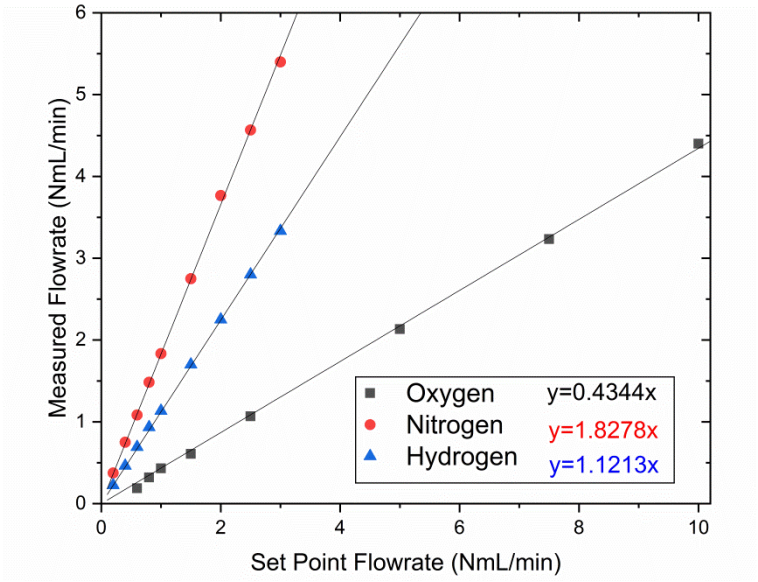

Figure B-1 Calibration of the Brooks Instrument gas mass flow controller.

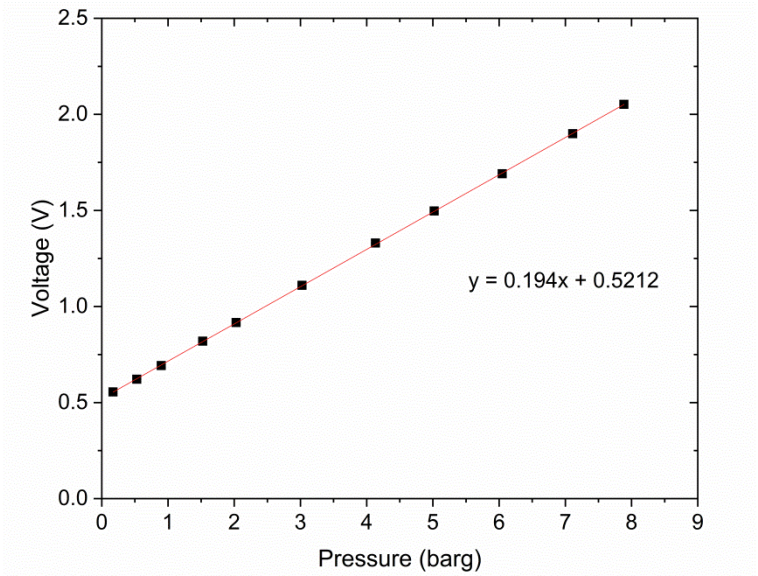

Figure B-2 Calibration of the Zaiput Hastelloy, 300 psi, liquid pressure sensor

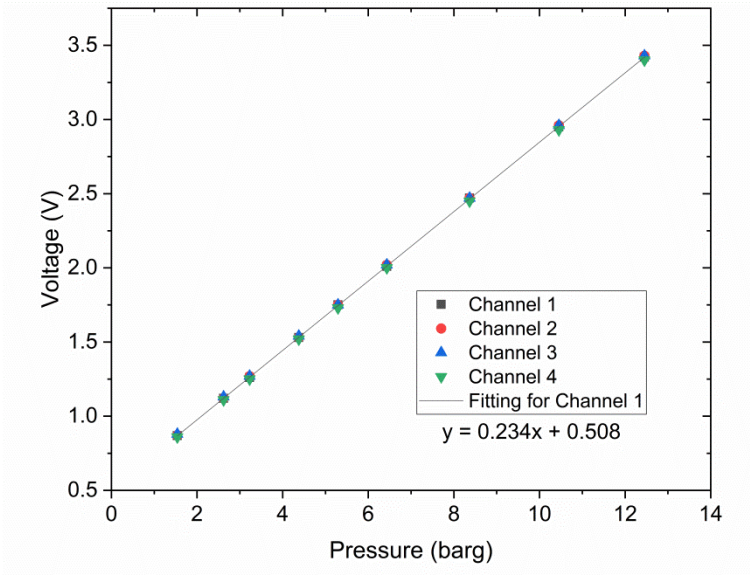

Figure B-3 Calibration of the Honeywell 40PC, 250 psig gas pressure sensors

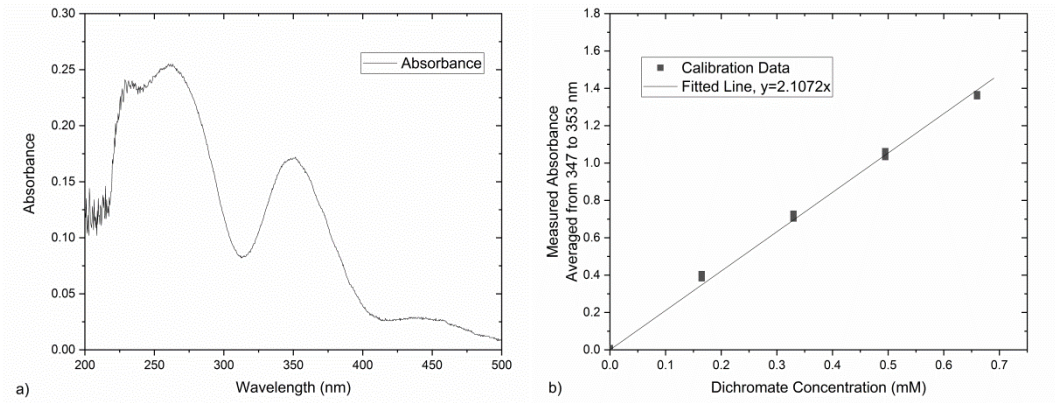

Figure B-4 Calibration of the UV-vis spectrometer for measuring dichromate concentration, used in external mass transfer experiments.

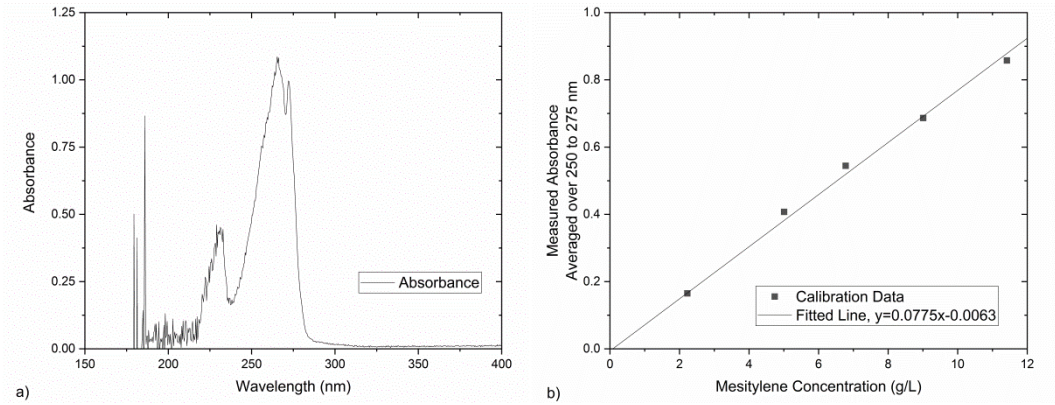

Figure B-5 Calibration of the UV-vis spectrometer for measuring mesitylene concentration, used in RTD experiments for the string reactor.

The calibration of the GC using mesitylene as an internal standard is shown below in Figure B-6. The response factors for each species obtained from these calibrations can then be used to calculate the concentration of each species according to Eq (B-1).

$$C_i = \frac{A_i}{A_{mesitylene}} * C_{mesitylene} * RF_i \quad \text{(B-1)}$$

Where C_i is the unknown concentration of species i to be measured, $C_{mesitylene}$ is the known concentration of internal standard mesitylene that is present in the sample, RF_i is the response factor of species i obtained from the calibration graphs, A_i is the peak area of species i obtained from the GC and $A_{mesitylene}$ is the peak area of mesitylene obtained from the GC.

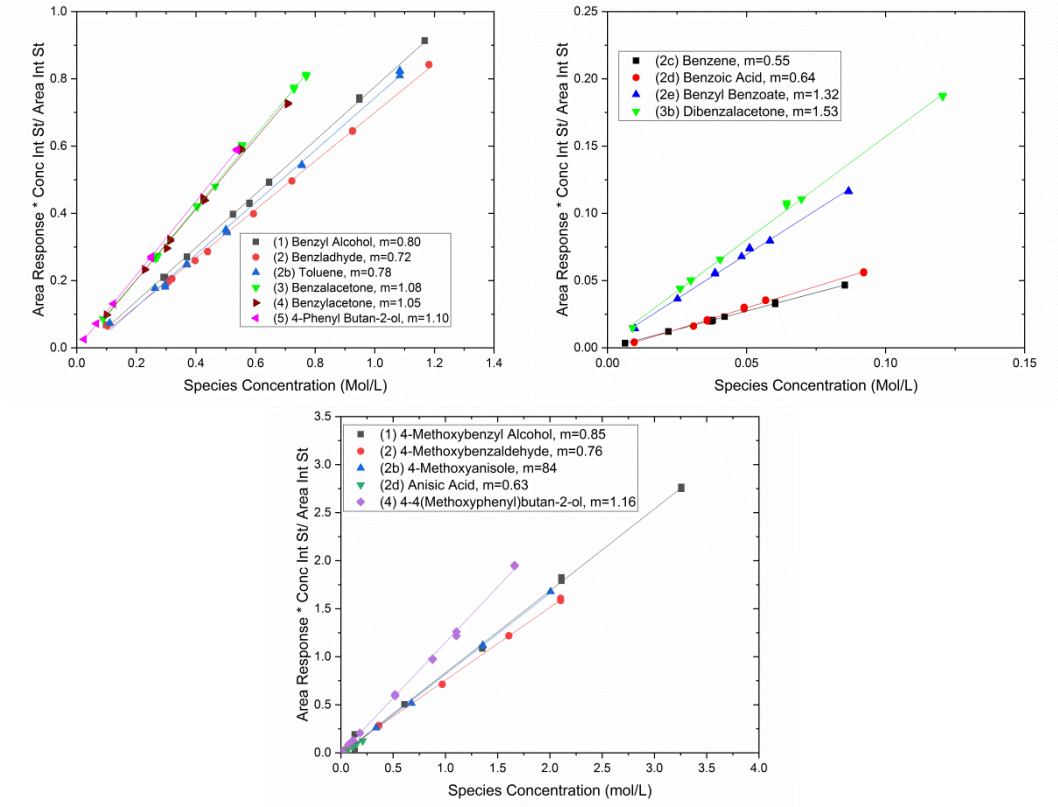

Figure B-6 Calibration of the GC for the benzyl alcohol and 4-methoxy benzyl alcohol systems. The y-axis is the ratio of the peak area of species i compared to the peak area of the internal standard (mesitylene) multiplied by the known concentration of internal standard.

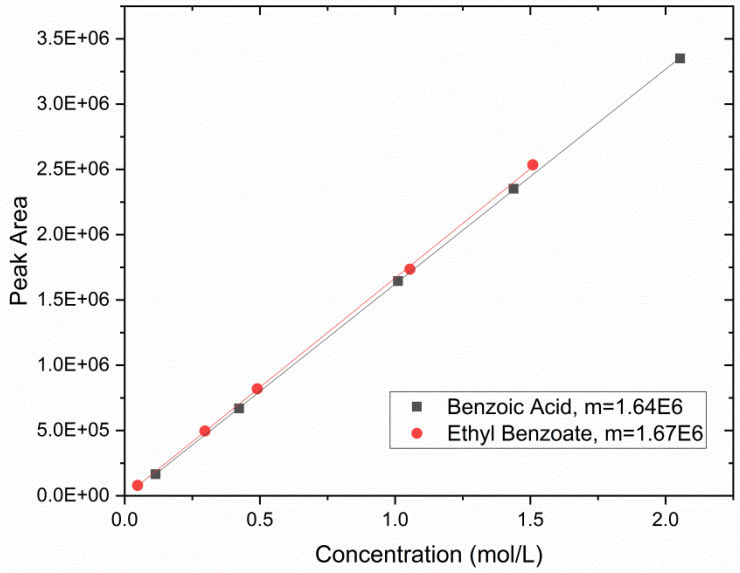

Figure B-7 Calibration of the HPLC for benzoic acid and ethyl benzoate with a dilution factor of 250 with UV detection at 274 nm.

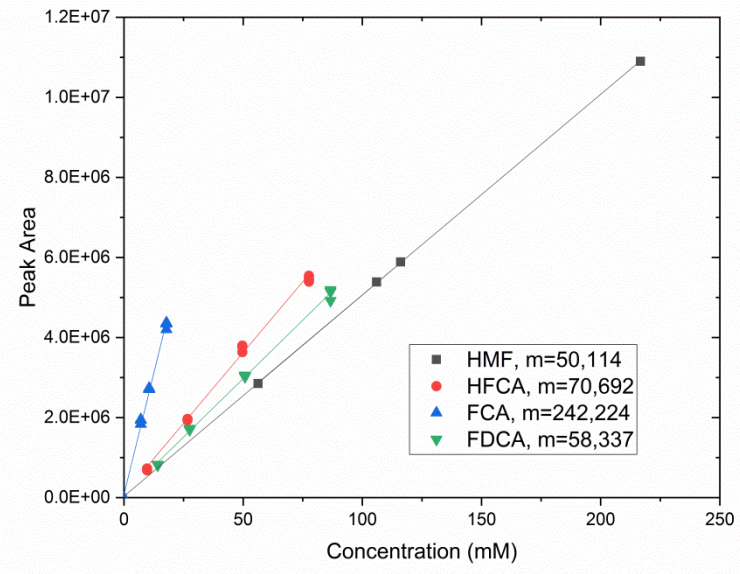

Figure B-8 Calibration of the HPLC for HMF, HFCA, FCA and FDCA with a dilution factor of 20 with UV detection at 210 nm.

Appendix C: Multistep Reactions in Isolation (SI from Ch 3)

C.1 Deactivation Correction Procedure

When studying the coupling and reduction reactions in isolation, it was observed that both reactions underwent considerable deactivation. In order to be able to use as much of the data collected as possible, a linear deactivation procedure was applied. The linear deactivation equations are shown in Eq (C-1) and Eq (C-2), where *r* is the reaction rate (mol/g/s), a_{cat} is catalyst activity, k_d is the deactivation constant (h^{-1}) and *t* is time (h) on stream. In order to estimate the deactivation constant, each day would start and end with the same experimental condition, this is shown in Figure C-1 for a representative example of benzylacetone (**3**) reduction. Then only using the data from the start and end of the day which were conducted at the same experimental conditions, the deactivation constant is found by fitting a straight line, as shown in Figure C-1 b. The corrected rate of reaction or outlet concentration can then be found using Eq (C-3) and Eq (C-4). It is known that this deactivation correction procedure is an over simplified approximation, as it assumes that the rate of deactivation is independent of process conditions, location in the bed and time on stream. However, this approximation is considered a suitable compromise for the purposes of this study, as studying the mechanism and extent of deactivation was not the objective of this work, and it would be a very difficult task.

$$r_{Observed} = a_{cat}\, r_{True} \tag{C-1}$$

$$a_{cat} = 1 - k_d\, t \tag{C-2}$$

$$r_{True} = \frac{r_{Observed}}{1 - k_d\, t} \tag{C-3}$$

$$C_{True} = \frac{C_{Observed}}{1 - k_d\, t} \tag{C-4}$$

C.2 Nanoparticle supported catalysts for aldol condensation reaction

Note that in the experiments where AuPd and Pd/TiO_2 were used for the coupling reaction instead of just the TiO_2 that is normally used, it was confirmed in a separate experiment that the presence of the nanoparticles does not impact the results of the reaction, as shown in Figure C-2.

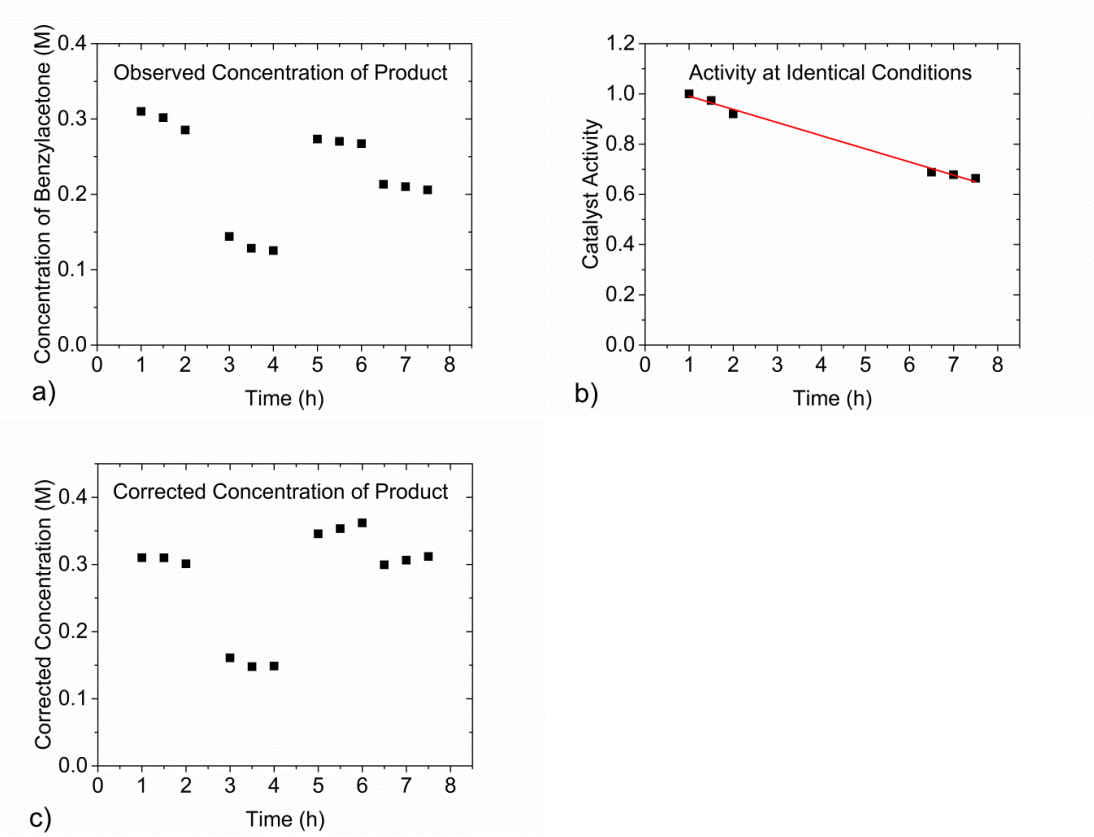

Figure C-1 Deactivation correction procedure.

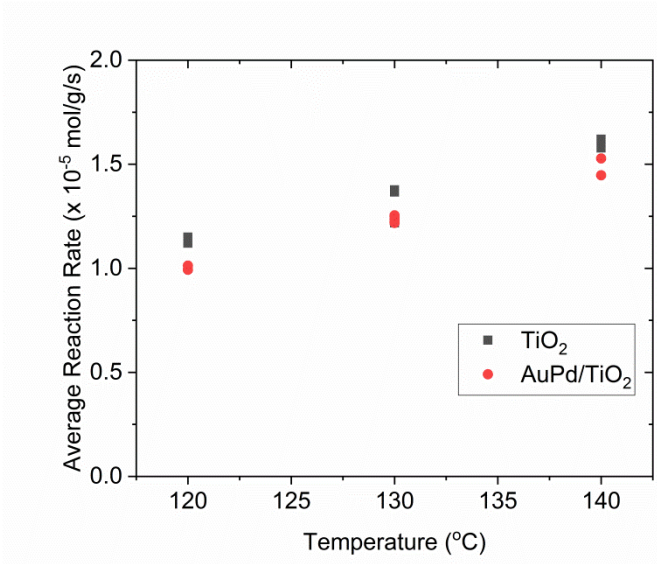

Figure C-2 Average reaction rate (mol/g/s) against temperature for 7.7 mg of TiO_2 catalyst with 1.05 M benzaldehyde (**2**) feed and 8.5 mg of $AuPd/TiO_2$ catalyst with 1.14 M benzaldehyde (**2**) feed. Both experiments are conducted at 10 µL/min with a catalyst particle size of 63-75 µm.

Appendix D: Tube Reactor Characterisation & LabVIEW Automation (SI from Ch 5)

D.1 Reactor Characterisation: Plug Flow Assumption

In order to use the tube reactor for kinetic experiments, it was first necessary to study the reactor behaviour and choose an appropriate reactor model to describe the system. This involved studying the reactor hydrodynamics and heat transfer properties. When assessing the flow and heat transfer characteristics of this reactor, the values of the various physical properties, such as density and viscosity, were approximated as the values of pure ethanol. This approximation was reasonable as the feed solution consisted of approximately 70-75% ethanol and only 15-20% benzoic acid and 10% water by mass. Therefore neglecting the presence of water and benzoic acid is not expected to significantly affect the results of this analysis. The viscosity, μ, and density, ρ, of pure ethanol at a range of temperatures was taken from the Dortmund Data Bank [275, 276] and are shown below in Figure D-1 a and b.

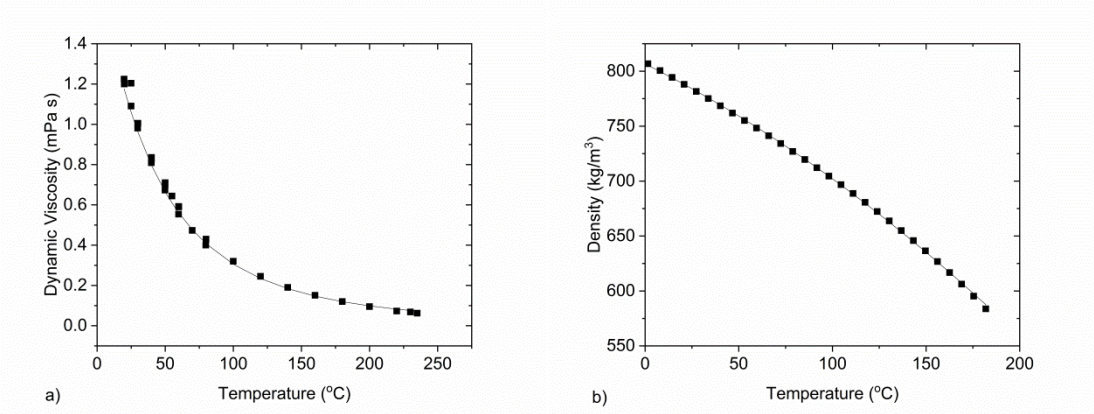

Figure D-1 Dynamic viscosity and density of ethanol as a function of temperature, taken from the Dortmund Data Bank.

An analytical expression for the viscosity (mPa·s) of ethanol was obtained using the Vogel equation, Eq (D-1), with the parameters from the Dortmund Data Bank [277] and temperature, T, in Kelvin. A polynomial expression was fitted to the experimental density values obtained from the Dortmund Data Bank, Eq (D-2), where temperature is in Kelvin and density is in kg/m^3.

$$\mu = \exp\left(-7.3714 + \frac{2770}{74.6787 + T}\right) \quad \text{(D-1)}$$

$$\rho = -0.0019413\,T^2 + 0.20877\,T + 894.471 \quad \text{(D-2)}$$

The molecular diffusivity of benzoic acid in the reaction solution (approximated as pure ethanol), D_m, was calculated using the Wilke-Chang empirical correlation, Eq (D-3) which calculates diffusivity in cm^2/s [273].

$$D_m = \frac{7.4 * 10^{-8}(\varphi M_2)^{0.5} T}{\mu_2 V_1^{0.6}} \quad \text{(D-3)}$$

Here, subscripts 1 and 2 are for the solute and solvent respectively, φ is the association parameter of the solvent, which is 1.5 for alcohols, M is the molecular weight (g/mol), μ is the viscosity (centipoises), V is the molar volume (ml/mol) and T is the temperature (K). For benzoic acid in ethanol the molecular weight of the solvent is 46.07 g/mol, the molar volume of benzoic acid is 92.5 mL/mol and the density and viscosity exhibit a temperature dependence described above. Using these values, the molecular diffusion coefficient of benzoic acid in ethanol as a function of temperature was calculated and shown in Figure D-2.

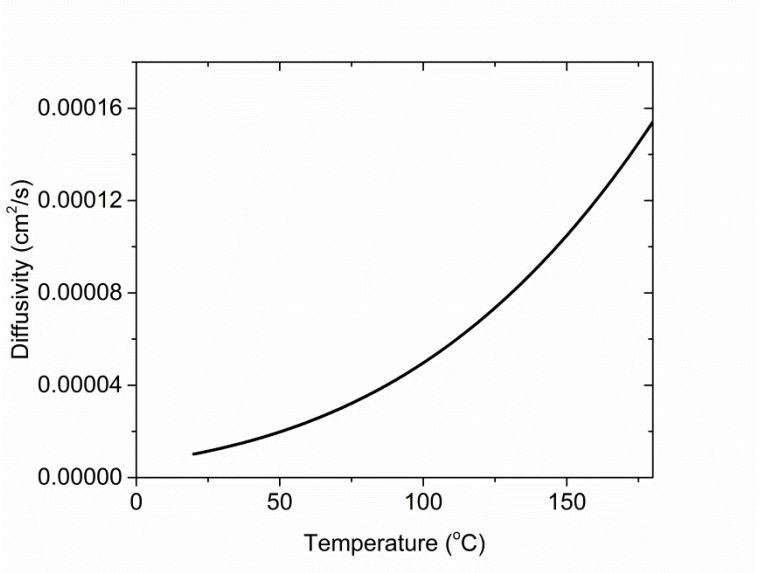

Figure D-2 Molecular diffusion coefficient of benzoic acid in ethanol, calculated using the Wilke-Chang equation.

The reactor was designed with a small internal diameter of 250 µm and a long length of 2 m to try and ensure that the reactor behaved as closely to a plug flow reactor as possible, as this simplifies the analysis of the results. The plug flow assumption was verified by computing the vessel dispersion number N_L at the upper and lower flowrate limits (5-100 µL/min), and checking that the values were below 0.01, which is the commonly used criterion for plug flow behaviour [278]. The vessel dispersion number is the inverse of the Pecklet number, Pe_L, and is shown in Eq (D-4).

$$N_L = \frac{1}{Pe_L} = \frac{D_{ax}}{uL} \quad \text{(D-4)}$$

where D_{ax} is the axial dispersion coefficient (m^2/s), u is the average velocity (m/s) and L is the length (m). The axial dispersion coefficient D_{ax}, was calculated using the Aris expression, Eq (D-5), where d_t is the tube diameter (m) and D_m is the molecular diffusion coefficient (m^2/s).

$$D_{ax} = D_m + \frac{u^2 d_t^2}{192\, D_m} \tag{D-5}$$

The validity of plug flow was assessed at 100 °C, where the values of density, viscosity and molecular diffusion coefficient are 702 kg/m^3, 0.3054 mPa·s and $4.97*10^{-5}$ cm^2/s. The validity of the axial dispersion model and the Aris expression were confirmed by examining the reactor operating point on a map given by Levenspiel [278]. The vessel dispersion number was then calculated to range from $5.7*10^{-5}$ to 0.001 for flowrates of 5 to 100 µL/min. These vessel dispersion numbers were significantly lower than the criterion for small deviation from plug flow of 0.01, hence verifying that the reactor exhibited plug flow behaviour.

D.2 Reactor Characterisation: Heating Assumption

In this work the reactor volume was defined as the volume of tubing submerged in the oil bath. This is based on the assumption that the reaction fluid changes from room temperature to reaction temperature and vice versa, instantaneously at the point where the reactor tubing enters and leaves the oil bath. This assumption is validated first for heating to reaction temperature, and then for cooling to quench temperature with the following heat transfer calculations, which are adopted from the heat exchanger literature [279].

The rate of heat flow needed, Q (J/s), to increase the reaction fluid temperature from room temperature, T_{room} (K), to the oil bath temperature, T_{bath} (K), is given by [279]

$$Q = \dot{m} C_{p\,EtOH} (T_{bath} - T_{room}) \tag{D-6}$$

where $C_{p\,EtOH}$ ($J\,kg^{-1}\,K^{-1}$) is the specific heat capacity of ethanol (assumed to be 2440 $J\,kg^{-1}\,K^{-1}$[280]) and $\dot{m}$ (kg/s) is the mass flowrate of reaction fluid (assumed to be pure ethanol). The worst case scenario was heating ethanol from 25 °C to 140 °C. The fastest flowrate used in steady state experiments was 20 µL/min and the fastest flowrate used in transient experiments (in chapter 6) was 100 µL/min. For these two scenarios the heat flow required, calculated from Eq (D-6), was 0.07 and 0.38 W.

The heat exchange area, *A* (m^2), required to achieve this temperature difference is calculated using

$$Q = UA\Delta T_{LM} \tag{D-7}$$

where U is the overall heat transfer coefficient (W m^{-2} K^{-1}) and ΔT_{LM} is the log mean temperature difference (K) [279, 281]. It is not possible to use the oil bath temperature as the outlet temperature, since this required an infinite heat transfer area, hence a value 0.1 ^{o}C lower was used. The log mean temperature difference was calculated to be 16.3 ^{o}C using Eq (D-8).

$$\Delta T_{LM} = \frac{(T_{bath} - T_{in}) - (T_{bath} - T_{out})}{ln\left(\frac{T_{bath} - T_{in}}{T_{bath} - T_{out}}\right)} \quad \text{(D-8)}$$

U is found from the sum of the three heat resistances, convection within the reactor, conduction through the tube and convection outside the tube [279, 281].

$$\frac{1}{U} = \frac{1}{h_i} + \frac{d_i}{2\lambda_t} ln\left(\frac{d_o}{d_i}\right) + \frac{d_i}{d_o h_o} \quad \text{(D-9)}$$

where h_i is the heat transfer coefficient (W m^{-2} K^{-1}) inside the tube, d_i and d_o are the inner and outer diameters of the reactor tube, which had values of 0.00025 m and 0.00158 m respectively, λ_t is the thermal conductivity of the PEEK reactor tubing (0.25 W m^{-1} K^{-1}) and h_o is the heat transfer coefficient (W m^{-2} K^{-1}) on the outside of the tube. The inner heat transfer coefficient was found from the Nusselt number calculated using the empirical correlation for laminar flow in tubes shown in Eq (D-11) [279, 281]

$$Nu = \frac{h_i d_i}{\lambda_{EtOH}} \quad \text{(D-10)}$$

$$Nu = 1.86\left(RePr\frac{d_i}{L}\right)^{1/3} \quad \text{(D-11)}$$

where Pr is the Prandtl number and L is the tubing length. In this work, a very low Nusselt number of less than 1 was calculated. However, if a Nusselt number of less than 3.5 is calculated, then a value of 3.5 should be used [281, 282]. From the Nusselt number the internal heat transfer coefficient of 2400 W m^{-2} K^{-1} was calculated from Eq (D-10), where λ_{EtOH} is the thermal conductivity of ethanol (0.171 W m^{-1} K^{-1}) [283].

The outer heat transfer coefficient, h_o, for the tube in the glycerol filled agitated oil bath was estimated from empirical correlations. The correlation for a six-bladed impeller in a fully baffled vessel was used, as shown in Eq (D-12). While the small oil bath used in this work is not a fully baffled vessel with a six-blade impeller, only order of magnitude accuracy was needed for these calculations.

$$\frac{h_o d_o}{\lambda_{EtOH}} = 0.17\left(\frac{\rho N d_{imp}^2}{\mu}\right)^{0.67}\left(\frac{C_{p\,EtOH}\mu}{\lambda_{EtOH}}\right)^{0.37}\left(\frac{d_o}{d_v}\right)^{0.5} \quad \text{(D-12)}$$

In Eq (D-12), N is the number of rotations per second (which was 10 from the hot plate stirrer set point), d_{imp} is the diameter of the impeller (0.03 m) and d_v is the diameter of the vessel (0.1 m). The physical properties of glycerol were taken from the literature

[284, 285]. At 140 °C glycerol has a density of 1187 kg/m^3, a viscosity of 0.0051 Pa·s, a specific heat capacity of 270 J kg^{-1} K^{-1} and a thermal conductivity of 0.285 W m^{-1} K^{-1}. Using these values, the outer heat transfer coefficient was estimated to be 1678 W m^{-2} K^{-1}.

Combining the values for the conductivity of the reactor wall λ_t with the internal and external heat transfer coefficients (2400 and 1678 W m^{-2} K^{-1}), the overall heat transfer coefficient was 690 W m^{-2} K^{-1}. Using Eq (D-7) the area and hence length of tubing required for heating was calculated, for the fastest flowrate used in steady state experiments of 20 µL/min; only 0.8 cm of tubing was required, which can be considered negligible compared to the 2 m reactor length. For the fastest flowrate used in transient experiments the length of tubing required was 4 cm. This larger value is still considered negligible, as it is only 2% of the reactor length.

The length of tubing required to cool the reaction fluid was calculated in the same way, except an external heat transfer coefficient of 10 W m^{-2} K^{-1} was chosen, as a typical value for natural convection in air around a tube [286]. This gave an overall U value of 59 W m^{-2} K^{-1}, showing that cooling was slower. However, the objective here was not to cool back down to room temperature, but to quench the reaction. Since the reaction is effectively quenched at 60 °C it was only necessary to cool to this value. The log mean temperature difference was then calculated to be 67 °C and the required cooling length for the fastest steady state experiment of 20 µL/min flowrate was only 1.6 cm, which could be considered negligible. For the fastest transient experiment of 100 µL/min flowrate the required cooling length was 8 cm, which corresponds to 4% of the reactor length. This was small enough to be neglected.

These calculations indicate that it was reasonable to assume the reactor heats up and cools down instantly upon entering and leaving the oil bath, especially for the steady state experiments and hence the reactor volume could be calculated as the tube volume submerged in the oil bath.

D.3 Automation using LabVIEW, Python and Excel

The LabVIEW code developed in this work allowed the user to run a list of pre-selected experimental conditions, or to run a campaign of steady-state experiments, which were designed online by MBDoE algorithms written and executed in Python. In both cases the LabVIEW code ran an experimental condition for a duration of time specified by the user to ensure the reactor reached steady-state. When the specified time limit was reached, the LabVIEW code read the most recent HPLC measurement and took this value as the steady-state outlet concentration for that experimental condition. These

experimental conditions and outlet concentrations were then written in a “Record” Excel file with all the previous experimental results. LabVIEW then called Python to perform parameter estimation using the “Record” Excel file as the Python function input. The computed parameter statistics were then displayed on the LabVIEW screen and were also written to the “Record” Excel file. The LabVIEW code measured and recorded the temperatures, flowrates and pressures every 5 s and saved the values in a separate “Process Value” Excel file, allowing the user to examine the experimental conditions at some later date. Additionally, the LabVIEW code had safety shut down features, where if any temperature or pressure exceeded a user specified value the pumps and heater were automatically turned off. All LabVIEW code consists of a “block diagram” where the code is written, and a “front panel” user interface. The front panel for this LabVIEW code is shown in Figure D-3.

LabVIEW is a graphical programming language where programmes are not written as lines of code but instead are drawn as flowsheets with logic and loop structures. A simplified version of the LabVIEW block diagram used for the steady-state experiments is shown in Figure D-4 illustrating how online MBDoE was implemented. The central component of the LabVIEW code is a *while* loop, which contains a *timed* loop and also a *case structure*. In LabVIEW a *timed* loop repeats a given set of commands at a given frequency until a time limit is reached, in this case the frequency is every 5 s and the time limit is the experimental duration, which is specified by the user. A *case structure* is the LabVIEW equivalent of an “if, else-if, else” logic structure, and this is used in Figure D-4 to allow different commands to be given for different experiments. To assist the reader understanding the LabVIEW code, the algorithm is also shown in Table D-1.

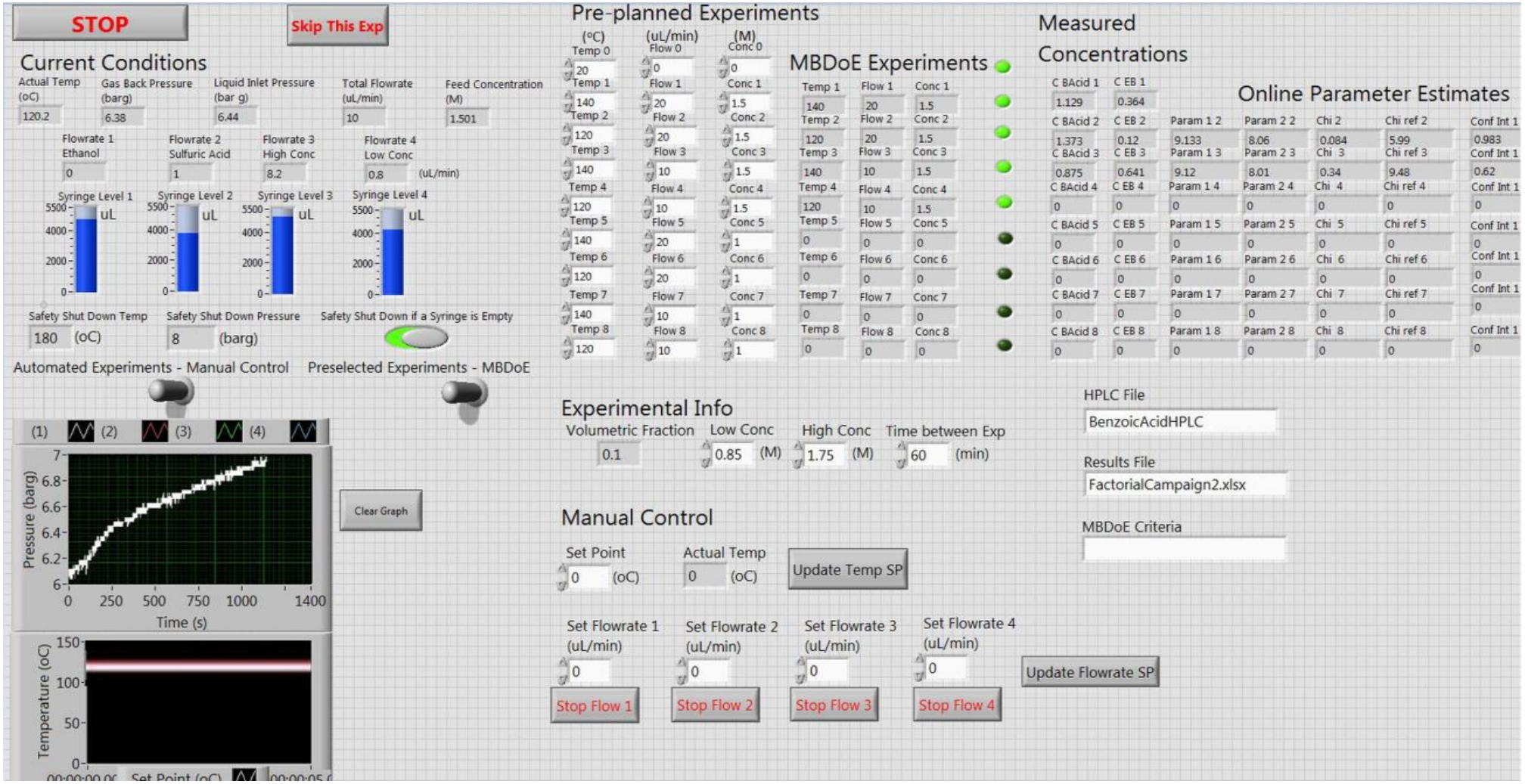

Figure D-3 LabVIEW user interface (front panel) for the steady-state experiments.

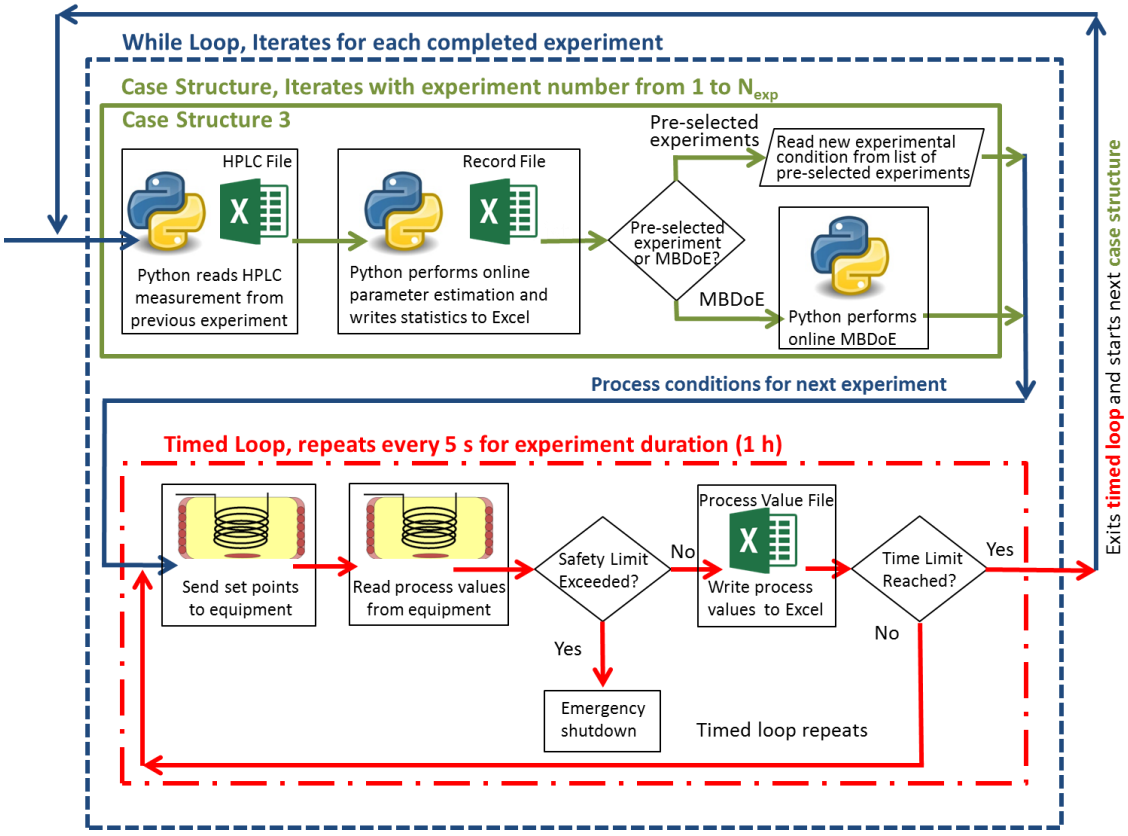

Figure D-4 Simplified LabVIEW block diagram showing the major flows of information and decision making.

Table D-1 The algorithm applied in the LabVIEW code for the automated steady-state campaigns.

Step	Activity	Task in flow chart
1	Read the 1st set point values from the user input fields and send these values to the relevant process equipment.	Case Structure 1 (not shown in Figure D-4 due to space limitations)
2	While waiting for the experiment duration, the following tasks are completed every 5 s: • Read the process values. • Compare process values to the safety shut down values (if values are exceeded the safety shut down procedure is triggered). • Record the process values in an Excel spreadsheet.	Timed Loop
3	When the experiment duration (specified by user) is reached, the 1st experiment ends and the following commands are carried out • Using Python read the most recent HPLC values from the HPLC Excel file and store these values along with their corresponding experimental conditions. • Read the 2nd set point values from the user input field and send these values to the relevant process equipment.	Case Structure 2 (not shown in Figure D-4 due to space limitations)
4	While waiting for the experiment duration, the following tasks are completed every 5 s: • Read the process values. • Compare process values to the safety shut-down values (if values are exceeded the safety shut-down procedure is triggered). • Record the process values in an Excel spreadsheet.	Timed Loop
5	When the experiment duration (specified by user) is reached, the 2nd experiment ends and the following commands are carried out • Using Python read the most recent HPLC values from the HPLC Excel file and store these values along with the corresponding experimental conditions. • Using Python perform parameter estimation using all previously collected data and record the estimate values and corresponding statistics on the screen and in an Excel file. • If "MBDoE" is selected, using Python perform MBDoE to calculate the experimental conditions for the next experimental conditions and send these values to the relevant process equipment. • If "Pre-selected Experiments" is selected, read the next set point values from the user input field and send these values to the relevant process equipment.	Case Structure 3-8 (case structures 3-8 were identical)
6	Steps 4 and 5 are repeated for the 4th to N_{exp}th experimental conditions	Timed Loop & Case Structures 3 to N_{exp}
7	When the N_{exp}th experiment ends, the following commands are carried out • Using Python read the most recent HPLC values from the HPLC Excel file and store these values along with the corresponding experimental conditions. • Using Python perform parameter estimation using all previously collected data and record the estimate values and corresponding statistics on the screen and in an Excel file. • Shut Down all equipment	Case Structure N_{exp}+1 (not shown in Figure D-4 due to space limitations)

Appendix E: Transient Experiments (SI from Ch 6)

E.1 Sensitivity of MBDoE to Parameter Estimates

In order to test the sensitivity of the transient MBDoE designs on the values of the initial guess for the kinetic parameters *KP1* and *KP2*, the MBDoE design procedure was repeated 5 times, once with the factorial parameter estimates that were actually used for the design of experiments in chapter 6, and then 4 more times with poor guesses for the parameter values, as shown in Figure E-1. As shown in Table E-1, the guesses for the parameter estimates resulted in a wide spread in activation energies and pre exponential factors when converted back to the original Arrhenius parameter values. The sensitivity of MBDoE to the initial guess is then tested with these parameter values for both **Ramp F** and **Ramp FT** experiments.

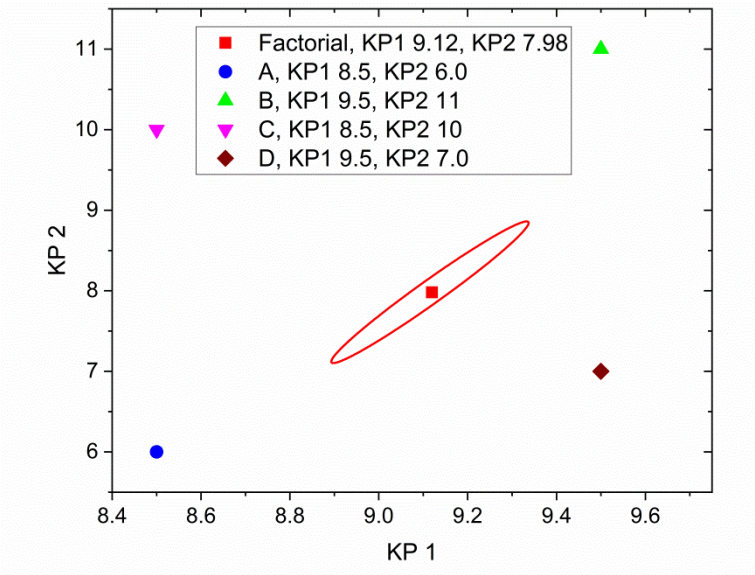

Figure E-1 Parameter guesses used to test the sensitivity of MBDoE to the initial parameter estimate.

Table E-1, the parameter estimates used for the MBDoE design of transient experiments to test the sensitivity of MBDoE to the initial parameter estimates for this case study.

	KP1	*KP2*	k_0 (s^{-1})	E_A (J/mol)	k at 100°C (*10^5 s^{-1})	k at 120°C (*10^5 s^{-1})	k at 140°C (*10^5 s^{-1})
Factorial Estimates	9.12	7.98	1.17E+07	79,800	0.78	2.88	9.40
A	8.5	6.0	3.95E+04	60,000	1.58	4.21	10.25
B	9.5	11	1.17E+11	110,000	0.47	2.84	14.50
C	8.5	10	1.32E+10	100,000	1.33	6.85	30.11
D	9.5	7.0	3.49E+05	70,000	0.56	1.75	4.94

As can be observed in Figure E-2 and Figure E-3, the design of the flowrate profile for **Ramp F** experiments is influenced by the value of the initial guess, however it can be observed that the flow profile for all MBDoE experiments are very similar regardless of the values of the parameter estimates. In all cases the MBDoE designed flowrate is very low, whereas the intuitively designed experiment has a very large flowrate varying from 100 to 1 µL/min. The value of the MBDoE designed feed concentration was always 1.55 M regardless of the initial parameter estimate. Additionally, the fixed temperature value designed by MBDoE was not very sensitive to the initial parameter guess, as all the temperature profiles designed for the second **Ramp F** experiment were almost identical, as shown in Figure E-3 b, and many of the temperature profiles for the first **Ramp F** experiment also were very similar, as show in Figure E-2 b.

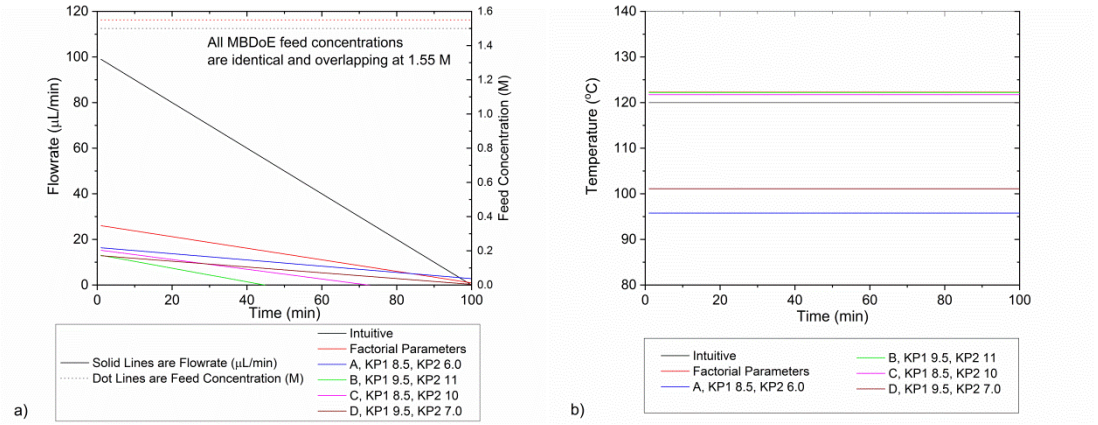

Figure E-2 Control variable profiles (a is flowrate and feed concentration, b is temperature) for the first **Ramp F** experiments when designed intuitively (black) and when designed by MBDoE using different values for the parameter estimates.

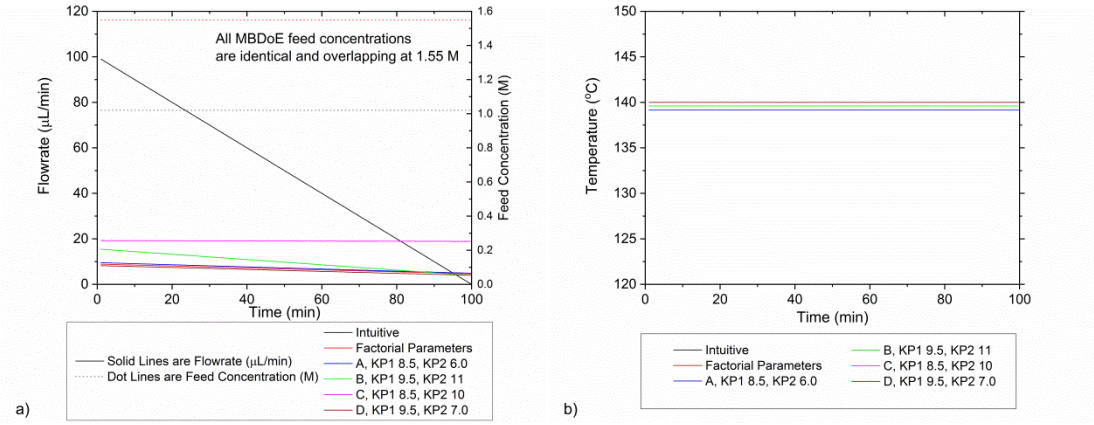

Figure E-3 Control variable profiles (a is flowrate and feed concentration, b is temperature) for the second **Ramp F** experiments when designed intuitively (black) and when designed by MBDoE using different values for the parameter estimates.

In order to quantify how good or bad these designs were, the expected covariance matrix of each of these experiments was then calculated using what is believed to be the correct parameter estimate values of *KP1* = 9.12 and *KP2* = 7.98. Therefore, this calculation shows how effective experiments are when they are designed using the wrong values of the parameter estimate (without having to physically conduct the experiments). The 95% confidence ellipsoids obtained from each of the MBDoE designs is then shown in Figure E-4, where it can be observed that in all cases the confidence ellipsoid of the MBDoE designs are similar in size and are always significantly smaller than the intuitively designed experiment. Therefore, this shows that for this case study that MBDoE is not particularly sensitive to the value of the initial parameter estimate.

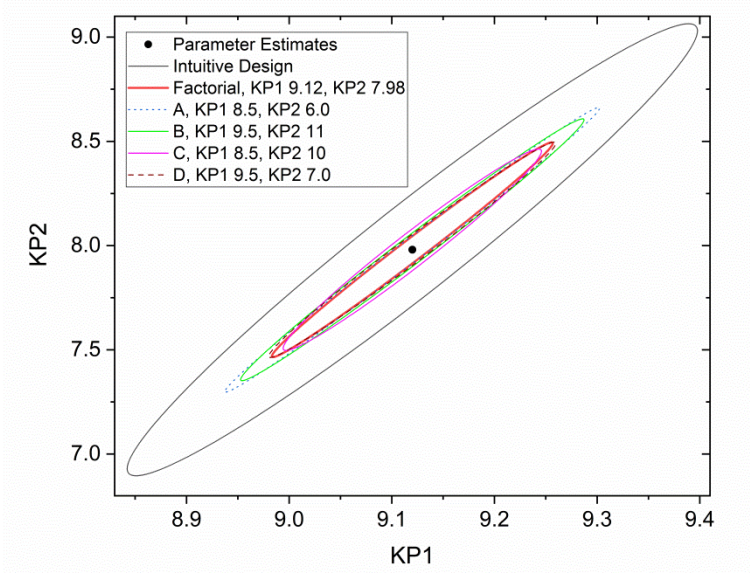

Figure E-4 95% Confidence ellipsoids comparing the statistical certainty of the kinetic parameters KP1 and KP2 for the **Ramp F** experiments designed intuitively (black) and designed by MBDoE with different values for the parameter estimates.

The same procedure is then repeated for the **Ramp FT** experiments. It can be shown in Figure E-5 that the design profile of MBDoE experiments is not very sensitive to the initial parameter estimates and that in all cases a very low flowrate profile is designed which is very different from the intuitively designed flowrate profile. The MBDoE temperature profiles were all quite similar regardless of the initial parameter estimate and the MBDoE feed concentration was always identical for all MBDoE designs.

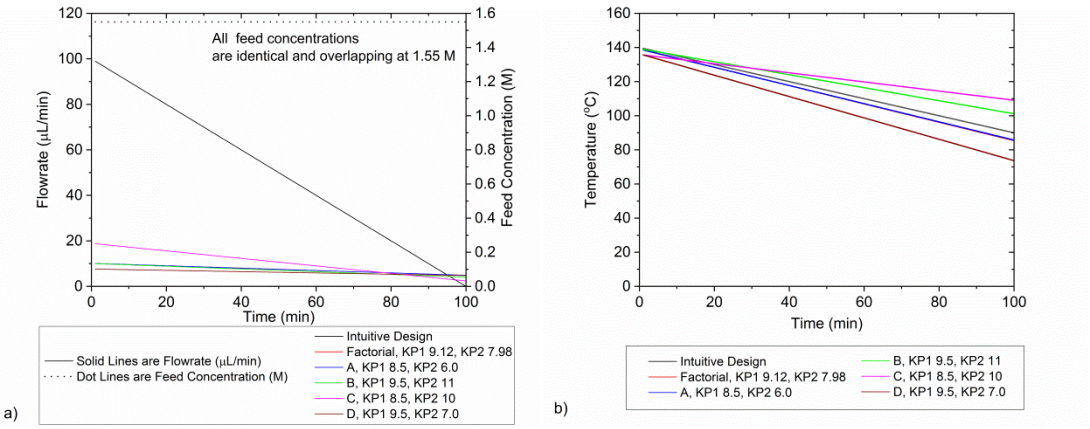

Figure E-5 The control variable profiles for the **Ramp FT** experiments when designed intuitively (black) and when designed by MBDoE using different values for the parameter estimates.

It was again shown that the MBDoE designs which were created using the wrong parameter values were still very good designs and were significantly superior than the intuitively designed experiment as shown by the confidence ellipsoids in Figure E-6. This demonstrates that for this case study that MBDoE is not very sensitive to the initial parameter guess, and therefore that MBDoE is a valuable technique even in the case of low certainty in the initial parameter guess.

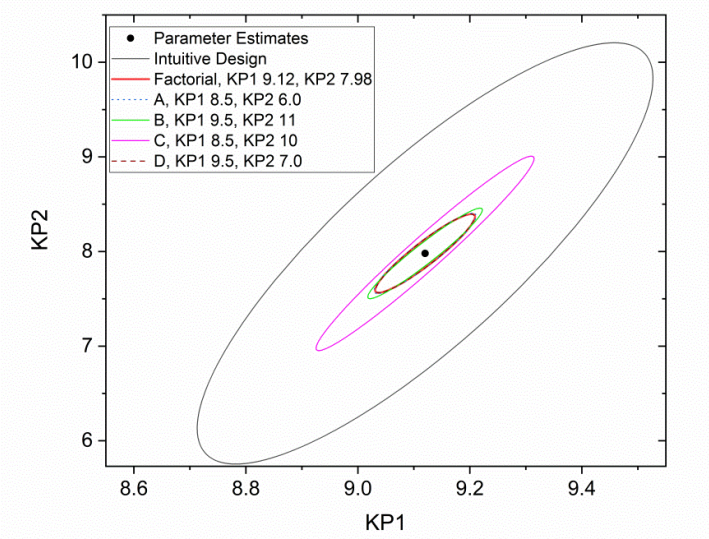

Figure E-6 95% Confidence ellipsoids comparing the statistical certainty of the kinetic parameters KP1 and KP2 for the **Ramp FT** experiments designed intuitively (black) and designed by MBDoE with different values for the parameter estimates.

E.2 Raw Data

Raw Data: Intuitively designed Ramp F 1

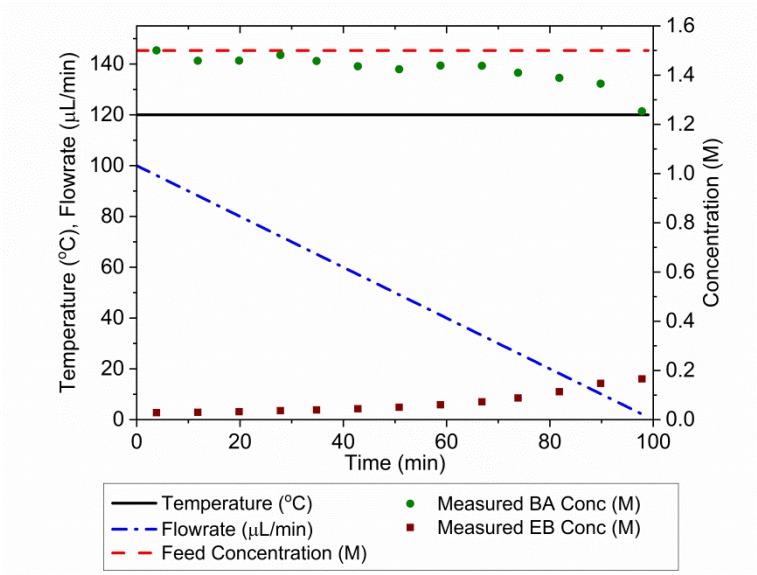

Figure E-7 Control variable profile and outlet concentrations of benzoic acid (BA) and ethyl benzoate (EB) for the first intuitively designed **Ramp F** experiment.

Table E-2 Experimental measurements for the first intuitively designed **Ramp F** experiment.

t_M Time the sample was measured	t_L Time the sample left the reactor	t_{In} Time the sample entered the reactor	τ Sample residence time	X Conversion	Outlet Concentration Benzoic Acid	Outlet Concentration Ethyl Benzoate
s	s	s	s	%	M	M
0	0	NA	NA	4.0	1.44	0.03
229	202	141	61	0.0	1.50	0.03
709	679	613	66	2.7	1.46	0.03
1189	1156	1084	72	2.7	1.46	0.03
1669	1632	1552	80	1.3	1.48	0.04
2089	2049	1960	88	2.7	1.46	0.04
2569	2523	2423	100	4.0	1.44	0.04
3049	2996	2880	115	5.3	1.42	0.05
3529	3465	3330	136	4.0	1.44	0.06
4009	3931	3766	164	4.0	1.44	0.07
4429	4331	4131	200	6.0	1.41	0.09
4909	4772	4512	260	7.3	1.39	0.11
5389	5168	4817	351	8.7	1.37	0.15
5869	5421	4979	442	16.7	1.25	0.17

Raw Data: Intuitively designed Ramp F 2

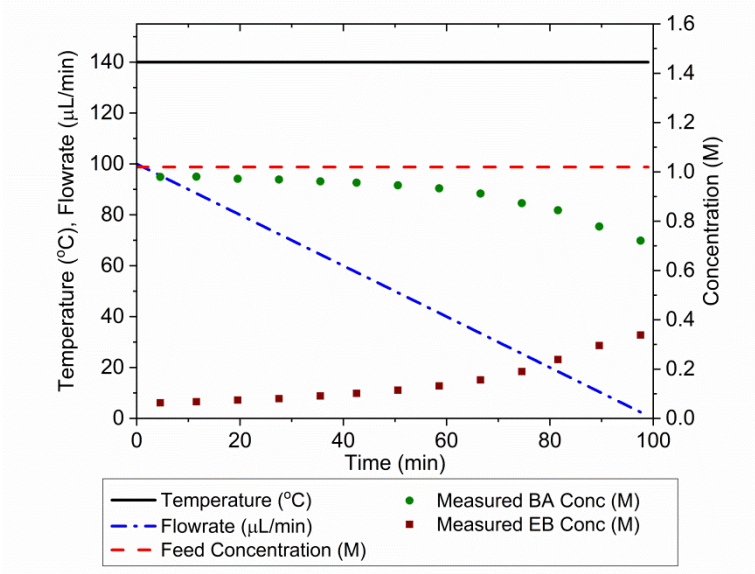

Figure E-8 Control variable profile and outlet concentrations of benzoic acid (BA) and ethyl benzoate (EB) for the second intuitively designed **Ramp F** experiment.

Table E-3 Experimental measurements for the second intuitively designed **Ramp F** experiment

t_M Time the sample was measured	t_L Time the sample left the reactor	t_{In} Time the sample entered the reactor	τ Sample residence time	X Conversion	Outlet Concentration Benzoic Acid	Outlet Concentration Ethyl Benzoate
s	s	s	s	%	M	M
273	245	184	61	3.9	0.98	0.06
693	663	597	66	3.9	0.98	0.07
1173	1140	1068	72	4.9	0.97	0.07
1653	1617	1537	80	4.9	0.97	0.08
2133	2092	2003	89	5.9	0.96	0.09
2553	2507	2407	100	5.9	0.96	0.10
3033	2980	2865	115	6.9	0.95	0.11
3513	3450	3315	135	8.8	0.93	0.13
3993	3915	3752	163	10.8	0.91	0.16
4473	4372	4168	204	14.7	0.87	0.19
4893	4758	4500	258	17.7	0.84	0.24
5373	5157	4809	348	23.5	0.78	0.30
5853	5417	4977	440	29.4	0.72	0.34

Raw Data: MBDoE designed Ramp F 1

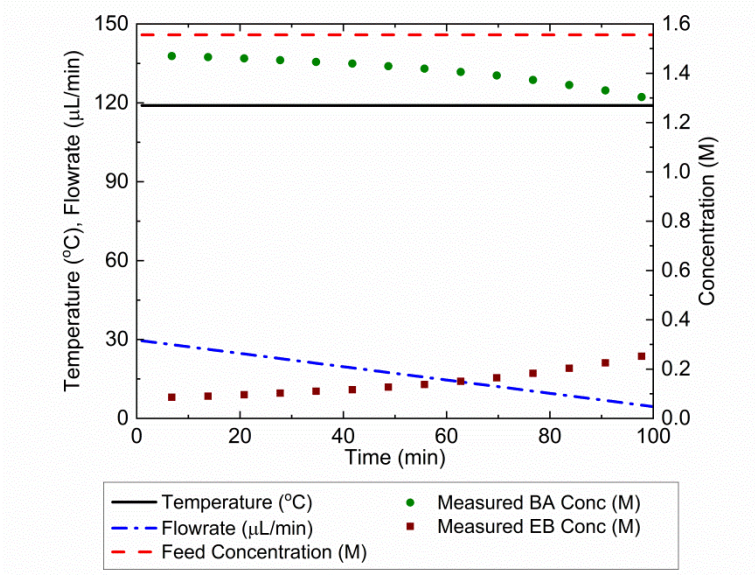

Figure E-9 Control variable profile and outlet concentrations of benzoic acid (BA) and ethyl benzoate (EB) for the first MBDoE designed **Ramp F** experiment.

Table E-4 Experimental measurements for the first MBDoE designed **Ramp F** experiment

t_M Time the sample was measured	t_L Time the sample left the reactor	t_{In} Time the sample entered the reactor	τ Sample residence time	X Conversion	Outlet Concentration Benzoic Acid	Outlet Concentration Ethyl Benzoate
s	s	s	s	%	M	M
408	314	110	204	5.8	1.47	0.09
828	728	511	217	5.8	1.47	0.09
1248	1141	910	231	6.4	1.46	0.10
1667	1552	1304	248	7.1	1.45	0.10
2084	1959	1693	267	7.1	1.45	0.11
2504	2368	2080	288	7.7	1.44	0.12
2923	2774	2460	314	8.3	1.43	0.13
3342	3177	2833	344	9.0	1.42	0.14
3763	3578	3198	380	9.6	1.41	0.15
4182	3972	3549	422	10.9	1.39	0.17
4603	4360	3885	474	12.2	1.37	0.18
5024	4736	4199	537	13.5	1.35	0.20
5444	5094	4481	613	14.7	1.33	0.23
5864	5422	4722	700	16.7	1.30	0.25

Raw Data: MBDoE designed Ramp F 2

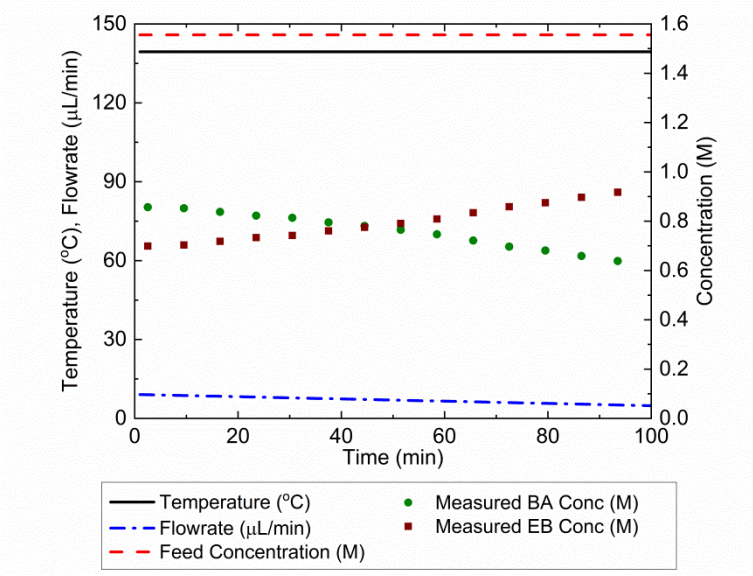

Figure E-10 Control variable profile and outlet concentrations of benzoic acid (BA) and ethyl benzoate (EB) for the second MBDoE designed **Ramp F** experiment.

Table E-5 Experimental measurements for the second MBDoE designed **Ramp F** experiment

t_M Time the sample was measured	t_L Time the sample left the reactor	t_{In} Time the sample entered the reactor	τ Sample residence time	X Conversion	Outlet Concentration Benzoic Acid	Outlet Concentration Ethyl Benzoate
s	s	s	s	%	M	M
152	NA	NA	NA	44.9	0.86	0.70
571	271	NA	NA	45.5	0.85	0.70
991	680	17	663	46.2	0.84	0.72
1411	1089	403	685	47.4	0.82	0.73
1830	1496	787	709	48.1	0.81	0.74
2251	1904	1170	734	48.7	0.80	0.76
2670	2309	1549	760	50.0	0.78	0.78
3090	2714	1925	789	51.3	0.76	0.79
3510	3117	2298	820	51.9	0.75	0.81
3931	3520	2668	852	53.8	0.72	0.83
4350	3920	3032	888	55.1	0.70	0.86
4770	4318	3393	925	56.4	0.68	0.87
5190	4715	3748	966	57.7	0.66	0.90
5610	5109	4098	1010	59.0	0.64	0.92

Raw Data: Intuitively designed Ramp FT

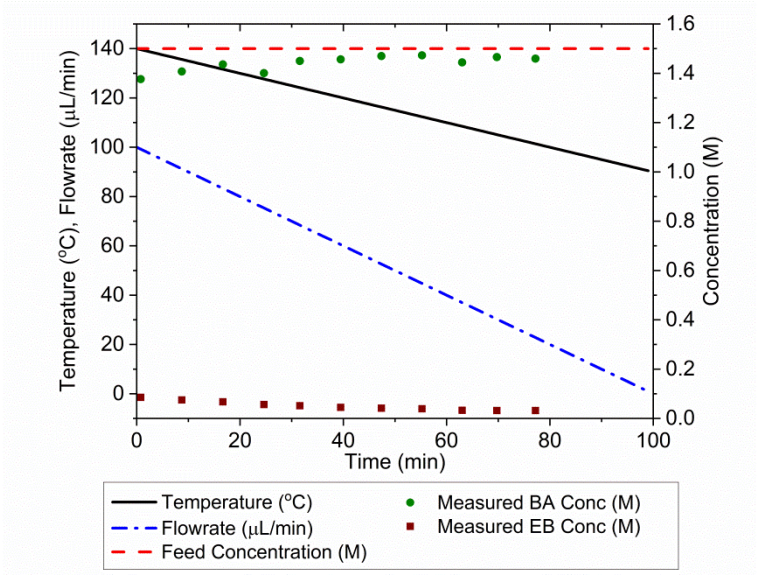

Figure E-11 Control variable profile and outlet concentrations of benzoic acid (BA) and ethyl benzoate (EB) for the intuitively designed **Ramp FT** experiment.

Table E-6 Experimental measurements for the intuitively designed **Ramp FT** experiment

t_M Time the sample was measured	t_L Time the sample left the reactor	t_{In} Time the sample entered the reactor	τ Sample residence time	T_{in} Reactor temperature at time t_{In}	T_L Reactor temperature at time t_L	X Conversion	Outlet Conc. Benzoic Acid	Outlet Conc. Ethyl Benzoate
s	s	s	s	°C	°C	%	M	M
73	46	NA	NA	140.0	139.6	8.0	1.38	0.09
553	524	460	64	136.2	135.6	6.0	1.41	0.07
1033	1001	931	70	132.2	131.7	4.0	1.44	0.07
1513	1478	1400	78	128.3	127.7	6.7	1.40	0.06
1933	1894	1809	85	124.9	124.2	3.3	1.45	0.05
2413	2369	2273	96	121.1	120.3	2.7	1.46	0.05
2893	2842	2732	110	117.2	116.3	2.0	1.47	0.04
3373	3313	3185	128	113.5	112.4	2.0	1.47	0.04
3853	3780	3626	154	109.8	108.5	4.0	1.44	0.03
4273	4183	3998	185	106.7	105.1	2.0	1.47	0.03
4753	4631	4394	238	103.4	101.4	2.7	1.46	0.03

Raw Data: MBDoE designed Ramp FT

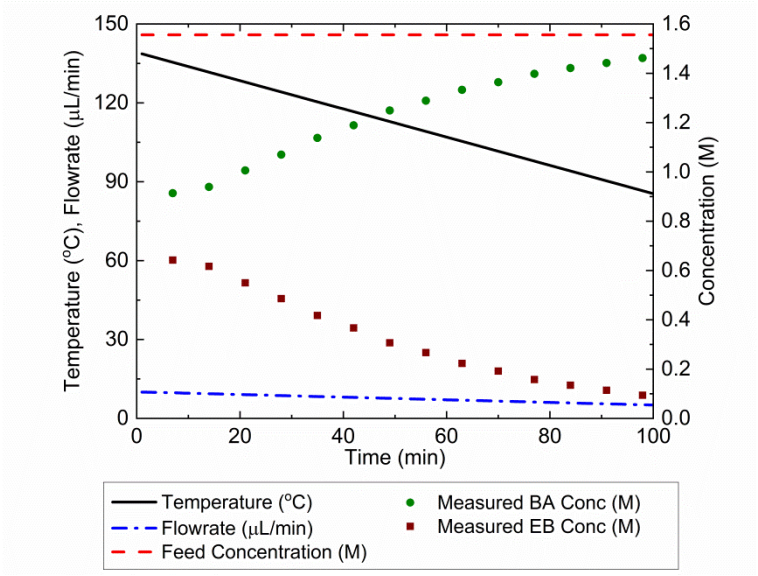

Figure E-12 Control variable profile and outlet concentrations of benzoic acid (BA) and ethyl benzoate (EB) for the MBDoE designed **Ramp FT** experiment.

Table E-7 Experimental measurements for the MBDoE designed **Ramp FT** experiment

t_M Time the sample was measured	t_L Time the sample left the reactor	t_{In} Time the sample entered the reactor	τ Sample residence time	T_{in} Reactor temperature at time t_{In}	T_L Reactor temperature at time t_L	X Conversion	Outlet Conc. Benzoic Acid	Outlet Conc. Ethyl Benzoate
s	s	s	s	°C	°C	%	M	M
419	150	NA	NA	139.2	137.9	41.5	0.91	0.64
840	561	NA	NA	139.2	134.2	39.6	0.94	0.62
1260	971	354	617	136.0	130.5	35.1	1.01	0.55
1679	1379	739	639	132.6	126.9	31.2	1.07	0.49
2099	1786	1123	663	129.1	123.2	26.7	1.14	0.42
2519	2193	1505	688	125.7	119.6	23.5	1.19	0.37
2939	2599	1883	716	122.3	115.9	19.7	1.25	0.31
3359	3003	2258	745	119.0	112.3	17.1	1.29	0.27
3779	3406	2629	777	115.7	108.7	14.5	1.33	0.22
4199	3807	2996	811	112.4	105.1	12.6	1.36	0.19
4619	4206	3358	848	109.1	101.6	10.0	1.4	0.16
5038	4602	3714	888	106.0	98.0	8.7	1.42	0.13
5457	4995	4064	931	102.8	94.5	7.5	1.44	0.11
5876	5386	4407	979	99.8	91.0	6.2	1.46	0.09

Appendix F: String Reactor Characterisation (SI from Ch7)

F.1 Catalyst Description and Motivation for String Reactor

Amberlyst-15 is a sulfonic acid, macroreticular polymeric resin based on crosslinked styrene divinylbenzene copolymers. The catalyst particles are spherical with particle diameters ranging from 0.35 mm to 1.18 mm and each catalyst sphere is composed of a porous network of agglomerates of randomly packed gel microspheres, which gives the catalyst a high surface area and porosity [239, 240]. The catalyst is commonly used industrially for esterification reactions due to its high porosity and stability. In this work it was originally intended to use the catalyst in a micropacked bed reactor by grinding and sieving the catalyst to a particle size of 50-75 µm. However, it was found that the mechanical properties of the catalyst were not suited to this. Instead it was decided to use the catalyst in its commercial form, as spheres. For packed bed reactors it is desirable to have the reactor diameter at least ten times greater than the particle diameter to minimise the wall effect (fluid bypass at the reactor walls where local reactor porosity is higher) [287, 288], however for the large Amberlyst-15 particle size, this would lead to a reactor diameter of at least 3.5 mm. This reactor would be too large for the microreactor platform that had already been developed, as it would require high flowrates that the 5 mL syringe pumps would not be able to provide without needing to be refilled at regular intervals. Therefore, instead of using a standard packed bed reactor, it was decided to use a bead string reactor, where the reactor internal diameter is only slightly larger than the catalyst particle. The bead string reactor consisted of a PTFE tubing (VICI Jour) with external diameter of 1.58 mm and internal diameter of 1 mm, into which Amberlyst-15 spheres obtained from the 710-850 µm dry sieve fraction was loaded, as shown in Figure F-1. As Amberlyst swells when in contact with solvents, this dry particle size range resulted in an average wet diameter of 825 µm as measured by a microscope (VHX-600 Digital Microscope, Keyence). A typical reactor was loaded with 0.1 g of Amberlyst-15 resulting in a catalyst bed length of 30 cm. In addition to requiring lower flowrates that were compatible with the current automated reactor set up, string reactor designs have been reported in the literature to offer a number of advantages including i) providing plug flow behaviour with negligible bypass or axial dispersion [289], ii) possessing efficient heat transfer due to the large surface area to volume ratio [289], iii) allowing the use of similar superficial velocities to those that are used in industrial scale reactors [46, 48, 289, 290] iv) increased reproducibility between reactors as packing is always uniform [46, 289] v) ease of scale-up through parallelisation [47] and vi) they use industrial sized catalyst pellets instead of smaller particles or powders, hence allowing the study of any catalyst pellet skin effects [291].

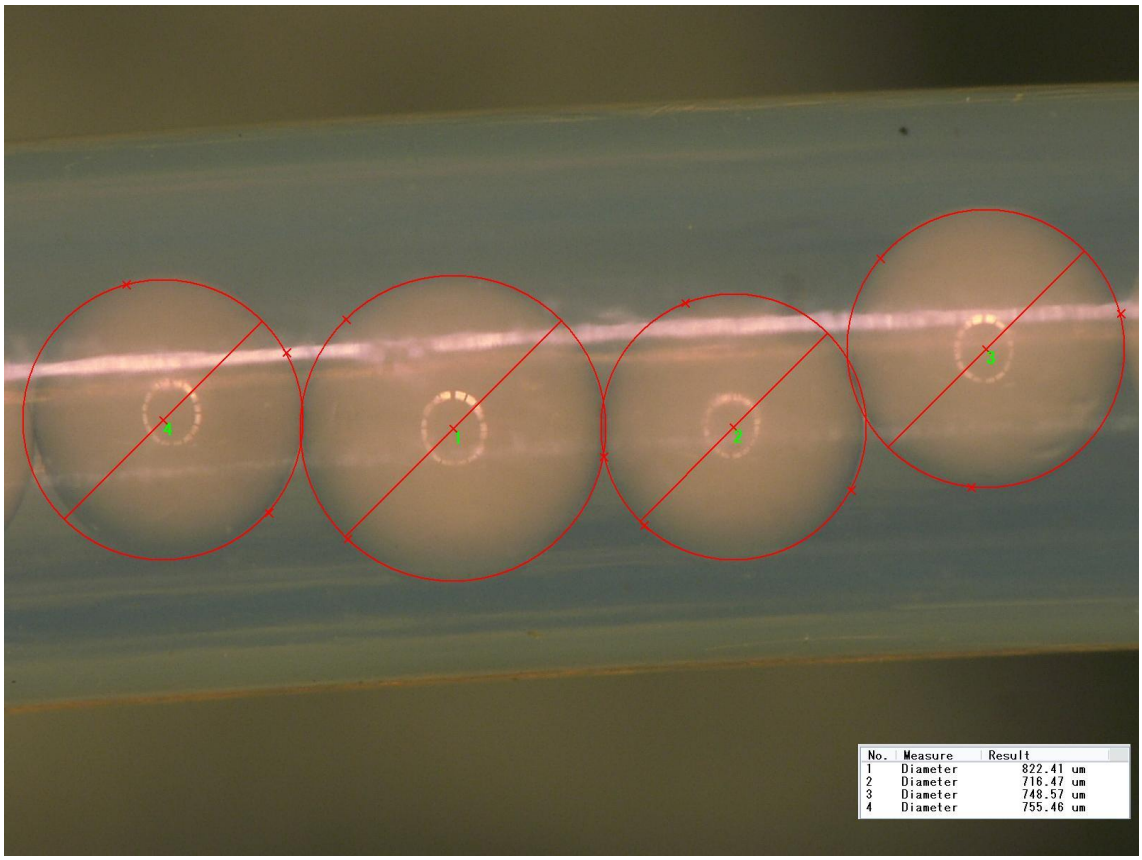

Figure F-1 Image of the string reactor loaded with dry Amberlyst-15 catalyst particles from the 710-850 µm sieve fraction.

F.2 Residence Time Distribution Study

F.2.1 Materials & Methods

An important aspect of the bead string reactor design was to ensure the reactor could be modelled as a plug flow reactor to allow easier data analysis. This was evaluated by conducting a RTD study at four different flowrates, (10, 20, 40 and 80 µL/min), representative of those used in kinetic experiments. A step tracer change was achieved using a four-way switching valve with two identical 5 mL glass syringes (Hamilton) mounted on the same syringe pump (PhD Ultra, Harvard) and the tracer was measured with a UV flow cell, as shown in Figure F-2.

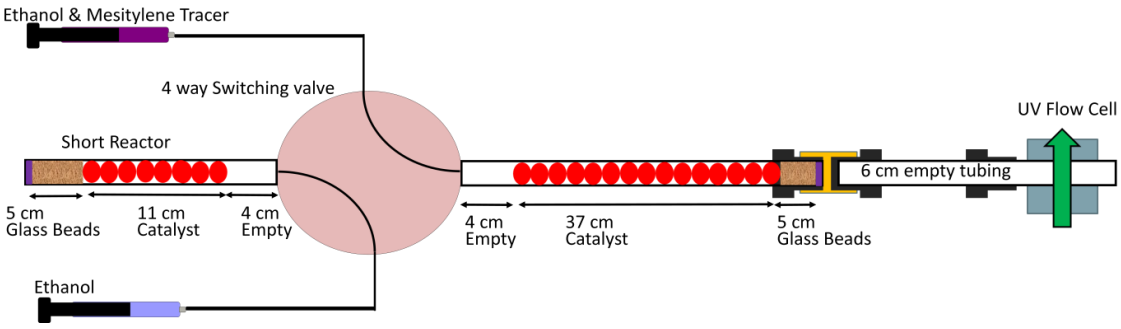

Figure F-2 Experimental set-up for the RTD study of a 1000 µm I.D. string reactor filled with Amberlyst-15 spheres from the 710-850 µm dry sieve fraction.

The tracer chosen for this RTD experiment was 12 g/L mesitylene in ethanol solvent, as mesitylene did not absorb on the Amberlyst-15 catalyst while more common UV tracers such as basic blue dye did, and hence could not be used. The mesitylene tracer showed a linear response at the wavelength range of 250-275 nm when measured with an Ocean Optics UV-vis-ES USB 2000+ spectrometer combined with an Ocean Optics DH-2000BAL light source with both deuterium and halogen bulbs. The calibration is shown in Appendix B.

It was not possible to directly study the RTD of the string reactor on its own, as there were a number of unavoidable additional components in the flow path between the four-way switching valve and the UV detection point. These included the small empty section before the start of the string reactor, the 5 cm section of glass beads at the reactor outlet and the UV flow cell which required 6 cm of empty tubing, as shown in Figure F-2. Therefore, in order to study the RTD of just the packed section of the string reactor without the contribution from these other elements, two RTD studies were performed with two separate string reactors; a long one and a short one, but crucially both reactors were identical in their additional components before and after the string reactor section [292]. Using deconvolution it was possible to obtain the RTD of only the packed section of the string reactor of length equal to the difference between the long and short lengths studied. The two string reactors were packed with 0.1479 and 0.0336 g of Amberlyst-15 catalyst from the dry sieve fraction 710-850 µm resulting in wet reactor lengths of 37 and 11 cm respectively, hence the deconvolution would give the RTD of a 26 cm long string reactor. During experiments the reactors were helically coiled with a diameter of 6 cm.

Mathematically the RTD function, E(t) is described in Eq (F-1). If the RTD experiment is conducted using the injection of a pulse of tracer, Eq (F-1) can be used directly.

$$E(t) = \frac{C(t)}{\int_0^\infty C(t)dt} \qquad \text{(F-1)}$$

However, in this work, a step change experiment was conducted so the RTD is instead obtained by smoothing, normalising and differentiating the raw absorbance data measured during each experiment.

Obtaining the RTD of the 26 cm string reactor by deconvolution is quite challenging, as deconvolution requires conversion from the time domain to the frequency domain which is highly sensitive to noise and requires significant signal filtering making [293]. Instead the RTD of the 26 cm string reactor was obtained by convolution of the experimentally measured RTD of the short reactor with an estimated RTD of the 26 cm string reactor, and fitting the resulting convoluted RTD to experimentally measured RTD of the long reactor. Fitting is achieved by changing the parameters of the model for the estimated RTD of the 26 cm string reactor [62, 292, 294]. This method requires a model for the expected RTD of the string reactor with one or more parameters. In our work, we assumed that the string reactor could be described by the axial dispersion model

$$\frac{\partial C}{\partial t} = D\frac{\partial^2 C}{\partial x^2} - u\frac{\partial C}{\partial x} \tag{F-2}$$

where D is the axial dispersion coefficient (m^2/s), C is tracer concentration (mol/L), u is superficial velocity (m/s), t is time as measured from the start of the step change (s) and x is axial position along the reactor (m). Depending on if there is a small or large deviation from plug flow, the axial dispersion model can be solved with open-open boundary conditions to give the RTD expressions shown in Eq (F-3) and Eq (F-4) respectively [272, 278].

$$E = \sqrt{\frac{u^3}{4\pi D L_{eq}}}\, exp\left(-\frac{\left(L_{eq} - ut\right)^2}{4DL_{eq}/u}\right) \tag{F-3}$$

$$E = \frac{u}{\sqrt{4\pi Dt}}\, exp\left(-\frac{\left(L_{eq} - ut\right)^2}{4Dt}\right) \tag{F-4}$$

As the axial dispersion model was originally derived for empty tubes, the model is adapted to include L_{eq} which is the equivalent length, described by Eq (F-5), accounting for the volume of the catalyst spheres in the tube, similar approaches have been reported in the literature [62].

$$L_{eq} = L(\Phi_{rxr}) + L(1 - \Phi_{rxr}) * \Phi_p \tag{F-5}$$

where L is the actual string reactor length (m), Φ_{rxr} is the reactor voidage (the fraction of reactor volume available for flow) and Φ_p is the porosity of the catalyst. It was assumed that the actual values of Φ_{rxr} and Φ_p were unknown and hence L_{eq} was treated as a parameter, so the RTD consisted of two parameters, D and L_{eq}. Using

either Eq (F-3) or Eq (F-4) to describe the unknown RTD of the string reactor, a convolution was performed [278] according to Eq (F-6), where the experimental data of outlet tracer concentration of the short string reactor (11 cm) were convoluted with the expression for the unknown RTD of a 26 cm string reactor section to obtain the experimental outlet tracer concentration of the long string reactor (37 cm).

$$C_{out}(t) = \int_0^t C_{in}(t')E(t-t')dt' \tag{F-6}$$

The parameters *D* and L_{eq} were fitted to minimise the difference between the experimental data obtained from the long reactor and the convoluted RTD. This is done by first smoothing and differentiating the raw data using Origin software, before performing the previously described method of convolution and fitting using the SLSQP (Sequential Least Squares Programming) algorithm on Python. This procedure was repeated for both the small and large deviation from plug flow models, shown in Eq (F-3) and Eq (F-4), to allow the identification of the most suitable model. The appropriateness of the model was assessed by visual inspection, comparing the resulting theoretical convoluted RTD of the long reactor with the corresponding experimental results.

F.2.2 Results & Discussion

The RTD experiments were analysed using both the small and large deviation from plug flow models and the resulting parameter estimates for *D* and L_{eq} for both models are shown in Table F-1 for all flowrates studied. While the two models gave almost identical parameter estimates, the large deviation model was more appropriate, as the resulting vessel dispersion number, *D/uL* was on average slightly greater than 0.01 which is commonly used as the criteria to decide between the two models [278]. The results for each flowrate studied are also shown in Figure F-3, where the experimentally measured RTD of the short and long string reactors, as well as the deconvoluted RTD of the 26 cm reactor section are shown. In order to demonstrate that the analysis method is satisfactory, in Figure F-3 the convolution of the short reactor RTD and the deconvoluted RTD of the 26 cm string reactor is also shown; and this convolution closely matches the experimental data from the long reactor experiments, hence validating the analysis procedure.

Table F-1 Parameter estimates for the deconvoluted RTD of a 26 cm string reactor assuming the small and large deviation from plug flow axial dispersion models.

	Small Deviation From Plug Flow			Large Deviation From Plug Flow		
Flowrate (µL/min)	**D (m^2/s)**	**L_{eq} (m)**	**D/uL = Pe^{-1} (-)**	**D (m^2/s)**	**L_{eq} (m)**	**D/uL = Pe^{-1} (-)**
10	$4.58 * 10^{-7}$	0.225	0.0096	$4.65 * 10^{-7}$	0.222	0.0099
20	$1.35 * 10^{-6}$	0.217	0.0147	$1.40 * 10^{-6}$	0.214	0.0154
40	$2.91 * 10^{-6}$	0.206	0.0166	$3.12 * 10^{-6}$	0.203	0.0180
80	$4.63 * 10^{-6}$	0.191	0.0143	$5.00 * 10^{-6}$	0.189	0.0156

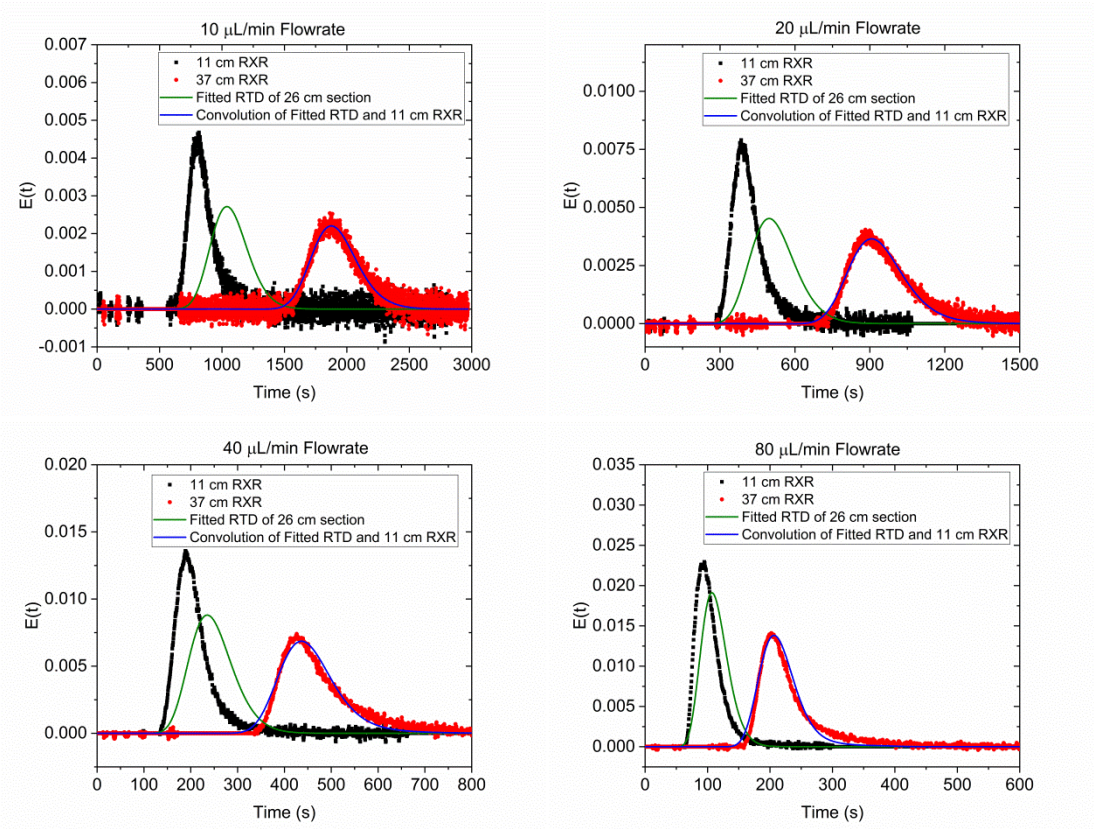

Figure F-3 Experimentally measured RTD for the 11 and 37 cm string reactor set-ups and estimated RTD of the 26 cm section of string reactor, obtained by convolution and fitting, assuming the large deviation from plug flow axial dispersion model.

In the literature, a string reactor RTD study consisting of cylindrical shaped catalyst pellets in tubes with circular cross sections demonstrated plug flow behaviour, with vessel dispersion numbers in the range of 0.001 to 0.005 [289], almost an order of magnitude lower than what was obtained in this work. Similarly, another liquid phase string reactor study using spherical particles of 4 mm diameter in 4 x 4 mm^2 square channels found that the flow could not be described by the axial dispersion model due to very long tails in the RTD, indicating the presence of stagnant zones [295]. Comparing our work with the above, the differences in flow behaviour can largely be attributed to the differences in catalyst and channel shape in each of the string reactors. The lowest dispersion is obtained when the area available for flow between

the catalyst particle and the channel wall is kept small to prevent stagnant zones; this is achieved with cylindrical pellets in tubes with circular cross sections.

As the vessel dispersion numbers obtained in the RTD study were as large as 0.018, it was not immediately clear if the string reactor could be modelled as a plug flow reactor during the kinetic experiments. The impact of axial dispersion depends on the kinetic rate law and conversion, with axial dispersion reactors giving similar results to plug flow reactors only when operating at low levels of conversion, but at higher conversion levels axial dispersion leads to lower conversion for the same reactor volume [291].

An analysis of the impact of dispersion on the reactor performance can be conducted if the reactor is modelled as homogenous, as for a homogenous first order reaction the outlet concentration of the reactor is described analytically according to

$$\frac{C_{out}}{C_{in}} = \frac{4a\ exp\left(\frac{1}{2}\frac{uL}{D}\right)}{(1+a)^2 exp\left(\frac{a}{2}\frac{uL}{D}\right) - (1-a)^2 exp\left(\frac{-a}{2}\frac{uL}{D}\right)} \quad \text{(F-7)}$$

where u is velocity (m/s), L is reactor length (m), D is axial dispersion (m^2/s), k is the homogenous rate constant (s^{-1}) and a is given by

$$a = \sqrt{1 + 4k\tau(D/uL)} \quad \text{(F-8)}$$

In order to estimate a value for the homogenous rate constant k (s^{-1}), some initial kinetic experiments were conducted using the experimental set up described in Chapter 7. The initial experimental data used to estimate the homogenous rate constant are shown in Table F-2, note that these experiments were conducted at the highest temperature that the catalyst can operate at, as it was desired to assess the impact of axial dispersion at high conversion levels where the effect of axial dispersion is most significant. With this experimental data, and an ideal plug flow reactor model with a first order reaction, shown in Eq (F-9), integrated from volume 0 to 251 µL, which is the volume of the 32 cm reactor which was used for these experiments, the homogenous rate constant k, was then estimated as 0.00074 min^{-1}.

$$\frac{dC}{dV} = \frac{kC}{v} \quad \text{(F-9)}$$

Table F-2 Experiments used for initial fitting to assess the expected deviation of the string reactor from ideal plug flow behaviour. Experimental data were obtained from a string reactor packed with 0.1156 g of Amberlyst-15 from the 850-940 µm dry sieve fraction, resulting in a packed bed length of 32 cm.

Temperature (°C)	Flowrate (µL/min)	Feed Conc Benzoic Acid (M)	Outlet Conc Benzoic Acid (M)	Outlet Conc Ethyl Benzoate (M)
120	40	1.5	1.111	0.381
120	40	1	0.749	0.273
120	20	1.5	0.920	0.630
120	20	1	0.602	0.448

The impact of axial dispersion was quantified using Eq (F-7), for a reactor of length 32 cm and an inlet concentration of 1.5 M. The deviation between axial dispersion and plug flow models is greatest at high conversions, therefore this analysis was conducted at the lowest flowrate studied of 15 µL/min. However, it was also observed in the RTD study that the deviation from plug flow operation for this string reactor increased at increasing flowrates, therefore the analysis was conducted for a second time at the maximum flowrate of 60 µL/min. The axial dispersion coefficient for the 15 µL/min was estimated as $1.4*10^{-6}$ m^2/s, while for the 60 µL/min the axial dispersion coefficient was estimated as $5*10^{-6}$ m^2/s; these values were conservative estimates based on the results from Table F-1. The results are shown in Figure F-4, where it can be seen that for 15 µL/min flow rate, the outlet concentration predicted by the axial dispersion model was 0.718 M, while the ideal plug flow reactor predicts 0.713 M. For the 60 µL/min flow rate the outlet concentration predicted by the axial dispersion model was 1.246 M, while the ideal plug flow reactor predicts 1.2454. In both cases the difference between the axial dispersion model and the plug flow model was sufficiently small compared to the experimental error of 0.03 and 0.0165 M, so that the effect of axial dispersion was negligible for this system and hence the reactor can be modelled as a PFR.

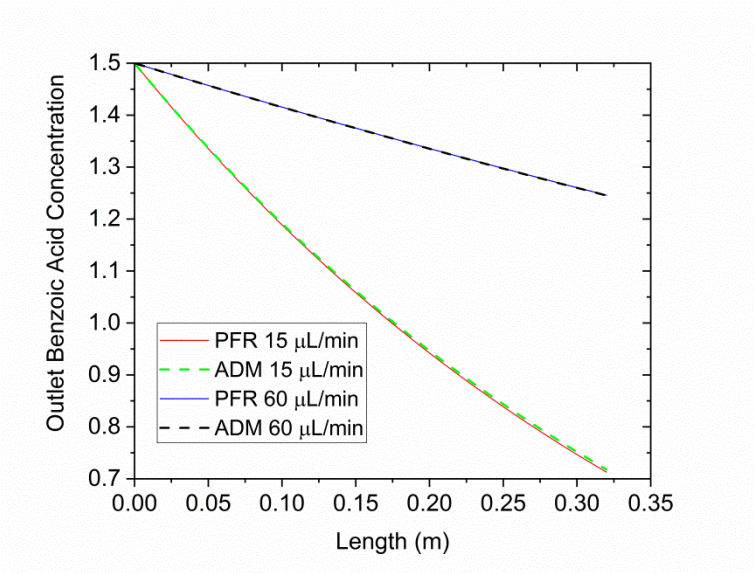

Figure F-4 Model prediction for the outlet concentration of benzoic acid for both the Plug Flow Reactor (PFR) model, and the Axial Dispersion Model (ADM), for a 32 cm long string reactor where the reaction is modelled as first order with a rate constant of 0.00074 s^{-1}.

F.3 External Mass Transfer Study

In order to perform kinetic studies it is necessary to either confirm that there are no mass transfer resistances or account for the mass transfer, which requires mass transfer coefficients from the literature or from experiments. As string reactors are less common than fixed bed reactors, there is less information available in the literature, hence experiments and simulations were conducted to study mass transfer.

F.3.1 Materials & Methods

External mass transfer in the string reactor was studied using the copper dissolution method where copper reacts with acidified dichromate solution, as shown in Eq (F-10) [7]. This process consists of two parts, the diffusion of the chromate ion $Cr_2O_7^{2-}$ from the liquid bulk through the diffusion layer to the copper surface, and then the chemical reaction between the chromate ion and the Cu^{2+} ions. Since the chemical reaction is very fast, the process is controlled by external mass transfer. Therefore, the rate of external mass transfer can be studied by measuring the consumption of $Cr_2O_7^{2-}$ with UV-Vis spectroscopy. The feed used was 0.33 mM $K_2Cr_2O_7$ and 0.3 M H_2SO_4 in deionised water, these concentrations were chosen to minimise the influence of natural convection and ionic migration [7, 296]. Both $K_2Cr_2O_7$ and H_2SO_4 reagents were purchased from Alfa Aesar.

$$3Cu + K_2Cr_2O_7 + 7H_2SO_4 \rightarrow 3CuSO_4 + K_2SO_4 + Cr_2(SO_4)_3 + 7H_2O \qquad \text{(F-10)}$$

The experimental set-up, is shown in Figure F-5. A syringe pump (PhD Ultra, Harvard Apparatus) and a 10 mL glass syringe (Hamilton) were used to deliver the desired

flowrate of feed solution to the string reactor loaded with spherical glass beads of diameter range 710-940 µm (Sigma Aldrich) and a small section of 3 copper spheres. Inert glass beads were used instead of Amberlyst-15 in the reactor as the Amberlyst-15 was found to react with the potassium dichromate ion. It was also necessary to use glass wool and a small layer of smaller glass spheres (425-600 µm diameter, Sigma Aldrich) to hold the copper and glass beads in place, instead of the normally used nickel mesh because the nickel mesh reacted with the chromate ions. A blank test using the glass spheres and glass wool without any copper verified that only a negligible amount of reaction occurred in the absence of copper. The copper spheres used in this study were obtained from Redhill and they had a mean diameter of 947.2 µm and a standard deviation of 11 µm as measured using the Keyence microscope. The number of copper spheres loaded into the reactor was varied to produce the required conversion levels (30-80%) for the different flowrates studied. Three copper spheres were used for studying flowrates of 20-100 µL/min, and 10 copper spheres were used to study flowrates from 100 to 300 µL/min. In addition to conducting experiments in the string reactor of interest to this work (1 mm diameter), a 1.59 mm diameter reactor was also used to study the effect of aspect ratio (ratio of tube diameter to particle diameter) on the mass transfer in string reactors. Experiments were conducted at room temperature (24-25 ^{o}C). For each flowrate studied, two or three samples of 300 µL were collected in small volume UV cuvettes (1.5 mL semi-micro PMMA, BRAND GMBH+) before measuring the absorbance using UV-Vis (Ocean Optics USB2000+ UV-vis-ES spectrometer, 250 nm optic fibres, DT-Mini-2-GS Ocean Optics light source). The absorbance was measured as an average over the wavelength range 343-353 nm to measure the $Cr^{(VI)}$ absorbance peak and the calibration is shown in Appendix B.

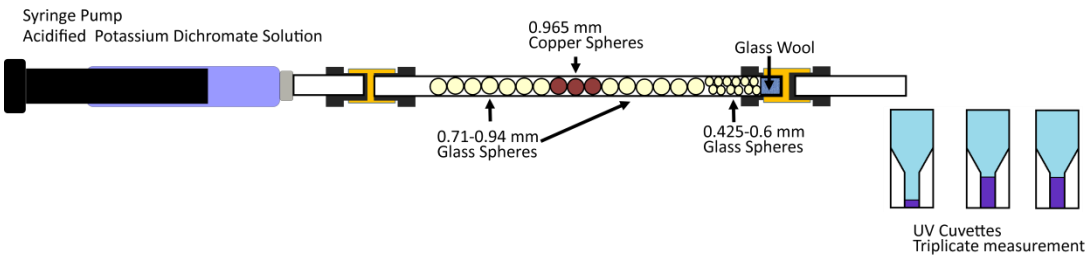

Figure F-5 Experimental set-up for the external mass transfer studies using the copper dissolution method.

In order to obtain mass transfer coefficients from the measurements of the outlet potassium dichromate concentration, a mass balance is required. While it was demonstrated that the string reactor behaved approximately as a plug flow reactor, this is only valid for long string reactors. For the external mass transfer experiment, the

length of the packed bed was just the length of the copper section, l_{cu}, which was only 3 or 10 copper beads, resulting in a length of less than 1 cm. This length was so short that significant axial dispersion was expected, as vessel dispersion numbers in the range of 0.4 - 1.65 were expected for the 1 mm string reactor. Therefore the reactor was modelled using the axial dispersion model

$$D\frac{\partial^2 C}{\partial x^2} - u\frac{\partial C}{\partial x} - k_{SL}a\,C = 0 \qquad \text{(F-11)}$$

Where C is the concentration of potassium dichromate (M), k_{LS} is the liquid solid mass transfer coefficient (m^2/s), *a* is the specific surface area of the copper (m^{-1}), u is the superficial velocity (m/s) and *D* is the axial dispersion coefficient (m^2/s). This equation can be solved by applying the Danckwerts boundary conditions shown in Eq (F-12) and (F-13), leading to the expression for outlet concentration shown in Eq (F-14) [7]. With this equation, the liquid solid mass transfer coefficient can be estimated.

$$at\ x = 0, \qquad u\big(C(0^-) - C(0^+)\big) = -D\frac{dC}{dx} \qquad \text{(F-12)}$$

$$at\ x = l_{cu}, \qquad \frac{dC}{dx} = 0 \qquad \text{(F-13)}$$

$$\frac{C(l_{Cu})}{C(0)} = \frac{4B * \exp(\frac{ul_{Cu}}{2D})}{(1+B)^2 exp\left(\frac{Bul_{Cu}}{2D}\right) - (1-B)^2 exp\left(-\frac{Bul_{Cu}}{2D}\right)} \qquad \text{(F-14)}$$

$$Where \quad B = \sqrt{1 + \frac{4k_{LS}aD}{u^2}}$$

With the liquid solid mass transfer coefficient the Sherwood number can be calculated according to Eq (F-15).

$$Sh = \frac{k_{LS}d_{cu}}{D_M} \qquad \text{(F-15)}$$

where D_M is the molecular diffusion coefficient of the dichromate ion at room temperature, taken from the literature as $1.375*10^{-9}$ m^2/s [7]. Mass transfer results and correlations are most often presented in the literature as Sherwood numbers as a function of Reynolds numbers, where the Reynolds number is Eq (F-16).

$$Re = \frac{\rho u d_{cu}}{\mu} \qquad \text{(F-16)}$$

where ρ and μ are the density (kg/m^3) and dynamic viscosity ($kg\ m^{-1}\ s^{-1}$) of the dichromate solution. The ratio of density and viscosity is kinematic viscosity, whose value reported in the literature as $9.5*10^{-7}$ (m^2/s) [13].

The results of this work are then compared against the Wakao and Funazkri [297] correlation, Eq (F-17), which is valid for micropacked bed reactors.

$$Sh = 2 + 1.1Re^{0.6}Sc^{0.33} \quad \text{(F-17)}$$

F.3.2 Results & Discussions

The results of the mass transfer study are shown in Figure F-6, where it can be observed that the Sherwood numbers obtained for the 1 mm string reactor were found to be far greater than that predicted by the commonly used correlations in the literature, as shown in Figure F-6. However, when the reactor diameter was increased to 1.59 mm, the Sherwood numbers obtained decreased significantly and started matching the Wakao and Funazkri correlation which is commonly used for packed bed reactors. This large difference between the two reactors is explained by their different aspect ratios. Aspect ratio is the ratio of reactor diameter to particle diameter and in the literature string reactors are often defined as reactors with an aspect ratio of less than 1.4. In this work the 1 mm reactor had an aspect ratio of only 1.06 while the 1.59 mm reactor had an aspect ratio of 1.69. Therefore, only the 1 mm reactor can be defined as a string reactor, while the 1.59 mm reactor is between that of a string reactor and a packed bed reactor (which ideally has an aspect ratio greater than 10 to minimise the negative influence of the wall effect). These results then indicate that the correlations available in the literature for packed bed reactors do not apply to string reactors with very low aspect ratios. Similar results in the literature have also reported that for low aspect ratio packed beds, that mass transfer coefficients increase with decreasing aspect ratio [7]. Possibly the increase in mass transfer in string reactors is caused by great variations in reactor voidage along its axial length. In packed bed reactors with large aspect ratios the typical reactor voidage is 0.385 to 0.465, and while there are some variations in voidage along the radial direction near the reactor wall [298], the reactor voidage is not known to vary significantly along the axial direction. In comparison the voidage of a string reactor with spherical beads has large periodic variation in voidage along the axial direction from almost 1 at the point where two beads meet, to just 0.11 at the most constricted point at the centre of a sphere. This results in very high velocities at the constricted points in the reactor, which may contribute to the increased rates of mass transfer obtained in this study.

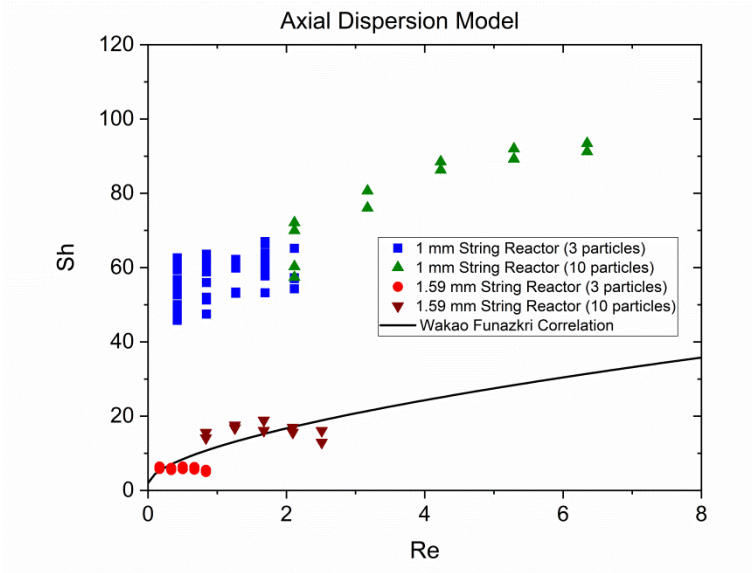

Figure F-6 Sherwood number against Reynolds number for the 1mm and 1.59mm string reactor packed with 947 µm copper spheres.

Within the overall objective of this work, to rapidly identify kinetics for an esterification reaction, it was only required to check if the rate of liquid solid mass transfer was sufficiently high that it could be neglected from the kinetic model. The importance of the rate of external mass transfer can be assessed using the Mear's criterion for external mass transfer [272]

$$\frac{-r_A'\rho_b Rn}{k_{LS}C_{BA\ bulk}} < 0.15 \qquad \text{(F-18)}$$

where r_A' is the rate of mass transfer per mass of catalyst (kmol s^{-1} kg^{-1}), ρ_b is the bulk density of catalyst (kg/m^3), R is the radius of the catalyst particle (m), n is the reaction order, k_{LS} is the liquid-solid mass transfer coefficient (m/s) and $C_{BA\ bulk}$ is the concentration of benzoic acid in the bulk solution (kmol/m^3).

Using the high temperature experimental data shown in Table F-2, the value for the rate of reaction per mass of catalyst is approximated as the average rate of reaction along the length of the string reactor using

$$r_A' = \frac{v\left(C_{BA,in} - C_{BA,out}\right)}{W} \qquad \text{(F-19)}$$

where v is the volumetric flowrate (L/s), $C_{BA,in}$ and $C_{BA,out}$ are the concentrations of benzoic acid at the inlet and outlet (mol/L) and W is the mass of catalyst (g). The observed rate of reaction is then found to be <2.3*10^{-6} kmol s^{-1} kg^{-1}. The bulk catalyst density is calculated according to

$$\rho_b = \rho_c(1 - \Phi_{rxr}) \qquad \text{(F-20)}$$

where ρ_c is the pellet catalyst density (770 kg/m^3 according to the manufacturer specifications), and Φ_{rxr} is the porosity of the string reactor, calculated to be 0.55 for the 1mm string reactor packed with 825 µm spheres. The bulk catalyst density in the reactor is then 350 kg/m^3. Using these values for observed rate of reaction and bulk catalyst density, along with a catalyst radius of 412 µm, a bulk concentration of 1.5 kmol/m^3, a liquid solid mass transfer coefficient of 8*10^{-5} (m/s) and assuming a first order reaction, the dimensionless ratio of reaction rate to mass transfer rate in Eq (F-18) is calculated to be 0.0027, which is significantly less than the criteria of 0.15, hence indicating that external mass transfer can be ignored.

F.4 Internal Mass Transfer Analysis

The catalyst used in this work, Amberlyst-15, is a macroreticular polymeric resin based on crosslinked styrene divinylbenzene copolymers. This means it has a complicated internal structure consisting of pores and channels between agglomerates of minute spherical gel particles [239, 240]. When ground and dried the Amberlyst-15 is found to consist of a pores ranging in size from 40-80 nm, which makes up the macroreticular structure [240]. The gel microspheres are much smaller than 1 µm and they themselves have a gel porosity [239, 240]. Therefore there are two internal mass transfer resistances that must be considered, the resistances in the large catalyst sphere and then the resistances in the small microspheres within the catalyst sphere. Note that the large catalyst sphere size is the size obtained when sieving the catalyst, this is the size of the bead in the bead string reactor which is typically 825 µm in this work.

First the internal mass transfer resistances inside the large catalyst sphere are assessed using the Weisz-Prater criterion for internal mass transfer resistances assuming a first order reaction. The Weisz-Prater criterion is

$$C_{WP} = \frac{-r_A'(obs)\rho_c R^2}{D_e C_{BA,s}} \qquad \text{(F-21)}$$

where $r_A'(obs)$ is the observed rate of reaction per mass of catalyst, 2.3*10^{-6} kmol s^{-1} kg^{-1} (estimated from the initial kinetic experiments shown in Table F-2), ρ_c is the density of the catalyst pellet, 770 kg/m^3, R is the radius of the catalyst particle 4.125*10^{-3} m, $C_{BA,s}$ is the concentration of benzoic acid at the catalyst surface 1.5 kmol/m^3 and D_e is the effective diffusivity of benzoic acid in the pellet (m^2/s), which is calculated according to

$$D_e = \frac{D_M \Phi_p \sigma}{\tau} \qquad \text{(F-22)}$$

where D_M is the molecular diffusivity of benzoic acid in the ethanol solvent, Φ_p is the catalyst pellet porosity, σ is the constriction factor and τ is the catalyst tortuosity. The catalyst porosity was 0.31, based on the reported pore volume and catalyst density of 0.4 ml/g and 770 g/L given by the supplier. The constriction factor and tortuosity factor are unknown and are lumped together with a value of 3.75, based on common tortuosity values in other catalysts [272]. The molecular diffusivity of benzoic acid in the ethanol solvent was calculated using the Wilke Chang equation, as already shown in Appendix D. In order to take a worst possible estimate of the internal mass transfer resistances, we evaluate the mass transfer resistances at the highest temperature of 120 ^{o}C, as this produces the highest reaction rate. The molecular diffusivity at 120 ^{o}C, has a value of $6*10^{-9}$ m^2/s. The effective diffusivity in the catalyst pores is then estimated as $4.93*10^{-10}$ m^2/s, resulting in a Weisz-Prater number of 0.4 which is less than the commonly used criteria for internal mass resistances of 1. Therefore, internal mass transfer resistances within the large catalyst sphere can be ignored for this reaction [272]. This result implies that the rate of reaction does not vary with the size of the Amberlyst-15 particle used, and that the internal pore structure in the particle is sufficient to ensure that all of the microspheres inside the catalyst particle are exposed to the same external concentrations. This conclusion has been reported many times in the literature for a variety of similar esterification reactions, where internal mass transfer was assessed by calculations or by studying a wide range of particle sizes [231, 237, 238, 241, 299-301].

The internal mass transfer resistances inside the microspheres were not assessed in this work. However, Pöpken et al reported that if the Amberlyst-15 particles are ground in a mill, and a sieve fraction of less than 63 μm is used, that the rate of reaction doubles [241]. Pöpken et al do not present this as evidence of internal mass transfer resistances in the macro sphere, as they also report that the reaction rate is independent of the sieve fraction of Amberlyst-15 particles used. Instead they attribute this to a “mass transfer limitation, which is only of importance when the catalyst is subjected to grinding or abrasion”, which implies that they are breaking the microspheres and hence increasing the surface area of microspheres in the catalyst. This result suggests that there are internal mass transfer resistances in the microspheres. Therefore, due to presence of internal mass transfer resistances in the microspheres all of the kinetic data generated in this work is from the mass transfer limited regime and all rate laws and activation energies reported in this paper are apparent rate laws and apparent activation energies. However, this result has limited relevance to industry where the catalyst is always used in the sphere form without grinding or abrasion. Therefore, an apparent rate law would still be industrially useful.

Appendix G: HMF Raw Data & Modelling (SI from Ch 8)

G.1 Raw Data

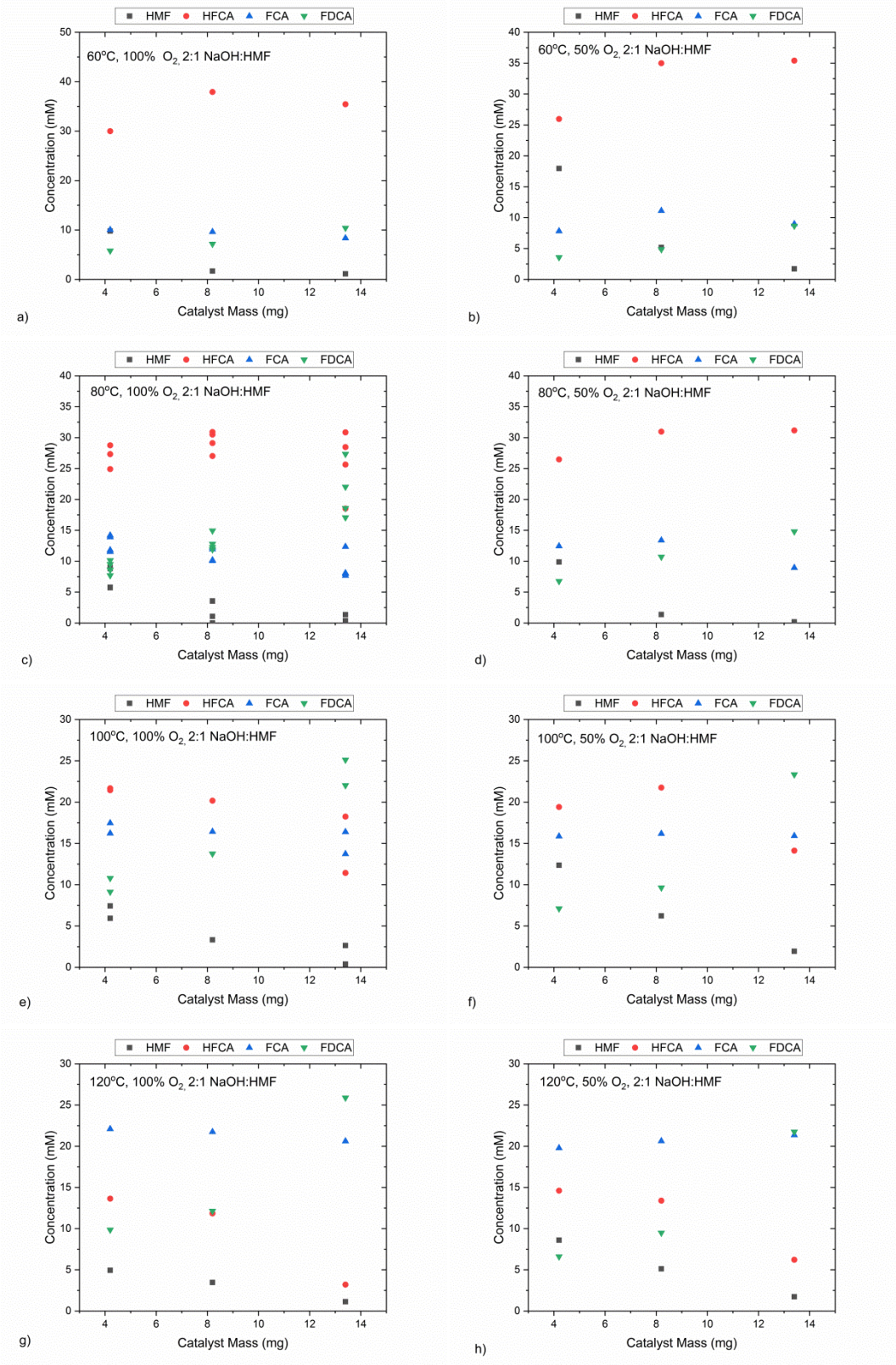

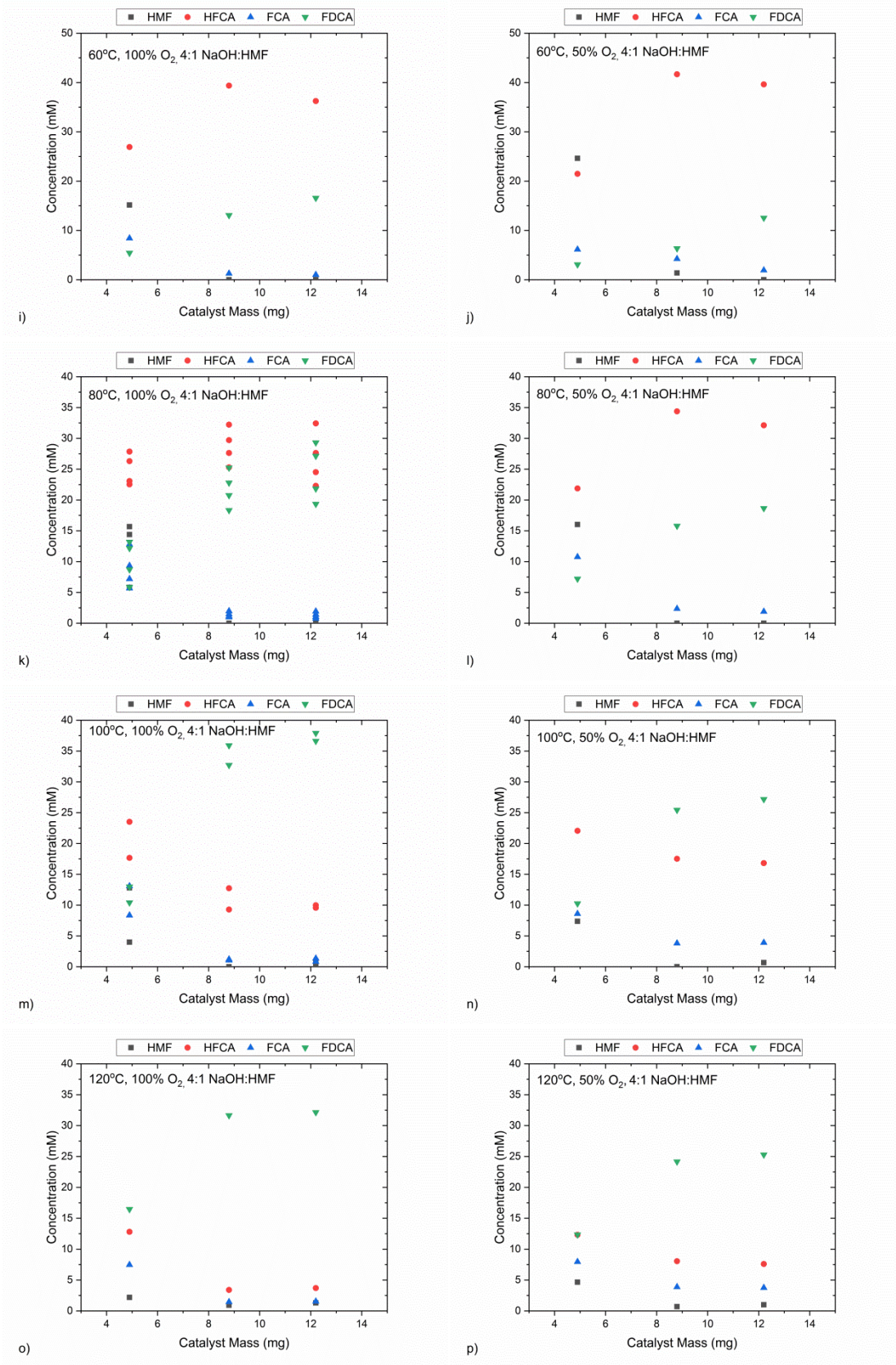

Figure G-1 Concentration profile along the packed bed reactor for each experimental condition of temperature, NaOH:HMF ratio and oxygen composition studied in the factorial experiments.

G.2 Linear Regression Model

The HMF data set (excluding the data points with an unsatisfactory mole balance) was inputted into a linear response model where temperature, concentration of base, oxygen fraction and catalyst mass were treated as continuous variables and the reactor the experiment was conducted in was treated as a nominal effect variable. Unfortunately, the experimental design for the factorial experiments was not ideal. For example the low base concentration experiments were conducted in reactors A, C and E, while the high base concentration experiments were conducted in reactors B, D and F. Therefore, it was difficult to distinguish between the reactor effect and the base concentration effect. Similarly it was difficult to separate the catalyst mass effect from the reactor effect. However, the results of the linear regression model, shown in Table G-1, indicate that the reactor the experiment was conducted in was a significant factor.

Table G-1 Effect tests of linear regression model from JMP

Source	Number of parameters	Degrees of Freedom	Sum of Squares	F ratio	Prob > F
Temperature	1	1	286.7	39.48	<0.001
Oxygen Fraction	1	1	157.1	21.63	<0.001
Base Conc	1	0	0	-	
Catalyst Mass	1	0	0	-	
Reactor	5	3	115.1	5.28	<0.001

G.3 Kinetic Parameter Estimation Results

The results of the kinetic parameter estimation are shown below for both the trend and first order model, when the gas liquid mass transfer coefficient is treated as a parameter to be estimated and when it is given a fixed value.

Table G-2 Parameter estimates for the first order model. Poorly estimated parameters that fail the t-test are highlighted in red.

	KP1 RXN1	KP1 RXN1 95% CI	KP1 RXN2	KP1 RXN2 95% CI	KP1 RXN3	KP1 RXN3 95% CI
RXR A	3.37	0.46	4.12	0.43	3.85	0.48
RXR B	4.73	0.35	5.22	0.35	4.52	0.41
RXR C	3.20	0.39	4.69	0.28	4.00	0.31
RXR D	3.67	0.76	6.05	0.28	3.21	0.69
RXR E	3.22	0.58	5.07	0.22	3.97	0.26
RXR F	**1.00**	**65.03**	6.32	0.36	3.23	0.97
Common to All Reactors			**Estimate**	**95% CI**		
	KP2 RXN1		1.29	0.65		
	KP2 RXN2		2.67	0.56		
	KP2 RXN3		**0.56**	**0.9**		
	$k_{GL}a_{T_M}$	**(min^{-1})**	**3925**	**186900**		

Table G-3 Parameter estimates for the first order model where $k_{GL}a_{T_M}$ is fixed at the value of 612 min^{-1}. Poorly estimated parameters that fail the t-test are highlighted in red.

	KP1 RXN1	KP1 RXN1 95% CI	KP1 RXN2	KP1 RXN2 95% CI	KP1 RXN3	KP1 RXN3 95% CI
RXR A	3.32	0.12	4.07	0.13	3.80	0.22
RXR B	4.69	0.11	5.19	0.17	4.49	0.26
RXR C	3.17	0.24	4.66	0.12	3.97	0.18
RXR D	3.59	0.77	6.02	0.15	3.18	0.65
RXR E	3.21	0.53	5.06	0.15	3.96	0.21
RXR F	**1.39**	**40.19**	6.29	0.35	3.23	0.95
Common to All Reactors			**Estimate**	**95% CI**		
	KP2 RXN1		1.32	0.59		
	KP2 RXN2		2.69	0.52		
	KP2 RXN3		**0.57**	**0.88**		
	$k_{GL}a_{T_M}$	(min^{-1})	612	NA		

Table G-4 Parameter estimates for the trend model. Poorly estimated parameters that fail the t-test are highlighted in red.

	KP1 RXN1	KP1 RXN1 95% CI	KP1 RXN2	KP1 RXN2 95% CI	KP1 RXN3	KP1 RXN3 95% CI
RXR A	10.47	0.14	11.14	0.16	8.07	0.28
RXR B	10.86	0.12	11.26	0.18	8.76	0.29
RXR C	10.56	0.22	11.97	0.13	8.21	0.22
RXR D	10.02	1.15	12.27	0.25	7.46	0.63
RXR E	10.61	0.71	12.51	0.19	8.08	0.23
RXR F	10.17	2.67	12.50	0.45	7.43	0.93
Common to All Reactors			**Estimate**	**95% CI**		
	KP2 RXN1		1.13	0.52		
	KP2 RXN2		2.23	0.47		
	KP2 RXN3		**0.93**	**0.99**		
	$k_{GL}a_{T_M}$	**(min^{-1})**	**89.3**	**72**		

Table G-5 Parameter estimates for the trend model where $k_{GL}a_{T_M}$ is fixed at the value of 612 min^{-1}. Poorly estimated parameters that fail the t-test are highlighted in red.

	KP1 RXN1	KP1 RXN1 95% CI	KP1 RXN2	KP1 RXN2 95% CI	KP1 RXN3	KP1 RXN3 95% CI
RXR A	10.55	0.09	11.23	0.12	8.15	0.26
RXR B	10.92	0.09	11.32	0.17	8.82	0.28
RXR C	**7.99**	**33.50**	12.31	0.71	8.28	0.66
RXR D	10.10	1.05	12.31	0.24	7.51	0.63
RXR E	**7.84**	**73.04**	12.74	0.80	8.22	0.79
RXR F	10.24	2.24	12.53	0.40	7.49	0.90
Common to All Reactors			**Estimate**	**95% CI**		
	KP2 RXN1		1.18	0.5		
	KP2 RXN2		2.20	0.64		
	KP2 RXN3		**0.81**	**1.03**		
	$k_{GL}a_{T_M}$	(min^{-1})	612	NA		

G.4 Dissolved Oxygen Concentration in the Packed Bed Reactor

Previously when assessing the external and internal mass transfer resistances using the Mear's and Weisz Prater criteria it was assumed that the rate of oxygen mass transfer from the gas to the bulk liquid was fast, so that the concentration of oxygen could assumed to be saturated in the bulk liquid. It is difficult to assess the validity of this assumption as it was found that it was not possible to precisely estimate the gas liquid mass transfer coefificent. For example, it was estimated to be both 89.3 ± 72 and 3925 ± 186,900 min^{-1}, while the literautre suggested a value of 612 min^{-1}. However, for all four situations considered in this work (the first order model and the trend model, where $k_{GL}a$ is a parameter and when it is fixed at 612 min^{-1}) the dissolved oxgen concentration in the liquid bulk along the length of the reactor is simulated for a single experimental condition using the corresponding parameter estimates from Table G-2 to Table G-5. From the simulated dissovled oxygen profiles, shown in Figure G-2 a-d, it can be observed that in almost all cases that the dissovled oxygen concentration is approximately equal to the saturated value, hence validating the earlier assumption. Only for the trend model where the mass transfer parameter was estiamted to be 89.3 min^{-1} was it shown that the liquid was not saturated with oxygen. These simualted oxygen profiles also help to explain why it was so hard to estimate the mass transfer coefficient, as they show that in all cases the rate of oxygen transport is resonably fast and that the dissolved oxygen concentration is qutie high. It is generally harder to precisely estiamte fast mass transfer coefficients, as there is very little change in the model response when a high value of the mass transfer coefficient is used. Therefore, instead of obtaining a precise parameter estimate, all that can be said with confidence is that the mass transfer coefficient is high.

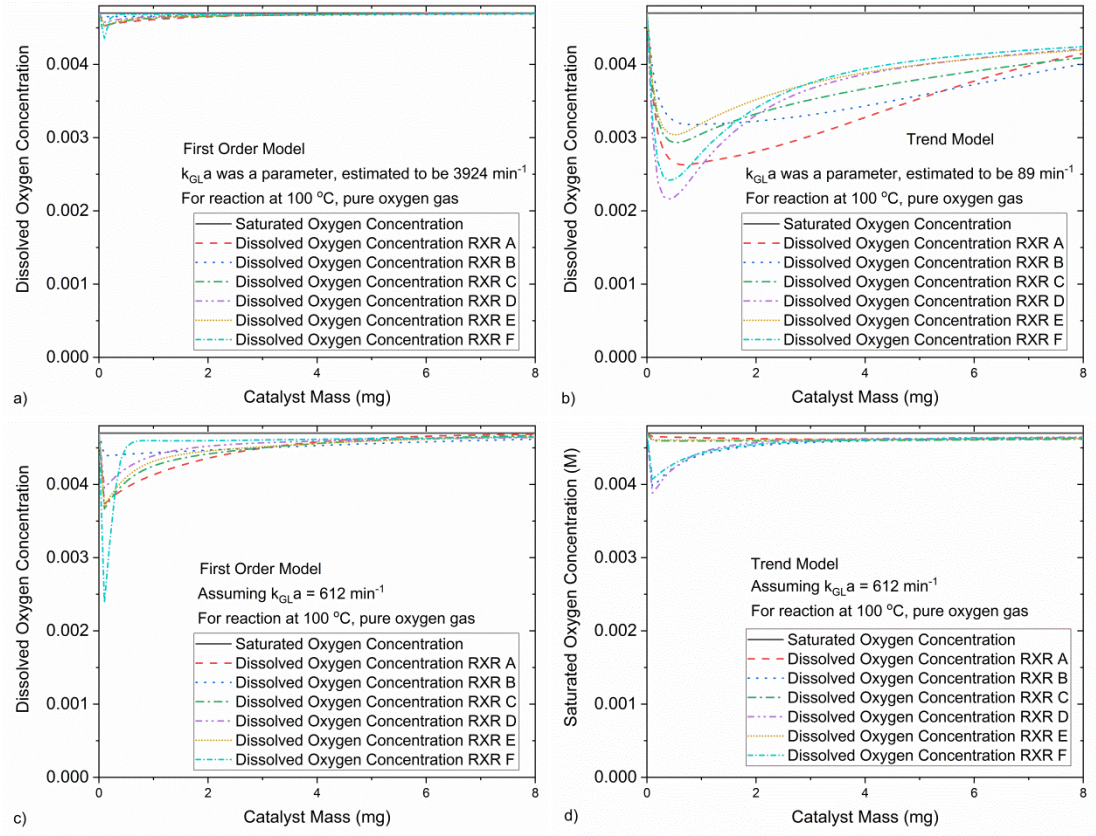

Figure G-2 Dissolved oxygen concentration along the length of the packed bed calculated for an experiment conducted at 100 °C, with 20 µL/min liquid flowrate, 2 NmL/min pure oxygen flowrate and a feed concentration of 50 mM HMF and 200 mM NaOH.